Sensing, uptake and excretion of pyruvate in gamma-proteobacteria

Dissertation

der Fakultät für Biologie

der Ludwig-Maximilians-Universität München

zur Erlangung des Doktorgrades (Dr. rer. nat.)

vorgelegt von

Stephanie Friederike Paulini

München, März 2023

Diese Dissertation wurde angefertigt
unter der Leitung von Prof. Dr. Kirsten Jung
im Bereich Mikrobiologie
an der Ludwig-Maximilians-Universität München

Erstgutachterin: Prof. Dr. Kirsten Jung
Zweitgutachterin: Prof. Dr. Bärbel Stecher
Datum der Abgabe: 06.03.2023
Datum der mündlichen Prüfung: 11.07.2023

Eidesstattliche Erklärung

Ich versichere hiermit an Eides statt, dass die vorgelegte Dissertation von mir selbstständig und ohne unerlaubte Hilfe angefertigt wurde. Des Weiteren erkläre ich, dass ich nicht anderweitig ohne Erfolg versucht habe, eine Dissertation einzureichen oder mich der Doktorprüfung zu unterziehen. Die folgende Dissertation liegt weder ganz, noch in wesentlichen Teilen einer anderen Prüfungskommission vor.

München, den 06.03.2023

Stephanie Paulini

Statutory Declaration

I declare that I have authored this thesis independently, that I have not used other than the declared sources/resources. As well I declare, that I have not submitted a dissertation without success and not passed the oral exam. The present dissertation (neither the entire dissertation nor parts) has not been presented to another examination board.

Munich, 06.03.2023

Stephanie Paulini

Table of Contents

Nomenclature

All genes are written in italics, all proteins are written with a first capital letter. Gene deletions are indicated by the symbol Δ, gene fusions are indicated by the symbol : and gene replacements are indicated by the symbol ::. Antibiotic resistances are indicated by the abbreviated name of the antibiotic with an superscripted R, for instance amp^R.

Abbreviations

amp	ampicillin
AMP	adenosine monophosphate
ATP	adenosine-5'-triphosphate
bp, kb	base pair(s), kilo base pairs
°C	degree Celsius
cm	chloramphenicol
CRP	cyclic AMP receptor protein
DNA	desoxy ribonucleid acid
dNTPs	desoxyribose nucleoside triphosphates
e.g. (*exempli gratia*)	for example
gent	gentamicin
GFP	green fluorescent protein
i.e. (*id est*)	that is
kan	kanamycin
OD_{600}	optical density at 600 nm
PEP	phosphoenolpyruvate
P_{gene}	promoter region of the indicated gene
RLU	relative light units (luminescence)
RNA	ribonucleid acid
ROS	reactive oxygen species
rpm	revolutions per minute
RT	room temperature
strep	streptomycin
TM	transmembrane domain
VBNC	viable but nonculturable
w/v	weight per volume
WT	wild type

Publications originating from this thesis

Chapter 2:

Gasperotti AF, Göing S, Ruiz EF, Forne I, Jung K. 2020. Function and regulation of the pyruvate transporter CstA in *Escherichia coli*. Int J Mol Sci 21:E9068. https://doi.org/10.3390/ijms21239068

Chapter 3:

Göing S, Gasperotti AF, Yang Q, Defoirdt T, Jung K. 2021. Insights into a pyruvate sensing and uptake system in *Vibrio campbellii* and its importance for virulence. J Bacteriol 203:e00296-21. https://doi.org/10.1128/jb.00296-21

Chapter 4:

Paulini S, Fabiani FD, Weiß AS, Moldoveanu AL, Helaine S, Stecher B, Jung K. 2022. The Biological Significance of Pyruvate Sensing and Uptake in *Salmonella enterica* Serovar Typhimurium. Microorganisms 10:1751. https://doi.org/10.3390/microorganisms10091751

Further publications not included in this thesis:

Weiss AS, Burrichter AG, Durai Raj AC, von Strempel A, Meng C, Kleigrewe K, Münch PC, Rössler L, Huber C, Eisenreich W, Jochum LM, Göing S, Jung K, Lincetto C, Hübner J, Marinos G, Zimmermann J, Kaleta C, Sanchez A, Stecher B. 2022. *In vitro* interaction network of a synthetic gut bacterial community. ISME J 16:1095-1109. https://doi.org/10.1038/s41396-021-01153-z

Göing S, Jung K. 2021. Viable but nonculturable gastrointestinal bacteria and their resuscitation. Arch Gastroenterol Res 2: 55-62.

Contributions to publications presented in this thesis

Chapter 2:

The study was designed by Kirsten Jung and Ana Florencia Gasperotti. Stephanie Paulini, née Göing, performed the chemotaxis assays. Elena Fajardo Ruiz performed the DNA affinity capture assay. Ignasi Forné performed the protein analysis via mass spectrometry. Ana Florencia Gasperotti performed all remaining experiments. All authors contributed in writing the material and methods section. The main manuscript was written by Ana Florencia Gasperotti and Kirsten Jung. All authors contributed in reviewing and editing the draft manuscript.

Chapter 3:

The study was designed by Kirsten Jung and Stephanie Paulini, née Göing. Ana Florencia Gasperotti performed the transport experiments. Qjang Yang and Tom Defoirdt performed the *Artemia* infection assays. Stephanie Paulini performed all genetic work and all remaining experiments. All authors contributed in writing the material and methods section. The main manuscript was written by Stephanie Paulini and Kirsten Jung. All authors contributed in reviewing and editing the draft manuscript.

Chapter 4:

The study was designed by Kirsten Jung and Stephanie Paulini. Florian D. Fabiani performed strain construction and experiments regarding transport and external pyruvate measurements. Anna S. Weiß and Bärbel Stecher performed the *in vivo* experiments regarding infection of gnotobiotic mice. Ana Laura Moldoveanu and Sophie Helaine performed the *in vivo* experiments regarding antibiotic survival in macrophages. Stephanie Paulini performed all remaining genetic work and experiments. All authors contributed in writing the material and methods section. The main manuscript was written by Stephanie Paulini and Kirsten Jung. All authors contributed in reviewing and editing the draft manuscript.

We hereby confirm the statements above:

Stephanie Paulini, née Göing

Prof. Dr. Kirsten Jung

Summary

Bacteria are found almost everywhere on earth and can flexibly adapt to changing conditions. They can for instance produce specific transporter proteins to utilize organic compounds as soon as they detect their presence in the environment. They also balance intracellular metabolite concentrations by excreting them when the levels rise too high. This dissertation focuses on sensing, uptake and excretion of one central metabolite, pyruvate.

Pyruvate sensing and uptake systems were investigated and compared in three different gamma-proteobacteria, *Escherichia coli*, *Vibrio campbellii*, and *Salmonella enterica* serovar Typhimurium. The results presented here show that *E. coli* has two different two-component systems for pyruvate sensing (BtsS/BtsR and PyrS/PyrR) and three pyruvate transporters (BtsT, YhjX and CstA), whereas the pathogen *S.* Typhimurium has one pyruvate sensing system (BtsS/BtsR) and two pyruvate transporters (BtsT and CstA), and the marine pathogen *V. campbellii* has one pyruvate sensing system (BtsS/BtsR) and only one pyruvate transporter (BtsU). It is found that the three model bacteria not only possess different numbers and types of pyruvate sensing and uptake systems, but they phenotypically differ when pyruvate uptake is prevented by deletion of the corresponding transporter genes, especially when infecting their respective hosts.

In addition, the excretion of pyruvate by *E. coli* was investigated with the aim of finding the responsible pyruvate exporter protein(s). Several large-scale screening methods were established and performed, leading to a selection of promising candidates. The energetics of pyruvate export were studied using right-side-out membrane vesicles.

The results of this dissertation suggest that pyruvate sensing, uptake and excretion are important for all three model species – not only to catabolize this compound, but also to balance intracellular pyruvate levels and benefit from its other properties, such as protection against reactive oxygen species, recovery from persistence, promotion of virulence, or gaining an advantage in a competitive environment. Comparative molecular analysis of the systems for sensing and uptake of an important metabolite such as pyruvate in different species has provided new insights into the successful adaptation of bacteria to different environmental conditions.

Zusammenfassung

Bakterien sind fast überall auf der Erde zu finden und können sich flexibel an wechselnde Bedingungen anpassen. So können sie zum Beispiel spezifische Transporterproteine produzieren, um wertvolle Verbindungen wie Metabolite genau dann aufzunehmen, sobald sie deren Vorhandensein in der Umwelt wahrnehmen. Außerdem gleichen sie intrazelluläre Metabolit-Konzentrationen aus, indem sie die Verbindungen ausscheiden, wenn die Level zu hoch ansteigen. Der Fokus dieser Dissertation liegt auf der Wahrnehmung, Aufnahme und Ausscheidung des zentralen Metaboliten Pyruvat.

In den drei Modell-Gammaproteobakterien *Escherichia coli*, *Vibrio campbellii* und *Salmonella enterica* serovar Typhimurium wurden Pyruvat-Wahrnehmungs- und -Aufnahmesysteme untersucht und verglichen. Die hier präsentierten Ergebnisse zeigen, dass *E. coli* zwei verschiedene Zweikomponentensysteme zur Wahrnehmung von Pyruvat besitzt (BtsS/BtsR und PyrS/PyrR), sowie drei Pyruvat-Transporter (BtsT, YhjX und CstA), während der Krankheitserreger *S.* Typhimurium ein Pyruvat-Wahrnehmungssystem besitzt (BtsS/BtsR) und zwei Pyruvat-Transporter (BtsT und CstA). Das pathogene Meeresbakterium *V. campbellii* hingegen besitzt ein System zur Wahrnehmung von Pyruvat (BtsS/BtsR) und nur einen Pyruvat-Transporter (BtsU). Es zeigt sich, dass die drei Modellbakterien nicht nur eine unterschiedliche Anzahl und Art von Pyruvat-Wahrnehmungs- und -Aufnahmesystemen besitzen, sondern auch abweichende Phänotypen zeigen, wenn die Aufnahme von Pyruvat durch eine Deletion der verantwortlichen Transporter-Gene verhindert wird – insbesondere bei einer Wirtsinfektion.

Des Weiteren wurde die Ausscheidung von Pyruvat durch *E. coli* untersucht, mit dem Ziel, das/die verantwortliche/n Pyruvat-Exporterprotein/e zu finden. Verschiedene Screening-Methoden wurden etabliert, die zu einer Auswahl vielversprechender Kandidaten führten. Die Energetik des Pyruvat-Exports wurde anhand von Membranvesikeln analysiert.

Die Ergebnisse dieser Dissertation weisen darauf hin, dass die Wahrnehmung, Aufnahme und Ausscheidung von Pyruvat für alle drei Modellbakterien wichtig ist – doch nicht nur, um es zu verstoffwechseln, sondern auch um die intrazelluläre Konzentration konstant zu halten und von seinen anderen Eigenschaften zu profitieren, wie etwa dem Schutz vor oxidativem Stress oder der Förderung von Regeneration und Virulenz. Die vergleichende molekulare Analyse der Systeme zur Wahrnehmung und Aufnahme eines so wichtigen Metaboliten wie Pyruvat in verschiedenen Spezies liefert neue Erkenntnisse über die erfolgreiche Anpassung von Bakterien an unterschiedliche Umweltbedingungen.

1 Introduction

1.1 Bacteria perceive their environment

Bacteria can be found in almost every place on earth and are able to cope with frequent changes in their environment. These can be physical or chemical challenges, like temperature, pressure or pH shifts, oxygen limitation, toxins or radiation, but also changes in nutrient availability, host-pathogen interactions or fluctuating competitive conditions in their habitat. Survival and even thriving of bacteria under these environmental alterations is possible because they flexibly adapt to their surroundings and make use of specific cell features only when they are necessary. To do so, they need to permanently monitor their environment and respond fast and adequately to different positive or negative cues by activating the appropriate cellular processes resulting in advantageous phenotypic changes.

This phenotypic adaptation in accordance to environmental cues is achieved on a molecular level by signal transduction, i.e. first perceiving the signal with a sensor and second translating it with an effector into a regulatory change, which can be altering gene expression, translation or protein activity [1]. Three different systems are known to fulfil this task of signal transduction: One-component systems, alternative sigma factors and two-component systems. One-component (ToxR-like) systems are the evolutionary oldest and predominant systems and comprise both sensor and effector in one protein, usually subdivided into two domains [2]. Sigma factors are essential components of the RNA polymerase inducing gene expression. Based on specific environmental signals, primary housekeeping sigma factors can be substituted by alternative sigma factors. Extracytoplasmic function sigma factors, the largest group of alternative sigma factors, represent another mechanism of bacterial signal transduction [3]. The third group of signal transduction systems, two-component systems, are described in more detail in the following section.

1.2 Signal transduction by two-component systems

Two-component systems have evolved from the simpler one-component systems [4]. They are found in all three domains of life and are among the most abundant proteins in bacteria [4-6]. On average, bacteria possess 25 two-component systems, but the number correlates with the genome size and with the constancy of the specific niche they live in [7, 8]. The obligate intracellular *Mycoplasma genitalium* for instance has no two-component system at all,

Myxococcus xanthus, a bacterium living in a rapidly changing environment, has 132, *Bacillus subtilis* has 36, *Enterococcus faecalis* has 17, *Salmonalla enterica* has 30, and the model bacterium *Escherichia coli* possesses 30 two-component systems [9-12].

Two-component systems consist of a (mostly membrane-integrated) sensor histidine kinase and a soluble response regulator [13]. Typically, the sensor histidine kinase perceives a stimulus from the environment with its input domain (input), transfers the information across the bacterial cell membrane and usually autophosphorylates at a histidine residue in its conserved transmitter domain. The phosphoryl group is subsequently transferred to an aspartate residue in the conserved receiver domain of the response regulator, whereupon its effector domain changes its conformation and modulates gene expression (output) [6, 11]. This process is illustrated in Figure 1. There are also variants of this phosphotransfer prototype, such as hybrid kinases or phosphorelays, in which a multistep transfer of the phosphoryl group is necessary before the signal reaches the response regulator [14].

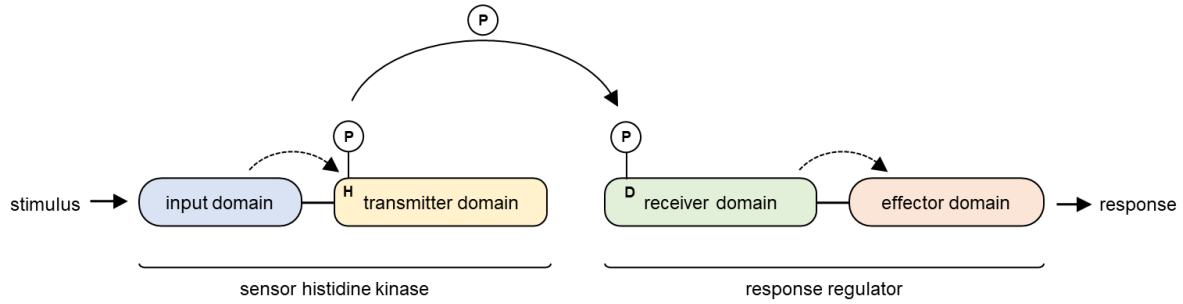

Figure 1. Signal transduction by a two-component system. Typically, a stimulus (temperature, nutrients, pH, osmolarity, etc.) is perceived by the sensor histidine kinase, which autophosphorylates at a conserved histidine residue (H) and transfers the phosphoryl group (P) to a conserved aspartate residue (D) in the receiver domain of the response regulator, resulting in a cellular response by modulating gene expression (enzymatic activity, metabolism, transport, activation of virulence, etc.).

1.3 Transporter gene expression upon signal transduction

The cellular response which is following upon signal transduction can range from changes in metabolism over motility up to collective behavior. We are still far from knowing all signals sensed and all functions regulated by two-component systems [15]. In Figure 2, an overview of all two-component systems in *E. coli* with their hitherto known stimuli and regulatory outcomes can be found. The chemotaxis signal transduction system, which induces changes in movement

upon signal perception, is a specific case of two-component signaling [16]. Moreover, in several cases, no simple stimulus-reaction processes but rather complex regulatory networks determine the final reaction of cells to an environmental stimulus and signal transduction pathways can also be interconnected [17].

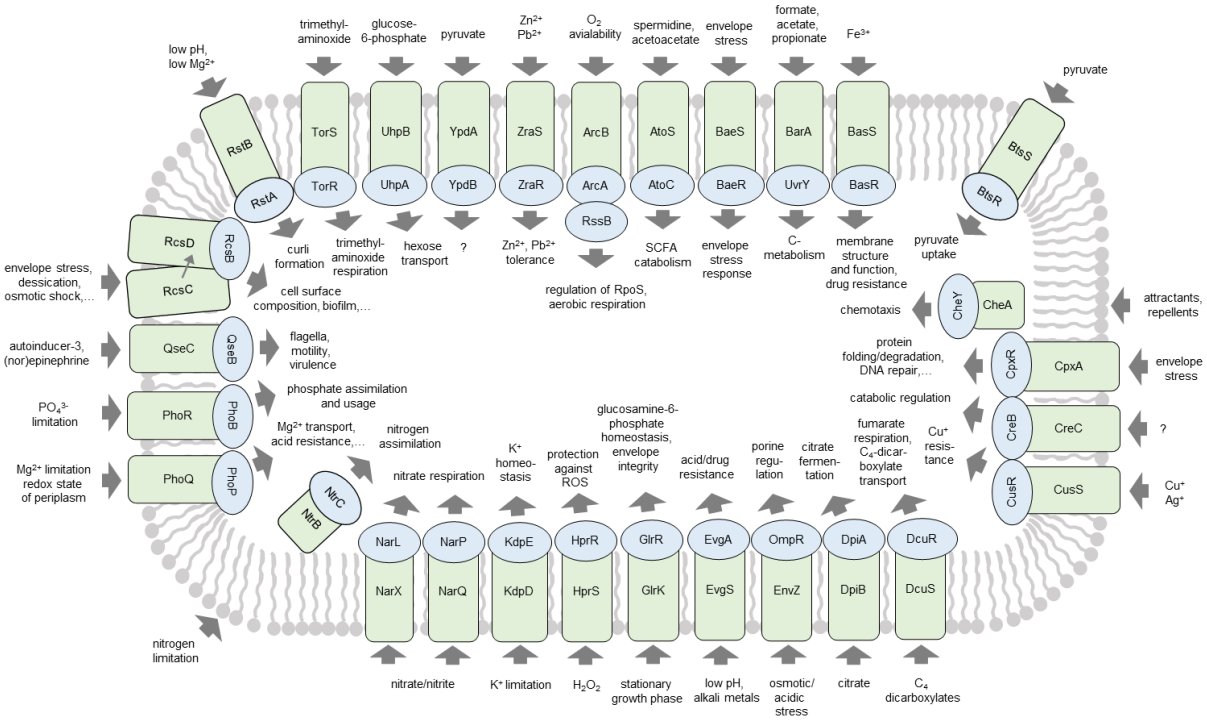

Figure 2. Two-component systems in *E. coli*. Schematic illustration of sensor histidine kinases (green) and their corresponding response regulators (blue) with so far known input signals and output responses. Unknown stimuli or responses are depicted with a question mark. C-metabolism: carbon-metabolism; ROS: reactive oxygen species; SCFA: short chain fatty acids. Modified after Vilhena [18].

One important reaction on sensing a signal is the production of a transporter protein. To make use of valuable compounds, for instance metabolites, bacteria must take them up into the cell with specific transport proteins enabling the transfer across the membrane, may it be actively or passively [19]. As not every compound is present at every time, it is a good strategy to only or increasingly produce a transporter protein if it is needed. This adaptation saves energy and also space in the bacterial membrane. For this end, it is useful for bacteria to couple the expression of transporter protein genes with sensing systems on recognizing the corresponding molecule to be taken up. Transporters can also interact directly with histidine kinases and function as co-sensors [20]. For several transporter systems it was shown that their expression relies on an induction by a two-component system: In *E. coli,* for instance *kdpFABC* (coding

for a potassium transport system) is induced by KdpD/KdpE [21], *dctA* (coding for a C4-dicarboxylate transport protein) is induced by DcuS/DcuR [22], *citT* (coding for a citrate-succinate antiporter) is induced by CitA/CitB [23], *mgtA* (coding for a magnesium-transporting ATPase) is induced by PhoQ/PhoP [24] or *uhpT* (coding for a sugar-phosphate antiporter) is induced by UhpB/UhpA [25]. The two-component system BtsS/BtsR, which induces expression of *btsT* coding for a pyruvate transporter, is another example that will be described in detail in chapters 1.5.1 and 1.5.2. Being able to rapidly take up valuable compounds as soon as they are present can depict an important advantage in a competitive environment, for example in the intestinal microbiota.

1.4 The role of primary metabolites in the intestinal microbiota

The intestine and its microbiota build a complex ecosystem with interaction networks of numerous bacterial communities and metabolites in distinct niches [26]. Every member of the intestinal microbiota has other capabilities and needs [27]. Stable survival in this competitive environment is only possible with a strategy to receive enough resources in a co-existence with other members [28]. Thus, it is a balance between competition and cooperation that shapes and conserves the microbial community composition and determines its functions.

Bacteria in the intestine consume compounds which are either diet-derived, host-derived or excreted by other microbes [29]. It was found that a driver of the microbial community assembly are the networks of trophic interactions, in which the metabolic excretions of one species are the primary resource for another, the so-called cross-feeding [30]. These very complex networks build the foundation of several functions of the intestinal microbiota, be it valuable as well as undesirable ones [31].

Synthetic microbial communities are commonly used in gut microbiome research. It is advantageous to start investigating impacts on colonization and infection within a defined, well-characterized consortium, before going on to an even more complex native microbiota. The oligo mouse microbiota (OMM^{12}) consists of twelve bacterial species representing the five major bacterial phyla in the murine intestine. It provides colonization resistance against enteropathogens and was shown to stably colonizes the mouse gut [32]. Colonization and infection experiments with mice carrying the OMM^{12} can reveal parts of the complex puzzle regarding mechanisms and processes in the murine host, as well as the microbiota's function for health and disease.

1.5 Pyruvate as one important primary metabolite

Pyruvate – the conjugate base of pyruvic acid, the simplest of the alpha-keto acids – is one of the most important molecules in both pro- and eukaryotic cells. It is the end product of glycolysis and can enter the tricarboxylic acid circle via acetyl-CoA under aerobic conditions. Under anaerobic conditions, it can also be fermented, making it a hub between aerobic and anaerobic metabolism. Furthermore, it can be used as a substrate to produce amino acids, fatty acids or sugars via gluconeogenesis. The node position of pyruvate in metabolism is schematically illustrated in figure 3.

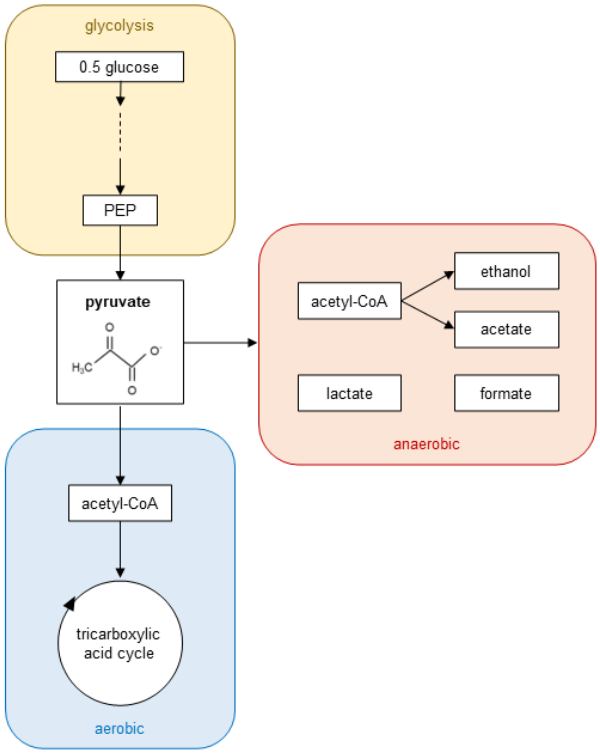

Figure 3. Pyruvate as a central player in metabolism. Rough schematic illustration of metabolic pathways with pyruvate at a central position, as a hub between aerobic and anaerobic metabolism, and also as a substrate for amino acid and fatty acid synthesis.

But pyruvate is not only a central player in metabolism. It also serves as a scavenger of reactive oxygen species (ROS) like H_2O_2 by being oxidatively decarboxylated [33-37]. By this means, it can for instance prevent lipid peroxidation [38] and some bacteria were found to secrete pyruvate to protect themselves from H_2O_2 released by their competitors [39]. The ROS scavenging property of pyruvate is also important for the resuscitation of viable but nonculturable (VBNC) bacteria: This deeply dormant state is characterized by a loss of

culturability in standard cultivation media, with the cells however still being metabolically active on a very low level [40]. More than hundred bacterial species have been found to enter this state which can depict a survival strategy for harsh conditions, such as antibiotic treatments, radiation or nutrient limitations [41]. For the resuscitation of the cells from the VBNC state, i.e. to regain culturability, pyruvate was found to be a crucial factor [42-45] – even beyond its role as an antioxidant for the oxidatively stressed cells: It was demonstrated that pyruvate is taken up as a first substrate by VBNC *E. coli* cells during resuscitation and allows the cells to return to the metabolic active state [46]. Moreover, *Pseudomonas aeruginosa* cells were shown to stay viable over weeks when provided with pyruvate [47]. This points out that pyruvate is a perfect metabolite for bacteria to recover from or to prevent a persisting state.

Pyruvate furthermore plays an important role for the fitness and virulence of several bacterial pathogens: In *Yersenia pseudotuberculosis*, pyruvate metabolism and excretion were found to control fitness and virulence, which could also be demonstrated in infection experiments with mice [48]. The carboxylation of pyruvate was shown to be crucial for the replication of the intracellular pathogen *Listeria monocytogenes* in mammalian host cells as well as for virulence in mice [49]. The opportunistic pathogen *P. aeruginosa* requires pyruvate and pyruvate fermentation for microcolony formation [50]. It was further demonstrated that biofilms established by *P. aeruginosa* or *S. aureus* could be dispersed by the depletion of pyruvate [51]. For *Salmonella enterica* serovar Typhimurium, it was shown that pyruvate metabolism is important for the pathogen's virulence in human cell culture [52] and the growth of *S. enterica* is promoted by pyruvate released from mammalian apoptotic cells [53]. Moreover, pyruvate enhances the pathogenicity of *Staphylococcus aureus* by inducing the production of virulence factors [54]. In *Clostridioides difficile*, however, external pyruvate downregulates the expression of virulence genes [55], and *Vibrio parahaemolyticus*, a cold stress resistant seafood-borne pathogen, was found to be suppressed to grow at low temperature by the addition of pyruvate [56],

For the human host, it was shown that cancer cells produce high amounts of pyruvate and convert it to lactate as they switch to elevated glycolysis rates, even when enough oxygen is present, a phenomenon known as aerobic glycolysis or Warburg effect [57]. This could have an impact on the microbiota of cancer patients. Moreover, in mice infected with the pathogen *S. enterica*, pyruvate concentrations are higher than in uninfected mice [53]. All these research results highlight that pyruvate might be strongly involved in bacterial pathogenicity, infection and host inflammation.

1.5.1 Pyruvate sensing

It has been shown that bacteria can sense pyruvate in their environment. Several two-component systems belonging to the LytS/LytTR family – one of the most distributed families of bacterial two-component systems, members of which often regulate the expression of virulence factors [58] – have been found to be involved in pyruvate sensing. *E. coli* possesses two LytS/LytTR-type two-component systems, which share a high degree of protein sequence similarity: The BtsS/BtsR two-component system (formerly known as YehU/YehT [59]) and the PyrS/PyrR two-component system (formerly known as YpdA/YpdB [60]). Both systems were shown to sense pyruvate, but with different affinities: BtsS is activated by pyruvate starting from a threshold concentration of 50 µM [59] and BtsR then initiates the expression of the target gene *btsT* (formerly known as *yjiY*) [61], which codes for the high-affinity pyruvate transporter BtsT [62], as explained in the next chapter. In contrast, PyrS requires a minimal pyruvate concentration of 600 µM to activate via PyrR the expression of the target gene *yhjX*, which codes for a transporter protein with unknown function [63]. Both systems are also interconnected: BtsS/BtsR downregulates the expression of *yhjX*, whereas PyrS/PyrR activates the expression of *btsT* [64]. These cross-regulations were found to be slightly different in pathogenic *E. coli* bacteria, with BtsS and YpdB interacting to regulate expression of *yhjX*. [65]. Moreover, the central carbon metabolism has an influence on this pyruvate sensing circuit, as the cyclic AMP receptor protein complex (CRP-cAMP) was found to upregulate *btsT*, and the carbon storage regulator A (CsrA) regulates both genes on a post-transcriptional level, albeit *btsT* negatively and *yhjX* positively [61, 64]. The pyruvate sensing network in *E. coli* is illustrated in figure 4.

It was also shown that this pyruvate-sensing network is expressed very heterogeneously and that pyruvate sensing might be important to balance the physiological state of *E. coli* cells within a population, since a larger proportion of mutants lacking both pyruvate sensing systems formed persister cells upon antibiotic stress and were unable to overexpress the green fluorescent protein (GFP) [66]. Furthermore, it was suggested that BtsR is involved in biofilm regulation [67] and both target genes *btsT* and *yhjX* were found to be significantly upregulated in uropathogenic *E. coli* (UPEC) during acute and chronic urinary tract infections in mice [68].

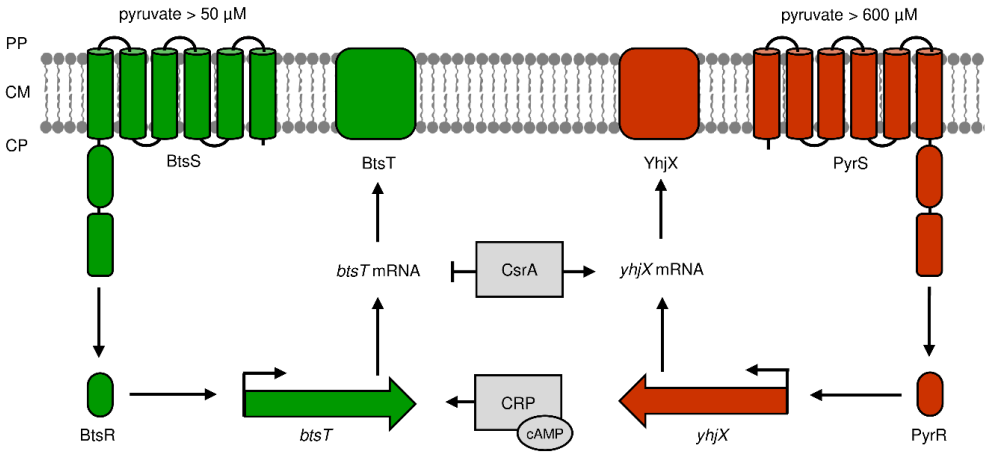

Figure 4. Network of pyruvate sensing systems in *E. coli*. Schematic illustration of the two pyruvate sensing systems in *E. coli* and their regulation. The sensor histine kinases BtsS and PyrS with the response regulators BtsR and PyrR activate the expression of *btsT* and *yhjX*, both coding for transporter proteins, upon sensing different concentrations of external pyruvate. The systems are further regulated by the central carbon metabolism via the carbon storage regulator A (CsrA) and the cyclic AMP receptor protein complex (CRP-cAMP). Activating (⊥) and inhibitory (→) effects are indicated. PP, periplasm; CM, cytoplasmic membrane; CP, cytoplasm.

In *Staphylococcus epidermidis*, LytS/LytR is also suggested to sense pyruvate and activate its uptake, whereby the responsible target gene has not been identified yet [69]. A LytS/LytR homolog in *Clostridioides difficile* was shown to downregulate toxin gene expression upon sensing pyruvate [55]. Also in *Bacillus subtilis*, LytS/LytT senses external pyruvate and induces expression of the pyruvate transport system PftAB [70], and in *Sinorhizobium fredii*, sensing of pyruvate with the two-component system RpuS/RpuR activates expression of *mctP*, a gene coding for a pyruvate transporter [71].

A comparative analysis of LytS/LytTR-type two-component systems in gamma-proteobacteria revealed that they cluster into two different types: The BtsS/BtsR-type and the PyrS/PyrR-type [72]. The majority of gamma-proteobacteria harbors only the predominant BtsS/BtsR system, but some few genera have homologs of both types (like *E. coli*), indicating that PyrS/PyrR serves as a supplementary system [72]. In addition to *E. coli*, for six representative gamma-proteobacteria (*Citrobacter freundii*, *S. enterica*, *Enterobacter aerogenes*, *Xenorhabdus szentirmaii*, *Y. enterocolitica* and *V. campbellii*), a common binding motive was identified in the promoter region of the putative target gene and it was shown that the expression of this gene was activated by pyruvate [72]. This indicates that the LytS/LytTR-type two-component system might also perform pyruvate sensing in these species. Nevertheless, apart from *E. coli*, pyruvate

sensing as well as its biological significance has not yet been demonstrated or investigated directly in any other gamma-proteobacterium. One study has focused on the BtsS/BtsT-type two-component system in *S.* Typhimurium, but could not identify its stimulus or significance [73], although this operon might be a relevant target for adaptive evolution, since it accumulated non-synonymous mutations over time [74]. The target gene *btsT* (formerly *cstA1* or *yjiY*), has been found to be required for flagella mediated infection [75]. This indicates that pyruvate sensing might play an important role for *S.* Typhimurium. In Table 1, the so far known bacterial systems for pyruvate sensing are summarized.

Table 1. So far known bacterial systems for pyruvate sensing, uptake and excretion (in chronological order of their identification).

	gene(s)	species	reference
pyruvate sensing systems	*lytS*/*lytR*	*Staphylococcus epidermidis*	[69]
	pyrS/pyrR	*Escherichia coli*	[63]
	lytS/lytR	*Clostridioides difficile*	[55]
	btsS/*btsR*	*Escherichia coli*	[59]
	lytS/*lytT*	*Bacillus subtilis*	[70]
	rpuS/*rpuR*	*Sinorhizobium fredii*	[71]
pyruvate uptake systems	*mctP*	*Rhizobium leguminosarum*	[76]
	mtcC	*Corynebacterium glutamicum*	[77]
	pftAB	*Bacillus subtilis*	[70]
	btsT	*Escherichia coli*	[62]
	lrgAB	*Streptococcus mutans*	[78]
	mctP	*Sinorhizobium fredii*	[71]
pyruvate export system	*pftAB*	*Bacillus subtilis*	[70]

1.5.2 Pyruvate uptake

In the last twenty years, several transporters in various bacterial species were identified to be capable for the uptake of pyruvate, mostly besides other substances: For *E. coli*, it has been suggested already in 1967 that a separate pyruvate uptake system exists [79], in 1987 it was shown that pyruvate is actively transported into the cells [80] and in 2013 evidence was found that *E. coli* possesses at least two pyruvate uptake systems [81]. Based on the findings in 2017 that the two-component system BtsS/BtsR senses pyruvate (see chapter 1.5.1) and the assumption that the target gene *yhjY* might be involved in pyruvate uptake [59], YjiY was

shortly after confirmed as a specific, high-affinity pyruvate/H^+ symporter and renamed BtsT [62]. BtsT is a member of the peptide transporter carbon starvation (CstA) family, which belongs to the amino acid/polyamine/organocation (APC) superfamily. Evidence was found that BtsT has 18 transmembrane domains with an intracellular N-terminus and that it transports pyruvate with high affinity (K_m: 16.5 µM) [62].

Since the two-component system PyrS/PyrR also senses pyruvate, albeit with a lower affinity, it was assumed that its target gene *yhjX* might also code for a pyruvate transporter, possibly one with a lower affinity than BtsT [63]. This would complete the hypothetic model, as BtsS/BtsR and PyrS/PyrR with their target proteins BtsT and YhjX form a regulatory network [64], which was suggested to function as a fine-tuning of nutrient uptake for an optimally balanced metabolic state of the population [66]. However, the role of the transporter YhjX, belonging to the major facilitator superfamily, has not been solved yet. Strikingly, mutants lacking both *btsT* and *yhjX* are still able to grow on pyruvate as sole carbon source. This leads to the assumption that *E. coli* possesses – even besides YhjX as a second suggested pyruvate transporter – another yet undiscovered pyruvate transport system. It was suggested that in addition to an inducible, highly specific pyruvate uptake system, at least one second constitutive uptake system exists [81]. A recent study based on a transposon library in combination with a toxic pyruvate analog suggested CstA as a constitutively expressed pyruvate transporter [82]. CstA was originally described as a peptide transporter [83] and shares a high degree of similarity (75 %) with BtsT [62]. To this end, CstA might be another pyruvate transporter in *E. coli*. In other model gamma-proteobacteria, nothing is known yet about the function and role of pyruvate uptake. Table 1 gives an overview of all so far characterized bacterial pyruvate uptake systems.

In *Rhizobium leguminosarum*, the permease MctP transports pyruvate besides alanine and other monocarboxylates [76], and in *Corynebacterium glutamicum*, the monocarboxylate transport system MtcC acts as a secondary carrier also for pyruvate besides acetate and propionate, with the expression of *mtcC* being activated in the presence of external pyruvate [77]. As mentioned in the previous chapter, the two-component system LytS/LytT in *B. subtilis* activates a gene coding for the pyruvate-specific transport system PftAB [70]. In *Streptococcus mutans*, LrgAB was identified as a stationary phase-specific pyruvate uptake system, expression of which requires the two-component system LytS/LytR [78]. The transporter MctP in *Sinorhizobium fredii* was shown to transport pyruvate as well, induced by the two-component system RpuS/RpuR upon sensing pyruvate, as mentioned in the previous chapter [71].

In eukaryotic cells, the mitochondrial pyruvate carriers MCP1 and MCP2 transport pyruvate across the mitochondrial membrane [84]. Mitochondrial pyruvate transport was shown to play an important role for the differentiation of memory T cells [85], for the regulation of tumor initiation [86], for fever and neuroinflammation [87] as well as for different neurogenerative diseases and metabolic disorders [88]. The impact of blocking the mitochondrial pyruvate carriers has been investigated with increasing interest in the last years.

1.5.3 Pyruvate excretion

It is known that cells excrete pyruvate under specific conditions. Already in the late 1979s and early 1980s, pyruvate excretion was directly shown and investigated [89, 90]. It is assumed that pyruvate excretion happens mainly due to a so-called overflow metabolisms: To keep intracellular pyruvate concentrations constant under conditions of high pyruvate production, for instance if cells are cultivated under carbon excess, the compound is not fully metabolized, but excreted into the medium and later taken up again [72, 91-93].

When grown in media containing glucose, pyruvate excretion could often be observed, for instance in several marine luminous bacteria [89], in *Y. pseudotuberculosis* [48], in *S. mutans* [78], in *Streptomyces alboniger* [94], in *S. lividans* [95] and in *B. subtilis* [70]. For *E. coli* and several other gamma-proteobacteria, it was shown that pyruvate is excreted when the cells are grown in LB medium, which is rich in amino acids, and that they reclaim the compound in a later growth phase [72]. *Synechococcus elongatus* excretes pyruvate under nitrogen deprivation [96]. Interestingly, bacteria of the genus *Vibrio* were found to excrete extraordinarily high amounts of pyruvate [72, 89].

Furthermore, for some species not only the excretion of pyruvate was observed, but also a specific benefit of this procedure – apart from balancing intracellular pyruvate levels – could be determined: Pathogenic oral streptococci protect themselves against H_2O_2 of commensal competitors by excreting pyruvate to detoxify the harmful ROS [39]. This useful property of pyruvate excretion was also suggested before for *S. mutans* [78]. So far, the only known bacterial pyruvate exporter is PftAB of *B. subtilis* (see Table 1), which is not only able to specifically import, but also export pyruvate [70]. It is suggested for *E. coli*, that a specific system for pyruvate excretion exists [81], but it has not been identified yet.

Eukaryotic cells also excrete pyruvate. It was shown that different types of human and murine cells, both malignant and nonmalignant, excrete pyruvate into their growth medium and that

the amount even increases when catalase is added, indicating that the excreted pyruvate serves as an antioxidant defense mechanism [34]. This is also a reason why pyruvate is often added to cell culture media. Moreover, oxygenated cancer cells were found to excrete pyruvate for hypoxic cancer cells to allow the tumor as a whole to adapt to hypoxia [97]. The pyruvate excretion of mammalian apoptotic cells was further found to support the growth of the pathogen *S.* Typhimurium in cell culture experiments [53]. In return, intestinal immune cells were shown to be activated by pyruvate [98]. These data suggest an important role for pyruvate excretion in the context of human disease – and that it has a strong influence on the bacteria nearby.

1.6 Aims of this thesis

The aim of this thesis is to investigate sensing, uptake and excretion of pyruvate in three model gamma-proteobacteria, namely *E. coli*, *V. campbellii* and *S.* Typhimurium, using methods of various scales, from focused direct measurements with single cells up to *in vivo* infection experiments with animal models. This allows a broader comparison and a deeper understanding of the function and relevance of pyruvate for different species, including pathogens.

So far, in *E. coli*, sensing of pyruvate has been investigated well. One pyruvate transporter, BtsT, has been characterized and one, YhjX, has been suggested, but since a mutant of both these transporters can still grow on pyruvate as sole carbon source, there must be further pyruvate transporter(s), which shall be identified within this thesis. It also needs to be elaborated how a functional redundancy with different transporters for the same substrate can be regulated and explained (see chapter 2).

In *V. campbellii* and in *S.* Typhimurium, nothing is known yet about pyruvate sensing and uptake. Both species possess orthologs of the BtsS/BtsR two-component system and were found to excrete pyruvate during growth and to take it up again, indicating that an uptake system for pyruvate exists in these species. *V. campbellii* is a bioluminescent pathogen for fish and shrimps and represents a major burden for the marine aquaculture economy. *S.* Typhimurium is one of the best-known food-borne pathogens which can cause gastroenteritis as well as systemic infection in humans. Since pyruvate has been shown to be crucial for the virulence of several pathogens, it is important to elucidate the function and impact to perceive and use pyruvate for these two species. To this end, identifying pyruvate sensing and uptake systems in *V. campbellii* and *S.* Typhimurium is also part of this thesis (see chapters 3 and 4).

Another aim of this thesis is to investigate pyruvate excretion in *E. coli*. Apart from PftAB of *B. subtilis*, which was assumed to transport pyruvate not only in but also out of the cell, so far no study exists which has characterized a molecular system exporting pyruvate. Here, large-scale screening methods and direct pyruvate export measurements in the model bacterium *E. coli* will be established to identify the responsible pyruvate exporter protein(s). Thereby, the relevance of pyruvate excretion shall be revealed, especially since this is an until now completely unexplored but yet very relevant topic (see chapter 5).

2 Function and regulation of the pyruvate transporter CstA in *Escherichia coli*

Gasperotti AF, Göing S, Ruiz EF, Forne I, Jung K. 2020. Int J Mol Sci 21:E9068. https://doi.org/10.3390/ijms21239068

International Journal of
Molecular Sciences

MDPI

Article

Function and Regulation of the Pyruvate Transporter CstA in *Escherichia coli* †

Ana Gasperotti [1], Stephanie Göing [1], Elena Fajardo-Ruiz [1], Ignasi Forné [2] and Kirsten Jung [1,*]

1 Department of Microbiology, Ludwig-Maximilians-Universität München, 82152 Martinsried, Germany; ana.gasperotti@lmu.de (A.G.); stephanie.goeing@lmu.de (S.G.); e.fajardoruiz@gmail.com (E.F.-R.)
2 Protein Analysis Unit, BioMedical Center (BMC), Ludwig-Maximilians-Universität München, 82152 Martinsried, Germany; ignasi.forne@lrz.uni-muenchen.de
* Correspondence: jung@lmu.de
† This article is dedicated to Ron Kaback, a fascinating scientist and mentor.

Received: 8 October 2020; Accepted: 23 November 2020; Published: 28 November 2020

Abstract: Pyruvate is a central metabolite that connects many metabolic pathways in living organisms. To meet the cellular pyruvate requirements, the enterobacterium *Escherichia coli* has at least three pyruvate uptake systems—the H^+/pyruvate symporter BtsT, and two thus far less well-characterized transporters, YhjX and CstA. BtsT and CstA belong to the putative carbon starvation (CstA) family (transporter classification TC# 2.A.114). We have created an *E. coli* mutant that cannot grow on pyruvate as the sole carbon source and used it to characterize CstA as a pyruvate transporter. Transport studies in intact cells confirmed that CstA is a highly specific pyruvate transporter with moderate affinity and is energized by a proton gradient. When cells of a reporter strain were cultured in complex medium, *cstA* expression was maximal only in stationary phase. A DNA affinity-capture assay combined with mass spectrometry and an in-vivo reporter assay identified Fis as a repressor of *cstA* expression, in addition to the known activator cAMP-CRP. The functional characterization and regulation of this second pyruvate uptake system provides valuable information for understanding the complexity of pyruvate sensing and uptake in *E. coli*.

Keywords: secondary transporter; pyruvate uptake; global regulator Fis; stationary phase; catabolite repression

1. Introduction

Pyruvate plays a central role in metabolism. It is formed by the degradation of glucose, alanine, and aromatic compounds, and constitutes the branching point that leads (via acetyl-coA) to the tricarboxylic acid cycle and to fatty acid synthesis, to amino acids, such as alanine, and to gluconeogenesis (via oxaloacetate). Under anaerobic conditions, bacteria can switch to fermentation, and reduce organic compounds to maintain the balance of NAD^+/NADH. Pyruvate is then reduced to lactate, oxidized to formate, or decarboxylated to acetaldehyde. This makes pyruvate an important node for the switch between aerobic and anaerobic metabolism.

Pyruvate also plays essential roles in regulating bacterial survival and virulence, as pyruvate is a prominent nutrient in eukaryotic host environment [1–6]. In recent years, it has been shown that bacteria are able to sense external pyruvate and modulate gene expression accordingly [7,8]. Pyruvate sensing and uptake have also been shown to be crucial for the resuscitation of viable but non culturable (VBNC) *E. coli* cells [9].

Since pyruvate is a central metabolite, the intracellular levels of the compound must be tightly regulated [10]. The excretion of pyruvate, during overflow metabolism, is a common feature of many

bacterial species when cultivated under conditions of carbon excess, and contributes to metabolic balancing between carbon uptake and consumption [7,11–16]. Not surprisingly, excretion and reuptake of pyruvate are tightly regulated at multiple levels. In *E. coli*, at least two systems for pyruvate uptake have been proposed—one inducible and the other constitutively active [17].

It was already shown that *E. coli* possess two related histidine kinase/response regulator systems (HK/RR), BtsS/BtsR and YpdA/YpdB (recently renamed PyrS/PyrR) that control the expression of the inducible pyruvate uptake systems [13,14,18,19]. BtsS/BtsR is a high-affinity pyruvate sensing system, while pyruvate acts as a low-affinity stimulus for the PyrS/PyrR system. Both systems regulate the expression of the pyruvate/H^+ symporter BtsT [20], as well as YhjX, a putative low-affinity pyruvate transporter belonging to the major facilitator superfamily [14,21].

BtsT is a secondary transporter with 18 predicted transmembrane helices, which belongs to a small family of transporters named after CstA (the "Putative Peptide Transporter Carbon Starvation Family", transporter classification TC# 2.A.114) [22]. CstA is an inner membrane protein consisting of 701 amino acids, which was originally described as a putative peptide transporter [23]. It is highly conserved across many species and is involved in biofilm formation, motility, and agglutination [24]. BtsT displays high sequence similarity (75.4%) and identity (61.1%) to CstA [20]. Recently, CstA was identified as constitutively expressed pyruvate transporter by transposon mutagenesis in *E. coli* [21]. Nevertheless, its mode of action and substrate specificity remain unknown. Other members of the CstA family were characterized in vivo, e.g., CstA of *Campylobacter jejuni* [24], CstA, and YjiY of *Salmonella enterica* serovar Typhimurium [25], and the corresponding genes are upregulated under carbon starvation. Knockout mutants have a lower growth rate in the presence of peptides as nitrogen source [23,24]. Furthermore, *cstA* and *yjiY* mutants of *S*. Typhimurium are both impaired in the utilization of several dipeptides [25].

cstA expression is regulated at the transcriptional level by the cAMP receptor protein (CRP) under carbon starvation, and negatively regulated at the translational level by the carbon storage regulator CsrA [23,26]. The putative CRP binding site is located about 80 nucleotides upstream from the transcriptional start site, which is unusual for an σ^{70}-dependent promoter [27], indicating that the binding of another factor might be required for regulation [23]. Thus far, no other transcriptional regulators have been identified.

In this work, we focused on studying pyruvate uptake in *E. coli*. For this purpose, we generated a triple mutant that is unable to take up pyruvate. We used this mutant to demonstrate that CstA is a specific pyruvate transporter with moderate substrate-binding affinity. CstA is capable of restoring growth on pyruvate as sole carbon (C)-source, as well as chemotactic movement towards it. Our analysis of the *cstA* expression pattern revealed indications that at least two regulators are involved. Using a DNA affinity-capture assay in combination with reporter strains we identified Fis as a repressor for *cstA* transcription.

2. Results

2.1. Construction of a Mutant that Is Unable to Grow on and Take up Pyruvate

Based on previous work, we hypothesized that *E. coli* possess at least three pyruvate uptake systems, namely BtsT (known pyruvate transporter), YhjX, and CstA [14,20,21]. BtsT was the first pyruvate transporter characterized in *E. coli* [20]. Later, CstA was found also to be involved in pyruvate uptake [21]. Even though the function of YhjX remains elusive, it seems to be involved in pyruvate uptake as well [14,21]. In order to study pyruvate uptake by single transporters in *E. coli*, a mutant deficient in uptake of and growth on pyruvate was required, in order to minimize background activities. For this purpose, we generated the strain *E. coli* MG1655 Δ*btsT* Δ*cstA* Δ*yhjX* (designated as "3Δ mutant").

Growth of the 3Δ mutant was tested in media with different C-sources to make sure no other activity was altered. When this mutant was grown in LB medium, it behaved exactly like the wild-type

(wt) strain (Figure 1A). The same results were observed when the strains were grown in M9 minimal medium with glucose (Figure 1B) or succinate as sole C-source (Figure 1C). As expected, only when the cells were inoculated into M9 minimal medium with 40 mM pyruvate as sole C- and energy source, the 3Δ mutant was unable to grow (Figure 1D). Single deletion mutants and all possible combinations of double mutants showed no significant growth defect on pyruvate ([20] and Suppl. Figure S1) indicating that each transporter alone can sustain growth on pyruvate.

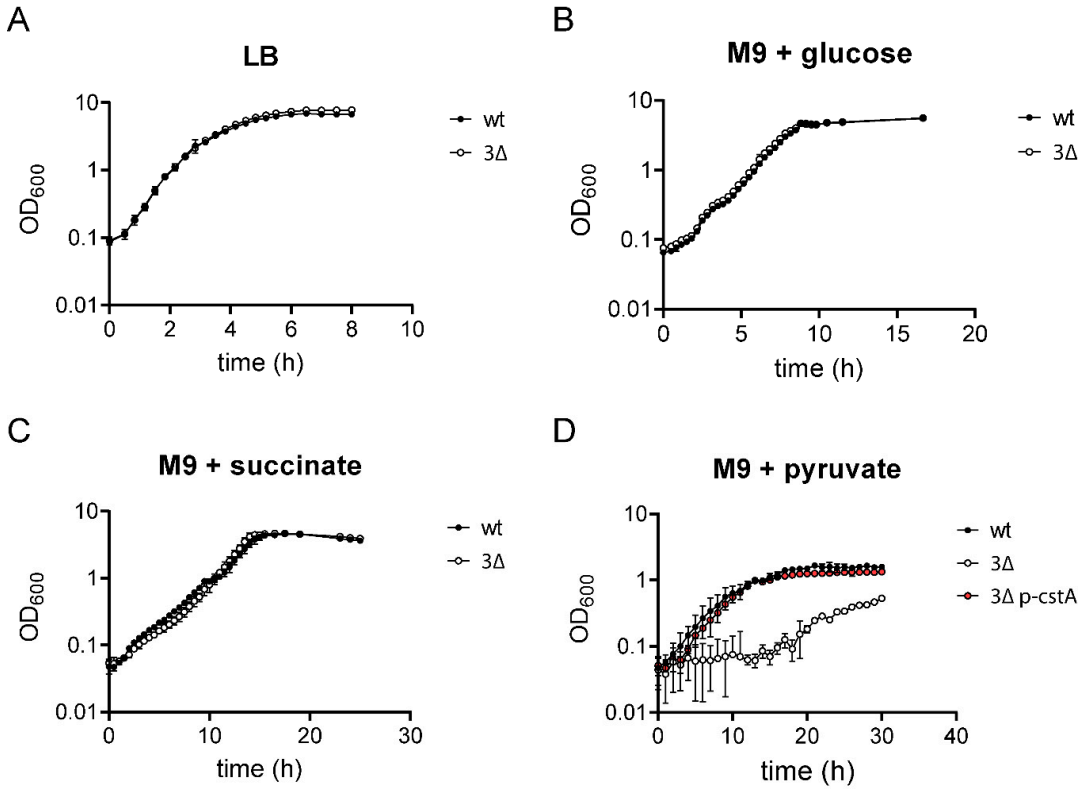

Figure 1. Growth of *E. coli* MG1655 and the triple mutant (3Δ) in media containing different C-sources. Cells of *E. coli* MG1655 (dark circles), the triple mutant (white circles), or the triple mutant complemented with pBAD24-cstA6H (pink circles) were grown in the indicated media at 37 °C under constant agitation. Samples were taken and OD_{600} was measured at different time points. (**A**) LB medium. (**B**) M9 minimal medium with 40 mM glucose. (**C**) M9 minimal medium with 40 mM succinate. (**D**) M9 minimal medium with 40 mM pyruvate. wt: Wild-type strain, 3Δ: Triple mutant, 3Δ p-cstA: Triple mutant complemented with pBAD24-cstA6H. The graphs show the means and standard deviations of three independent replicates.

It was previously shown that the influx of sugars influences chemotaxis toward them by modulating the phosphotransferase system (PTS) activity [28]. This applies to other metabolites, including pyruvate, as well. Therefore, we hypothesized that *E. coli* cells need to uptake pyruvate in order to respond chemotactically to it. To test this hypothesis, we assessed the ability of both wt and 3Δ mutant to chemotactically respond to pyruvate. In this case, since the 3Δ mutant is unable to grow on pyruvate, we assessed chemotaxis using the plug-in-pond assay so that the attractant gradient is not generated metabolically. Cells grown in LB were washed with M9 medium lacking a C-source, mixed with warm soft agar, and placed in a petri dish containing two plugs (one containing glucose, and one with pyruvate). After three hours, chemotaxis rings were observed. As shown in Figure 2A, *E. coli* is able to react chemotactically to both glucose and pyruvate, but the 3Δ mutant is impaired in its response to pyruvate (Figure 2A).

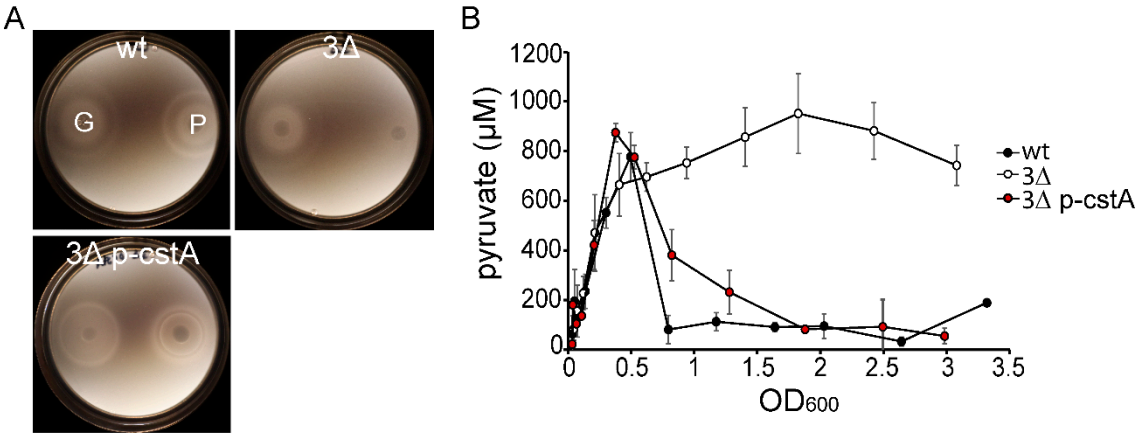

Figure 2. Phenotypic characterization of the 3Δ mutant. (**A**) Chemotaxis. The plug-in-pond assay was utilized to test chemotaxis towards pyruvate and glucose. Agar plugs containing 50 mM pyruvate (P) and glucose (G), respectively, were placed in a petri dish and covered with a suspension of cells in soft agar (0.25%, *w*/*v*). Plates were left to solidify and then incubated at 37 °C for 3 h. The pictures are representative of three independent assays. (**B**) Pyruvate overflow and uptake. *E. coli* MG1655 (wt, black circles), the 3Δ mutant (white circles) and the 3Δ mutant complemented with pBAD24-cstA6H (pink circles) were grown in LB medium at 37 °C, and samples were taken every 20 min. OD_{600} was measured and samples were centrifuged to collect the supernatant. Pyruvate concentrations in the supernatants were determined and values were plotted against OD_{600}. Wt: Wild-type strain, 3Δ: Triple mutant, 3Δ p-cstA: Triple mutant complemented with pBAD24-cstA6H. The graph shows the means and standard deviations of three independent replicates.

In order to demonstrate that the observed defects in growth and chemotaxis are due to the inability of the 3Δ mutant to uptake external pyruvate, we quantified the amounts of extracellular pyruvate present in a culture of the 3Δ mutant growing in LB-medium. For this purpose, we took samples every 20 min and measured the concentration of pyruvate released into the medium due to overflow metabolism (Figure 2B). Pyruvate excretion was not affected by the absence of all three transporters, as indicated by the increase in the external pyruvate concentration in both wt and 3Δ mutant cultures. When overflow ceased, and starvation gradually set in, only the wt strain was able to transport the pyruvate back into the cells, as seen by a decrease in the extracellular concentration (Figure 2B, black circles). The 3Δ mutant, however, was unable to take up pyruvate, and the extracellular concentration of pyruvate remained constant (approximately 800 μM) over time (Figure 2B, white circles).

Taken together, these results indicate that BtsT, CstA, and YhjX are required for pyruvate uptake and necessary for growth on pyruvate as sole C- and energy source.

2.2. CstA Restores Growth and Chemotaxis towards Pyruvate

To assess the function of CstA as a pyruvate transporter, we transformed the 3Δ mutant with either pBAD24 (control) or pBAD24-cstA6H (p-cstA) to check whether *cstA* alone can complement the previously described phenotypes. All the experiments were conducted in the absence of inducer (arabinose), as the leakiness of the P_{BAD} promoter should provide a sufficient amount of CstA to allow complementation. Indeed, the 3Δ mutant carrying *cstA in trans* grows at the wild-type rate on M9 minimal medium with pyruvate as sole C- and energy source, indicating the full restoration of pyruvate transport (Figure 1D). Our previous results showed that pyruvate must be taken up in order to function as a chemo-effector. Therefore, we tested the ability of the complemented mutant to respond chemotactically towards pyruvate. When complemented with *cstA*, chemotaxis towards pyruvate was fully restored (Figure 2A). We also measured the extracellular levels of pyruvate produced due to

overflow metabolism. The complemented 3Δ mutant and the wt strain were found to show similar decreases in external pyruvate (Figure 2A), indicating that CstA is indeed a pyruvate transporter.

2.3. CstA Is a Specific Pyruvate Transporter with Moderate Affinity

To characterize CstA biochemically, uptake of [^{14}C]pyruvate into intact cells was measured. To this end, the 3Δ mutant was transformed with either pBAD24 or pBAD24-cstA6H (p-cstA) and pyruvate uptake was analyzed by rapid filtration assay. To avoid fast metabolization, all assays were performed at 15 °C. The wt strain showed a linear rate of pyruvate uptake for 60 s before reaching saturation (Figure 3A). Indirect methods demonstrated that the 3Δ mutant is unable to take up pyruvate (Figure 2B), although small amounts of [^{14}C]pyruvate were detected in these cells (Figure 3A). This could be explained by simple diffusion of the protonated form of pyruvate or the presence of unspecific transporters that are not able to support growth. Mutant cells complemented with *cstA* displayed similar uptake rates to the wt indicating a full complementation (Figure 3A).

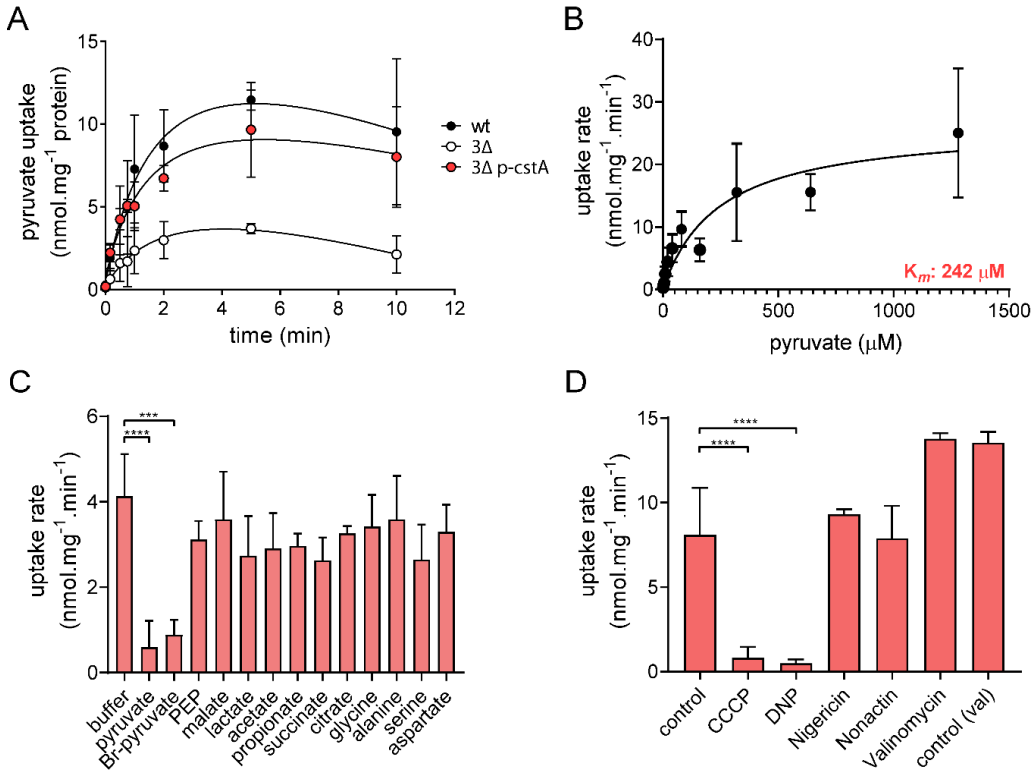

Figure 3. Characterization of pyruvate uptake mediated by CstA in intact cells. (**A**) Time course of pyruvate uptake by *E. coli* strains. Rates of [^{14}C]pyruvate uptake were measured at a final pyruvate concentration of 10 μM at 15 °C in *E. coli* MG1655 (black circles), the triple mutant (3Δ, white circles), and the triple mutant complemented with pBAD24-cstA6H (3Δ p-cstA, pink circles). (**B**) The K_m value was determined by quantification of the initial rate of pyruvate uptake by CstA in the presence of increasing concentrations of pyruvate. The values were corrected by subtracting the diffusion rates (i.e., uptake rate measured for the 3Δ mutant). The best-fit curve was determined by nonlinear regression using the Michaelis–Menten equation. (**C**) Substrate specificity. The effect of the different substrates on pyruvate uptake was measured by simultaneously adding 1 mM substrate and 10 μM [^{14}C]pyruvate. (**D**) Effects of the indicated protonophores and ionophores on pyruvate uptake by CstA. Cells were preincubated at room temperature with the inhibitors for 30 min before adding 10 μM [^{14}C]pyruvate. Control: Transport activity in Tris/MES buffer. Control (val): Transport activity in phosphate buffer, used to assess valinomycin effect (see Methods). All experiments were performed in triplicate; the error bars indicate the standard deviations of the mean. One-way ANOVA (multiple comparisons) was performed using GraphPad Prism, comparing each treatment to the control. Significant differences: **** $p < 0.0001$, *** $p < 0.001$.

To determine the K_m for pyruvate uptake, we quantified the initial rate of pyruvate uptake by CstA in the presence of different initial concentrations of pyruvate (Figure 3B). To properly calculate the uptake due to CstA, the rates were corrected for the background values measured in the 3Δ mutant transformed with the empty vector. The K_m of CstA for pyruvate in intact cells was estimated to be 242 µM—a rather moderate level of substrate affinity compared to that of BtsT (K_m 16.5 µM) [20].

The specificity of CstA was also evaluated by adding a 100-fold excess of several compounds to test for their ability to compete for the pyruvate binding site (Figure 3C). Only pyruvate itself or Br-pyruvate (a synthetic analogue) were found to act as competitors. None of the other compounds used significantly reduced the rate of pyruvate uptake. Like BtsT [20], CstA seems to have an extremely narrow substrate specificity.

Considering that previous observations revealed that pyruvate transport by BtsT is driven by the proton motive force [20] and that BtsT and CstA share high sequence similarity, we tested the effect of various ionophores on pyruvate uptake by CstA. We used 2,4-dinitrophenol (DNP), carbonyl cyanide m-chlorophenyl hydrazone (CCCP), nonactin, valinomycin, and nigericin for this purpose (Figure 3D). DNP and CCCP are hydrophobic protonophores, valinomycin is a highly selective ionophore for K^+, while nonactin forms complexes with K^+, Na^+, NH^+_4, and nigericin promotes potassium-proton antiport. Pyruvate uptake by CstA was only affected by CCCP and DNP (Figure 3D), indicating that transport depends on a proton gradient.

2.4. CstA Is Expressed in Late Exponential and Stationary Phase

The results reported so far were obtained with a 3Δ mutant in which *cstA* was expressed under the control of the P_{BAD} promoter. CstA was recently reported to be a constitutively expressed pyruvate transporter [21]. Indeed, previous results showed that *cstA* expression is under control of σ^{70}, the housekeeping sigma factor [29]. However, in a *lacZ* reporter strain, *cstA* expression was also found to be induced under nutrient limitation, and the CRP-binding site was identified in the promoter region of the gene [23]. To analyze the regulation of *cstA* expression in more detail, we generated a reporter strain in which the promoter region of *cstA* (300 bp upstream of the starting codon) was fused to the *luxCDABE* operon of *Photorhabdus luminescens* [30]. Cells were grown in LB medium, and *cstA* expression started in late exponential phase and further increased in stationary phase (Figure 4A). It should be noted that bioluminescence in cells usually decreases dramatically when entering the stationary phase. This phenomenon, known as abrupt decrease in luciferase activity (ADLA) [31,32], is caused by a decrease in the availability of reduced flavin mononucleotide ($FMNH_2$) and ATP. Despite these limitations, we found strong stimulation of luciferase activity of cells in the stationary phase, suggesting strong promoter activation. These results are consistent with the previous observation that *cstA* is induced under nutrient limitation [23].

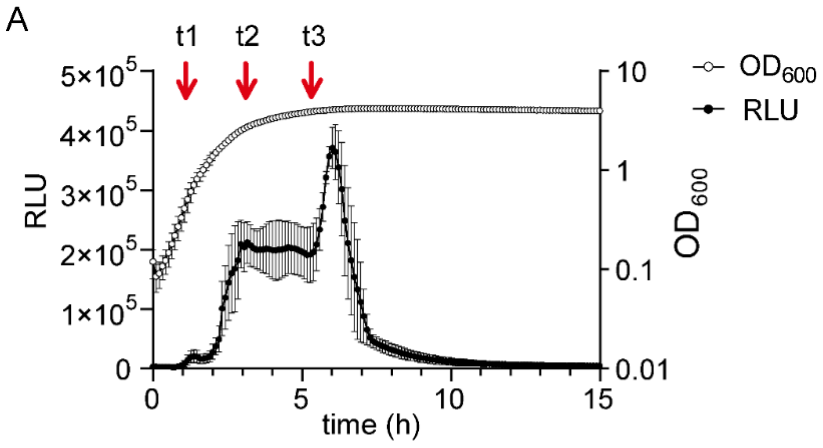

Figure 4. *Cont.*

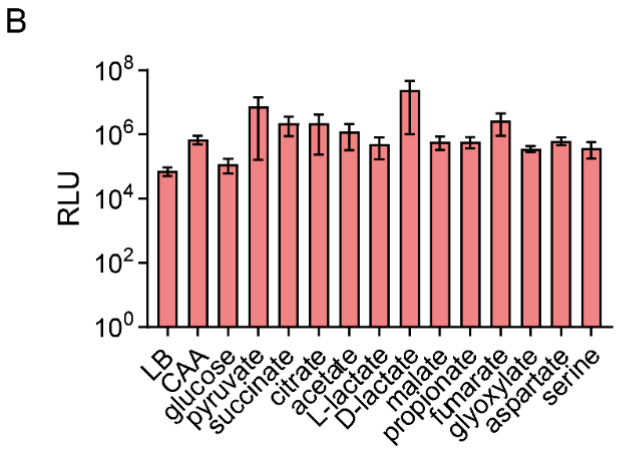

Figure 4. Activation of the *cstA* promoter under various growth conditions. The promoter region of *cstA* (300 bp upstream the gene) was cloned into a reporter plasmid containing the *luxCDABE* operon of *P. luminescens*. *E. coli* MG1655 cells were transformed with this plasmid and grown at 37 °C in the indicated media. Luminescence levels and OD_{600} was measured over time. (**A**) Expression pattern of *cstA*. Luminescence normalized to an optical density (OD_{600}) of 1 (RLU) and growth of cells in LB medium over time. The arrows indicate the time points (t1, t2 and t3) at which samples were collected for DNA affinity-capture assay. (**B**) Expression pattern of *cstA* in cells grown in M9 minimal medium supplemented with 40 mM of the indicated C-sources. The maximal luciferase activity normalized to an optical density (OD_{600}) of 1 (RLU) served as the measure for *cstA* expression. The histogram shows the maximal levels of *cstA* expression recorded in each case. All experiments were performed in triplicate, and the error bars indicate the standard deviations of the mean. CAA, casamino acids.

When cells were grown in M9 minimal medium with different C-sources, the fold-change of *cstA* expression was always >1000-fold (compared to the background noise of 100 RLU), indicating full activation of the promoter (Figure 4B and Figure S2). Although *cstA* is regulated by CRP, we observed an activation when cells were grown in the presence of glucose (Figure 4B). However, under this condition, *cstA* expression was strongly delayed and only started in the stationary phase, when the glucose was consumed (Figure S2). Considering the sensitivity of the bioluminescent output to the energy state of the cultures, the maximum levels of *cstA* expression were quite similar for all C-sources tested (Figure 4B), which suggests that no external stimuli are required for the activation of this gene. In contrast, a carbon source-specific expression was found for the BtsS/BtsR-dependent expression of *btsT* [13].

In summary, the high expression level in stationary phase (Figure 4A and Figure S2) indicated the presence of at least a second regulator besides CRP, which was already suggested by Schultz and Martin [23].

2.5. Identification of Fis as a Regulator of cstA

The growth-phase-dependent expression pattern of *cstA* prompted us to search for this putative second regulator. For this purpose, we used a DNA affinity-capture assay [33,34] to identify proteins bound to the promoter region of *cstA*. Cells were grown in LB medium and harvested at the three indicated time points (Figure 4A, t1-3, red arrows). Subsequently, putative regulators were captured out of whole cell extracts with beads conjugated with a DNA fragment encompassing the *cstA* promoter region (positions -300 to -1). The same procedure was done with a DNA fragment of 300 bp within the *cstA* coding sequence, which served as control. LC-MS was used to analyze the samples. All proteins that were found to be enriched (2-fold or higher) in the beads conjugated with the *ctsA* promoter DNA compared to the control are listed in Table 1. Regulators and otherwise unknown proteins were studied in more detail (Table 1).

Table 1. Identification of proteins bound to the *cstA* promoter. List of proteins enriched in the *cstA* promoter compared to the control fragment for each timepoint (t1, t2, t3). The uncharacterized proteins or regulators that were further studied aremarked with *.

Time Point	Protein	UniProt Description	Fold Change
t1	AtpE	ATP synthase subunit c	2.47
	DeoR *	Regulator	1.97
	Fis *	Regulator	3.53
	HemY	Heme metabolic process	1.82
	MraZ *	Regulator	1.85
	RpmG	50S ribosomal protein	3.19
	XseB	Exodeoxyribonuclease 7 small subunit	2.10
	YdjA	Putative NAD(P)H nitroreductase	1.98
t2	AceA	Isocitrate lyase	2.06
	DeoR *	Regulator	2.19
	IhfA	Integration host factor	2.22
	Lpp	Major outer membrane lipoprotein	2.00
	Rph	Truncated inactive ribonuclease PH	1.77
	RplW	30S ribosomal protein S5	1.94
	RpmA	50S ribosomal protein L27	2.85
	RpsT	30S ribosomal protein S20	1.95
	YgbI *	Uncharacterized HTH-type transcriptional regulator	2.08
	YhfW *	Uncharacterized protein	2.70
t3	DeoR *	Regulator	2.00
	JayE	Putative protein from lambdoid prophage	3.34
	Lpp	Major outer membrane lipoprotein	2.01
	RhlB	ATP-dependent RNA helicase RhlB	2.13
	RnpA	Ribonuclease P protein component	2.68
	YcaC	Probable hydrolase YcaC	1.73
	YgbI *	Uncharacterized HTH-type transcriptional regulator	1.83

The deletion mutants for the five selected genes (Table 1), and a Δ*crp* mutant were each transformed with the reporter plasmid, and the *ctsA* promoter activity of cells grown in LB medium was measured (Figure S3). As a control, a reporter plasmid carrying the *lux* operon under the control of the promoter region of *btsT* was used [13]. As expected, the absence of CRP completely abolished expression of both transporter genes (Figure 5A). As shown in Figure 5A, of the five regulators identified, only the Δ*fis* mutant showed enhanced luminescence compared to the wt strain, indicating that the Fis protein acts as a repressor for *cstA*. None of the other regulators significantly affected the expression of *btsT* or *ctsA*.

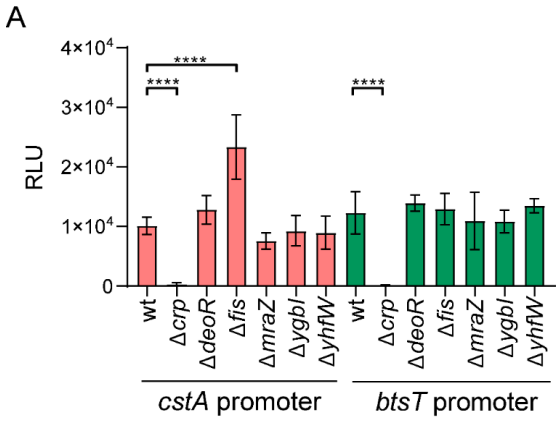

Figure 5. *Cont.*

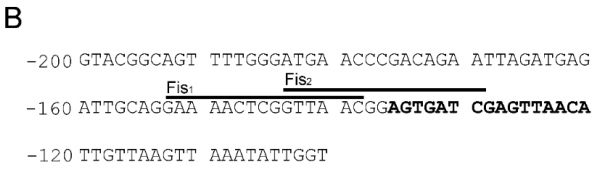

Figure 5. (**A**) Promoter activities of *cstA* and *btsT* in *E. coli* mutants. A luciferase-based reporter assay was used to monitor the promoter activities of *cstA* and *btsT* in the indicated *E. coli* mutants. All strains were transformed with the plasmid pBBR1-*cstA*prom-*lux* or pBBR1-*btsT*prom-*lux*. Bacteria were cultivated in LB medium under aerobic conditions, and the growth and activity of the reporter were continuously monitored. The maximal luciferase activity normalized to an optical density (OD_{600}) of 1 (RLU) served as the measure for *cstA* or *btsT* (formerly *yjiY*) promoter activity. All experiments were performed in triplicate, and the error bars indicate the standard deviations of the mean. One-way ANOVA (multiple comparisons) was performed using GraphPad Prism comparing each mutant to the wt, significant differences (**** $p < 0.0001$) were found for Δ*crp* (for both reporter genes) and Δ*fis*. (**B**) Analysis of the promoter region of *cstA*. Fragments of the nucleotide sequence of the *cstA* upstream region (positions −200 to −120) within which the binding motifs for CRP and Fis were identified. The CRP binding site (bold letters) corresponds to the sequence previously published [23]. For Fis, the motif $G_{-7}N_{-6}N_{-5}N_{-4}R_{-3}N_{-2}N_{-1}N_0N_1N_2Y_3N_4N_5N_6C_7$, based on Shao et al. [35], was used. Two possible binding sites with the specific characteristics where found (Fis_1 and Fis_2), both of which are close to the CRP binding site.

Fis (Factor for Inversion Stimulation) is a DNA-binding protein. In *E. coli*, Fis varies in abundance depending on the growth conditions and growth phase. Fis is most abundant in cells grown in rich medium during early exponential growth, but its level decreases during stationary phase. The role of Fis as a transcriptional regulator has been demonstrated for more than 200 genes [36]. Shao et al. [35] characterized the DNA-binding sequence of Fis in *E. coli* and found a highly variable sequence with four highly conserved positions, $G_{-7}N_{-6}N_{-5}N_{-4}R_{-3}N_{-2}N_{-1}N_0N_1N_2Y_3N_4N_5N_6C_7$. Analysis of the promoter region of *cstA* (-300/+0) revealed two binding sites with the previously described characteristics (Figure 5B). This result further corroborates a possible role of Fis in the expression of *cstA*. Interestingly, one of the predicted binding sites for Fis partially overlaps with the binding site of CRP [23] (Figure 5B), suggesting that Fis might also interfere with the binding of CRP in exponentially growing cells.

3. Discussion

Pyruvate is a central metabolite under both aerobic and anaerobic growth conditions. During glycolysis, glucose is converted into two molecules pyruvate. Some organisms have the Entner-Doudoroff pathway, in which 2-keto-3-desoxy-6-phosphogluconate is cleaved directly to pyruvate and glyceraldehyde 3-phosphate. The latter molecule is converted to pyruvate by the enzymes of the glycolytic pathway. In addition, bacteria can grow in amino acid-rich media, and alanine, serine, cysteine, glycine, and tryptophan are catabolized to pyruvate. Under these conditions, fast-growing bacteria excrete pyruvate rather than metabolizing it completely [7,11,15]. This so-called overflow metabolism is part of a global physiological response to the protein demands associated with energy production and biomass synthesis [37]. Pyruvate levels seem to reflect the quantitative relationship between carbon and nitrogen availability in the cell, and affect amino acid biosynthesis [16].

Taking uptake and export into account, it is not surprising that both in pro- and eukaryotic organisms the intracellular pyruvate concentration is much lower than the maximum external concentration. It ranges from 40 µM in cells to about 100 µM in plasma and serum, but can reach 2 mM in bacterial supernatants and up to 10 mM in blood of diabetics [7,38–40].

Moreover, there is increasing evidence for a role of pyruvate and other α-keto acids in biological fitness and resuscitation of dormant cells in bacterial communities [9,41]. Over the past few years, several pyruvate transporters have been characterized in different microorganisms, such as MctC in *Corynebacterium glutamicum* [42], MctP in *Rhizobium leguminosarum* [43], LrgAB in *S. mutans* [1], PftAB in *Bacillus subtilis* [8] and BtsT in *E. coli* [20].

Two HK/RR systems responsible for pyruvate sensing, BtsS/BtsR and PyrS/PyrR were previously identified [13,14,18,44]. These systems are activated by external pyruvate and induce the expression of two genes each of which codes for a transporter, BtsT and YhjX, respectively. We went on to characterize BtsT as a high affinity pyruvate/H^+ symporter [20]. Even though the precise function of YhjX remains elusive, there are indications that it might function as another inducible pyruvate transporter [14,21]. Besides these two inducible uptake systems, Hwang et al. [21] showed that the peptide transporter CstA might also be involved in pyruvate uptake.

Here we have created a strain lacking all three of these transporter genes (*E. coli* Δ*btsT* Δ*cstA* Δ*yhjX*), and show that this mutant, unlike any of the single or double mutants, is unable to grow on pyruvate as sole C- and energy source (Figure 1 and Figure S1). These results confirm that each of the three transporters is capable of mediating pyruvate uptake in *E. coli*, although BtsT, CstA, and YhjX probably act with different affinities and specificities. Furthermore, the triple mutant has lost the ability to sense pyruvate as chemoattractant (Figure 2A) and this is most likely due to its inability to take up the compound (Figure 2B). It was previously shown that *E. coli* responds chemotactically to pyruvate via the PTS network, whereby the addition of pyruvate affects protein interactions within the PTS network and these signals are further propagated to the chemotaxis pathway [28]. PTS activity obviously reflects the levels of other metabolites, including glycerol, oxaloacetate, and serine, and the Sourjik group [28] has proposed that sensing of these metabolites might be mediated by the pyruvate to phosphoenolpyruvate (PEP) ratio, which in turn has an impact on the phosphorylation state of the PTS network. Our results suggest that pyruvate uptake also plays a role in this network by regulating the intracellular levels of pyruvate, and therefore modifying the pyruvate/PEP ratio. Further experiments in this direction need to be conducted in order to understand the relationship between pyruvate uptake, PTS network and chemotaxis.

In this study, we have focused on the characterization of CstA as a pyruvate transporter. As mentioned previously, Hwang et al. [21] showed that a mutant lacking *cstA* was less susceptible than the wt strain to the toxic pyruvate analog 3-fluoropyruvate. Our finding that the triple mutant complemented with CstA alone was sufficient to enable this strain to utilize pyruvate as sole C- and energy source and chemoattractant (Figure 1D, Figure 2) is compatible with the previous result. We studied the function of CstA in intact cells and characterized the protein as a specific pyruvate transporter with a moderate affinity for its substrate. The measured K_m value was 242 μM (Figure 3B). The protonophores CCCP and DNP had a significant inhibitory effect on pyruvate transport, indicating that the transport of pyruvate is driven by a protonmotive force. Similar results were described for BtsT, although this transporter has a 15-fold higher affinity for pyruvate than CstA [20]. BtsT and CstA are unusual secondary transporters insofar as they have 18 transmembrane helices. Both belong to the same transporter family (transporter classification TC# 2.A.114) [22] and share high sequence similarity (75.4%) and identity (61.1%). The number of amino-acid substitutions that differentiates them is sufficient to explain the difference between their respective affinities for pyruvate.

Besides their basic function, the two transporters share some regulatory elements. Expression of both genes is regulated by the cyclic AMP receptor protein (CRP), and the carbon storage regulator A (CsrA) post-transcriptionally inhibits synthesis of the transporters [13,23,26]. The main difference in regulation is that *btsT* is tightly controlled by the BtsS/BtsR HK/RR system [13], while *cstA* is under control of the general sigma factor RpoD (σ^{70}) [23].

The question of how P_{cstA} activation is regulated is important for understanding the pyruvate metabolism of *E. coli*. Using a reporter plasmid, we monitored *cstA* promoter activity in cells grown under different conditions. In contrast to *btsT*, expression seems to be independent of the C-source (Figure 4B). Our analysis of the *cstA* expression pattern revealed evidence for the existence of more than one regulator, which had previously been postulated [23]. We were able to identify Fis (factor for inversion stimulation) as a regulator of the expression of *cstA* (Figure 5A). This protein negatively regulates *cstA* as indicated by the fact that *cstA* expression is significantly increased in a Δ*fis* mutant. Moreover, by using a DNA capture assay, we found Fis to be specifically enriched in the promoter

region of *cstA* in early-log-phase cells (Table 1, t1). Fis is the most abundant nucleoid-associated protein during the exponential growth phase in rapidly growing cultures [45]. The intracellular Fis levels peak during early exponential growth and then decrease, falling to very low levels in the stationary phase [46]. Analysis of Fis-dependent gene regulation showed that the expression of 231 genes was significantly altered during one or more growth stages, the majority of them being downregulated by Fis [36]. Fis is able to interact specifically with highly variable DNA sequences. The general binding motif $G_{-7}N_{-6}N_{-5}N_{-4}R_{-3}N_{-2}N_{-1}N_0N_1N_2Y_3N_4N_5N_6C_7$ has been derived from base substitution analysis, with the −7G, -3R, +3Y, and +7C bases serving as major determinants for high-affinity binding, while the nucleotide combination −4A/+4T severely hinders binding and an AT-rich central region (N_{-2} to N_2) facilitates Fis–DNA interactions [35]. On examination of the promoter region of *cstA*, we found two possible binding sites for Fis (Figure 5B, Fis_1 and Fis_2). Both sites possess the four major determinants for high-affinity binding, but also at least one nucleotide that reduces binding. Therefore, we speculate that Fis has a low to moderate affinity for these two possible binding sites, which could explain why there is only a two-fold increase of *cstA* expression in the Δ*fis* mutant. Both binding sites are in close proximity to the identified CRP binding site (Figure 5B). Therefore, we propose that Fis acts not only as repressor of *ctsA*, but also blocks access of CRP to its binding site in exponentially growing cells. As the cells approach stationary phase, levels of Fis drop, and the regulator is released from the DNA, thereby permitting binding of CRP and activation of *ctsA* expression (Figure 4A, first peak). In stationary phase cells, in which levels of Fis should be negligible, maximum *cstA* expression can be achieved. Our findings suggest that the timing and level of *cstA* activation is dependent on the growth stage of the population.

When *E. coli* cells are grown in LB medium, *btsT* and *yhjX* are expressed in the mid-exponential growth phase [13,14,44], whereas *cstA* is mainly expressed in stationary phase. Therefore, planktonic *E. coli* cells produce at least one pyruvate transporter in all growth stages. In liquid culture, the excretion of pyruvate during overflow metabolism is followed by rapid uptake so that levels of external pyruvate are low in stationary phase (Figure 2B). CstA may be more important in *E. coli* biofilms, which are stratified in exponential- and stationary-phase cells, and allow exchange of pyruvate [47]. The pyruvate uptake system LrgAB in *S. mutans* is also known to be expressed in stationary phase, but is the only system responsible for the uptake of extracellular pyruvate in this species [1].

Functional redundancy of transporters and sensory systems has been shown for several nutrients and may be a usual strategy for many bacteria, allowing them to increase the range of response in constantly fluctuating environments. Growth under suboptimal nutrient concentrations requires adaptations [48,49], and CstA might be part of this adaptation network to scavenge pyruvate. The results presented here add another piece of information to the puzzle of *E. coli's* tightly and dynamically regulated pyruvate uptake systems.

4. Materials and Methods

4.1. Bacterial Strains and Plasmids

In this study, we used the strains and plasmids listed in Table 2. The primers used to generate the deletion mutants or plasmids are provided in Table S1.

E. coli mutants were generated by using the Quick and easy *E. coli* gene deletion kit, which uses the RED®/ET® recombinase system (Gene Bridges). Shortly, an FRT-PGK-gb2-neo-FRT (kanamycin cassette) was amplified by PCR with flanking regions corresponding to each transporter and introduced into the genomic DNA via Red/ET recombination. The kanamycin marker was subsequently removed from the chromosome using a FLP recombinase. For double and triple mutants, the transporter genes were deleted sequentially. For complementation assays and transport studies, the cells were transformed with vector pBAD24-cstA6H, which codes for CstA-6His, and pBAD24 as control. In all cases, no arabinose was added to the culture, and the leakiness of the P_{BAD} promoter allowed sufficient expression of *cstA* for complementation. To test promoter activity, we used plasmid

pBBR1-cstAprom-lux, a promoter-based luciferase reporter construct obtained by cloning the promoter region of *cstA* (300 bp upstream the starting codon) in front of the *luxCDABE* operon [30].

Table 2. List of strains and plasmids.

Strains		
	E. coli MG1655	[50]
	E. coli BW25113	[51]
	JW5702 (*E. coli* BW25113 Δ*crp*)	[51]
	JW0824 (*E. coli* BW25113 Δ*deoR*)	[51]
	JW3229 (*E. coli* BW25113 Δ*fis*)	[51]
	JW0079 (*E. coli* BW25113 Δ*mraZ*)	[51]
	JW2705 (*E. coli* BW25113 Δ*ygbI*)	[51]
	JW3343 (*E. coli* BW25113 Δ*yhfW*)	[51]
	E. coli MG1655 Δ*btsT* Δ*yhjX* Δ*cstA* (3Δ)	This study
	E. coli MG1655 Δ*btsT* Δ*cstA*	This study
	E. coli MG1655 Δ*btsT* Δ*yhjX*	This study
	E. coli MG1655 Δ*cstA* Δ*yhjX*	This study
	E. coli MG1655 Δ*btsT*	[20]
	E. coli MG1655 Δ*cstA*	This study
	E. coli MG1655 Δ*yhjX*	[14]
Plasmids		
	pBAD24	[52]
	pBAD24-*cstA6His* (pBAD24-cstA6H)	This study
	pBBR1-*cstA*prom-lux	This study
	pBBR *yjiY-lux* (pBBR1-*btsT*prom-lux)	[13]

4.2. Growth Conditions

All strains were grown overnight in LB medium (10 g/L tryptone, 5 g/L yeast extract, 10 g/L NaCl) or M9 minimal medium [53] containing 40 mM of the indicated C-source. When required, media were supplemented with ampicillin (100 µg/mL) or gentamicin (20 µg/mL). Cells from the overnight culture were transferred to the corresponding fresh medium and grown under agitation (200 rpm) at 37 °C. Growth was monitored over time by measuring the optical density at 600 nm (OD_{600}).

4.3. Determination of the Extracellular Pyruvate Concentration

To determine the pyruvate concentration in the supernatant, *E. coli* cells (MG1655, MG1655 Δ*btsT* Δ*cstA* Δ*yhjX* pBAD24 or MG1655 Δ*btsT* Δ*cstA* Δ*yhjX* pBAD24-cstA) were grown in LB medium with constant agitation at 37 °C. Every 20 min samples were taken and the OD_{600} was determined. The pyruvate extraction procedure was adapted from O'Donell-Tormey et al. [54] with some modifications. Briefly, a 1 mL aliquot was withdrawn from the culture flask and centrifuged at 14,000× *g* for 5 min. Five hundred microliters of the supernatant were transferred to a 2 mL Eppendorf tube containing 125 µL of ice-cold 2 M $HClO_4$ and incubated for 5 min on ice. Afterwards, the acid was neutralized with 125 µL of 2.5 M $KHCO_3$, and then the precipitated $KClO_4$ and proteins were removed by centrifugation at 14,000× *g* for 10 min. For the assay, the supernatant was diluted 1:5 in 100 mM PIPES buffer pH 7.5. The assay was performed as follows: 200 µL of the diluted samples with 200 µM NADH+H^+ were added into 96-well plates and the absorbance (A1) was measured at 340 nm. Five microliters of 80 U/mL LDH (Roche) were added and then the sample was incubated at 37 °C in the dark for 30 min. The absorbance (A2) at 340 nm was read again. The change of absorbance at 340 nm (ΔA = A1 − A2) was used to calculate the pyruvate concentration. For the standard curve 0, 50, 100, 150, and 200 µM pyruvate in PIPES was used.

4.4. Chemotaxis Assay

For the plug-in-pond assay, the three *E. coli* strains (MG1655, MG1655 Δ*btsT* Δ*cstA* Δ*yhjX* pBAD24, or MG1655 Δ*btsT* Δ*cstA* Δ*yhjX* pBAD24-cstA) were grown in LB medium until OD_{600}: 0.6–0.8. The plug-in-pond assay was carried according to Reyes-Darias et al. [55] with some modifications. Briefly, bacteria were collected by low-speed centrifugation (800× *g*) and then washed twice with M9 medium (with no C-source) and resuspended at OD_{600}: 0.8. A 100 µL aliquot of melted agar (1.5%, *w*/*v* in M9 medium) containing the chemoattractant was placed in a petri dish. After the agar had solidified, 12 mL of bacterial suspension (OD_{600}: 0.4 in M9 medium with 0.25% *w*/*v* agar) was poured around the agar plug. Plates were incubated at 37 °C and monitored for up to 3 h.

4.5. Promoter Activity Assay

Promoter activity of *cstA* or *btsT* (as control) was explored in vivo with a luciferase-based reporter gene assay. For this purpose, different *E. coli* mutants were transformed with the plasmid pBBR1-*cstA*prom-lux or pBBR *btsT*prom-*lux* [13]. Cells from an overnight culture were inoculated at a starting OD_{600} of 0.05 into LB medium or M9 minimal medium supplemented with 40 mM of different C-sources in 96-well plates. Plates were then incubated under constant agitation at 37 °C. OD_{600} and luminescence were measured in intervals of 10 min for the total period of 18 h (Clariostar). The maximum luminescence levels (relative light units (RLU) expressed in counts per second per OD_{600}) were determined for each growth condition.

4.6. Transport Measurements with Intact Cells

E. coli strain MG1655 Δ*btsT* Δ*cstA* Δ*yhjX* was transformed with pBAD24 or pBAD24-cstA6H. Cells grown in LB medium in the absence of arabinose were harvested in mid-log phase. Cells were washed and resuspended in transport buffer (100 mM Tris/MES (morpholineethanesulfonic acid) pH 7.5, 5 mM $MgCl_2$) to an absorbance of 5 (420 nm) thereby adjusting the total protein concentration to 0.35 mg/mL. Uptake of [^{14}C]pyruvate (55 mCi/mmol, Biotrend) was measured at a total substrate concentration of 10 µM at 15 °C. At each time point, transport was terminated by the addition of stop buffer (100 mM potassium phosphate pH 6.0, 100 mM LiCl) followed by rapid filtration through membrane filters (MN gf-5 0.4 µm; Macherey-Nagel). Afterwards, the filters were dissolved in 5 mL of scintillation fluid (MP Biomedicals, Santa. Ana, CA, USA), and radioactivity was determined in a liquid scintillation analyzer (PerkinElmer, Downers Grove, IL, USA). To test substrate specificity, [^{14}C]pyruvate (10 µM) uptake was tested in the presence of an excess of the corresponding non-radioactive compounds (1 mM). The effects of protonophores and ionophores were tested after preincubation of cells in transport buffer supplemented with 2 mM DNP, 20 µM CCCP, 6 µM nigericin, 10 µM nonactin, or dimethyl sulfoxide (DMSO) (as a control) at 25 °C for 30 min. In the case of valinomycin, cells were preincubated in 100 mM potassium phosphate buffer, pH 7.5, at 25 °C for 30 min, as control [^{14}C]pyruvate uptake was measured in the same buffer without valinomycin.

4.7. DNA Affinity Capture Assay

To identify putative transcriptional regulators of *cstA*, we used a DNA capture assay [33,34]. A biotinylated P_{cstA} fragment was generated by PCR using primers labeled with biotin at the 5′ end. As a control, a biotinylated DNA fragment located within the *cstA* coding sequence was used; 600 pmol of the DNA fragments was immobilized with streptavidin-coated magnetic beads (NEB) according to the manufacturer's instructions. For the preparation of protein extract, *E. coli* MG1655 was cultivated in 800 mL of LB medium until the indicated growth phase. Cells were harvested at 4 °C, washed with cold protein binding buffer B (20 mM Tris pH 8.0, 1mM EDTA, 0.05% (*v*/*v*) TritonX100, 10% (*v*/*v*) glycerol, 1 mM DTT, 100 mM NaCl), resuspended in 8 mL of the same buffer, and disrupted with a French press. The supernatant was incubated with the previously coated magnetic beads at room temperature for 30 min. After extensive washing to remove unspecific bound proteins, the magnetic

beads were subjected to trypsin digestion using the iST 8x kit (PreOmics) following the protocol provided by the manufacturer.

4.8. Mass Spectrometry

For LC-MS purposes, desalted peptides were injected in an Ultimate 3000 RSLCnano system (Thermo Scientific, Waltham, MA, USA), separated in a 15-cm analytical column (75 µm ID with ReproSil-Pur C18-AQ 2.4 µm from Dr. Maisch) with a 50-min gradient from 5 to 60% acetonitrile in 0.1% formic acid. The effluent from the HPLC was directly electrosprayed into a Qexactive HF (Thermo) operated in data-dependent mode to automatically switch between full-scan MS and MS/MS acquisition. Survey full-scan MS spectra (from *m/z* 375–1600) were acquired with a resolution of R = 60,000 at *m/z* 400 (AGC target of 3×10^6). The 10 most intense peptide ions with charge states between 2 and 5 were sequentially isolated to a target value of 1×10^5 and fragmented at 27% normalized collision energy. Typical mass spectrometric conditions were spray voltage, 1.5 kV; no sheath and auxiliary gas flow; heated capillary temperature, 250 °C; ion selection threshold, 33,000 counts.

MaxQuant 1.6.10.43 was used to identify proteins and quantify them by iBAQ with the following parameters: Database, uniprot_AUP000000625_Ecoli_20200512; MS tol, 10 ppm; MS/MS tol, 20 ppm Da; Peptide FDR, 0.1; Protein FDR, 0.01 Min. peptide Length, 7; Variable modifications, Oxidation (M); Fixed modifications, Carbamidomethyl (C); Peptides for protein quantitation, razor and unique; Min. peptides, 1; Min. ratio count, 2. Identified proteins were considered as interaction partners of the promoter region of cstA if their MaxQuant iBAQ values displayed a log fold change of 2 or higher compared to the control. The mass spectrometry proteomics data have been deposited into the ProteomeXchange Consortium via the PRIDE [56] partner repository with the dataset identifier PXD021798.

Supplementary Materials: Supplementary materials can be found at http://www.mdpi.com/1422-0067/21/23/9068/s1.

Author Contributions: Conceptualization, A.G. and K.J.; data curation, A.G. and I.F.; formal analysis, A.G., S.G., E.F.-R. and I.F.; funding acquisition, K.J.; investigation, A.G., S.G. and E.F.R.; methodology, A.G., I.F. and K.J.; project administration, K.J.; supervision, A.G. and K.J.; writing—original draft, A.G. and K.J.; writing—review and editing, A.G., S.G., E.F.R., I.F. and K.J. All authors have read and agreed to the published version of the manuscript.

Funding: This research was funded by the Deutsche Forschungsgemeinschaft (JU270/19-1 to K.J. and Project number 395357507 - SFB1371 to K.J.)

Acknowledgments: We thank Ingrid Weitl for excellent technical assistance, Ivica Kristoficova for the construction of the plasmid pBAD24-cstA6H, and Luitpold Fried for the construction of the *E. coli* MG1655 Δ*btsT* Δ*cstA* and *E. coli* MG1655 Δ*cstA* strains.

Conflicts of Interest: The authors declare no conflict of interest.

References

1. Ahn, S.J.; Deep, K.; Turner, M.E.; Ishkov, I.; Waters, A.; Hagen, S.J.; Rice, K.C. Characterization of LrgAB as a stationary phase-specific pyruvate uptake system in *Streptococcus mutans*. *BMC Microbiol.* **2019**, *19*, 1–15. [CrossRef]
2. Steiner, B.D.; Eberly, A.R.; Hurst, M.N.; Zhang, E.W.; Green, H.D.; Behr, S.; Jung, K.; Hadjifrangiskou, M. Evidence of cross-regulation in two closely related pyruvate-sensing systems in uropathogenic *Escherichia coli*. *J. Membr. Biol.* **2018**, *251*, 65–74. [CrossRef] [PubMed]
3. Tuntufye, H.N.; Lebeer, S.; Gwakisa, P.S.; Goddeeris, B.M. Identification of avian pathogenic *Escherichia coli* genes that are induced in vivo during infection in chickens. *Appl. Environ. Microbiol.* **2012**, *78*, 3343–3351. [CrossRef] [PubMed]
4. Schär, J.; Stoll, R.; Schauer, K.; Loeffler, D.I.M.; Eylert, E.; Joseph, B.; Eisenreich, W.; Fuchs, T.M.; Goebel, W. Pyruvate carboxylase plays a crucial role in carbon metabolism of extra and intracellularly replicating *Listeria monocytogenes*. *J. Bacteriol.* **2010**, *192*, 1774–1784. [CrossRef] [PubMed]
5. Harper, L.; Balasubramanian, D.; Ohneck, E.A.; Sause, W.E.; Chapman, J.; Mejia-Sosa, B.; Lhakhang, T.; Heguy, A.; Tsirigos, A.; Ueberheide, B.; et al. *Staphylococcus aureus* responds to the central metabolite pyruvate to regulate virulence. *mBio* **2018**, *9*, 1–17. [CrossRef]

6. Bücker, R.; Heroven, A.K.; Becker, J.; Dersch, P.; Wittmann, C. The pyruvate-tricarboxylic acid cycle node: A focal point of virulence control in the enteric pathogen *Yersinia pseudotuberculosis*. *J. Biol. Chem.* **2014**, *289*, 30114–30132. [CrossRef]
7. Behr, S.; Brameyer, S.; Witting, M.; Schmitt-Kopplin, P.; Jung, K. Comparative analysis of LytS/LytTR-type histidine kinase/response regulator systems in gamma-proteobacteria. *PLoS ONE* **2017**, *12*, 1–14. [CrossRef]
8. Charbonnier, T.; Le Coq, D.; McGovern, S.; Calabre, M.; Delumeau, O.; Aymerich, S.; Jules, M. Molecular and physiological logics of the pyruvate-induced response of a novel transporter in *Bacillus subtilis*. *mBio* **2017**, *8*, 1–18. [CrossRef]
9. Vilhena, C.; Kaganovitch, E.; Grünberger, A.; Motz, M.; Forné, I.; Kohlheyer, D.; Jung, K. Importance of pyruvate sensing and transport for the resuscitation of viable but nonculturable *Escherichia coli* K-12. *J. Bacteriol.* **2018**, 201. [CrossRef]
10. Vemuri, G.N.; Altman, E.; Sangurdekar, D.P.; Khodursky, A.B.; Eiteman, M.A. Overflow metabolism in *Escherichia coli* during steady-state growth: Transcriptional regulation and effect of the redox ratio. *Appl. Environ. Microbiol.* **2006**, *72*, 3653–3661. [CrossRef]
11. Paczia, N.; Nilgen, A.; Lehmann, T.; Gätgens, J.; Wiechert, W.; Noack, S. Extensive exometabolome analysis reveals extended overflow metabolism in various microorganisms. *Microb. Cell Fact.* **2012**, *11*, 1–14. [CrossRef] [PubMed]
12. Behr, S.; Fried, L.; Jung, K. Identification of a novel nutrient-sensing histidine kinase/response regulator network in *Escherichia coli*. *J. Bacteriol.* **2014**, *196*, 2023–2029. [CrossRef] [PubMed]
13. Kraxenberger, T.; Fried, L.; Behr, S.; Jung, K. First insights into the unexplored two-component system YehU/YehT in *Escherichia coli*. *J. Bacteriol.* **2012**, *194*, 4272–4284. [CrossRef] [PubMed]
14. Fried, L.; Behr, S.; Jung, K. Identification of a target gene and activating stimulus for the YpdA/YpdB histidine kinase/response regulator system in *Escherichia coli*. *J. Bacteriol.* **2012**, *195*, 807–815. [CrossRef] [PubMed]
15. Ruby, E.G.; Nealson, K.H. Pyruvate production and excretion by the luminous marine bacteria. *Appl. Environ. Microbiol.* **1977**, *34*, 164–169. [CrossRef]
16. Chubukov, V.; Gerosa, L.; Kochanowski, K.; Sauer, U. Coordination of microbial metabolism. *Nat. Rev. Microbiol.* **2014**, *12*, 327–340. [CrossRef]
17. Kreth, J.; Lengeler, J.W.; Jahreis, K. Characterization of pyruvate uptake in *Escherichia coli* K-12. *PLoS ONE* **2013**, *8*, 6–12. [CrossRef]
18. Miyake, Y.; Inaba, T.; Watanabe, H.; Teramoto, J.; Yamamoto, K.; Ishihama, A. Regulatory roles of pyruvate-sensing two-component system PyrSR (YpdAB) in *Escherichia coli* K-12. *FEMS Microbiol. Lett.* **2019**, *366*, 1–9. [CrossRef]
19. Ogasawara, H.; Ishizuka, T.; Yamaji, K.; Kato, Y.; Shimada, T.; Ishihama, A. Regulatory role of pyruvate-sensing BtsSR in biofilm formation by *Escherichia coli* K-12. *FEMS Microbiol. Lett.* **2020**, *366*, 1–10. [CrossRef]
20. Kristoficova, I.; Vilhena, C.; Behr, S.; Jung, K. BtsT, a novel and specific Pyruvate/H+ symporter in *Escherichia coli*. *J. Bacteriol.* **2018**, *200*, 1–11. [CrossRef]
21. Hwang, S.; Choe, D.; Yoo, M.; Cho, S.; Kim, S.C.; Cho, S.; Cho, B.K. Peptide transporter CstA imports pyruvate in *Escherichia coli* K-12. *J. Bacteriol.* **2018**, *200*, 1–14. [CrossRef] [PubMed]
22. Saier, M.H.; Reddy, V.S.; Tamang, D.G.; Västermark, Å. The transporter classification database. *Nucleic Acids Res.* **2014**, *42*, 251–258. [CrossRef] [PubMed]
23. Schultz, J.E.; Matin, A. Molecular and functional characterization of a carbon starvation gene of *Escherichia coli*. *J. Mol. Biol.* **1991**, *218*, 129–140. [CrossRef]
24. Rasmussen, J.J.; Vegge, C.S.; Frøkiær, H.; Howlett, R.M.; Krogfelt, K.A.; Kelly, D.J.; Ingmer, H. *Campylobacter jejuni* carbon starvation protein A (CstA) is involved in peptide utilization, motility and agglutination, and has a role in stimulation of dendritic cells. *J. Med. Microbiol.* **2013**, *62*, 1135–1143. [CrossRef]
25. Garai, P.; Lahiri, A.; Ghosh, D.; Chatterjee, J.; Chakravortty, D. Peptide-utilizing carbon starvation gene *yjiY* is required for flagella-mediated infection caused by *Salmonella*. *Microbiology* **2016**, *162*, 100–116. [CrossRef]
26. Dubey, A.K.; Baker, C.S.; Suzuki, K.; Jones, A.D.; Pandit, P.; Romeo, T.; Babitzke, P. CsrA regulates translation of the *Escherichia coli* carbon starvation gene, *cstA*, by blocking ribosome access to the *cstA* transcript. *J. Bacteriol.* **2003**, *185*, 4450–4460. [CrossRef]
27. Gralla, J.D. Bacterial gene regulation from distant DNA sites. *Cell* **1989**, *57*, 193–195. [CrossRef]
28. Somavanshi, R.; Ghosh, B.; Sourjik, V. Sugar influx sensing by the phosphotransferase system of *Escherichia coli*. *PLoS Biol.* **2016**, *14*, 1–19. [CrossRef]

29. Schultz, J.E.; Latter, G.I.; Matin, A. Differential regulation by cyclic AMP of starvation protein synthesis in *Escherichia coli*. *J. Bacteriol.* **1988**, *170*, 3903–3909. [CrossRef]
30. Gödeke, J.; Heun, M.; Bubendorfer, S.; Paul, K.; Thormann, K.M. Roles of two *Shewanella oneidensis* MR-1 extracellular endonucleases. *Appl. Environ. Microbiol.* **2011**, *77*, 5342–5351. [CrossRef]
31. Koga, K.; Harada, T.; Shimizu, H.; Tanaka, K. Bacterial luciferase activity and the intracellular redox pool in *Escherichia coli*. *Mol. Genet. Genom.* **2005**, *274*, 180–188. [CrossRef] [PubMed]
32. Galluzzi, L.; Karp, M. Intracellular redox equilibrium and growth phase affect the performance of luciferase-based biosensors. *J. Biotechnol.* **2007**, *127*, 188–198. [CrossRef] [PubMed]
33. Park, S.S.; Ko, B.J.; Kim, B.G. Mass spectrometric screening of transcriptional regulators using DNA affinity capture assay. *Anal. Biochem.* **2005**, *344*, 152–154. [CrossRef] [PubMed]
34. Kalinowski, J. *Intracellular Signaling and Gene Target Analysis in Bacterial Signaling*; Kramer, R., Jung, K., Eds.; Wiley-VCH Verlag GmbH & Co. KgaA: Weinheim, Germany, 2010; pp. 463–472.
35. Shao, Y.; Feldman-Cohen, L.S.; Osuna, R. Functional characterization of the *Escherichia coli* Fis-DNA binding sequence. *J. Mol. Biol.* **2008**, *376*, 771–785. [CrossRef]
36. Bradley, M.D.; Beach, M.B.; de Koning, A.P.J.; Pratt, T.S.; Osuna, R. Effects of Fis on *Escherichia coli* gene expression during different growth stages. *Microbiology* **2007**, *153*, 2922–2940. [CrossRef]
37. Basan, M.; Hui, S.; Okano, H.; Zhang, Z.; Shen, Y.; Williamson, J.R.; Haw, T. Overflow metabolism in *Escherichia coli* results from efficient proteome allocation. *Nature* **2015**, *528*, 99–104. [CrossRef]
38. Anderson, J.; Marks, V. Pyruvate in diabetes mellitus, concentrations in urine and blood. *Lancet* **1962**, *1*, 1159–1161. [CrossRef]
39. Mathioudakis, D.; Engel, J.; Welters, I.D.; Dehne, M.G.; Matejec, R.; Harbach, H.; Henrich, M.; Schwandner, T.; Fuchs, M.; Weismüller, K.; et al. Pyruvate: Immunonutritional effects on neutrophil intracellular amino or alpha-keto acid profiles and reactive oxygen species production. *Amino Acids* **2011**, *40*, 1077–1090. [CrossRef]
40. Mühling, J.; Fuchs, M.; Campos, M.E.; Gonter, J.; Engel, J.M.; Sablotzki, A.; Menges, T.; Weiss, S.; Dehne, M.G.; Krüll, M.; et al. Quantitative determination of free intracellular α-keto acids in neutrophils. *J. Chromatogr. B Anal. Technol. Biomed. Life Sci.* **2003**, *789*, 383–392. [CrossRef]
41. Hawver, L.A.; Giulietti, J.M.; Baleja, J.D.; Ng, W.L. Quorum sensing coordinates cooperative expression of pyruvate metabolism genes to maintain a sustainable environment for population stability. *mBio* **2016**, *7*, 1–11. [CrossRef]
42. Jolkver, E.; Emer, D.; Ballan, S.; Krämer, R.; Eikmanns, B.J.; Marin, K. Identification and characterization of a bacterial transport system for the uptake of pyruvate, propionate, and acetate in *Corynebacterium glutamicum*. *J. Bacteriol.* **2009**, *191*, 940–948. [CrossRef] [PubMed]
43. Hosie, A.H.F.; Allaway, D.; Poole, P.S. A monocarboxylate permease of *Rhizobium leguminosarum* is the first member of a new subfamily of transporters. *J. Bacteriol.* **2002**, *184*, 5436–5448. [CrossRef] [PubMed]
44. Behr, S.; Kristoficova, I.; Witting, M.; Breland, E.J.; Eberly, A.R.; Sachs, C.; Schmitt-Kopplin, P.; Hadjifrangiskou, M.; Jung, K. Identification of a high-affinity Pyruvate receptor in *Escherichia coli*. *Sci. Rep.* **2017**, *7*, 1–10. [CrossRef] [PubMed]
45. Azam, T.A.; Iwata, A.; Nishimura, A.; Ueda, S.; Ishihama, A. Growth phase-dependent variation in protein composition of the *Escherichia coli* nucleoid. *J. Bacteriol.* **1999**, *181*, 6361–6370. [CrossRef] [PubMed]
46. Ball, C.A.; Osuna, R.; Ferguson, K.C.; Johnson, R.C. Dramatic changes in Fis levels upon nutrient upshift in *Escherichia coli*. *J. Bacteriol.* **1992**, *174*, 8043–8056. [CrossRef]
47. Serra, D.O.; Klauck, G.; Hengge, R. Vertical stratification of matrix production is essential for physical integrity and architecture of macrocolony biofilms of *Escherichia coli*. *Environ. Microbiol.* **2015**, *17*, 5073–5088. [CrossRef]
48. Ferenci, T. Regulation by nutrient limitation. *Curr. Opin. Microbiol.* **1999**, *2*, 208–213. [CrossRef]
49. Ferenci, T. Hungry bacteria—Definition and properties of a nutritional state. *Environ. Microbiol.* **2001**, *3*, 605–611. [CrossRef]
50. Blattner, F.R.; Plunkett, G.; Bloch, C.A.; Perna, N.T.; Burland, V.; Riley, M.; Collado-Vides, J.; Glasner, J.D.; Rode, C.K.; Mayhew, G.F.; et al. The complete genome sequence of *Escherichia coli* K-12. *Science* **1997**, *277*, 1453–1462. [CrossRef]
51. Baba, T.; Ara, T.; Hasegawa, M.; Takai, Y.; Okumura, Y.; Baba, M.; Datsenko, K.A.; Tomita, M.; Wanner, B.L.; Mori, H. Construction of *Escherichia coli* K-12 in-frame, single-gene knockout mutants: The Keio collection. *Mol. Syst. Biol.* **2006**, *2*, 2006.0008. [CrossRef]

52. Guzman, L.M.; Belin, D.; Carson, M.J.; Beckwith, J. Tight regulation, modulation, and high-level expression by vectors containing the arabinose $P_{(BAD)}$ promoter. *J. Bacteriol.* **1995**, *177*, 4121–4130. [CrossRef] [PubMed]
53. Harwood, C.R.; Cutting, S.M. (Eds.) Chemically defined growth media and suplements. In *Molecular Biological Methods for Bacillus*; Wiley: London, UK, 1990; p. 548.
54. O'donnell-Tormey, J.; Nathan, C.F.; Lanks, K.; Deboer, C.J.; De La Harpe, J. Secretion of pyruvate: An antioxidant defense of mammalian cells. *J. Exp. Med.* **1987**, *165*, 500–514. [CrossRef]
55. Reyes-Darías, J.A.; Garcia-Fontana, C.; Corral-Lugo, A.; Rico-Jiménez, M.; Krell, T. Qualitative and quantitative assays for flagellum-mediated chemotaxis. *Methods Mol. Biol.* **2014**, *1149*, 87–97.
56. Perez-Riverol, Y.; Csordas, A.; Bai, J.; Bernal-Llinares, M.; Hewapathirana, S.; Kundu, D.J.; Inuganti, A.; Griss, J.; Mayer, G.; Eisenacher, M.; et al. The PRIDE database and related tools and resources in 2019: Improving support for quantification data. *Nucleic Acids Res.* **2019**, *47*, D442–D450. [CrossRef] [PubMed]

3 Insights into a pyruvate sensing and uptake system in *Vibrio campbellii* and its importance for virulence

Göing S, Gasperotti AF, Yang Q, Defoirdt T, Jung K. 2021. J Bacteriol 203:e00296-21. https://doi.org/10.1128/jb.00296-21

AMERICAN SOCIETY FOR MICROBIOLOGY | Journal of Bacteriology®

RESEARCH ARTICLE

Insights into a Pyruvate Sensing and Uptake System in *Vibrio campbellii* and Its Importance for Virulence

Stephanie Göing,[a] Ana Florencia Gasperotti,[a] Qian Yang,[b] Tom Defoirdt,[b] Kirsten Jung[a]

[a]Department of Microbiology, Ludwig-Maximilians-Universität München, Munich, Germany
[b]Center for Microbial Ecology and Technology, Ghent University, Ghent, Belgium

ABSTRACT Pyruvate is a key metabolite in living cells and has been shown to play a crucial role in the virulence of several bacterial pathogens. The bioluminescent *Vibrio campbellii*, a severe infectious burden for marine aquaculture, excretes extraordinarily large amounts of pyruvate during growth and rapidly retrieves it by an as-yet-unknown mechanism. We have now identified the responsible pyruvate transporter, here named BtsU, and our results show that it is the only pyruvate transporter in *V. campbellii*. Expression of *btsU* is tightly regulated by the membrane-integrated LytS-type histidine kinase BtsS, a sensor for extracellular pyruvate, and the LytTR-type response regulator BtsR. Cells lacking either the pyruvate transporter or sensing system show no chemotactic response toward pyruvate, indicating that intracellular pyruvate is required to activate the chemotaxis system. Moreover, pyruvate sensing and uptake were found to be important for the resuscitation of *V. campbellii* from the viable but nonculturable state and the bacterium's virulence against brine shrimp larvae.

IMPORTANCE Bacterial infections are a serious threat to marine aquaculture, one of the fastest growing food sectors on earth. Therefore, it is extremely important to learn more about the pathogens responsible, one of which is *Vibrio campbellii*. This study sheds light on the importance of pyruvate sensing and uptake for *V. campbellii*, and reveals that the bacterium possesses only one pyruvate transporter, which is activated by a pyruvate-responsive histidine kinase/response regulator system. Without the ability to sense or take up pyruvate, the virulence of *V. campbellii* toward gnotobiotic brine shrimp larvae is strongly reduced.

KEYWORDS LytTR, pyruvate transport, chemotaxis, histidine kinase, overflow metabolism, viable but nonculturable cells

Pyruvate is one of the most important molecules in both pro- and eukaryotic cells. Being the end product of glycolysis and—converted to acetyl coenzyme A—the starting compound of the citric acid cycle and fatty acid synthesis, as well as a substrate for fermentation in the case of oxygen limitation, pyruvate acts as the hub between aerobic and anaerobic metabolism (1). It can also be converted into carbohydrates via gluconeogenesis and be used to produce amino acids like alanine. Moreover, pyruvate serves as a scavenger for reactive oxygen species (ROS) such as H_2O_2, since it inactivates them by a nonenzymatic oxidative decarboxylation reaction (2–6).

For a wide variety of microbial pathogens, it has been demonstrated that pyruvate and its metabolism are crucial for fitness and virulence, including *Borrelia burgdorferi*, *Leptospira interrogans*, *Listeria monocytogenes*, *Vibrio parahaemolyticus*, *Yersinia pseudotuberculosis*, *Staphylococcus aureus*, and uropathogenic *Escherichia coli* (7–12). Furthermore, pyruvate has been shown to play a role in the resuscitation of viable but nonculturable (VBNC) bacteria (13–15). Many different species can enter this dormant state of low metabolic activity, which enables them to withstand stressful environmental conditions. By this means, they can for instance survive antibiotic treatments without being detected by

Citation Göing S, Gasperotti AF, Yang Q, Defoirdt T, Jung K. 2021. Insights into a pyruvate sensing and uptake system in *Vibrio campbellii* and its importance for virulence. J Bacteriol 203:e00296-21. https://doi.org/10.1128/JB.00296-21.

Editor Ann M. Stock, Rutgers University-Robert Wood Johnson Medical School

Address correspondence to Kirsten Jung, jung@lmu.de.

Received 1 June 2021
Accepted 25 July 2021
Accepted manuscript posted online 2 August 2021
Published 23 September 2021

standard cultivation methods (16, 17). In *E. coli*, pyruvate was also found to be important for the formation of persister cells, as well as for protein overproduction (18). Beyond that, pyruvate has become a focus of attention in the context of metabolic engineering for industrial applications (19, 20). In eukaryotes, two mitochondrial pyruvate carriers, MCP1 and MCP2, were identified which transport pyruvate across the mitochondrial membrane (21). Moreover, pyruvate was found to be important for cancer cells to cope with hypoxia (22) and for activation of human intestinal immune cells (23).

Vibrio harveyi ATCC BAA-116, a model organism for quorum sensing that was reclassified as *V. campbellii* in 2010 (24), is a marine, motile, luminous gammaproteobacterium and an opportunistic pathogen for fish, shrimps, squids, and other marine invertebrates (25–27). Aquaculture is one of the fastest growing food-producing sectors on earth and now accounts for 50% of the world's fish consumed (28). To prevent the loss of entire aquaculture populations owing to infections, antimicrobial treatments are often unavoidable, although these measures can lead to severe problems such as antimicrobial resistances (29). This underlines the need to investigate pathogens such as *V. campbellii*, including their virulence and metabolism, in more detail. It has been known since the 1970s that bacteria of the genus *Vibrio* excrete large amounts (up to 3 mM) of pyruvate during exponential growth and rapidly take it up again, whereas other genera excrete much smaller amounts, usually in the micromolar range (30, 31). The physiological function of this excretion and reuptake of pyruvate is not fully understood, but it presumably represents a form of overflow metabolism to avoid excessive accumulation of pyruvate in the cells and rebalance intracellular pyruvate levels—a typical adaptation phenomenon during shifts from aerobic to anaerobic growth (32–34). However, why *Vibrio*, in contrast to other genera, should excrete such extraordinary amounts of pyruvate remains unclear.

In the model organism *E. coli*, two different histidine kinase/response regulator systems are known to be responsible for pyruvate sensing. One consists of the histidine kinase BtsS (formerly known as YehU) and the response regulator BtsR (formerly known as YehT) (31, 35), the other comprises the histidine kinase YpdA and the response regulator YpdB. These LytS/LytTR systems are found in many bacterial phyla, especially in plant and human pathogens, but most species harbor only one of the two systems (31). In *E. coli*, BtsS has been shown to sense pyruvate at very low concentrations, and BtsR then activates transcription of *btsT* (formerly known as *yjiY*), which codes for the high-affinity pyruvate/H^+ symporter BtsT, a member of the CstA transporter family with 18 predicted transmembrane domains (36, 37). In addition to BtsT, *E. coli* possesses at least one other pyruvate transporter (38–40).

V. campbellii can grow on pyruvate as a sole carbon source, which indicates that it must be able to take up the compound by a hitherto-unknown means. Work by Behr et al. (31) has shown that the species possesses homologs of the *btsS*/*btsR* system of *E. coli* (VIBHAR_RS04665 and VIBHAR_RS04660) and of the pyruvate transporter gene *btsT* (VIBHAR_RS04670), but to date nothing is known about this gene cluster nor about pyruvate sensing or transport in *V. campbellii*. Since bacteria of the genus *Vibrio* excrete and take up large amounts of pyruvate (30, 31), we hypothesized that the system must play an important role for the cells. This study reports first insights into pyruvate sensing and uptake in *V. campbellii* and its relevance for this pathogen. Deletion mutants of the respective homologous genes were generated and investigated in terms of several phenotypes to reveal gene functions and relevance.

Our results show that BtsU, the transporter protein encoded by the ortholog of the *E. coli btsT* gene, is the only pyruvate transporter in *V. campbellii*. In the presence of pyruvate, its expression is activated by the sensor kinase BtsS via the response regulator BtsR. Further characterization of the deletion mutants demonstrates the importance of the system for chemotaxis, resuscitation from the viable but nonculturable (VBNC) state, and virulence.

RESULTS AND DISCUSSION

Characterization of the homologs of the *E. coli* genes *btsS*, *btsR*, and *btsT* in *V. campbellii*. Pyruvate sensing by the two-component system BtsS/BtsR and uptake by the transporter BtsT in *E. coli* has been described in detail in recent years (15, 18, 31, 35–37, 41).

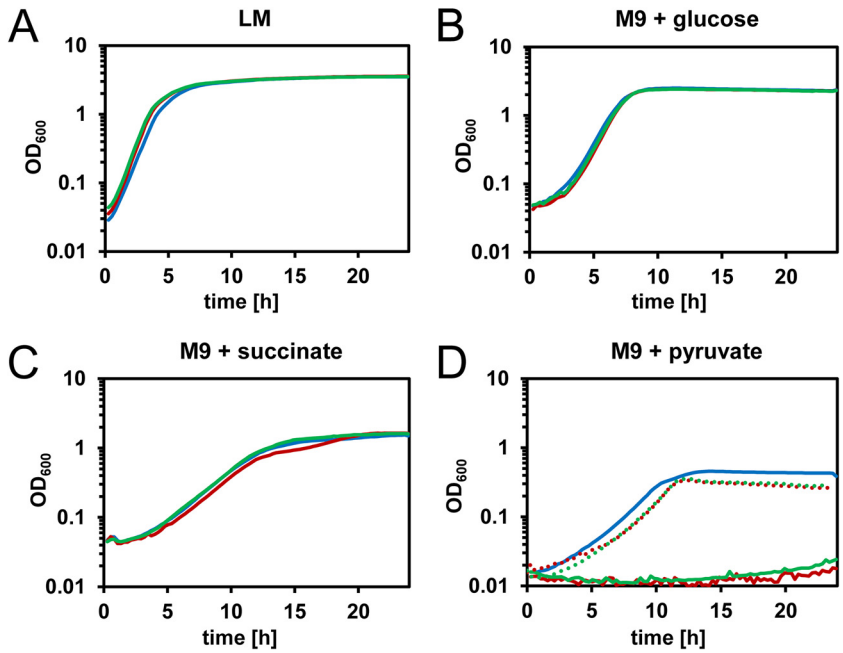

FIG 1 *V. campbellii* Δ*btsU* and Δ*btsSR* cells are unable to grow on pyruvate. *V. campbellii* wild-type (blue line), Δ*btsU* (red line) and Δ*btsSR* (green line) cells were grown in a plate reader (Tecan) at 30°C in LM medium (A) or in M9 minimal medium (2% [wt/vol] NaCl) with 20 mM glucose (B), 20 mM sodium succinate (C), or 20 mM sodium pyruvate (D). The *V. campbellii* Δ*btsU* and Δ*btsSR* strains were complemented with full-length *btsU* and *btsSR*, respectively, at the native loci via double homologous recombination. Complemented Δ*btsU* (red dotted line) and Δ*btsSR* (green dotted line) cells were grown in M9 minimal medium (2% [wt/vol] NaCl) with 20 mM sodium pyruvate.

The full-length amino acid sequences of these proteins were used to identify homologs of the *E. coli* genes *btsT*, *btsS*, and *btsR* in *V. campbellii* by a local alignment search against the *V. campbellii* ATCC BAA-1116 genome, using Protein BLAST (42). In contrast to their counterparts in *E. coli*, all three genes are located adjacent to each other in the *V. campbellii* genome: VIBHAR_RS04670 (the homolog of *E. coli*'s *btsT*, old locus tag VIBHAR_00986), VIBHAR_RS04665 (the homolog of *E. coli*'s *btsS*, old locus tag VIBHAR_00985), and VIBHAR_RS04660 (the homolog of *E. coli*'s *btsR*, old locus tag VIBHAR_00984). Using the online tool Clustal Omega (43), we compared the corresponding amino acid sequences with the sequences of the *E. coli* proteins and found the following identity values: 19% for BtsT (coverage 66.2%), 57% for BtsS (coverage 98.9%), and 50% for BtsR (coverage 99.6%).

VIBHAR_RS04670 codes for an uncharacterized transporter protein, parts of which are assigned by Pfam analysis to CstA, a member of the carbon starvation family (44). A topology prediction for the 53-kDa protein (449 amino acids) with the online tool TMPred predicted 12 transmembrane domains (45), whereas the *E. coli* BtsT, also a member of the CstA family, has 18 predicted transmembrane domains (37). Therefore, we propose to rename VIBHAR_RS04670 as *btsU* (transporter BtsU) to reflect the low similarity of its predicted product to BtsT. VIBHAR_RS04665 codes for a LytS-type sensor histidine kinase of 556 amino acids (61 kDa), and VIBHAR_RS04660 encodes a LytTR-type response regulator of 242 amino acids (27 kDa). These two genes are named *btsS* and *btsR* here, in accordance with their respective homologs in *E. coli*, coding for the proteins BtsS and BtsR, respectively.

***V. campbellii* cells lacking *btsU* or *btsSR* are unable to grow on pyruvate.** We constructed in-frame deletion mutants for the transporter gene (Δ*btsU*), as well as for the genes of the two-component system (Δ*btsS* and Δ*btsR* as single gene deletions and Δ*btsSR* as a double deletion of both genes) to learn more about their functions in *V. campbellii*. The deletion mutants were tested for several phenotypes.

All strains grew equally well in LM medium, and in minimal medium supplemented with glucose or succinate (Fig. 1A to C). However, in minimal medium with pyruvate as

sole carbon source, only the wild type was able to grow (Fig. 1D). Mutants lacking either the transporter (Δ*btsU*) or the two-component system (Δ*btsSR*) did not grow on pyruvate at all. In complemented *V. campbellii* deletion mutants, growth on pyruvate was restored to the wild-type level (Fig. 1D). Thus, we conclude that BtsU is the only pyruvate transporter in *V. campbellii*, and we suggest that its transcription might be activated (as in *E. coli*) by the two-component system BtsSR upon detection of external pyruvate. These results stand in clear contrast to phenotypes of the *E. coli* Δ*btsT* and Δ*btsSR* strains, which are able to grow on pyruvate, as expected in light of the presence of alternative pyruvate transporters (35, 37). This also highlights the much greater importance of this pyruvate sensing and uptake system for *V. campbellii*, since there are no substitutes.

We also assessed swimming motility, cell aggregation, pH changes during growth in Luria marine (LM) medium, and the amount of excreted indole, and found no significant differences between the deletion mutants of *V. campbellii* and the wild type (see Fig. S1 in the supplemental material). The same was true for bioluminescence and macrocolony formation, indicating that the system does not play any role in processes that are regulated by quorum sensing (see Fig. S1).

***V. campbellii btsU* expression is activated by the two-component system BtsSR in the presence of pyruvate.** Growth defects of both mutant strains on pyruvate as sole carbon source implied that not only the transporter BtsU but also the two-component system BtsSR is crucial for pyruvate uptake and is thus presumably necessary for the expression of *btsU*. To determine whether the two-component system fulfills the same function in *V. campbellii* as in *E. coli*, namely, activation of the transporter gene *btsU* when pyruvate is present to be taken up (36), we monitored *btsU* expression in LM medium in mutants lacking either one or both of the genes *btsS* and *btsR*. Using a reporter construct of the *btsU* promoter fused to the *mcherry* gene, chromosomally integrated upstream of the native locus, *btsU* expression could be monitored over time at the transcriptional level in both wild-type and mutant cells.

The results showed that the *btsU* promoter was activated only in the presence of BtsSR (Fig. 2A), demonstrating that this two-component system is crucial for expression of *btsU* in *V. campbellii*. Sensing of pyruvate thus serves as a precondition for pyruvate uptake. In the Δ*btsU* deletion mutant, the reporter gene fused to the *btsU* promoter was upregulated 10-fold relative to its expression in the wild type (Fig. 2A). *V. campbellii* seems to register the absence of its sole pyruvate transporter, which leads to an even stronger attempt to produce it to take up the metabolite. It is also reasonable that in wild-type cells the presence of the transporter BtsU causes negative feedback of its expression. The exact mechanism of this feedback regulation requires further analysis, and transcriptional or posttranscriptional regulatory mechanisms are conceivable.

When wild-type cells harboring the reporter construct for the *btsU* promoter were grown in M9 minimal medium supplemented with different carbon sources, the strongest transcriptional induction of *btsU* was observed in the presence of pyruvate (Fig. 2B). This result supports the assumption that expression of *btsU* is activated specifically by pyruvate via BtsSR in order to enable the sensed metabolite to be transported into the cells. To further determine this dependence of *btsU* expression on pyruvate, wild-type cells were grown in M9 minimal medium with different pyruvate concentrations and a constant basic level of succinate (20 mM) as the carbon source. Expression levels attributable to the presence of succinate, as well as the autofluorescence of the cells, were subtracted. Transcriptional activation of *btsU* increased in accordance with the concentration of pyruvate, with a threshold concentration of 500 μM being required for induction (Fig. 2C). The pyruvate concentration resulting in half-maximal *btsU* expression was estimated to be 3 ± 0.5 mM. Based on these data, we conclude that transcription of the pyruvate transporter gene *btsU* is activated by the two-component system BtsSR in a pyruvate-concentration dependent manner.

***V. campbellii* excretes large amounts of pyruvate during growth, and BtsU is required for reuptake of the compound from the medium.** To further characterize the relevance of pyruvate sensing and uptake in *V. campbellii*, different phenotypes of

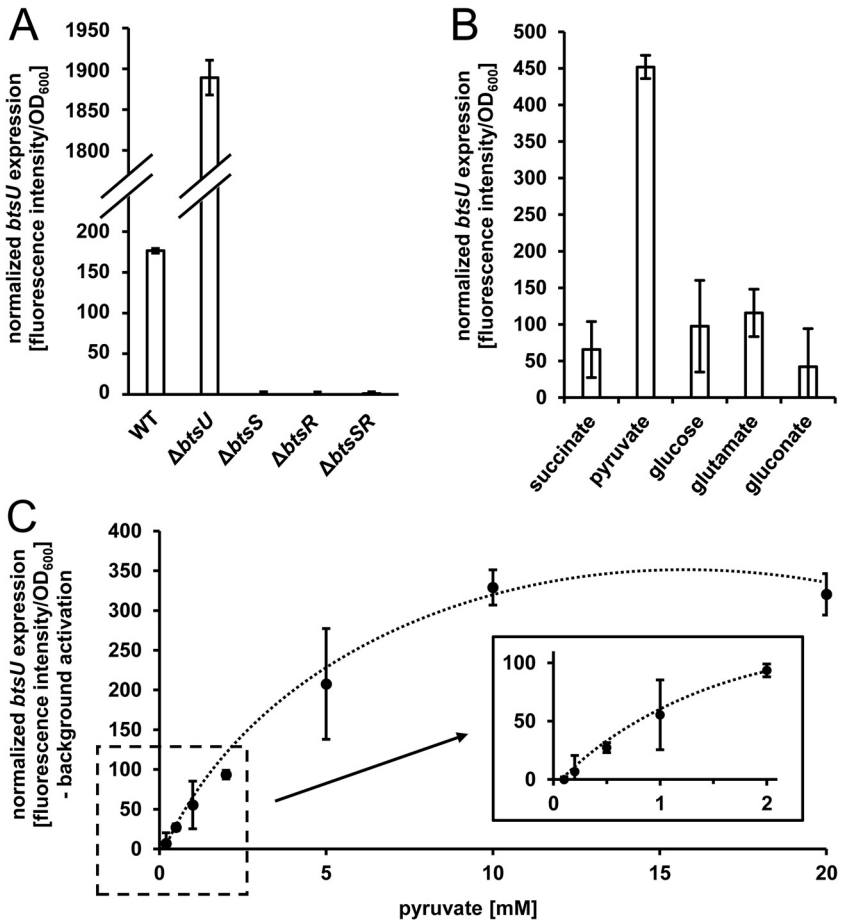

FIG 2 *V. campbellii btsU* expression is activated by the two-component system BtsSR in the presence of pyruvate. *V. campbellii* wild-type, Δ*btsU*, Δ*btsS*, Δ*btsR*, and Δ*btsSR* cells carrying a chromosomally integrated reporter comprising the promoter of *btsU* fused to *mcherry* (P_{btsU}-*mcherry*) were grown in a plate reader (Tecan) at 30°C in different media. Activation of the *btsU* promoter was monitored by measuring the intensity of mCherry fluorescence, normalized to an OD_{600} of 1. (A) Promoter activation of *btsU* in *V. campbellii* wild type and the indicated deletion mutants in LM medium. (B) Promoter activation of *btsU* in *V. campbellii* wild type by different carbon sources. Cells were grown in M9 minimal medium (2% [wt/vol] NaCl) supplemented with 20 mM sodium succinate, sodium pyruvate, glucose, sodium glutamate or sodium gluconate. (C) Promoter activation of *btsU* in *V. campbellii* wild type as a function of pyruvate concentration. Cells were grown in M9 minimal medium (2% [wt/vol] NaCl) with 20 mM sodium succinate as carbon source and different concentrations of sodium pyruvate. Baseline promoter activation by sodium succinate was subtracted (see panel B). All experiments were performed in triplicate, and error bars represent the standard deviations of the mean.

the deletion mutants were analyzed. It was shown previously that bacteria of the genus *Vibrio* excrete high levels of pyruvate during growth and then take it up again (30, 31). Measurements of external pyruvate concentrations in LM medium confirmed that *V. campbellii* excretes large amounts of pyruvate during exponential growth (Fig. 3). When the cell density had reached an optical density at 600 nm (OD_{600}) of ~2, the external pyruvate concentration was determined to be higher than 3 mM. In wild-type cultures, this peak was followed by a rapid decrease which reduced the concentration of the compound to the initial value. This finding shows that wild-type cells could rapidly and completely "reclaim" the pyruvate from the medium. Cells lacking the transporter protein BtsU or the sensing system BtsSR were unable to do so, and the external pyruvate concentration remained essentially unchanged after reaching its peak.

Thus, pyruvate reuptake from the medium after its excessive excretion depends entirely on the pyruvate transporter BtsU, transcription of which is activated after sensing of the excreted pyruvate by BtsSR. Other bacterial species do not excrete pyruvate

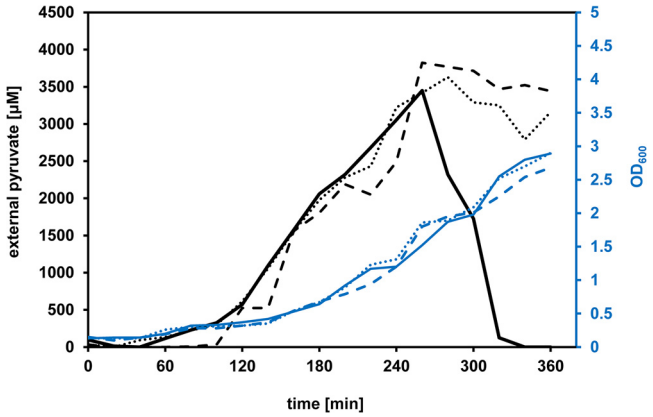

FIG 3 *V. campbellii* excretes large amounts of pyruvate and requires BtsU for its reuptake. *V. campbellii* wild-type (solid lines), Δ*btsU* (dotted lines), and Δ*btsSR* (dashed lines) cells were grown in LM medium at 30°C. Growth was monitored, and supernatant samples were collected to determine external pyruvate concentrations.

to such an extent (31). Therefore, pyruvate sensing and uptake presumably play an especially important role for *V. campbellii* in comparison to other microbes.

BtsU actively transports radiolabeled pyruvate, driven by the proton motive force. To ensure that the phenotypes of the deletion strains were indeed due to a defect in pyruvate uptake and to further characterize BtsU function, we directly monitored the transport of radiolabeled pyruvate by wild-type *V. campbellii* cells in comparison to Δ*btsU* and Δ*btsSR* cells. Experiments were done at 18°C to slow down the metabolization of pyruvate in the cells. The results clearly show that wild-type cells transported pyruvate with an uptake rate of 8 nmol of pyruvate per mg of total protein per min, whereas for Δ*btsU* and Δ*btsSR* cells no transport of pyruvate could be detected (Fig. 4A). These data support the conclusions drawn from the mutant phenotypes related to growth and the uptake of external pyruvate, i.e., that BtsU is the sole pyruvate transporter in *V. campbellii*, and that BtsSR serves as a pyruvate sensing system crucial for *btsU* expression.

To identify the driving force for pyruvate transport by BtsU in *V. campbellii*, various protonophores and ionophores were tested for their effect. Uptake of radiolabeled pyruvate was abolished by the addition of the hydrophobic protonophores carbonyl cyanide *m*-chlorophenyl hydrazone (CCCP) and 2,4-dinitrophenol (DNP), whereas the ionophores valinomycin (selective for K^+), nigericin (selective for K^+/H^+), and nonactin, which forms complexes with K^+, Na^+, NH_4^+, and other cations, had no obvious or specific effect on pyruvate transport (Fig. 4B). This indicates that pyruvate uptake by BtsU in *V. campbellii* is driven by the proton motive force.

Pyruvate sensing and uptake are required for chemotaxis toward pyruvate. As stated above, swimming motility of *V. campbellii* was not affected by the deletion of *btsU* or *btsSR* (see Fig. S1 in the supplemental material). Motile bacteria make use of a chemotaxis network system to perform directed movement along a chemical gradient, for instance toward nutrients and favorable environments, by changing the direction of rotation of their flagellum (46, 47). Chemotaxis has not yet been investigated in *V. campbellii*, unlike in its relatives *V. harveyi* and *V. cholerae* (47, 48). The *V. campbellii* deletion strains were tested for chemotaxis toward several compounds by using a plug-in-pond assay, in which cells are mixed with warm soft agar (0.3% [wt/vol] agar) and poured over hard agar plugs (1.5% [wt/vol] agar) containing the test compounds (Fig. 5). After incubation, movement of cells toward the test compounds is observed, and this serves as an indicator for chemotaxis.

We found that wild-type cells could swim along the gradient of pyruvate created by diffusion from the hard agar plugs and form circles of cell density around them, with the circle size increasing with the pyruvate concentration in the plug. Both Δ*btsU* and Δ*btsSR* strains were unable to migrate toward pyruvate (Fig. 5). In contrast, all strains

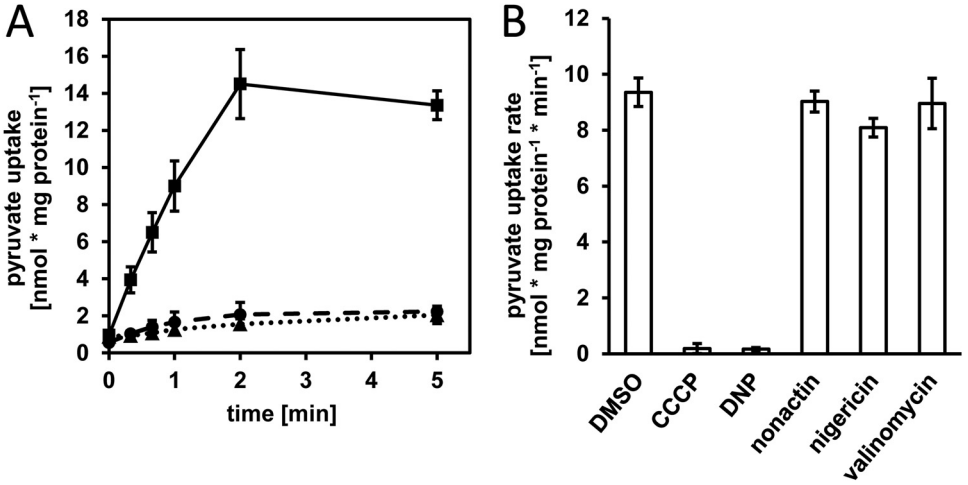

FIG 4 Pyruvate transport by BtsU in *V. campbellii*. (A) Uptake of [^{14}C]pyruvate by *V. campbellii* wild-type (solid line), Δ*btsU* (dotted line), and Δ*btsSR* (dashed) cells monitored over time at a final pyruvate concentration of 10 μM at 18°C. (B) The impact of different protonophores and ionophores on pyruvate transport was determined after preincubation of the cells with the indicated compounds at 25°C for 30 min. DMSO was used as a control. All experiments were performed in triplicate, and error bars represent standard deviations of the mean.

showed chemotaxis toward succinate (Fig. 5) and other compounds tested (see Fig. S3). Hence, the defect is specific for pyruvate. Being unable to detect and follow a gradient of pyruvate can be a severe disadvantage when the bacterium needs this important molecule, either as energy source or as a scavenger of ROS.

Since both cells lacking the transporter and cells lacking the two-component system were unable to perform chemotaxis toward pyruvate, transport of the compound into the cells must itself be crucial for functional chemotaxis toward pyruvate. We therefore suggest that pyruvate is in some way sensed intracellularly as an attractant by the chemotaxis system. It has been shown in *E. coli* that cytoplasmic pyruvate is sensed by the phosphotransferase (PTS) system—presumably based on the ratio of pyruvate to phosphoenolpyruvate—and that this signal is transmitted linearly to the chemotaxis pathway (49, 50). The exact mechanism of this signaling network still needs to be investigated, but an increase in intracellular pyruvate levels detected via the PTS system could also activate chemotaxis of *V. campbellii*.

Resuscitation of VBNC *V. campbellii* cells by pyruvate is impaired in mutants lacking BtsU or BtsSR. Earlier studies have demonstrated that pyruvate is an important factor for the resuscitation of VBNC bacteria owing to its function as a scavenger of ROS and the fact that it is a C-source that can easily be metabolized without prior phosphorylation (13–15). To test whether this also applies to *V. campbellii*, the VBNC state was induced in wild-type, Δ*btsU*, and Δ*btsSR* cells by long-term storage in the cold under nutrient limitation. Actively growing cells were adjusted to the same optical density in M9 minimal medium, with a higher salt concentration (2% [wt/vol] NaCl), but without any carbon source, and stored at 4°C. Periodic plating on LM agar plates showed a steady decrease in culturable cells over time (Fig. 6A). After 163 days, no colonies could be detected on the plates, indicating that the remaining living cells had entered the VBNC state. A characteristic change in cell morphology to a very small and rounded shape was observed for both wild-type and mutant cells (Fig. 6C), similar to that previously reported for VBNC bacteria, including members of the genus *Vibrio* (51–53).

Resuscitation experiments were performed by temperature upshift and addition of different nutrients. To exclude regrowth of any putatively remaining culturable cell, experiments were first done after 1 week of daily plating during which no colonies were detectable on the plates, and dilutions of the VNBC cell suspensions were used as suggested before (54, 55). Moreover, ampicillin was added to prevent growth of any

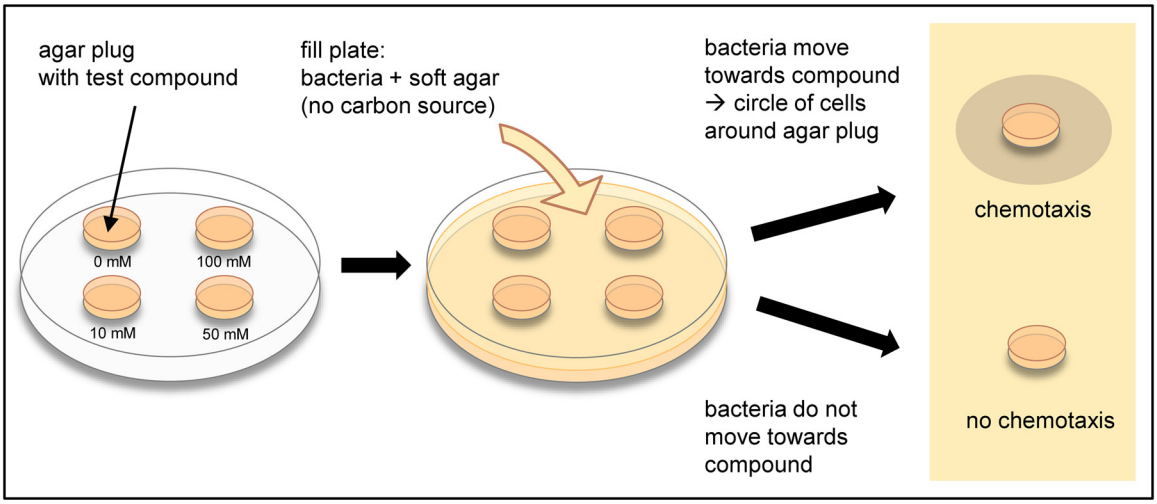

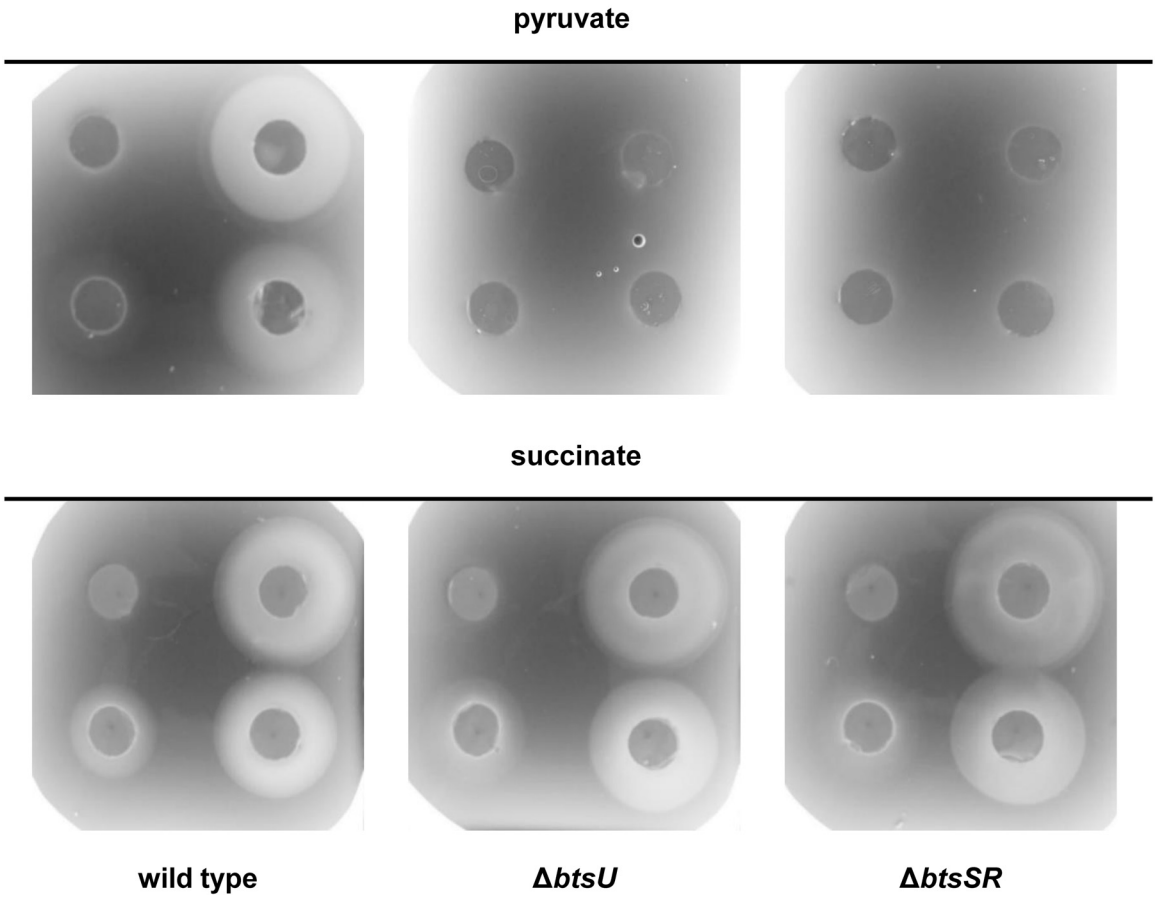

FIG 5 *V. campbellii* Δ*btsU* and Δ*btsSR* cells lost chemotactic response toward pyruvate. *V. campbellii* wild-type, Δ*btsU*, and Δ*btsSR* cells were tested for chemotaxis toward sodium pyruvate and sodium succinate in a plug-in-pond assay, which is schematically illustrated. Cells were mixed with soft agar (0.3% [wt/vol] agar) and poured over agar plugs (1.5% [wt/vol] agar) containing either sodium pyruvate or sodium succinate at concentrations of 0, 10, 50, and 100 mM (counterclockwise). Plates were incubated for 3 h at 30°C, and the images of cell accumulations are representative of three independent experiments.

contaminating bacteria, as *V. campbellii* is resistant to this antibiotic. VBNC *V. campbellii* cells were barely resuscitated by temperature upshift alone, but they did respond to the addition of nutrients (Fig. 6B). After 12 h of incubation, first colonies could be detected on plates, indicating the return of the cells to the culturable state. This could

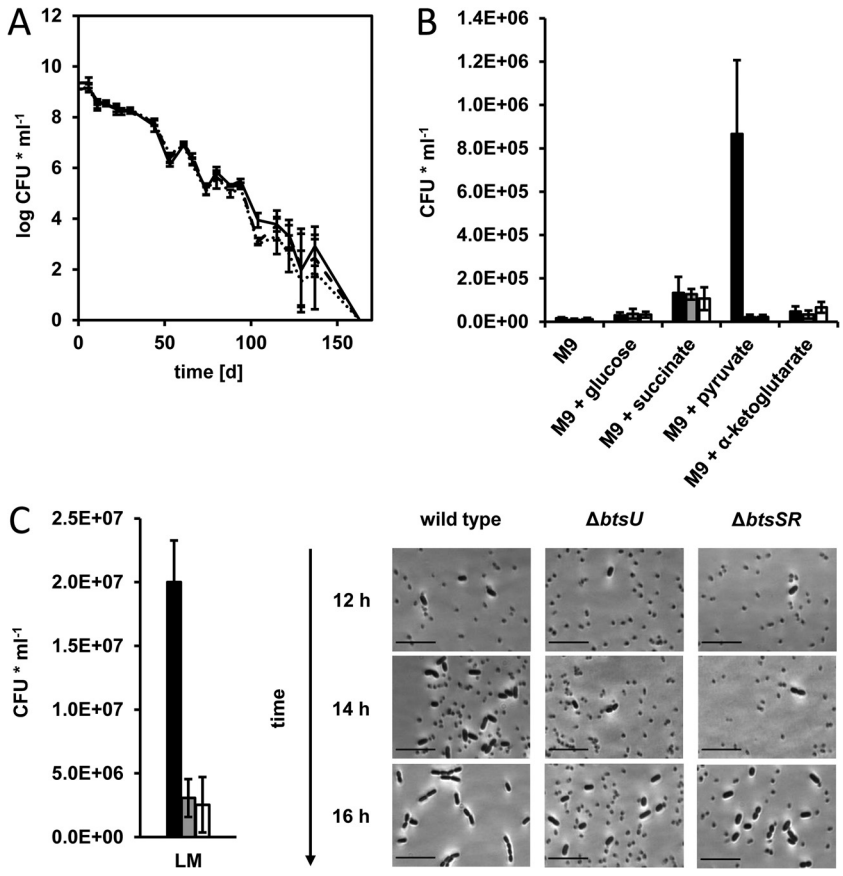

FIG 6 Induction of the VBNC state in *V. campbellii* and resuscitation by different nutrients. (A) The VBNC state was induced in *V. campbellii* wild-type (solid line), Δ*btsU* (dotted line), and Δ*btsSR* (dashed line) cells by long-term storage at 4°C under nutrient starvation in M9 minimal medium (2% [wt/vol] NaCl) without a carbon source. CFU on LM agar plates were determined periodically. (B) Resuscitation of wild-type (black), Δ*btsU* (gray), and Δ*btsSR* (white) VBNC cells upon temperature upshift to 30°C and addition of the indicated nutrients to M9 minimal medium (2% [wt/vol] NaCl). CFU on LM agar plates were determined after 14 h. (C) Resuscitation of wild-type (black), Δ*btsU* (gray), and Δ*btsSR* (white) VBNC cells in LM medium at 30°C. CFU on LM agar plates were determined after 14 h. Micrographs of wild-type, Δ*btsU*, and Δ*btsSR* cells during resuscitation in LM medium after the indicated time points are also shown. There is a mixture of small (VBNC) and large (growing) cells in the mutant cultures at 16 h. Scale bars, 10 μm.

also be seen under the microscope, as first cells were elongated and regained their normal shape (Fig. 6C). Numbers of colonies on plates were compared after 14 h of incubation in the presence of different compounds: the addition of succinate resuscitated more cells than the addition of glucose or α-ketoglutarate, which has been shown to promote resuscitation of other bacterial species (14). Addition of pyruvate led to the highest number of culturable cells—but only for the wild type, as the deletion mutants are unable to take up pyruvate. This demonstrates once again the importance of pyruvate and of the BtsSRU system for *V. campbellii*, which promotes efficient resuscitation from the VBNC state.

Addition of LM medium to the VBNC cells also restored culturability to a large extent (Fig. 6C). Interestingly, Δ*btsU* and Δ*btsSR* cells were impaired in resuscitation also in LM medium, which could also be followed under the microscope with less regularly shaped cells for the mutants compared to the wild type (Fig. 6C). LM medium contains at least 200 μM pyruvate (31). Thus, we conclude that the resuscitating effect of pyruvate is also the key factor in the resuscitation of VBNC *V. campbellii* cells in LM medium. Mutants unable to sense or take up pyruvate can enter the VBNC state and survive unfavorable conditions, but they are impaired in returning to the culturable state upon provision of pyruvate. Loss of the BtsSRU system thus puts dormant *V. campbellii*

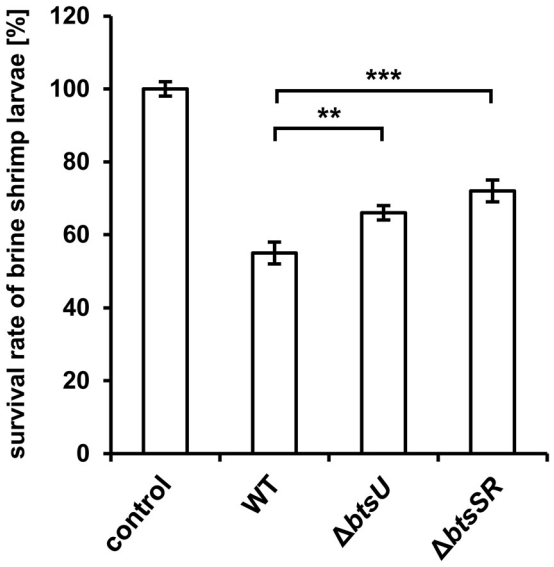

FIG 7 Reduced virulence of *V. campbellii* Δ*btsU* and Δ*btsSR* cells toward gnotobiotic brine shrimp larvae. Axenic *Artemia franciscana* larvae in sterile seawater (1 animal ml^{-1}) were challenged with *V. campbellii* wild-type, Δ*btsU*, and Δ*btsSR* cells at 10^7 cells ml^{-1}. Unchallenged animals were used as a control. After 48 h of incubation at 28°C, the survival of the larvae was determined. Experiments were performed in triplicate, and error bars represent standard deviations of the mean. *t* tests were performed to compare the treatments. Significant differences are indicated by asterisks (**, $P < 0.01$; ***, $P < 0.001$).

cells at a severe disadvantage, and pyruvate therefore plays an important role in this context too.

Virulence of *V. campbellii* toward gnotobiotic brine shrimp larvae is reduced in the absence of pyruvate sensing or uptake. It was shown previously for several bacterial pathogens that pyruvate is important for virulence and infection (7–12). Since *V. campbellii* is an important marine pathogen, we were interested in the relevance of the pyruvate sensing and uptake system described here for the virulence of the cells *in vivo*. To this end, we performed a standardized challenge test with gnotobiotic brine shrimp (*Artemia franciscana*) larvae to determine the ability of the bacteria to infect and kill their host. Wild-type *V. campbellii*, as well as Δ*btsU* and Δ*btsSR* cells, was added to sterile *Artemia* larvae cultures at 10^7 cells per ml. After 2 days of incubation at 28°C, the surviving brine shrimp larvae were counted. This number was then normalized to the number of live brine shrimp larvae in the control group, to which the pathogen was not added.

In the samples of *Artemia* larvae that were challenged with wild-type *V. campbellii* cells, the numbers of surviving larvae were almost 50% lower than in the control group, in which nearly all animals were still alive (Fig. 7). This illustrates how effectively the pathogen can infect and kill its host. In contrast, the relative survival of *Artemia* challenged with *V. campbellii* Δ*btsU* or Δ*btsSR* cells was significantly higher: In the group of animals exposed to Δ*btsU* cells, 66% survived the challenge, and in the group of animals treated with Δ*btsSR* cells even 72% survived (Fig. 7). We conclude that without pyruvate sensing and uptake, the virulence of *V. campbellii* toward gnotobiotic brine shrimp larvae is significantly reduced. The BtsSRU system, and hence pyruvate sensing and uptake, seem to be important for full virulence of the pathogen.

The expression of virulence factors in *V. campbellii* is regulated by quorum sensing (56). Here, we found no evidence that deletion of elements of the BtsSRU system affects quorum-sensing regulated processes, although we observed a clear effect on virulence. Thus, we suggest that pyruvate is linked to virulence in *V. campbellii* by a mechanism that is not connected with the quorum-sensing system. This might involve the ability of pyruvate to scavenge ROS. Zebrafish infected with *V. alginolyticus* were shown to produce high levels of ROS (57). Relating this to our study, with respect to

their ability to establish an infection, *V. campbellii* mutants that cannot take up pyruvate as an antioxidant against ROS may well be at a disadvantage in comparison to wild-type bacteria.

Conclusions. This study reveals first insights into pyruvate sensing and uptake in *V. campbellii* and its importance for this marine pathogen. Pyruvate is an indispensable metabolite for all living cells, since it not only functions as a central node of both aerobic and anaerobic metabolism but also protects cells against oxidative damage. *V. campbellii* excretes large amounts of pyruvate during growth, but nothing was previously known about the role of this compound for the pathogen. We demonstrate here that the sensor kinase BtsS senses pyruvate and activates expression of the only pyruvate transporter in this species, BtsU, via the response regulator BtsR. Inability to sense and thus to take up pyruvate affects many aspects of the normal behavior of this bacterium, including directed movement toward pyruvate, resuscitation from a dormant state and—most importantly—virulence. With regard to the increasing aquaculture production, to which *V. campbellii* presents a severe threat, this study is an important step toward a better understanding of the molecular mechanisms and factors that influence virulence. This study is not the first demonstrating the importance of pyruvate for fitness of and infection by pathogenic bacteria, indicating that this primary metabolite has a function that goes beyond its central role in metabolism and which makes it an extremely interesting and possibly so far underestimated molecule.

MATERIALS AND METHODS

Strains, plasmids, and oligonucleotides. *V. campbellii* and *E. coli* strains as well as plasmids used in this study are listed in Table 1. Oligonucleotide sequences are listed in Table S1 in the supplemental material. Clean in-frame deletions in *V. campbellii* were created by double homologous recombination using the pNPTS138-R6KT suicide plasmid (58). Upstream and downstream 800-bp regions of the respective gene were amplified from chromosomal DNA by PCR with appropriate oligonucleotides, retaining the first and last 15 bp of the coding sequence. The two DNA fragments were fused by overlapping PCR and cloned into the pNPTS138-R6KT plasmid following digestion with PstI and BamHI. Plasmids were then transferred into chemically competent *E. coli* DH5α λ*pir* cells (59). Plasmid sequences were confirmed by sequencing and transferred into *E. coli* WM3064 for conjugation with *V. campbellii*. Double homologous recombination was induced as previously described (58, 60). In short, mutants bearing single-crossover integrations were selected on LM agar plates containing kanamycin, then single clones were grown for 8 h in LM medium and selected for plasmid excision on LM agar plates containing 10% (wt/vol) sucrose. Kanamycin-sensitive clones were first checked for chromosomal in-frame gene deletions by colony PCR and finally confirmed by sequencing.

Complementation of *V. campbellii* Δ*btsU* and Δ*btsSR* strains with full-length genes inserted in the native locus was also done by double homologous recombination as described above, using the pNPTS138-R6KT plasmid (58) as the vector for amplified regions encompassing the respective full-length gene together with flanking up- and downstream regions. Correct complementation was confirmed by sequencing. Chromosomally integrated reporter constructs, with the *btsU* promoter fused to the *mcherry* gene upstream of the native locus, were assembled by single homologous recombination with the pNPTS138-R6KT plasmid as described previously (61). Briefly, a 500-bp region upstream of *V. campbellii btsU* was amplified by PCR and fused by overlapping PCR to the *mcherry* sequence, which was amplified by PCR from the pBAD-Cherry plasmid (62). This fragment was cloned into the pNPTS138-R6KT plasmid via restriction digestion using PstI and BamHI. For chromosomal integration of this reporter construct into the different *V. campbellii* strains, single homologous recombination was performed as described above.

Molecular biological methods. Molecular methods followed standard protocols (63) or were implemented according to manufacturer's instructions. Kits for the isolation of chromosomal DNA or plasmids and purification of PCR products were purchased from Südlabor. Enzymes were purchased from New England Biolabs. Chemicals were sourced from Roth or Merck.

Growth conditions. *V. campbellii* strains were grown overnight under agitation (200 rpm) at 30°C in Luria Marine (LM) medium (10 g liter^{-1} tryptone, 5 g liter^{-1} yeast extract, 20 g liter^{-1} NaCl) (64). Cells from the overnight culture were then transferred to the appropriate fresh medium. *E. coli* strains were grown under agitation (200 rpm) at 37°C in lysogeny broth (LB) medium (10 g liter^{-1} tryptone, 5 g liter^{-1} yeast extract, 10 g liter^{-1} NaCl) (65). The conjugation strain *E. coli* WM3064 was grown in the presence of 300 μM diaminopimelic acid. If necessary, media were supplemented with 50 μg ml^{-1} kanamycin sulfate and/or 100 μg ml^{-1} ampicillin sodium salt. To measure growth of *V. campbellii* strains on different carbon sources, cells were cultivated for 24 h at 30°C in M9 minimal medium (66) containing 2% (wt/vol) NaCl, supplemented with the carbon source to be tested (e.g., 20 mM sodium pyruvate). Growth was monitored by measuring the OD_{600} over time.

Analysis of *btsU* expression. Expression of *V. campbellii btsU* was determined by measuring fluorescence levels of the different *V. campbellii* reporter strains carrying a chromosomally integrated fusion of

TABLE 1 Strains and plasmids used in this study

Strain or plasmid	Genotype or description	Source or reference
Strains		
V. campbellii		
ATCC BAA-116 (BB120)	Wild type	24
Δ*btsU* strain	In-frame deletion of VIBHAR_00986	This study
Δ*btsS* strain	In-frame deletion of VIBHAR_00985	This study
Δ*btsR* strain	In-frame deletion of VIBHAR_00984	This study
Δ*btsSR* strain	In-frame deletion of VIBHAR_00984-00985	This study
Δ*btsU*::*btsU* strain	Complemented Δ*btsU*	This study
Δ*btsSR*::*btsSR* strain	Complemented Δ*btsSR*	This study
Wild-type P_{btsU}-*mcherry* strain	Wild type with chromosomally integrated reporter construct for *btsU* upstream of the native promoter	This study
Δ*btsU* P_{btsU}-*mcherry* strain	Δ*btsU* with chromosomally integrated reporter construct for *btsU* upstream of the native promoter	This study
Δ*btsS* P_{btsU}-*mcherry* strain	Δ*btsS* with chromosomally integrated reporter construct for *btsU* upstream of the native promoter	This study
Δ*btsR* P_{btsU}-*mcherry* strain	Δ*btsR* with chromosomally integrated reporter construct for *btsU* upstream of the native promoter	This study
Δ*btsSR* P_{btsU}-*mcherry* strain	Δ*btsSR* with chromosomally integrated reporter construct for *btsU* upstream of the native promoter	This study
E. coli		
DH5α λ*pir*	*endA1 hsdR17 glnV44 thi-1 recA1 gyrA96 relA1* ϕ80′ *lac*Δ(*lacZ*)M15 Δ(*lacZYA-argF*) *U169 zdg*-232::Tn*10 uidA*::*pir*$^+$	72
WM3064	*thrB1004 pro thi rpsL hsdS lacZ* ΔM15 RP4-1360 Δ(*araBAD*)*567* Δ*dapA1341*::[*erm pir*]	W. Metcalf, University of Illinois
Plasmids		
pNPTS138-R6KT	Plasmid backbone for in-frame deletions; *mobRP4*$^+$ *sacB* Kan^r	58
pNPTS138-R6KT-Δ*btsU*	Plasmid for in-frame deletion of *btsU* in *V. campbellii*	This study
pNPTS138-R6KT-Δ*btsS*	Plasmid for in-frame deletion of *btsS* in *V. campbellii*	This study
pNPTS138-R6KT-Δ*btsR*	Plasmid for in-frame deletion of *btsR* in *V. campbellii*	This study
pNPTS138-R6KT-Δ*btsSR*	Plasmid for in-frame deletion of *btsSR* in *V. campbellii*	This study
pNPTS138-R6KT-P_{btsU}-*mcherry*	Plasmid used to create *V. campbellii* strains with a chromosomally integrated reporter construct (P_{btsU}-*mcherry*) upstream of the native locus	This study
pBAD-Cherry	*mcherry* in pBAD33	62

the *btsU* promoter with the *mcherry* gene upstream of the native locus. To this end, cells from overnight cultures were inoculated at a starting OD_{600} of 0.05 into various media in 96-well plates. Plates were then incubated under constant agitation at 30°C and mCherry fluorescence (excitation at 580 nm, emission at 610 nm) was measured at intervals of 10 min for 24 h in a Tecan Infinite M200 Pro plate reader. Fluorescence levels (normalized to 1 OD_{600}) were determined for each condition in exponential growth phase. Autofluorescence of the cells was subtracted.

External pyruvate determination. Levels of excreted pyruvate were measured using a procedure adapted from O'Donell-Tormey et al. (3). *V. campbellii* strains were grown under agitation at 30°C in LM medium, and growth was monitored. At selected time points, 1-ml samples of supernatant were harvested by centrifugation at 4°C (10 min, 14,000 × *g*). Proteins were precipitated by the addition of 250 μl of ice-cold 2 M perchloric acid. After a 5-min incubation on ice, the samples were neutralized with 250 μl of 2.5 M potassium bicarbonate, and precipitates were removed by centrifugation (4°C, 10 min, 14,000 × *g*). Pyruvate concentrations of the clear supernatants, diluted 1:20 in 100 mM PIPES buffer (pH 7.5), were determined by using an enzymatic assay based on the conversion of pyruvate and $NADH + H^+$ to lactate by lactate dehydrogenase. The assay was performed as described before (39).

Pyruvate uptake measurement. To determine the uptake of pyruvate by *V. campbellii*, a transport assay was performed with radiolabeled pyruvate. Cells were grown under agitation at 30°C in LM medium and harvested in mid-log phase. Cells were pelleted at 4°C, washed twice, and resuspended in transport buffer (2.9 mM K_2HPO_4, 2.2 mM KH_2PO_4, 0.33 M NaCl, 30 mM $MgCl_2$, 6.8 M $CaCl_2$) to an absorbance of 5 at 420 nm, equivalent to a total protein concentration of 0.35 mg ml^{-1}. Uptake of [^{14}C]pyruvate (55 mCi $mmol^{-1}$; Biotrend) was measured at a total substrate concentration of 10 μM at 18°C. At various time intervals, transport was terminated by the addition of ice-cold stop buffer (100 mM potassium phosphate [pH 6.0], 100 mM LiCl), followed by rapid filtration through membrane filters (MN gf-5, 0.4-μm nitrocellulose; Macherey-Nagel). The filters were dissolved in 5 ml of scintillation fluid (MP Biomedicals), and radioactivity was determined in a liquid scintillation analyzer (Perkin-Elmer). The effects of protonophores and ionophores were tested after preincubation of cells in transport buffer supplemented with 20 μM carbonyl cyanide *m*-chlorophenylhydrazone (CCCP), 2 mM 2,4-dinitrophenol (DNP), 10 μM nonactin, 6 μM nigericin, 2 μM valinomycin, or dimethyl sulfoxide (DMSO; as control) at 25°C for 30 min.

Chemotaxis test. Chemotaxis of *V. campbellii* toward different compounds was tested using the plug-in-pond assay (67). Cells grown in LM medium were pelleted, resuspended to a final OD_{600} of 0.5 in M9 soft agar (M9 medium with 2% [wt/vol] NaCl and 0.3% [wt/vol] agar) without a carbon source, and poured into a petri dish, in which agar plugs (M9 medium with 2% [wt/vol] NaCl and 1.5% [wt/vol] agar) containing the test substances had been placed. Plates were incubated at 30°C for 3 h. Pictures were taken with a Canon EOS M50 camera.

Induction of the VBNC state. *V. campbellii* cells were grown under agitation at 30°C in LM medium, harvested by centrifugation in mid-log phase, and washed twice with sterile saline solution (2% [wt/vol] NaCl). Cells were resuspended in M9 minimal medium (2% [wt/vol] NaCl) without a carbon source to a final OD_{600} of 1 and stored at 4°C to induce long-term cold stress under nutrient limitation. Ampicillin sodium salt (100 μg ml^{-1}) was added to the medium to prevent contamination, since *V. campbellii* is naturally ampicillin resistant. Culturability was determined periodically by plating serial dilutions of samples on LM agar plates and counting CFU. When CFU could no longer be detected, cells were considered to be nonculturable.

Resuscitation from the VBNC state. VBNC cells were diluted 1:10 in different media and incubated under agitation at 30°C. At different time points, samples were taken, serial dilutions were plated on LM agar plates and CFU were counted. For microscopy, samples were centrifuged and resuspended in small volumes of sterile saline solution (2% [wt/vol] NaCl). Then, 3-μl drops were placed on agarose pads (2% [wt/vol] NaCl, 1% [wt/vol] agarose) and sealed with a cover slide. Microscopy was performed using a Leica DMI6000 B fluorescence microscope.

Axenic hatching of brine shrimp larvae. Samples (500 mg) of high-quality *Artemia franciscana* cysts (EG Type; INVE Aquaculture, Baasrode, Belgium) were hydrated in 45 ml of sterilized distilled water for 1 h. Sterile cysts were obtained by decapsulation based on the method described by Marques et al. (68). Briefly, 1.65 ml of NaOH (32% [wt/vol]) and 25 ml of NaOCl (50% available chlorine) were added to the hydrated cyst suspension to facilitate decapsulation. The process was stopped after 2 min by adding 35 ml of $Na_2S_2O_3$ (10 g liter^{-1}). Filtered (0.22 μm) aeration was provided during the reaction. The decapsulated cysts were washed with filtered (passed through a 0.45-μm membrane filter), autoclaved (moist heat at 121°C for 20 min) artificial seawater and then resuspended in 500 ml of filtered, autoclaved seawater and hatched for 28 h at 28°C with constant illumination (2000 lx). Air was bubbled into the suspension through a sterile glass tube extending to the bottom of the hatching vessel to ensure that all the cysts were kept in continuous motion (69). The axenity of cysts was verified by inoculating 1 ml of culture water into 9 ml of LM medium and incubating overnight at 28°C. After 28 h of hatching, batches of 30 larvae were counted and transferred to sterilized 50-ml glass tubes containing 30 ml of filtered and autoclaved seawater. Finally, the tubes were incubated on a rotor (4 rpm) and kept at 28°C. All manipulations were performed in a laminar-flow cabinet to maintain sterility of cysts and larvae.

Brine shrimp challenge test. The virulence of wild-type and mutant strains was determined in a standardized challenge test with gnotobiotic brine shrimp larvae. *V. campbellii* strains were grown to an OD_{600} of 1, and then cultures were washed with phosphate-buffered saline (pH 7.4) prior to inoculation of the brine shrimp samples at 10^5 CFU ml^{-1}. The challenge tests were performed as described by Defoirdt et al. (70) with some modifications. A suspension of autoclaved LVS3 bacteria (71) in filtered and autoclaved seawater was added at 10^7 cells ml^{-1} as feed to the culture water at the start of the challenge. Brine shrimp cultures to which only autoclaved LVS3 bacteria were added as feed were used as controls. The surviving larvae were counted 48 h after the addition of the pathogens. Each treatment was carried out in triplicate, and the experiment was repeated three times to verify reproducibility. At the end of the challenge, the sterility of the control treatments in each test was checked by adding 1 ml of rearing water to 9 ml of LM medium and incubating the mixture for 2 days at 28°C.

SUPPLEMENTAL MATERIAL

Supplemental material is available online only.

SUPPLEMENTAL FILE 1, PDF file, 0.4 MB.

ACKNOWLEDGMENTS

This research was funded by the Deutsche Forschungsgemeinschaft (JU270/19-1 to K.J. and project number 395357507-SFB1371 to K.J.).

REFERENCES

1. Postma PW, Lengeler JW, Jacobson GR. 1993. Phosphoenolpyruvate:carbohydrate phosphotransferase systems of bacteria. Microbiol Rev 57:543–594. https://doi.org/10.1128/mr.57.3.543-594.1993.
2. Kładna A, Marchlewicz M, Piechowska T, Kruk I, Aboul-Enein HY. 2015. Reactivity of pyruvic acid and its derivatives towards reactive oxygen species. Luminescence 30:1153–1158. https://doi.org/10.1002/bio.2879.
3. O'Donnell-Tormey J, Nathan CF, Lanks K, DeBoer CJ, de la Harpe J. 1987. Secretion of pyruvate: an antioxidant defense of mammalian cells. J Exp Med 165:500–514. https://doi.org/10.1084/jem.165.2.500.
4. Constantopoulos G, Barranger JA. 1984. Nonenzymatic decarboxylation of pyruvate. Anal Biochem 139:353–358. https://doi.org/10.1016/0003-2697(84)90016-2.
5. Varma SD, Hegde K, Henein M. 2003. Oxidative damage to mouse lens in culture. Protective effect of pyruvate. Biochim Biophys Acta 1621:246–252. https://doi.org/10.1016/s0304-4165(03)00075-8.
6. Woo YJ, Taylor MD, Cohen JE, Jayasankar V, Bish LT, Burdick J, Pirolli TJ, Berry MF, Hsu V, Grand T. 2004. Ethyl pyruvate preserves cardiac function and attenuates oxidative injury after prolonged myocardial ischemia. J Thorac Cardiovasc Surg 127:1262–1269. https://doi.org/10.1016/j.jtcvs.2003.11.032.
7. Troxell B, Zhang JJ, Bourret TJ, Zeng MY, Blum J, Gherardini F, Hassan HM, Yang XF. 2014. Pyruvate protects pathogenic spirochetes from H_2O_2 killing. PLoS One 9:e84625. https://doi.org/10.1371/journal.pone.0084625.
8. Schär J, Stoll R, Schauer K, Loeffler DI, Eylert E, Joseph B, Eisenreich W, Fuchs TM, Goebel W. 2010. Pyruvate carboxylase plays a crucial role in

carbon metabolism of extra- and intracellularly replicating *Listeria monocytogenes*. J Bacteriol 192:1774–1784. https://doi.org/10.1128/JB.01132-09.
9. Xie T, Pang R, Wu Q, Zhang J, Lei T, Li Y, Wang J, Ding Y, Chen M, Bai J. 2019. Cold tolerance regulated by the pyruvate metabolism in *Vibrio parahaemolyticus*. Front Microbiol 10:178. https://doi.org/10.3389/fmicb.2019.00178.
10. Bücker R, Heroven AK, Becker J, Dersch P, Wittmann C. 2014. The pyruvate-tricarboxylic acid cycle node: a focal point of virulence control in the enteric pathogen *Yersinia pseudotuberculosis*. J Biol Chem 289:30114–30132. https://doi.org/10.1074/jbc.M114.581348.
11. Harper L, Balasubramanian D, Ohneck EA, Sause WE, Chapman J, Mejia-Sosa B, Lhakhang T, Heguy A, Tsirigos A, Ueberheide B, Boyd JM, Lun DS, Torres VJ. 2018. *Staphylococcus aureus* responds to the central metabolite pyruvate to regulate virulence. mBio 9:e02272-17. https://doi.org/10.1128/mBio.02272-17.
12. Steiner BD, Eberly AR, Hurst MN, Zhang EW, Green HD, Behr S, Jung K, Hadjifrangiskou M. 2018. Evidence of cross-regulation in two closely related pyruvate-sensing systems in uropathogenic *Escherichia coli*. J Membr Biol 251:65–74. https://doi.org/10.1007/s00232-018-0014-2.
13. Liao H, Jiang L, Zhang R. 2018. Induction of a viable but non-culturable state in *Salmonella* Typhimurium by thermosonication and factors affecting resuscitation. FEMS Microbiol Lett 365:fnx249.
14. Mizunoe Y, Wai SN, Takade A, Yoshida S. 1999. Restoration of culturability of starvation-stressed and low-temperature-stressed *Escherichia coli* O157 cells by using H_2O_2-degrading compounds. Arch Microbiol 172:63–67. https://doi.org/10.1007/s002030050741.
15. Vilhena C, Kaganovitch E, Grünberger A, Motz M, Forné I, Kohlheyer D, Jung K. 2019. Importance of pyruvate sensing and transport for the resuscitation of viable but nonculturable *Escherichia coli* K-12. J Bacteriol 201:e00610-18. https://doi.org/10.1128/JB.00610-18.
16. Dong K, Pan H, Yang D, Rao L, Zhao L, Wang Y, Liao X. 2020. Induction, detection, formation, and resuscitation of viable but non-culturable state microorganisms. Compr Rev Food Sci Food Saf 19:149–183. https://doi.org/10.1111/1541-4337.12513.
17. Oliver JD. 2005. The viable but nonculturable state in bacteria. J Microbiol 43:Spec No:93-100.
18. Vilhena C, Kaganovitch E, Shin JY, Grünberger A, Behr S, Kristoficova I, Brameyer S, Kohlheyer D, Jung K. 2018. A single-cell view of the BtsSR/YpdAB pyruvate sensing network in *Escherichia coli* and its biological relevance. J Bacteriol 200:e00536-17. https://doi.org/10.1128/JB.00536-17.
19. Benson PJ, Purcell-Meyerink D, Hocart CH, Truong TT, James GO, Rourke L, Djordjevic MA, Blackburn SI, Price GD. 2016. Factors altering pyruvate excretion in a glycogen storage mutant of the cyanobacterium, *Synechococcus* PCC7942. Front Microbiol 7:475.
20. Jules M. 2017. The logics of metabolic regulation in bacteria challenges biosensor-based metabolic engineering. Microb Cell 5:56–59. https://doi.org/10.15698/mic2018.01.610.
21. Bricker DK, Taylor EB, Schell JC, Orsak T, Boutron A, Chen YC, Cox JE, Cardon CM, Van Vranken JG, Dephoure N, Redin C, Boudina S, Gygi SP, Brivet M, Thummel CS, Rutter J. 2012. A mitochondrial pyruvate carrier required for pyruvate uptake in yeast, *Drosophila*, and humans. Science 337:96–100. https://doi.org/10.1126/science.1218099.
22. Yin C, He D, Chen S, Tan X, Sang N. 2016. Exogenous pyruvate facilitates cancer cell adaptation to hypoxia by serving as an oxygen surrogate. Oncotarget 7:47494–47510. https://doi.org/10.18632/oncotarget.10202.
23. Morita N, Umemoto E, Fujita S, Hayashi A, Kikuta J, Kimura I, Haneda T, Imai T, Inoue A, Mimuro H, Maeda Y, Kayama H, Okumura R, Aoki J, Okada N, Kida T, Ishii M, Nabeshima R, Takeda K. 2019. GPR31-dependent dendrite protrusion of intestinal $CX3CR1^+$ cells by bacterial metabolites. Nature 566:110–114. https://doi.org/10.1038/s41586-019-0884-1.
24. Lin B, Wang Z, Malanoski AP, O'Grady EA, Wimpee CF, Vuddhakul V, Alves N, Jr, Thompson FL, Gomez-Gil B, Vora GJ. 2010. Comparative genomic analyses identify the *Vibrio harveyi* genome sequenced strains BAA-1116 and HY01 as *Vibrio campbellii*. Environ Microbiol Rep 2:81–89. https://doi.org/10.1111/j.1758-2229.2009.00100.x.
25. Pena LDdl, Lavilla-Pitogo CR, Paner MG. 2001. Luminescent vibrios associated with mortality in pond-cultured shrimp *Penaeus monodon* in the Philippines: species composition. Fish Pathol 36:133–138. https://doi.org/10.3147/jsfp.36.133.
26. Phuoc LH, Corteel M, Nauwynck HJ, Pensaert MB, Alday-Sanz V, Van den Broeck W, Sorgeloos P, Bossier P. 2008. Increased susceptibility of white spot syndrome virus-infected *Litopenaeus vannamei* to *Vibrio campbellii*. Environ Microbiol 10:2718–2727. https://doi.org/10.1111/j.1462-2920.2008.01692.x.
27. Austin B, Zhang XH. 2006. *Vibrio harveyi*: a significant pathogen of marine vertebrates and invertebrates. Lett Appl Microbiol 43:119–124. https://doi.org/10.1111/j.1472-765X.2006.01989.x.
28. FAO. 2020. The State of World Fisheries and Aquaculture 2020: sustainability in action. Food and Agriculture Organization of the United Nations, Rome, Italy.
29. Defoirdt T, Boon N, Sorgeloos P, Verstraete W, Bossier P. 2007. Alternatives to antibiotics to control bacterial infections: luminescent vibriosis in aquaculture as an example. Trends Biotechnol 25:472–479. https://doi.org/10.1016/j.tibtech.2007.08.001.
30. Ruby EG, Nealson KH. 1977. Pyruvate production and excretion by the luminous marine bacteria. Appl Environ Microbiol 34:164–169. https://doi.org/10.1128/aem.34.2.164-169.1977.
31. Behr S, Brameyer S, Witting M, Schmitt-Kopplin P, Jung K. 2017. Comparative analysis of LytS/LytTR-type histidine kinase/response regulator systems in γ-proteobacteria. PLoS One 12:e0182993. https://doi.org/10.1371/journal.pone.0182993.
32. Paczia N, Nilgen A, Lehmann T, Gätgens J, Wiechert W, Noack S. 2012. Extensive exometabolome analysis reveals extended overflow metabolism in various microorganisms. Microb Cell Fact 11:122. https://doi.org/10.1186/1475-2859-11-122.
33. Chubukov V, Gerosa L, Kochanowski K, Sauer U. 2014. Coordination of microbial metabolism. Nat Rev Microbiol 12:327–340. https://doi.org/10.1038/nrmicro3238.
34. Yasid NA, Rolfe MD, Green J, Williamson MP. 2016. Homeostasis of metabolites in *Escherichia coli* on transition from anaerobic to aerobic conditions and the transient secretion of pyruvate. R Soc Open Sci 3:160187. https://doi.org/10.1098/rsos.160187.
35. Kraxenberger T, Fried L, Behr S, Jung K. 2012. First insights into the unexplored two-component system YehU/YehT in *Escherichia coli*. J Bacteriol 194:4272–4284. https://doi.org/10.1128/JB.00409-12.
36. Behr S, Kristoficova I, Witting M, Breland EJ, Eberly AR, Sachs C, Schmitt-Kopplin P, Hadjifrangiskou M, Jung K. 2017. Identification of a high-affinity pyruvate receptor in *Escherichia coli*. Sci Rep 7:1388. https://doi.org/10.1038/s41598-017-01410-2.
37. Kristoficova I, Vilhena C, Behr S, Jung K. 2018. BtsT, a novel and specific pyruvate/H^+ symporter in *Escherichia coli*. J Bacteriol 200:e00599-17. https://doi.org/10.1128/JB.00599-17.
38. Hwang S, Choe D, Yoo M, Cho S, Kim SC, Cho S, Cho BK. 2018. Peptide transporter CstA imports pyruvate in *Escherichia coli* K-12. J Bacteriol 200:e00771-17. https://doi.org/10.1128/JB.00771-17.
39. Gasperotti A, Göing S, Fajardo-Ruiz E, Forné I, Jung K. 2020. Function and regulation of the pyruvate transporter CstA in *Escherichia coli*. Int J Mol Sci 21:9068. https://doi.org/10.3390/ijms21239068.
40. Fried L, Behr S, Jung K. 2013. Identification of a target gene and activating stimulus for the YpdA/YpdB histidine kinase/response regulator system in *Escherichia coli*. J Bacteriol 195:807–815. https://doi.org/10.1128/JB.02051-12.
41. Ogasawara H, Ishizuka T, Yamaji K, Kato Y, Shimada T, Ishihama A. 2019. Regulatory role of pyruvate-sensing BtsSR in biofilm formation by *Escherichia coli* K-12. FEMS Microbiol Lett 366:fnz251. https://doi.org/10.1093/femsle/fnz251.
42. Altschul SF, Gish W, Miller W, Myers EW, Lipman DJ. 1990. Basic local alignment search tool. J Mol Biol 215:403–410. https://doi.org/10.1016/S0022-2836(05)80360-2.
43. Sievers F, Wilm A, Dineen D, Gibson TJ, Karplus K, Li W, Lopez R, McWilliam H, Remmert M, Söding J, Thompson JD, Higgins DG. 2011. Fast, scalable generation of high-quality protein multiple sequence alignments using Clustal Omega. Mol Syst Biol 7:539. https://doi.org/10.1038/msb.2011.75.
44. Mistry J, Chuguransky S, Williams L, Qureshi M, Salazar Gustavo A, Sonnhammer ELL, Tosatto SCE, Paladin L, Raj S, Richardson LJ, Finn RD, Bateman A. 2021. Pfam: the protein families database in 2021. Nucleic Acids Res 49:D412–D419. https://doi.org/10.1093/nar/gkaa913.
45. Hofmann K, Stoffel W. 1993. TMbase: a database of membrane spanning protein segments. Biol Chem Hoppe-Seyler 374:166.
46. Bi S, Sourjik V. 2018. Stimulus sensing and signal processing in bacterial chemotaxis. Curr Opin Microbiol 45:22–29. https://doi.org/10.1016/j.mib.2018.02.002.
47. Boin MA, Austin MJ, Häse CC. 2004. Chemotaxis in *Vibrio cholerae*. FEMS Microbiol Lett 239:1–8. https://doi.org/10.1016/j.femsle.2004.08.039.
48. Xu X, Li H, Qi X, Chen Y, Qin Y, Zheng J, Jiang X. 2020. *cheA*, *cheB*, *cheR*, *cheV*, and *cheY* are involved in regulating the adhesion of *Vibrio harveyi*.

Front Cell Infect Microbiol 10:591751. https://doi.org/10.3389/fcimb.2020.591751.
49. Neumann S, Grosse K, Sourjik V. 2012. Chemotactic signaling via carbohydrate phosphotransferase systems in *Escherichia coli*. Proc Natl Acad Sci U S A 109:12159–12164. https://doi.org/10.1073/pnas.1205307109.
50. Somavanshi R, Ghosh B, Sourjik V. 2016. Sugar influx sensing by the phosphotransferase system of *Escherichia coli*. PLoS Biol 14:e2000074. https://doi.org/10.1371/journal.pbio.2000074.
51. Sun F, Chen J, Zhong L, Zhang XH, Wang R, Guo Q, Dong Y. 2008. Characterization and virulence retention of viable but nonculturable *Vibrio harveyi*. FEMS Microbiol Ecol 64:37–44. https://doi.org/10.1111/j.1574-6941.2008.00442.x.
52. Du M, Chen J, Zhang X, Li A, Li Y, Wang Y. 2007. Retention of virulence in a viable but nonculturable *Edwardsiella tarda* isolate. Appl Environ Microbiol 73:1349–1354. https://doi.org/10.1128/AEM.02243-06.
53. Nilsson L, Oliver JD, Kjelleberg S. 1991. Resuscitation of *Vibrio vulnificus* from the viable but nonculturable state. J Bacteriol 173:5054–5059. https://doi.org/10.1128/jb.173.16.5054-5059.1991.
54. Li L, Mendis N, Trigui H, Oliver JD, Faucher SP. 2014. The importance of the viable but non-culturable state in human bacterial pathogens. Front Microbiol 5:258.
55. Pinto D, Santos MA, Chambel L. 2015. Thirty years of viable but nonculturable state research: unsolved molecular mechanisms. Crit Rev Microbiol 41:61–76. https://doi.org/10.3109/1040841X.2013.794127.
56. Han B, Zheng X, Baruah K, Bossier P. 2020. Sodium ascorbate as a quorum-sensing inhibitor leads to decreased virulence in *Vibrio campbellii*. Front Microbiol 11:1054. https://doi.org/10.3389/fmicb.2020.01054.
57. Gong QY, Yang MJ, Yang LF, Chen ZG, Jiang M, Peng B. 2020. Metabolic modulation of redox state confounds fish survival against *Vibrio alginolyticus* infection. Microb Biotechnol 13:796–812. https://doi.org/10.1111/1751-7915.13553.
58. Lassak J, Henche AL, Binnenkade L, Thormann KM. 2010. ArcS, the cognate sensor kinase in an atypical Arc system of *Shewanella oneidensis* MR-1. Appl Environ Microbiol 76:3263–3274. https://doi.org/10.1128/AEM.00512-10.
59. Inoue H, Nojima H, Okayama H. 1990. High-efficiency transformation of *Escherichia coli* with plasmids. Gene 96:23–28. https://doi.org/10.1016/0378-1119(90)90336-p.
60. Brameyer S, Hoyer E, Bibinger S, Burdack K, Lassak J, Jung K. 2020. Molecular design of a signaling system influences noise in protein abundance under acid stress in different *γ-Proteobacteria*. J Bacteriol 202:e00121-20. https://doi.org/10.1128/JB.00121-20.
61. Fried L, Lassak J, Jung K. 2012. A comprehensive toolbox for the rapid construction of *lacZ* fusion reporters. J Microbiol Methods 91:537–543. https://doi.org/10.1016/j.mimet.2012.09.023.
62. Brameyer S, Kresovic D, Bode HB, Heermann R. 2015. Dialkylresorcinols as bacterial signaling molecules. Proc Natl Acad Sci U S A 112:572–577. https://doi.org/10.1073/pnas.1417685112.
63. Sambrook J, Fritsch E, Maniatis T. 1989. Molecular cloning: a laboratory manual, 2nd ed. Cold Spring Harbor Laboratory Press, Cold Spring Harbor, NY.
64. Bassler BL, Wright M, Showalter RE, Silverman MR. 1993. Intercellular signaling in *Vibrio harveyi*: sequence and function of genes regulating expression of luminescence. Mol Microbiol 9:773–786. https://doi.org/10.1111/j.1365-2958.1993.tb01737.x.
65. Bertani G. 1951. Studies on lysogenesis. I. The mode of phage liberation by lysogenic *Escherichia coli*. J Bacteriol 62:293–300. https://doi.org/10.1128/jb.62.3.293-300.1951.
66. Harwood CR, Cutting SM. 1990. Molecular biological methods for Bacillus. Wiley, Chichester, United Kingdom.
67. Darias JA, García-Fontana C, Lugo AC, Rico-Jiménez M, Krell T. 2014. Qualitative and quantitative assays for flagellum-mediated chemotaxis. Methods Mol Biol 1149:87–97. https://doi.org/10.1007/978-1-4939-0473-0_10.
68. Marques A, Dinh T, Ioakeimidis C, Huys G, Swings J, Verstraete W, Dhont J, Sorgeloos P, Bossier P. 2005. Effects of bacteria on *Artemia franciscana* cultured in different gnotobiotic environments. Appl Environ Microbiol 71:4307–4317. https://doi.org/10.1128/AEM.71.8.4307-4317.2005.
69. Sorgeloos P, Persoone G. 1975. Technological improvements for the cultivation of invertebrates as food for fishes and crustaceans. II. Hatching and culturing of the brine shrimp, *Artemia salina* L. Aquaculture 6:303–317. https://doi.org/10.1016/0044-8486(75)90110-6.
70. Defoirdt T, Bossier P, Sorgeloos P, Verstraete W. 2005. The impact of mutations in the quorum sensing systems of *Aeromonas hydrophila*, *Vibrio anguillarum* and *Vibrio harveyi* on their virulence towards gnotobiotically cultured *Artemia franciscana*. Environ Microbiol 7:1239–1247. https://doi.org/10.1111/j.1462-2920.2005.00807.x.
71. Verschuere L, Rombaut G, Huys G, Dhont J, Sorgeloos P, Verstraete W. 1999. Microbial control of the culture of *Artemia* juveniles through preemptive colonization by selected bacterial strains. Appl Environ Microbiol 65:2527–2533. https://doi.org/10.1128/AEM.65.6.2527-2533.1999.
72. Macinga DR, Parojcic MM, Rather PN. 1995. Identification and analysis of *aarP*, a transcriptional activator of the 2′-*N*-acetyltransferase in *Providencia stuartii*. J Bacteriol 177:3407–3413. https://doi.org/10.1128/jb.177.12.3407-3413.1995.

4 The biological significance of pyruvate sensing and uptake in *Salmonella enterica* serovar Typhimurium

Paulini S, Fabiani FD, Weiß AS, Moldoveanu AL, Helaine S, Stecher B, Jung K. 2022. Microorganisms 10:1751. https://doi.org/10.3390/microorganisms10091751

microorganisms

MDPI

Article

The Biological Significance of Pyruvate Sensing and Uptake in *Salmonella enterica* Serovar Typhimurium

Stephanie Paulini [1], Florian D. Fabiani [1,†], Anna S. Weiss [2], Ana Laura Moldoveanu [3], Sophie Helaine [3,‡], Bärbel Stecher [2,4] and Kirsten Jung [1,*]

[1] Department of Microbiology, Ludwig-Maximilians-University Munich, 82152 Planegg-Martinsried, Germany
[2] Max von Pettenkofer Institute of Hygiene and Medical Microbiology, Faculty of Medicine, Ludwig-Maximilians-University Munich, 80336 Munich, Germany
[3] MRC Centre for Molecular Bacteriology and Infection, Imperial College London, London SW7 2DD, UK
[4] German Center for Infection Research (DZIF), Partner Site LMU Munich, 80337 Munich, Germany
* Correspondence: jung@lmu.de; Tel.: +49-(0)89/2180-74500
† Present affiliation: Bayer AG, 13353 Berlin, Germany.
‡ Present affiliation: Department of Microbiology, Harvard Medical School, Boston, MA 02115, USA.

Abstract: Pyruvate ($CH_3COCOOH$) is the simplest of the alpha-keto acids and is at the interface of several metabolic pathways both in prokaryotes and eukaryotes. In an amino acid-rich environment, fast-growing bacteria excrete pyruvate instead of completely metabolizing it. The role of pyruvate uptake in pathological conditions is still unclear. In this study, we identified two pyruvate-specific transporters, BtsT and CstA, in *Salmonella enterica* serovar Typhimurium (*S*. Typhimurium). Expression of *btsT* is induced by the histidine kinase/response regulator system BtsS/BtsR upon sensing extracellular pyruvate, whereas expression of *cstA* is maximal in the stationary phase. Both pyruvate transporters were found to be important for the uptake of this compound, but also for chemotaxis to pyruvate, survival under oxidative and nitrosative stress, and persistence of *S*. Typhimurium in response to gentamicin. Compared with the wild-type cells, the Δ*btsT*Δ*cstA* mutant has disadvantages in antibiotic persistence in macrophages, as well as in colonization and systemic infection in gnotobiotic mice. These data demonstrate the surprising complexity of the two pyruvate uptake systems in *S*. Typhimurium.

Keywords: *Salmonella* Typhimurium; pyruvate transporter; chemotaxis; oxidative stress; persistence

Citation: Paulini, S.; Fabiani, F.D.; Weiss, A.S.; Moldoveanu, A.L.; Helaine, S.; Stecher, B.; Jung, K. The Biological Significance of Pyruvate Sensing and Uptake in *Salmonella enterica* Serovar Typhimurium. *Microorganisms* **2022**, *10*, 1751. https://doi.org/10.3390/microorganisms10091751

Academic Editor: Ute Römling

Received: 13 July 2022
Accepted: 24 August 2022
Published: 30 August 2022

1. Introduction

Pyruvate is a primary metabolite of central importance in all living cells. It is the end product of glycolysis and can enter the tricarboxylic acid cycle via acetyl-CoA under aerobic conditions; however, it can also be reduced to lactate under anaerobic conditions. Moreover, it is used as a precursor for the production of amino acids, fatty acids, and sugars. Bacteria tightly control intracellular pyruvate levels, which were reported to be between 7 and 100 mM [1–3]. In an amino acid-rich environment, fast-growing bacteria excrete pyruvate instead of metabolizing it completely, a phenomenon known as overflow metabolism, and take it up again later [4–7].

Pyruvate also scavenges reactive oxygen species (ROS). It inactivates hydrogen peroxide (H_2O_2) by being oxidized and rapidly decarboxylated [8–10]. Therefore, the secretion of pyruvate can also be seen as an antioxidant defense mechanism [11]. The role of pyruvate in the inactivation of ROS is important for the resuscitation of viable but non-culturable (VBNC) bacteria. Pyruvate is required to "wake up" cells from this dormant state and re-enter culturability [12–15]. *S*. Typhimurium was effectively resuscitated from the VBNC state using pyruvate [16].

Several reports have demonstrated the importance of pyruvate as focal point in metabolism and in virulence control of pathogens, such as *Yersinia pseudotuberculosis*, *S*.

Typhimurium, *Listeria monocytogenes*, and *Vibrio parahaemolyticus* [17–21]. *Pseudomonas aeruginosa*, *Staphylococcus aureus*, and *Chlostridium difficile* require extracellular pyruvate for biofilm formation [22–24]. Mammalian apoptotic cells also release pyruvate, which has been shown to promote the growth of *S*. Typhimurium [25]. This suggests an important role for pyruvate in host inflammation and infection.

In *E. coli*, BtsT and CstA have been characterized as substrate-specific pyruvate transporters, and a deletion mutant of these two transporter genes and the gene *yhjX* has lost the ability to grow on pyruvate, indicating that YhjX might also be a pyruvate transporter [26–28]. *btsT* and *yhjX* are activated by the histidine kinase/response regulator systems BtsS/BtsR and YpdA/YpdB (PyrS/PyrR), respectively, when the cells sense pyruvate [27,29–31], whereas *cstA* is induced by nutrient limitation in the stationary phase [26,32]. There are some monocarboxylate transporters that have broader substrate specificity and can also transport pyruvate: MctP in *Rhizobium leguminosarum* [33], MctC in *Corynebacterium glutamicum* [34], and PftAB in *Bacillus subtilis*, which is activated by the LytS/LytT two-component system [35], as well as LrgAB in *Streptococcus mutans* [36].

The enteric pathogen *Salmonella* is one of the leading causes of acute diarrheal disease, which affects more than 2 billion people worldwide each year [37]. *S*. Typhimurium was shown to excrete and likewise to reclaim pyruvate [4], as well as to grow on pyruvate as the sole carbon source [38], but no pyruvate transporter has been characterized yet. Homologs of *E. coli* genes *btsT* and *cstA* are found in *S*. Typhimurium, which we designate as *btsT* (locus tag SL1344_4463), previously known as *cstA1* or *yjiY*, and *cstA* (locus tag SL1344_0588). Both genes have been previously described to be involved in peptide utilization and in the colonization of *C. elegans* and mice [39,40]. Wong, et al. [41] investigated the histidine kinase/response regulator system BtsS/BtsR (previously known as YehU/YehT) in *S*. Typhi and Typhimurium and identified *btsT* as a predominantly regulated gene. Finally, an unusually high number of mutations over lineage development accumulated in the *btsSR* operon [42], suggesting that this system is targeted by adaptive evolution and is therefore of potential significance for the pathogen.

Here, we characterized BtsT and CstA as pyruvate transporters of *S*. Typhimurium and evaluated their importance for the pathogen in vitro and in vivo.

2. Materials and Methods

2.1. Strains, Plasmids, and Oligonucleotides

S. Typhimurium and *E. coli* strains as well as plasmids used in this study are listed in Table 1. Oligonucleotide sequences are listed in Supplementary Materials Table S1. Molecular methods followed standard protocols [43] or were implemented according to manufacturer's instructions.

S. Typhimurium SL1344 mutants were first generated in strain LT2 and then transduced with phage P22 to strain SL1344. Clean in-frame deletions of *btsT* and *btsSR* in SL1344 were created by λ-Red recombination [44]. One-step inactivation of *cstA* by insertion of a chromosomal kanamycin resistance cassette with flanking regions (FRT-aminoglycoside phosphotransferase-FRT) was performed as described by Datsenko and Wanner [45]. Gene deletions were checked by colony PCR and confirmed by sequencing. In *S*. Typhimurium M2702, clean in-frame deletion of *btsT* and gene inactivation of *cstA* by a chloramphenicol resistance cassette were performed by double homologous recombination using the pNPTS138-R6KT suicide plasmid as previously described [46,47]. *E. coli* DH5α λ*pir* cells were used for cloning. Plasmid sequences were confirmed by sequencing and transferred into *S*. Typhimurium by conjugation using the *E. coli* WM3064 strain. Double homologous recombination was induced as described before [13]. First, mutants with single-crossover integrations of the whole plasmid were selected on LB agar plates containing kanamycin. Then, the second crossover was induced by addition of 10% (*w/v*) sucrose and kanamycin-sensitive clones were checked by colony PCR. Gene deletions were confirmed by sequencing.

Table 1. Strains and plasmids used in this study. (^{R}—resistance).

Strain or Plasmid	Genotype or Description	Reference
***S.* Typhimurium strains**		
SL1344	Wild type; strep ^{R}	[48]
LT2	Wild type	DSMZ #17058
SL1344 Δ*btsT*	Mutant with in-frame deletion of *btsT* (SL1344_4463); strep ^{R}	this study
SL1344 Δ*cstA*	Mutant with in-frame replacement of *cstA* (SL1344_0588) by a kanamycin resistance cassette; strep ^{R} kan ^{R}	this study
SL1344 Δ*btsT* Δ*cstA*	Mutant with in-frame deletion of *btsT* (SL1344_4463) and replacement of *cstA* (SL1344_0588) by a kanamycin resistance cassette; strep ^{R} kan ^{R}	this study
SL1344 Δ*btsSR*	Mutant with in-frame deletion of *btsS* (SL1344_2137) and *btsR* (SL1344_2136); strep ^{R}	this study
M2702	Non-virulent SL1344 strain, Δ*invG* Δ*ssaV*; strep ^{R}	[49]
M2702 Δ*btsT* Δ*cstA*	Non-virulent mutant with in-frame deletion of *cstA* (SL1344_0588) and replacement of *btsT* (SL1344_4463) by a chloramphenicol resistance cassette; strep ^{R} cm ^{R}	this study
***E. coli*strains**		
DH5α λ*pir*	Cloning strain; *end*A1 *hsdR*17 *glnV*44 *thi*-1 *recA*1 *gyrA*96 *relA*1 φ80′*lac*Δ(*lacZ*)M15 Δ(*lacZYA-argF*)*U*169 *zdg*-232::Tn10 *uidA*::*pir*$^{+}$	[50]
WM3064	Conjugation strain; *thr*B1004 *pro thi rpsL hsdS lacZ* ΔM15 RP4-1360 Δ(*araBAD*)567 Δ*dapA*1341::[*erm pir*]	W. Metcalf, University of Illinois
Plasmids		
pNPTS138-R6KT	Plasmid backbone for in-frame deletions; *mobRP4+*; *sacB*, kan ^{R}	[47]
pNPTS138-R6KT-Δ*cstA*	Plasmid for in-frame deletion of *cstA* in SL1344; kan ^{R}	this study
pNPTS138-R6KT-Δ*btsT*::*cm* ^{R}	Plasmid for in-frame replacement of *btsT* by a chloramphenicol resistance cassette in SL1344; kan ^{R} cm ^{R}	this study
pBBR1-MCS5-*lux*	Plasmid backbone to insert a promoter sequence upstream of *luxCDABE* for a luciferase-based reporter assay; gent ^{R}	[51]
pBBR1-MCS5-P_{btsT}-*lux*	Luciferase-based reporter plasmid with the promoter region of SL1344 *btsT* upstream of *luxCDABE*; gent ^{R}	this study
pBBR1-MCS5-P_{cstA}-*lux*	Luciferase-based reporter plasmid with the promoter region of SL1344 *cstA* upstream of *luxCDABE*; gent ^{R}	this study
pBAD24	Plasmid backbone for expression; amp ^{R}	[52]
pBAD24-*btsT*	Expression plasmid for SL1344 *btsT*; amp ^{R}	this study
pBAD33	Plasmid backbone for expression; cm ^{R}	[52]
pBAD33-*cstA*	Expression plasmid for SL1344 *cstA*; cm ^{R}	this study
pKD46	λ-red recombinase expressing plasmid; amp ^{R}	[45]
pKD4	Template plasmid for kanamycin resistance cassette (FRT-aminoglycoside phosphotransferase-FRT); kan ^{R}	[45]

Complementation of deletion mutants was achieved by expressing the genes from plasmids. To this end, *btsT* and *cstA* were each amplified by PCR from SL1344 genomic DNA and cloned into plasmids pBAD24 and pBAD33, respectively, using restriction enzymes EcoRI and HindIII. Plasmids were transferred into the mutant strains by electroporation and leakiness of the arabinose promoter was sufficient for expression.

2.2. Growth Conditions

S. Typhimurium and *E. coli* strains were grown overnight under agitation (200 rpm) at 37 °C in LB medium (10 g/l tryptone, 5 g/l yeast extract, 10 g/l NaCl). The conjugation strain *E. coli* WM3064 was grown in the presence of 300 µM diaminopimelic acid. If necessary, media were supplemented with 50 µg/mL kanamycin sulfate, 100 µg/mL ampicillin sodium salt, 30 µg/mL chloramphenicol, and/or 20 µg/mL gentamicin sulfate to maintain plasmid(s) in the cells. To measure growth of *S*. Typhimurium strains on different carbon sources, cells were cultivated for 24 h at 37 °C in M9 minimal medium [53] supplemented with 4 µg/mL histidine and the C-sources as indicated. Growth was monitored by measuring the optical density at 600 nm (OD_{600}) over time.

2.3. Luciferase Reporter Assay for the Analysis of btsT and cstA Expression

Expression of *btsT* and *cstA* was determined using a luciferase-based reporter assay. Reporter plasmids for *btsT* or *cstA* expression (pBBR1-MCS5-P_{btsT}-*lux* or pBBR1-MCS5-P_{cstA}-*lux*) were constructed: Promoter regions of *btsT* and *cstA* (500 bp upstream of the start codon) were each amplified by PCR from SL1344 genomic DNA and cloned into the pBBR1-MCS5-*lux* vector, using restriction enzymes XbaI and XhoI. Plasmids were transferred into *S*. Typhimurium strains by electroporation. Cells harboring the reporter plasmid were grown in various media in 96-well plates, inoculated from overnight cultures to a starting OD_{600} of 0.05. Plates were then incubated under constant agitation at 37 °C, and OD_{600} as well as luminescence values were measured at intervals of 10 min for 24 h in a ClarioStar plate reader (BMG). Gene expression was presented in relative light units (RLU) normalized to OD_{600}.

2.4. External Pyruvate Determination

Levels of excreted pyruvate were measured using a procedure adapted from O'Donnell-Tormey et al. [11]. *S*. Typhimurium strains were grown under agitation at 37 °C in LB and growth was monitored. At selected time points, 1 mL samples of supernatant were harvested by centrifugation at 4 °C (10 min, 14,000× *g*). Proteins were precipitated by the addition of 250 µL ice-cold 2 M perchloric acid. After a 5 min incubation on ice, the samples were neutralized with 250 µL 2.5 M potassium bicarbonate, and precipitates were removed by centrifugation (4 °C, 10 min, 14,000× *g*). Pyruvate concentrations of the clear supernatants, diluted 1:5 in 100 mM PIPES buffer (pH 7.5), were determined using an enzymatic assay based on the conversion of pyruvate and NADH + H^+ to lactate by lactate dehydrogenase. The assay was performed as described before [26].

2.5. Pyruvate Uptake Measurement

To determine the uptake of pyruvate by *S*. Typhimurium, a transport assay was performed with radiolabeled pyruvate. Cells were grown under agitation at 37 °C in LB and harvested in mid-log phase. Cells were pelleted at 4 °C, washed twice, and resuspended in transport buffer (1 g/L $(NH_4)_2SO_4$, 10 g/L K_2HPO_4, 4.5 g/l KH_2PO_4, 0.1 g/L $MgSO_4$, pH 6.8) to an absorbance of 5 at 420 nm, equivalent to a total protein concentration of 0.35 mg/mL. Uptake of ^{14}C-pyruvate (55 mCi/mmol, Biotrend, Köln, Germany) was measured at a total substrate concentration of 10 µM at 18 °C. At various time intervals, transport was terminated by the addition of ice-cold stop buffer (100 mM potassium phosphate, pH 6.0, 100 mM LiCl) followed by rapid filtration through membrane filters (MN gf-5, 0.4 µm nitrocellulose, Macherey Nagel, Düren, Germany). The filters were dissolved

in 5 mL scintillation fluid (MP Biomedicals, Eschwege, Germany), and radioactivity was determined in a liquid scintillation analyzer (PerkinElmer, Waltham, MA, USA).

2.6. Motility Assay

Overnight cultures of *S*. Typhimurium were adjusted to an OD_{600} of 1 and 10 µL was inoculated into freshly poured swimming motility plates (10 g/l tryptone, 5 g/l NaCl, 0.3% agar, *w/v*) and incubated at 37 °C for 3 h. Pictures were taken with a EOS M50 camera (Canon, Tokyo, Japan) and images were analyzed using the software ImageJ [54]. The size of the ring was measured, and the size of each ring was expressed relatively to the average size of the wild-type ring.

2.7. Chemotaxis Test

Chemotaxis of *S*. Typhimurium towards different compounds was tested using the plug-in-pond assay [55]. Cells grown in LB were pelleted, resuspended to a final OD_{600} of 0.4 in M9 soft agar (M9 medium with 0.3% agar *w/v*), and poured into a petri dish, in which agar plugs (M9 medium with 1.5% agar, *w*/*v*) containing the test substances had been placed. Plates were incubated at 37 °C for 3 h. Pictures were taken with a EOS M50 camera (Canon, Tokyo, Japan).

2.8. Stress Assay

To test survival under oxidative and nitrosative stress, *S*. Typhimurium cells were grown in LB to an OD_{600} of 1.2, split into groups and either treated with 12.5 mM H_2O_2 for H_2O_2 stress, 250 µM spermine NONOate for NO stress, or with H_2O as a control. After 20 min incubation, catalase was added (for H_2O_2 only), and cells were plated in dilutions on LB to determine CFU. Survival under stress was calculated as the percentage of CFU in relation to the control condition and wild-type values were set to 100%.

2.9. Persister Formation

To investigate the persister formation, *S*. Typhimurium cells were grown in LB to an OD_{600} of 1.2 and diluted to an OD_{600} of 0.05 into fresh LB containing 50 µg/mL gentamicin. Every hour, cells were plated in dilutions on LB agar plates to determine CFU, which represent cells being able to survive the antibiotic treatment by forming persister cells.

2.10. Intramacrophage Antibiotic Survival Assays

S. Typhimurium strains were grown in LB for 16 h. Stationary phase bacteria were opsonized with 8% (*w/v*) mouse serum (Merck, Darmstadt, Germany) for 20 min and added to the bone marrow-derived macrophages at a multiplicity of infection (MOI) of 5. Infection was then synchronized by 5 min centrifugation at 100× *g*. The infected macrophages were incubated for 30 min at 37 °C with 5% CO_2 to allow for phagocytosis to occur. At 30 min following infection, the macrophages were washed three times with PBS, and half of the cells were lysed with 0.1% (vol/vol) Triton X-100 (Merck, Darmstadt, Germany)in PBS. Bacteria were then centrifuged at 16,000× *g* for 2 min at room temperature, following resuspension in PBS. The bacteria were diluted ten-fold in PBS and plated on LB agar to count the number of CFU prior to antibiotic treatment. With regards to the remaining macrophages, the three PBS washes were followed by addition of fresh medium (Dulbecco's modified eagle medium with high glucose (DMEM), 10% (vol/vol) fetal calf serum, 10 mM HEPES, 1 mM sodium pyruvate) containing 100 µg/mL cefotaxime. Cefotaxime was added to test intramacrophage antibiotic survival for 24 h. At 24 h following antibiotic treatment, the cells were washed three times with PBS, then lysed with 0.1% (vol/vol) Triton X-100 in PBS. Bacteria were then centrifuged at 16,000× *g* for 2 min at room temperature, following resuspension in PBS. The bacteria were diluted ten-fold in PBS and plated on LB agar to count the number of CFU following antibiotic treatment. The 24 h survival was expressed as a fold change of wild-type values.

2.11. Infection of Gnotobiotic Mice

All animal experiments were approved by the local authorities (Regierung von Oberbayern). Germ-free C57BL/6J mice and C57BL/6J mice colonized with defined bacterial consortia (OMM^{12}) were obtained from the animal housing facility of the Max von Pettenkofer-Institute (Ludwig-Maximilians-University, Munich, Germany). Mice were housed under germ-free conditions in flexible film isolators (North Kent Plastic Cages, London, UK) or in Han-gnotocages (ZOONLAB, Castrop-Rauxel, Germany). The mice were supplied with autoclaved ddH_2O and Mouse-Breeding complete feed for mice (Ssniff) ad libitum. For all experiments, female and male mice between 6 and 15 weeks were used, and animals were randomly assigned to experimental groups. Mice were not single housed and were kept in groups of 3–5 mice per cage during the experiment. All animals were scored twice daily for their health status.

For generation of the ASF mouse line, germ-free C57BL/6J mice were inoculated with a mixture of ASF^3 (ASF356, ASF361, ASF519). Mice were inoculated twice (72 h apart) with the bacterial mixtures (frozen glycerol stocks) by gavage (50 µL orally, 100 µL rectally). Mice were housed under germ-free conditions and were used 12 days post inoculation for experiments to ensure stable colonization of the consortium.

For infection experiments with virulent *S*. Typhimurium SL1344, OMM^{12} mice were treated with streptomycin by oral gavage with 50 µL of 500 mg/mL streptomycin one day before infection. For infection experiments with avirulent *S*. Typhimurium M2702, OMM^{12} and ASF^3 mice were not treated with streptomycin before infection. For all infection experiments, both *S*. Typhimurium wild-type and mutant cells were grown on MacConkey agar plates (Oxoid) containing streptomycin (50 mg/mL) at 37 °C. One colony was re-suspended in 5 mL LB containing 0.3 M NaCl and grown for 12 h at 37 °C on a wheel rotor. A subculture (1:20 dilution) was prepared in fresh LB containing 0.3 M NaCl and incubated for further 4 h. Bacteria were washed with ice-cold sterile PBS, pelleted, and re-suspended in fresh PBS. *S*. Typhimurium wild-type and mutant cells were mixed in a 1:1 ratio adjusted by OD_{600}. Mice were infected with the *S*. Typhimurium mix by oral gavage with 50 µL of bacterial suspension (approximately 4×10^6 CFU).

S. Typhimurium total loads in feces were determined on the first day after infection by plating on MacConkey agar with streptomycin (50 mg/mL). All mice were sacrificed by cervical dislocation four days after infection, and *S*. Typhimurium total loads in fecal and cecal contents, as well as from lymph nodes, spleen, and liver were determined by plating on MacConkey agar with streptomycin (50 mg/mL). From each plate, 50 colonies were picked onto MacConkey agar plates with streptomycin (50 mg/mL) and chloramphenicol (30 mg/mL) for M2702 mutants or kanamycin (30 mg/mL) for SL1344 mutants to determine the competitive index between wild-type and mutant strains.

3. Results and Discussion

3.1. S. Typhimurium Possesses Two Pyruvate Transporters, BtsT and CstA

Based on homology search, *S*. Typhimurium has two genes coding for putative pyruvate transporters: *btsT* (locus tag SL1344_4463) codes for a 77 kDa transporter protein that shares 96.6% identity with the *E. coli* BtsT, according to the online tool Clustal Omega [56]. *S*. Typhimurium *cstA* (locus tag SL1344_0588) codes for a 75 kDa transporter protein that shares 97.1% identity with the *E. coli* CstA. The genetic contexts of *btsT* and *cstA* are illustrated in Figure 1A. Both transporters belong to the CstA family (transporter classification: [TC] 2. A.114) [57] with at least 16 predicted transmembrane domains [58] and share 60.3% identity and 72.8% similarity with each other at 97.2% coverage, as illustrated in Figure 1B.

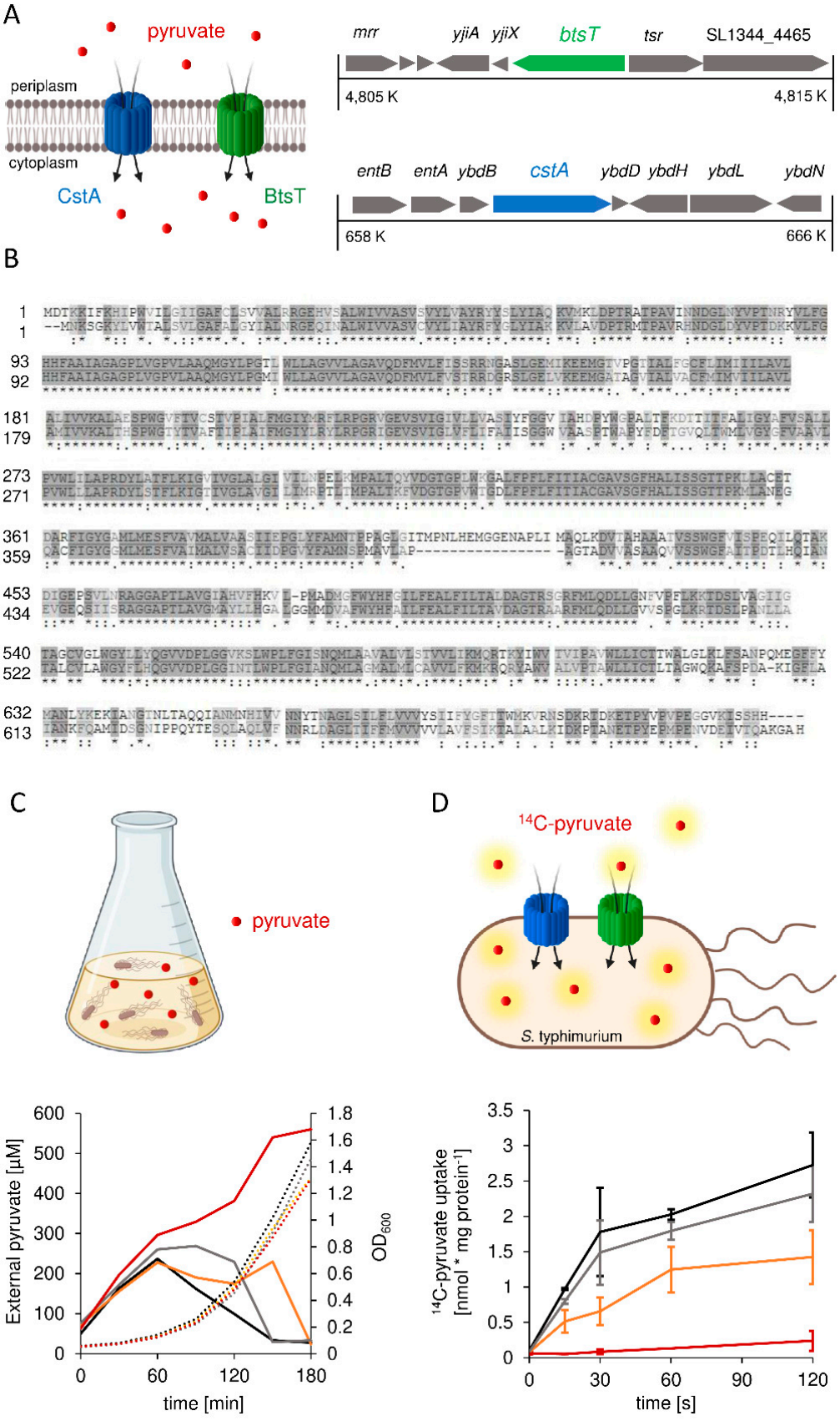

Figure 1. *S.* Typhimurium possesses two pyruvate transporters, BtsT and CstA. (**A**) Schematic illustration of the two transporters BtsT and CstA in *S.* Typhimurium responsible for the uptake of

pyruvate and the genetic context of their genes (*btsT* (SL1344_4463), *cstA* (SL1344_0588)). (**B**) Protein sequence alignment of BtsT (upper line) and CstA (lower line), created with the online tool Clustal Omega. (**C**) Alterations of the pyruvate concentration in LB medium (solid lines) owing to overflow and uptake during growth (dotted lines) of *S*. Typhimurium SL1344 wild-type cells (black), Δ*btsT* mutant (yellow), Δ*cstA* mutant (grey), and Δ*btsT*Δ*cstA* mutant (red). Samples were taken every 20 min. (**D**) Time course of [^{14}C]-pyruvate (10 µM) uptake by intact cells at 18 °C: SL1344 wild-type mutant (black), Δ*btsT* mutant (yellow), Δ*cstA* mutant (grey), and Δ*btsT*Δ*cstA* mutant (red). Error bars represent the standard deviations of the mean of three individual experiments. All illustrations were created with BioRender.

Gamma-proteobacteria excrete pyruvate when grown in amino acid-rich media, such as LB, owing to an overflow metabolism [4–6]. We measured the external pyruvate concentration during the growth of wild-type *S*. Typhimurium in LB (Figure 1C). At the beginning of exponential growth, the pyruvate concentration in the LB medium increased from 50 to 240 µM, followed by a rapid decrease back to the initial pyruvate concentration. For the double deletion mutant Δ*btsT*Δ*cstA*, we monitored the same pyruvate excretion as the wild-type cells but did not observe any subsequent decrease in the external pyruvate concentration; on the contrary, the concentration increased further, reaching 560 µM (Figure 1C). This indicates that the Δ*btsT*Δ*cstA* mutant did not reclaim pyruvate after excretion, which then accumulated in the medium. The Δ*btsT* and Δ*cstA* single deletion mutants both showed an increase and a decrease in external pyruvate concentration, similar to the wild type. However, it took longer for the pyruvate to be fully taken up in both single mutants, suggesting that both transporters function in a complementary manner.

To further confirm that BtsT and CstA are the only pyruvate transporters in *S*. Typhimurium, we performed transport experiments with radiolabeled pyruvate and intact cells. To avoid rapid metabolization, all assays were performed at 18 °C. For wild-type *S*. Typhimurium, we monitored the uptake of radiolabeled pyruvate over time (Figure 1D), with an initial uptake rate of 3.5 nmol per mg protein per minute, whereas for the double deletion mutant Δ*btsT*Δ*cstA*, no transport of radiolabeled pyruvate was observed (Figure 1D). Both single deletion mutants were able to take up pyruvate, but at a decreased rate (Figure 1D). For BtsT (Δ*cstA* mutant), we determined an initial uptake rate of 2.96 nmol pyruvate per mg per min, whereas the initial uptake rate for CstA (Δ*btsT* mutant) was 1.24 nmol per mg per min. This indicates that BtsT and CstA transport pyruvate in a complementary manner in *S*. Typhimurium.

3.2. Expression of btsT Is Activated by the Histidine Kinase Response Regulator System BtsS/BtsR in the Presence of Pyruvate, whereas Expression of cstA Is Dependent on the Growth Phase

To investigate growth-dependent *btsT* and *cstA* activation, we used luciferase-based reporter strains (Figure 2A). Cells were grown in LB medium, and a sharp *btsT* expression peak was observed at the beginning of the exponential growth phase (Figure 2C). This expression pattern is very similar to that observed in *E. coli* [29,30]. Expression of *cstA* started at the beginning of the stationary phase (Figure 2D). This expression pattern was similar for *E. coli cstA* and was explained by the induction of *cstA* under nutrient limitation as an effect of at least two regulators: cAMP-CRP and Fis [26,32]. In comparison, the maximal expression of *cstA* was about an order of magnitude higher than the expression of *btsT*.

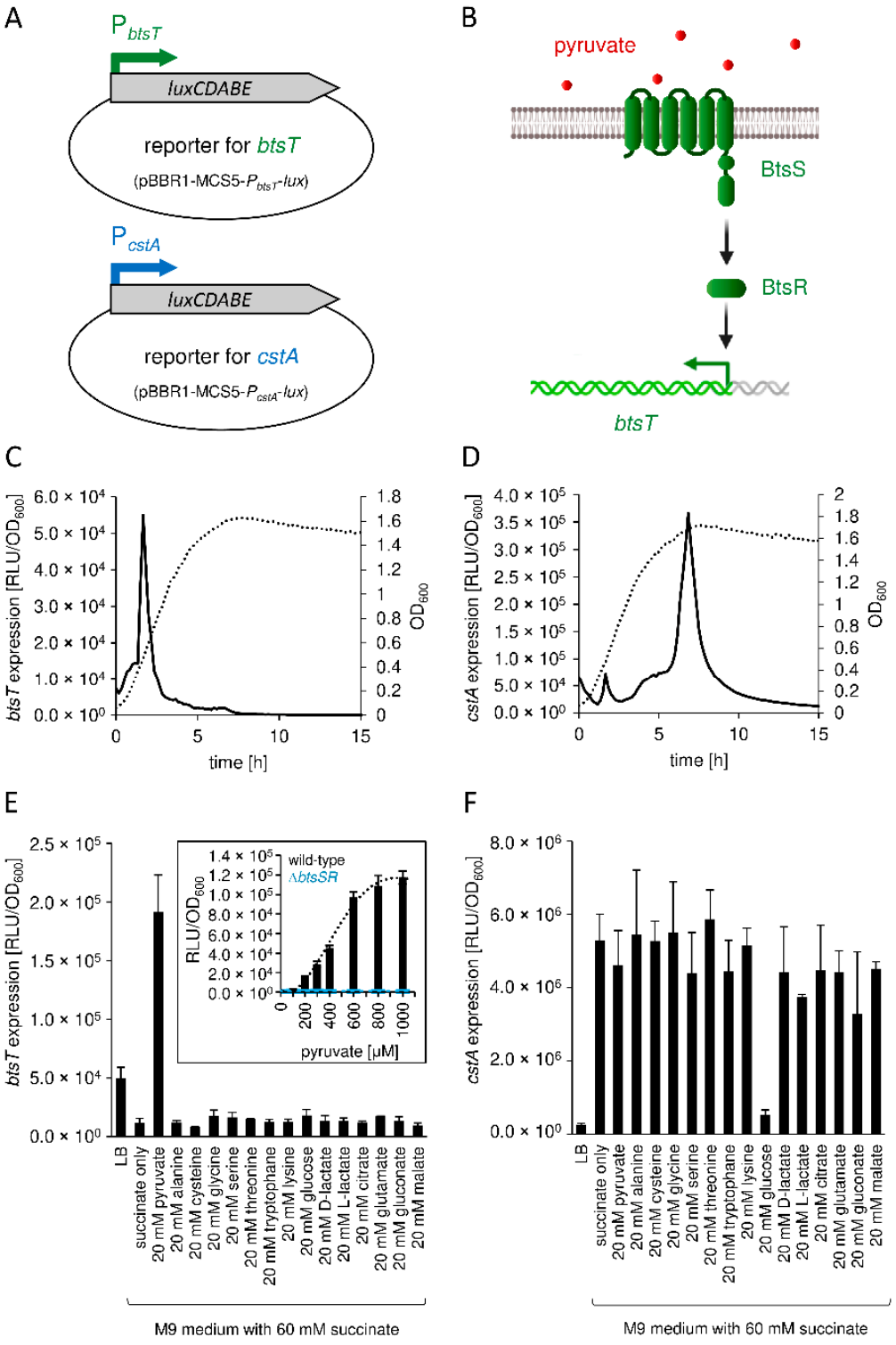

Figure 2. Expression of *btsT* and *cstA* in *S.* Typhimurium. (**A**) Schematic illustration of the luciferase-based, low copy reporter plasmids to monitor *btsT* (pBBR1-MCS5-P_{btsT}-*lux*) and *cstA* (pBBR1-MCS5-P_{cstA}-*lux*) expression. (**B**) Schematic illustration of the two-component system BtsS/BtsR in *S.* Typhimurium, with the histidine kinase BtsS sensing pyruvate and the response regulator BtsR inducing *btsT*. (**C**) Expression of *btsT* in *S.* Typhimurium SL1344 (pBBR1-MCS5-P_{btsT}-*lux*) during growth in LB medium at 37 °C. Luminescence (RLU normalized to OD_{600} = 1) (solid line) and growth (OD_{600})

(dotted line) were measured over time in a plate reader. The graphs show the means of three independent replicates; the standard deviations were below 10%. (**D**) Expression of *cstA* in S. Typhimurium SL1344 (pBBR1-MCS5-P_{cstA}-*lux*) during growth in LB medium. Experimental set-up as in (**C**); OD_{600} (dotted line), RLU per OD_{600} (solid line). The graphs show the means of three independent replicates; the standard deviations were below 10%. (**E**) Expression of *btsT* in SL1344 (pBBR1-MCS5-P_{btsT}-*lux*) grown in M9 minimal medium supplemented with 60 mM succinate and the indicated C-sources, each at 20 mM. Experimental set-up as in (**C**). The maximal RLUs per OD_{600} served as the measure for *btsT* expression. The value of the basal activation in the presence of succinate was subtracted. Inset: Expression of *btsT* in wild-type (black) or Δ*btsSR* (blue) cells as a function of pyruvate concentration. Cells were grown in M9 minimal medium with 60 mM succinate and different concentrations of pyruvate. The value of the basal activation in the presence of succinate was subtracted. (**F**) Expression of *cstA* in SL1344 (pBBR1-MCS5-P_{cstA}-*lux*) grown in M9 minimal medium. Experimental set-up as in (**E**). (**E**,**F**) Error bars represent the standard deviations of the mean of three independent replicates. Illustrations were partly created with BioRender.

We then measured the expression of *btsT* and *cstA* in cells grown in minimal medium containing different carbon (C) sources. Expression of *btsT* was exclusively activated in cells grown in minimal medium with pyruvate and barely in the presence of other compounds, such as amino acids or different carboxylic acids (Figure 2E). To further analyze the activation of *btsT* expression by pyruvate, cells were grown in minimal medium with different pyruvate concentrations (and 60 mM succinate as the basic C-source for growth, for which the activation value was subtracted). We monitored the concentration-dependent activation of *btsT* by pyruvate, with a threshold concentration of 200 µM required for induction and saturation of *btsT* expression at approximately 1 mM (inset panel in Figure 2E). The pyruvate concentration that resulted in half-maximal *btsT* expression was estimated to be 450 µM. In *E. coli*, *btsT* expression was shown to be activated by the LytS/LytTR-type two-component system BtsS/BtsR upon sensing pyruvate [30,59]. To test whether the BtsS/BtsR system is required for *btsT* activation in *S*. Typhimurium, we created a double deletion mutant lacking *btsS*, locus tag SL1344_2137, and *btsR*, locus tag SL1344_2136 (mutant Δ*btsSR*). Indeed, we could not detect *btsT* expression in the Δ*btsSR* mutant: In contrast to the wild-type cells, in which *btsT* expression increased with an increase of the pyruvate concentration, *btsT* expression was completely absent in Δ*btsSR* cells, independent of the pyruvate concentration (inset panel in Figure 2E). Additionally, in LB medium, no *btsT* expression at all could be observed in Δ*btsSR* cells (Supplementary Materials Figure S1). This result is consistent with the findings of Wong et al. [41]. We conclude that the transcriptional activation of *btsT* in *S*. Typhimurium follows the same pattern as that in *E. coli*, and that the pyruvate sensing BtsS/BtsR system activates *btsT* expression to mediate rapid uptake of the compound by BtsT (illustrated in Figure 2B).

In contrast to *btsT*, high expression of *cstA* was observed in cells independent of the C-source (Figure 2F). Expression of *cstA* was lower when cells were grown in amino acid-rich LB medium and in glucose-containing minimal medium, indicating a control by nutrient availability and catabolite repression. Indeed, *cstA* expression was always highest in stationary phase cells.

We also analyzed the expression of *btsT* and *cstA* in mutants with deletions of either *btsT*, *cstA*, or both *btsT* and *cstA* grown in LB medium, using cells transformed with reporter plasmids for *btsT* and *cstA* (Supplementary Materials Figure S1). We found a 12-fold upregulation of *btsT* in the Δ*btsT* mutant and a 50-fold upregulation in the Δ*btsT*Δ*cstA* mutant compared to that in the wild-type cells (Supplementary Materials Figure S1C). A similar feedback regulation was observed for *btsT* in the pathogen *Vibrio campbellii* [13], but the exact mechanism is unknown. In Δ*cstA* cells, the expression pattern of *btsT* over time was the same as that in the wild-type cells (Supplementary Materials Figure S1C). Moreover, the pattern and level of *cstA* expression in all mutants were identical to those in the wild-type cells (Supplementary Materials Figure S1B).

We concluded that *btsT* expression is activated by pyruvate, whereas *cstA* expression is induced in stationary phase and repressed by glucose.

3.3. Pyruvate Uptake by BtsT and CstA Is Required for Growth on Pyruvate and Chemotaxis to Pyruvate

In the next step, we investigated the biological impact of pyruvate uptake by BtsT and CstA in *S*. Typhimurium through phenotypical characterization of the Δ*btsT*Δ*cstA* mutant in comparison to the wild-type cells.

The *S*. Typhimurium Δ*btsT*Δ*cstA* deletion mutant was unable to grow on pyruvate as the sole C-source (Figure 3) but grew on other C-sources, such as glucose, or in complex media, such as LB (Supplementary Materials Figure S2A). Full complementation of the double deletion mutant Δ*btsT*Δ*cstA* was achieved by expressing both *btsT* and *cstA in trans* (Figure 3). The single deletion mutant Δ*btsT* was able to grow on pyruvate, although not as well as the wild-type cells, whereas the single deletion mutant Δ*cstA* grew on pyruvate similarly to the wild-type cells (Supplementary Materials Figure S2B). Expression of *btsT* alone was sufficient to restore growth almost to the level of wild-type cells, whereas expression of *cstA* alone could only partially restore growth (Figure 3).

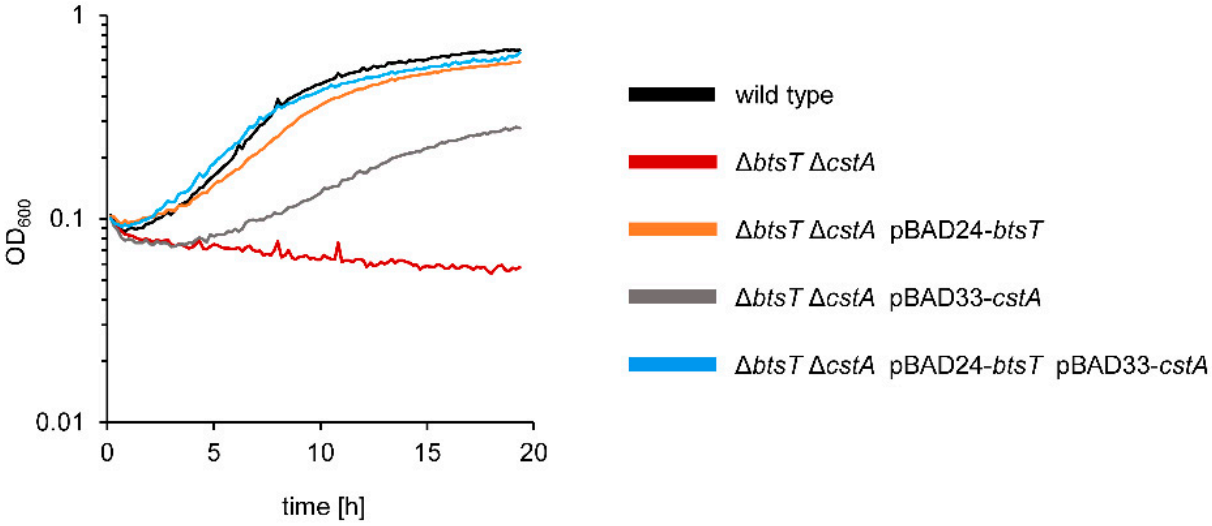

Figure 3. *S*. Typhimurium mutant Δ*btsT*Δ*cstA* is unable to grow on pyruvate. SL1344 wild-type cells and Δ*btsT*Δ*cstA* mutant harboring the indicated plasmid(s) were grown in M9 minimal medium with 60 mM pyruvate in a plate reader at 37 °C.

We then analyzed the chemotactic behavior of wild-type and Δ*btsT*Δ*cstA S*. Typhimurium cells using the plug-in-pond assay [55], in which cells are mixed with soft agar and poured into a petri dish containing agar plugs with potential attractants (Figure 4A). When the cells respond chemotactically to an attractant, a ring of clustered cells is visible around the agar plug. For wild-type *S*. Typhimurium, we observed chemotaxis to pyruvate by a clearly visible ring of accumulating cells (Figure 4A). In contrast, no ring was found in the Δ*btsT*Δ*cstA* mutant, indicating the loss of chemotaxis to pyruvate. This phenotype could be complemented by expressing *btsT* and *cstA in trans* (Supplementary Materials Figure S3).

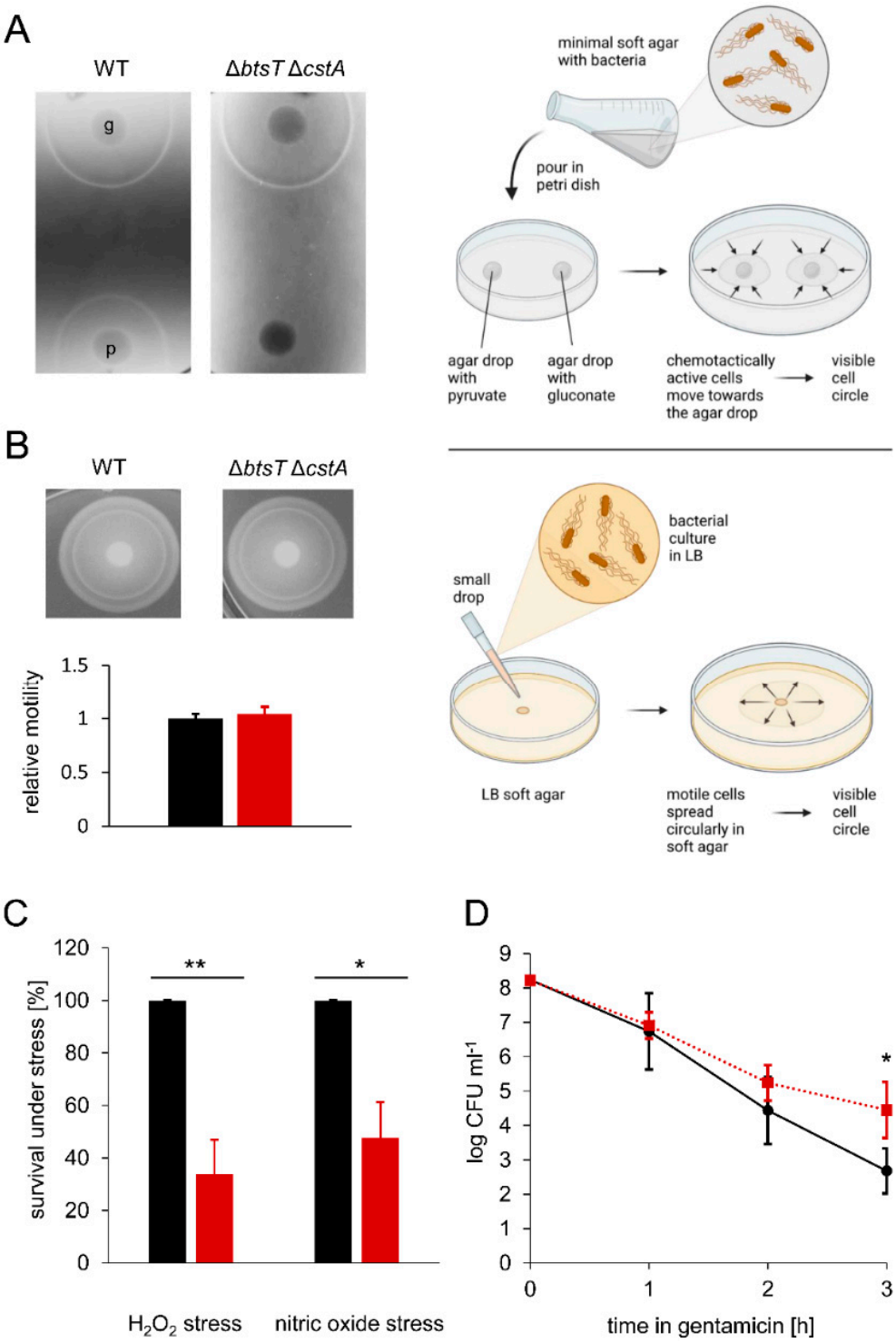

Figure 4. In vitro phenotypes of *S*. Typhimurium Δ*btsT*Δ*cstA* mutant. (**A**) Chemotaxis assay with schematic illustration: Chemotaxis was tested by mixing SL1344 wild-type (left) and Δ*btsT*Δ*cstA* (right) cells with 0.3% (*w/v*) M9 soft agar and pouring them over 1.5% (*w/v*) M9 agar plugs containing either 50 mM gluconate (g) or 50 mM pyruvate (p). Plates were incubated at 37 °C for 4 h, and the pictures are representative of three independent experiments. (**B**) Swimming motility assay with schematic illustration: Motility of SL1344 wild-type (left, black) and Δ*btsT*Δ*cstA* (right, red) cells was tested by spotting equal numbers of cells on 0.3% (*w/v*) LB soft agar, incubating the plates at 37 °C for

3 h, and measuring the cell ring diameter with the software ImageJ [54]. Images of rings are representative of four independent experiments and relative motility was determined in relation to the mean diameter of the wild-type ring. (**C**) Oxidative and nitrosative stress tests: SL1344 wild-type (black) and Δ*btsT*Δ*cstA* (red) cells were grown in LB medium to OD_{600} = 1.2, split in two groups and exposed to 12.5 mM H_2O_2 or 250 µM spermine NONOate or H_2O as control. After 20 min of incubation, catalase was added to the H_2O_2 treated group, and cells were plated in dilutions on LB plates to determine CFU. Survival under stress was calculated as the percentage of CFU in relation to the control condition, and wild-type values were set to 100%. Error bars represent the standard deviations of the mean of three independent experiments. (**D**) Formation of antibiotic-induced persister cells: SL1344 wild-type (black, circles) and Δ*btsT*Δ*cstA* (red, squares) cells were grown in LB medium to OD_{600} = 1.2 and diluted to OD_{600} = 0.05 into fresh LB containing 50 µg/mL gentamicin. Every hour, cells were plated in dilutions on LB plates to determine CFU. Error bars represent the standard deviations of the mean of three independent experiments. For statistical analysis, independent t-tests were performed using Excel (version 2207, Microsoft, Redmond, WA, USA). * $p < 0.05$, ** $p < 0.01$. All illustrations were created with BioRender.

To ensure that this defect did not result from impaired swimming motility, we analyzed the swimming motility of wild-type and mutant cells in LB soft agar, as illustrated in Figure 4B, and could not see any difference; both strains moved in the soft agar circularly away from the inoculation spot, where the cells had been dropped before, and formed visible rings of cells after 3 h of incubation (Figure 4B). The measurement of the ring sizes clearly shows that both strains could swim to the same extent. This finding is important, as it was previously claimed that motility and flagella biosynthesis are impaired in an *S*. Typhimurium Δ*btsT* mutant [39]. We could not confirm these previously published results, neither for the double deletion mutant Δ*btsT*Δ*cstA* (Figure 4B) nor for the single deletion mutants Δ*btsT* or Δ*cstA* (Supplementary Materials Figure S4). It should be noted that Garai et al. [39] did not report the successful complementation of deletion mutants.

Importantly, chemotaxis to other substances, such as gluconate, was not affected by deletions of *btsT* and *cstA*, as the double deletion mutant showed the same ring of accumulated cells as the wild-type cells (Figure 4A). These results indicate that pyruvate uptake is necessary for chemotaxis to pyruvate, leading to the conclusion that the chemotactic response must be activated by intracellular pyruvate. Similarly, for other gamma-proteobacteria it was described previously that the deletion of pyruvate transporter gene(s) impairs chemotaxis to pyruvate [13,26]. In *E. coli*, it has been shown that the phosphotransferase system (PTS) can sense pyruvate inside cells and that signals from the PTS are transmitted linearly to the chemotaxis system [60,61]. Thus, we assume that *S*. typhimurium must take up pyruvate, and the PTS monitors intracellular pyruvate levels via the ratio of pyruvate to phosphoenolpyruvate to trigger a chemotactic response to this compound.

3.4. Pyruvate Uptake Is Important to Survive Oxidative Stress, Nitrosative Stress, and Antibiotic Treatment

The production of ROS and nitric oxide (NO) is an important defense mechanism of the host to control the proliferation of intracellular pathogens, such as *S*. Typhimurium [62]. Pyruvate is a known scavenger of ROS [8–10]. Thus, we analyzed the importance of pyruvate uptake by *S*. Typhimurium under ROS and NO stress. We challenged wild-type and Δ*btsT*Δ*cstA S*. Typhimurium by exposing cells to hydrogen peroxide (H_2O_2) and nitrosative stress (NO) for 20 min. We found that the double mutant had a clear disadvantage compared to the wild-type cells (Figure 4C). Only half as many Δ*btsT*Δ*cstA* as wild-type cells were able to survive these stressful conditions, indicating that pyruvate uptake is important for *S*. Typhimurium to cope with oxygen and nitric radicals. We assume that intracellular pyruvate is required as a ROS scavenger and to compensate for the metabolic defects caused by NO. In the host environment, the concentration of H_2O_2 is lower than the concentration tested here, and the effect of the pyruvate uptake systems might be weaker. However, Kröger et al. [63] found a small, but detectable upregulation

of *btsT* and *cstA* under oxidative stress by treating cells for 12 min with a ten-fold lower concentration of H_2O_2 than in our setting, suggesting that the two transporters play a role under oxidative stress.

We also compared *S*. Typhimurium double pyruvate transporter mutant with the wild-type cells under antibiotic stress. Bacterial persisters survive exposure to antibiotics in laboratory media owing to their low metabolic activity and low growth rate [64,65]. We exposed wild-type and Δ*btsT*Δ*cstA S*. Typhimurium cells to gentamicin (50 µg/mL) and monitored the number of colony-forming units (CFU) over time. Only cells able to survive this stress form CFU. We observed a steep initial decrease in CFU for both strains, followed by a slower killing rate in the case of the mutant, which typically reveals the persister fraction of the population (Figure 4D). We hypothesize that the deficit in pyruvate uptake results in cells with lower metabolic activity, which are less harmed by antibiotic stress. Similarly, in *E. coli*, a pyruvate sensing network that tightly regulates the expression of two pyruvate transporters is important for balancing the physiological state of the entire population and increasing the fitness of single cells [66]. An *E. coli* mutant that is unable to produce the two major pyruvate transporters forms more persister cells than the wild-type cells [66]. We also quantified the persister fractions surviving other antibiotics, such as ampicillin and cefotaxime, in *S*. Typhimurium, but did not find any difference between the wild-type and mutant cells (data not shown).

3.5. Pyruvate Uptake Is Important to Recover from Intra-Macrophage Antibiotic Treatment

The facultative intracellular pathogen *S*. Typhimurium forms non-growing antibiotic persisters at high levels within macrophages [67], which have a different physiological state than persisters formed in vitro [68]. Therefore, we investigated whether pyruvate uptake plays a role in intra-macrophage antibiotic survival. As illustrated in Figure 5A, macrophages were infected with wild-type or Δ*btsT*Δ*cstA S*. Typhimurium cells, and after 30 min of incubation, the bacteria were recovered following lysis of half of the infected macrophages, and the number of surviving bacteria was determined by plating and counting CFU. The other half of the infected macrophages was challenged with cefotaxime for 24 h. After this treatment, the number of bacteria was determined, as described above. By comparing the number of CFU before and after cefotaxime treatment, the survival of *S*. Typhimurium cells in the macrophages during antibiotic stress was calculated.

The Δ*btsT*Δ*cstA* mutant had impaired survival to cefotaxime treatment within the macrophages compared to the wild-type cells (Figure 5A). These results show that pyruvate uptake plays a role in *S*. Typhimurium survival in cefotaxime-treated macrophages. The difference between wild-type and mutant cells in the intramacrophage survival assay was rather small. Although the macrophage environment and the in vitro conditions are not really comparable, we also measured only a low and homogeneous activation of *btsT* during growth of *S*. Typhimurium in InSPI2 medium [69] (Supplementary Materials Figure S5). For VBNC *E. coli* cells, we have previously shown that pyruvate is the first substrate taken up when cells return to the culturable state [15], and pyruvate is likewise important for the resuscitation of *S*. Typhimurium [16]. We propose that the uptake of pyruvate is important for the regrowth of *S*. Typhimurium from the persister state out of macrophages.

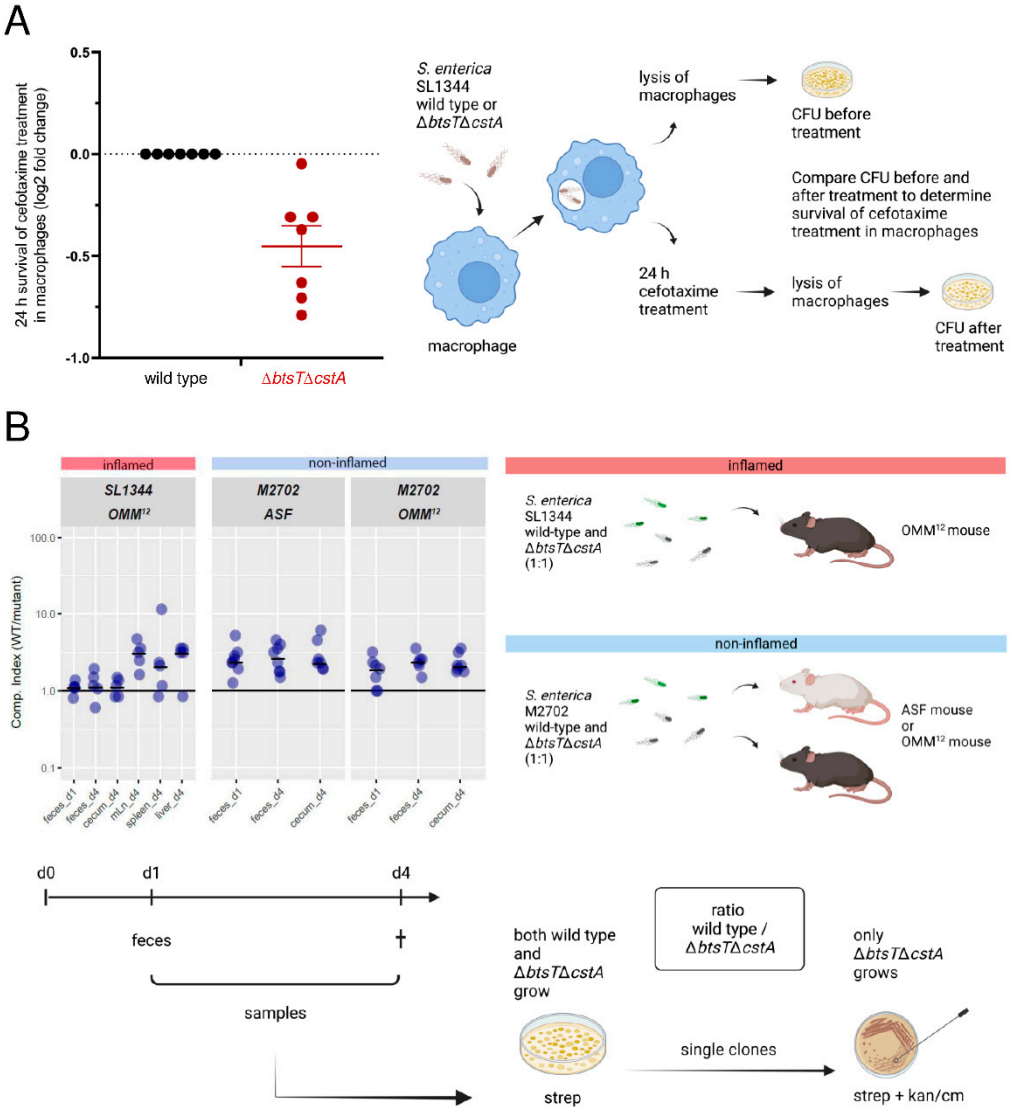

Figure 5. In vivo phenotypes of *S.* Typhimurium Δ*btsT*Δ*cstA* mutant. (**A**) Intra-macrophage antibiotic survival assay with schematic illustration: Bone marrow-derived macrophages were infected with either SL1344 wild-type (black) or Δ*btsT*Δ*cstA* (red) stationary-phase bacteria. After 30 min, one part of the macrophages was lysed, and the recovered bacteria were plated to determine CFUs. The other part of infected macrophages was treated with cefotaxime and incubated for 24 h, followed by macrophage lysis and plating to determine CFUs. The number of CFU after antibiotic treatment was set in relation to the number of CFU prior to antibiotic treatment. The 24 h antibiotic survival was then expressed as a fold-change of wild-type values. Using the paired student t-test on the 7 biological repeats a *p*-value of 2.83×10^{-6} was determined. (**B**) Competition assay in gnotobiotic mice with schematic illustration: OMM^{12} or ASF mice were inoculated with both wild-type and Δ*btsT*Δ*cstA* cells (ratio 1:1) of the virulent strain SL1344 or the avirulent strain M2702, respectively. One day after infection, fecal samples were collected and plated on MacConkey agar with streptomycin, which selects for all *S. enterica* cells owing to natural resistance. Four days after infection, all mice were sacrificed and samples from feces, cecum, lymph nodes, spleen, and liver were plated on MacConkey agar with streptomycin. Single colonies were streaked on MacConkey agar with streptomycin plus kanamycin (for SL1344) or chloramphenicol (for M2702) to select for Δ*btsT*Δ*cstA* cells. By this means, the competitive index could be determined, i.e., the ratio between wild-type and Δ*btsT*Δ*cstA* cells. All illustrations were created with BioRender.

3.6. Mutants Lacking Pyruvate Transporters Show a Slight Disadvantage in Colonization and Systemic Infection of Gnotobiotic Mice

S. Typhimurium colonizes the gut of its host, leading to inflammation, but it can also disseminate inside macrophages to other organs and cause systemic infection. In mice infected with *S*. Typhimurium, pyruvate concentrations were found to be significantly higher than those in uninfected mice [25]. Therefore, we investigated how the double deletion of pyruvate transporter genes in *S*. Typhimurium affects the colonization of gnotobiotic mice, as illustrated in Figure 5B. First, we used OMM^{12} mice, which stably carry a minimal consortium of 12 bacterial strains [70]. To reduce colonization resistance and allow infection by *S*. Typhimurium SL1344, OMM^{12} mice were pretreated with streptomycin. In a competition assay, OMM^{12} mice were infected with a 1:1 mixture of both SL1344 wild-type and Δ*btsT*Δ*cstA* mutant cells. One day after infection, fecal samples were taken, and four days after infection, mice were sacrificed, and samples from the cecum, feces, and different organs were collected. Notably, mice developed gut inflammation owing to infection with virulent *S*. Typhimurium SL1344. To determine the number of *S*. Typhimurium bacteria, samples were plated on streptomycin, an antibiotic that *S*. Typhimurium is resistant to. From these plates, 50 colonies were picked and streaked on kanamycin to determine the proportion of these cells as Δ*btsT*Δ*cstA* mutants, as only mutant cells carry the kanamycin resistance cassette. Thus, the competitive index, that is the ratio between the wild-type and mutant cells, was determined.

We found that, in all samples, the average competitive index was higher than 1, indicating that more SL1344 wild-type than Δ*btsT*Δ*cstA* cells were present (Figure 5B). In fecal samples, both one day and four days post infection, as well as in cecum samples, the competitive index was just slightly higher than 1, indicating that both the wild-type and mutant cells colonized equally well. However, in the lymph nodes, spleen, and liver, organs to which *S*. Typhimurium disseminates to cause systemic infection, an average competitive index of approximately 3 indicated a three times higher number of wild-type than mutant cells. These findings indicate that *S*. Typhimurium SL1344 Δ*btsT*Δ*cstA* cells, which cannot take up pyruvate, have a disadvantage in the systemic infection of OMM^{12} mice.

It has been shown that, in mice colonized with a different minimal bacterial consortium, the so-called altered Schaedler flora (ASF mice), more nutrients are available, *S*. Typhimurium *btsT* is upregulated, and no colonization resistance against the pathogen is provided [71]. We also investigated the competition between Δ*btsT*Δ*cstA* mutant and wild-type cells in these mice. Infection with SL1344 bacteria induces severe colitis in ASF mice that lack a sufficiently protective microbiota. Therefore, we generated deletions of both *btsT* and *cstA* in a non-virulent *S*. Typhimurium strain, M2702 (lacking the two virulence factors *invG* and *ssaV*), with the final Δ*btsT*Δ*cstA* mutant carrying a chloramphenicol resistance cassette to distinguish it from the wild-type cells. Competition experiments were performed as previously described and are illustrated in Figure 5B, with three differences compared to infection experiments with the virulent *S*. Typhimurium strain: no antibiotic treatment was carried out before infection and chloramphenicol instead of kanamycin was used to select for the mutant cells. Moreover, no organ samples from the lymph nodes, spleen, or liver were taken, as the non-virulent *S*. Typhimurium M2702 bacteria are able to colonize but not to systemically infect the mice.

In ASF mice, the average competitive index was higher than 1 for all samples (Figure 5B). Approximately three times more wild-type than Δ*btsT*Δ*cstA* mutant cells were counted in fecal and cecum samples. This indicates that avirulent *S*. Typhimurium bacteria unable to take up pyruvate had a disadvantage in colonizing the non-inflamed gut of ASF mice. Although the competitive index numbers were rather subtle, there was a clear difference between the wild-type and the mutant cells in samples taken from the cecum and feces. This trend was equally observable in the non-inflamed environment of OMM^{12} mice, indicating that the colonization differences of *S*. Typhimurium were not microbiota dependent.

We assume that for the non-virulent M2702 bacteria, the advantage of the wild-type cells might have already come to light in the gut, as they compete only there with the mutants. For the virulent SL1344 bacteria, in contrast, the advantage of wild-type cells could have led to more cells entering macrophages and traveling to organs such as lymph nodes or the liver. This could explain why the differences between wild-type and mutant cells regarding gut colonization were only found under non-virulent conditions. The microbiota did not show any influence on the competition between wild-type and mutant cells. Another explanation could be that the difference between the avirulent wild-type and mutant cells resulted from the different environment in the non-inflamed gut, where other nutrients are available. We conclude that pyruvate uptake delivers a small advantage for *S*. Typhimurium in both colonization and—if the cells are able to—systemic infection of gnotobiotic mice.

We expected to see a stronger disadvantage of the *S*. Typhimurium pyruvate transporter mutant in the in vivo experiments. However, extreme phenotypes cannot be expected in vivo by preventing the uptake of one compound. In macrophages, pyruvate uptake might help deal with oxidative stress, but there are other factors that are important and overlay this effect. In the gut, pyruvate is present, even more in the inflamed gut and during *Salmonella* infection, but the question is, if it is even available and necessary in this state for *S*. Typhimurium, so that it can depict an advantage. The intestine and its microbiome are a complex ecosystem with interaction networks of numerous bacterial communities and metabolites in distinct niches [72]. The minimal bacterial consortia used in this study are still what their name says, minimal, providing at most a model intestinal ecosystem [73], and their metabolic interactions are not yet fully solved [74]. We must consider that the importance of pyruvate putatively did not entirely come to light here, and both wild-type and mutant bacteria were not under pressure to give pyruvate uptake a strong impact on fitness and virulence, as they may have been in a more complex community.

4. Conclusions

This study is the first to describe pyruvate sensing and transport in *Salmonella* and its importance for the cells also beyond metabolism. Especially for relevant pathogens, it is very important to gain more and detailed knowledge about how they use specific compounds and what happens, if this usage is impaired. This can in the end not only help to better understand and fight frequent pathogens, but also to solve the complex puzzle of microbial interactions, niche formation, infection, and resistance in the intestine, that is still at the beginning of being understood.

It is quite remarkable that the lack of pyruvate uptake has consequences not only for the utilization of this primary metabolite, but also for chemotaxis and survival in oxidative, nitrosative, and gentamicin stress in *S*. Typhimurium. On the other hand, compared with the wild-type cells, the pyruvate transporter deletion mutant had a more moderate disadvantage in survival in macrophages or in colonization of the mouse intestine and systemic infection. The in vivo results reflect the complexity of the gut ecosystem and the diversity of factors leading to colonization and infection by pathogens such as *S*. Typhimurium. However, it is the transport proteins in particular that play a very crucial role in microbial communities, allowing for cross-feeding, but also achieving specificity as to which bacterium takes up which metabolite. This in turn contributes to community structure [74–76].

We and others have characterized pyruvate uptake systems in various gamma-proteobacteria. However, it remains unclear why different bacteria have different numbers of transporters and sensing systems. For *E. coli*, two pyruvate sensing systems and three pyruvate transporters (BtsT, YhjX, and CstA) were identified [26], whereas for *S*. Typhimurium, only one pyruvate sensing system and two pyruvate transporters (BtsT and CstA) were found. In contrast, the fish pathogen *Vibrio campbellii*, which excretes extraordinarily high amounts of pyruvate, harbors only one pyruvate sensing system and one transporter [13]. Moreover,

in contrast to pyruvate uptake systems, no exporter of pyruvate is known in any organism. As numerous bacteria excrete pyruvate, Tremblay et al [24] hypothesized that members of the gut microbiota might excrete pyruvate as a result of overflow metabolism, which then promotes the persistence of pathogens in the intestine. This metabolic cross-feeding of pyruvate was recently shown in another specific microbial community [75]. To gain more detailed knowledge of frequent pathogens on a molecular level regarding sensing systems, transporters, and their biological relevance might at some point tip the scales to understand the underlying functional structures and overcome worldwide burdens, such as severe gastroenteritis.

Supplementary Materials: The following supporting information can be downloaded at: https://www.mdpi.com/article/10.3390/microorganisms10091751/s1, Figure S1: Expression of *btsT* and *cstA* in *S*. Typhimurium mutants; Figure S2: Growth of *S*. Typhimurium mutants; Figure S3: *S*. Typhimurium Δ*btsT*Δ*cstA* mutant lost chemotactic response to pyruvate; Figure S4: Motility of *S*. Typhimurium is not affected by deletions of *btsT* or *cstA*; Figure S5: Expression of *btsT* in *S*. Typhimurium under SPI2-inducing conditions; Table S1: Oligonucleotides used in this study; References [46,47,54,69,77] are cited in the supplementary materials.

Author Contributions: Conceptualization, S.P., S.H., B.S. and K.J.; methodology, S.P., F.D.F., A.S.W., A.L.M., S.H., B.S. and K.J.; validation, S.P., F.D.F., A.S.W., A.L.M., S.H., B.S. and K.J.; formal analysis, S.P., F.D.F., A.S.W. and A.L.M.; investigation, S.P., F.D.F., A.S.W. and A.L.M.; resources, S.H., B.S. and K.J.; writing—original draft preparation, S.P. and K.J.; writing—review and editing, S.P., F.D.F., A.S.W., A.L.M., S.H., B.S. and K.J.; supervision, S.H., B.S. and K.J.; project administration, K.J. and B.S.; funding acquisition, K.J. and B.S. All authors have read and agreed to the published version of the manuscript.

Funding: This research was funded by the Deutsche Forschungsgemeinschaft, project number 395357507-SFB1371 to K.J. and B.S.

Institutional Review Board Statement: The animal study protocol was approved by the Institute Ethics Committee of the Max von Pettenkofer Institute, Ludwig-Maximilians-University, Munich, as well as the local authorities (Regierung von Oberbayern, AZ-55.2-1-54-2532-13-2015 approved 2015 and ROB-55.2-2532.Vet_02-20-84 approved 2020).

Informed Consent Statement: Not applicable.

Data Availability Statement: Not applicable.

Acknowledgments: The authors thank Raphaela Götz for her contribution in strain construction.

Conflicts of Interest: The authors declare no conflict of interest.

References

1. Yang, Y.T.; Bennett, G.N.; San, K.Y. The effects of feed and intracellular pyruvate levels on the redistribution of metabolic fluxes in *Escherichia coli*. *Metab. Eng.* **2001**, *3*, 115–123. [CrossRef] [PubMed]
2. Lowry, O.H.; Carter, J.; Ward, J.B.; Glaser, L. The effect of carbon and nitrogen sources on the level of metabolic intermediates in *Escherichia coli*. *J. Biol. Chem.* **1971**, *246*, 6511–6521. [CrossRef]
3. Snoep, J.L.; de Graef, M.R.; de Mattos, M.J.T.; Neijssel, O.M. Pyruvate catabolism during transient state conditions in chemostat cultures of *Enterococcus faecalis* NCTC 775: Importance of internal pyruvate concentrations and NADH/NAD^+ ratios. *J. Gen. Microbiol.* **1992**, *138*, 2015–2020. [CrossRef] [PubMed]
4. Behr, S.; Brameyer, S.; Witting, M.; Schmitt-Kopplin, P.; Jung, K. Comparative analysis of LytS/LytTR-type histidine kinase/response regulator systems in γ-proteobacteria. *PLoS ONE* **2017**, *12*, e0182993. [CrossRef]
5. Chubukov, V.; Gerosa, L.; Kochanowski, K.; Sauer, U. Coordination of microbial metabolism. *Nat. Rev. Microbiol.* **2014**, *12*, 327–340. [CrossRef]
6. Paczia, N.; Nilgen, A.; Lehmann, T.; Gätgens, J.; Wiechert, W.; Noack, S. Extensive exometabolome analysis reveals extended overflow metabolism in various microorganisms. *Microb. Cell Factories* **2012**, *11*, 122. [CrossRef]
7. Yasid, N.A.; Rolfe, M.D.; Green, J.; Williamson, M.P. Homeostasis of metabolites in *Escherichia coli* on transition from anaerobic to aerobic conditions and the transient secretion of pyruvate. *R. Soc. Open Sci.* **2016**, *3*, 160187. [CrossRef]
8. Constantopoulos, G.; Barranger, J.A. Nonenzymatic decarboxylation of pyruvate. *Anal. Biochem.* **1984**, *139*, 353–358. [CrossRef]
9. Kładna, A.; Marchlewicz, M.; Piechowska, T.; Kruk, I.; Aboul-Enein, H.Y. Reactivity of pyruvic acid and its derivatives towards reactive oxygen species. *Luminescence* **2015**, *30*, 1153–1158. [CrossRef]

10. Varma, S.D.; Hegde, K.; Henein, M. Oxidative damage to mouse lens in culture. Protective effect of pyruvate. *Biochim. Biophys. Acta* **2003**, *1621*, 246–252. [CrossRef]
11. O'Donnell-Tormey, J.; Nathan, C.F.; Lanks, K.; DeBoer, C.J.; de la Harpe, J. Secretion of pyruvate. An antioxidant defense of mammalian cells. *J. Exp. Med.* **1987**, *165*, 500–514. [CrossRef] [PubMed]
12. Dong, K.; Pan, H.; Yang, D.; Rao, L.; Zhao, L.; Wang, Y.; Liao, X. Induction, detection, formation, and resuscitation of viable but non-culturable state microorganisms. *Compr. Rev. Food Sci.* **2020**, *19*, 149–183. [CrossRef] [PubMed]
13. Göing, S.; Gasperotti, A.F.; Yang, Q.; Defoirdt, T.; Jung, K. Insights into a Pyruvate Sensing and Uptake System in *Vibrio campbellii* and Its Importance for Virulence. *J. Bacteriol.* **2021**, *203*, e0029621. [CrossRef]
14. Mizunoe, Y.; Wai, S.N.; Takade, A.; Yoshida, S. Restoration of culturability of starvation-stressed and low-temperature-stressed *Escherichia coli* O157 cells by using H_2O_2-degrading compounds. *Arch. Microbiol.* **1999**, *172*, 63–67. [CrossRef] [PubMed]
15. Vilhena, C.; Kaganovitch, E.; Grünberger, A.; Motz, M.; Forné, I.; Kohlheyer, D.; Jung, K. Importance of pyruvate sensing and transport for the resuscitation of viable but nonculturable *Escherichia coli* K-12. *J. Bacteriol.* **2019**, *201*, e00610-00618. [CrossRef]
16. Liao, H.; Jiang, L.; Zhang, R. Induction of a viable but non-culturable state in *Salmonella Typhimurium* by thermosonication and factors affecting resuscitation. *FEMS Microbiol. Lett.* **2018**, *365*, fnx249. [CrossRef] [PubMed]
17. Bücker, R.; Heroven, A.K.; Becker, J.; Dersch, P.; Wittmann, C. The pyruvate-tricarboxylic acid cycle node: A focal point of virulence control in the enteric pathogen *Yersinia pseudotuberculosis*. *J. Biol. Chem.* **2014**, *289*, 30114–30132. [CrossRef]
18. Schär, J.; Stoll, R.; Schauer, K.; Loeffler, D.I.; Eylert, E.; Joseph, B.; Eisenreich, W.; Fuchs, T.M.; Goebel, W. Pyruvate carboxylase plays a crucial role in carbon metabolism of extra- and intracellularly replicating *Listeria monocytogenes*. *J. Bacteriol.* **2010**, *192*, 1774–1784. [CrossRef] [PubMed]
19. Xie, T.; Pang, R.; Wu, Q.; Zhang, J.; Lei, T.; Li, Y.; Wang, J.; Ding, Y.; Chen, M.; Bai, J. Cold tolerance regulated by the pyruvate metabolism in *Vibrio parahaemolyticus*. *Front. Microbiol.* **2019**, *10*, 178. [CrossRef]
20. Abernathy, J.; Corkill, C.; Hinojosa, C.; Li, X.; Zhou, H. Deletions in the pyruvate pathway of *Salmonella* Typhimurium alter SPI1-mediated gene expression and infectivity. *J. Anim. Sci. Biotechnol.* **2013**, *4*, 5. [CrossRef]
21. van Doorn, C.L.R.; Schouten, G.K.; van Veen, S.; Walburg, K.V.; Esselink, J.J.; Heemskerk, M.T.; Vrieling, F.; Ottenhoff, T.H.M. Pyruvate Dehydrogenase Kinase Inhibitor Dichloroacetate Improves Host Control of *Salmonella enterica* Serovar Typhimurium Infection in Human Macrophages. *Front. Immunol.* **2021**, *12*, 739938. [CrossRef] [PubMed]
22. Goodwine, J.; Gil, J.; Doiron, A.; Valdes, J.; Solis, M.; Higa, A.; Davis, S.; Sauer, K. Pyruvate-depleting conditions induce biofilm dispersion and enhance the efficacy of antibiotics in killing biofilms in vitro and in vivo. *Sci. Rep.* **2019**, *9*, 3763. [CrossRef]
23. Petrova, O.E.; Schurr, J.R.; Schurr, M.J.; Sauer, K. Microcolony formation by the opportunistic pathogen *Pseudomonas aeruginosa* requires pyruvate and pyruvate fermentation. *Mol. Microbiol.* **2012**, *86*, 819–835. [CrossRef] [PubMed]
24. Tremblay, Y.D.N.; Durand, B.A.R.; Hamiot, A.; Martin-Verstraete, I.; Oberkampf, M.; Monot, M.; Dupuy, B. Metabolic adaption to extracellular pyruvate triggers biofilm formation in *Clostridioides difficile*. *ISME J.* **2021**, *15*, 3623–3635. [CrossRef] [PubMed]
25. Anderson, C.J.; Medina, C.B.; Barron, B.J.; Karvelyte, L.; Aaes, T.L.; Lambertz, I.; Perry, J.S.A.; Mehrotra, P.; Gonçalves, A.; Lemeire, K.; et al. Microbes exploit death-induced nutrient release by gut epithelial cells. *Nature* **2021**, *596*, 262–267. [CrossRef]
26. Gasperotti, A.; Göing, S.; Fajardo-Ruiz, E.; Forné, I.; Jung, K. Function and regulation of the pyruvate transporter CstA in *Escherichia coli*. *Int. J. Mol. Sci.* **2020**, *21*, 9068. [CrossRef]
27. Hwang, S.; Choe, D.; Yoo, M.; Cho, S.; Kim, S.C.; Cho, S.; Cho, B.K. Peptide transporter CstA imports pyruvate in *Escherichia coli* K-12. *J. Bacteriol.* **2018**, *200*, e00771-00717. [CrossRef] [PubMed]
28. Kristoficova, I.; Vilhena, C.; Behr, S.; Jung, K. BtsT, a novel and specific pyruvate/H^+ symporter in *Escherichia coli*. *J. Bacteriol.* **2018**, *200*, e00599-00517. [CrossRef]
29. Behr, S.; Fried, L.; Jung, K. Identification of a novel nutrient-sensing histidine kinase/response regulator network in *Escherichia coli*. *J. Bacteriol.* **2014**, *196*, 2023–2029. [CrossRef]
30. Behr, S.; Kristoficova, I.; Witting, M.; Breland, E.J.; Eberly, A.R.; Sachs, C.; Schmitt-Kopplin, P.; Hadjifrangiskou, M.; Jung, K. Identification of a high-affinity pyruvate receptor in *Escherichia coli*. *Sci. Rep.* **2017**, *7*, 1388. [CrossRef]
31. Fried, L.; Behr, S.; Jung, K. Identification of a target gene and activating stimulus for the YpdA/YpdB histidine kinase/response regulator system in *Escherichia coli*. *J. Bacteriol.* **2013**, *195*, 807–815. [CrossRef] [PubMed]
32. Schultz, J.E.; Matin, A. Molecular and functional characterization of a carbon starvation gene of *Escherichia coli*. *J. Mol. Biol.* **1991**, *218*, 129–140. [CrossRef]
33. Hosie, A.H.; Allaway, D.; Poole, P.S. A monocarboxylate permease of *Rhizobium leguminosarum* is the first member of a new subfamily of transporters. *J. Bacteriol.* **2002**, *184*, 5436–5448. [CrossRef]
34. Jolkver, E.; Emer, D.; Ballan, S.; Krämer, R.; Eikmanns, B.J.; Marin, K. Identification and characterization of a bacterial transport system for the uptake of pyruvate, propionate, and acetate in *Corynebacterium glutamicum*. *J. Bacteriol.* **2009**, *191*, 940–948. [CrossRef]
35. Charbonnier, T.; Le Coq, D.; McGovern, S.; Calabre, M.; Delumeau, O.; Aymerich, S.; Jules, M. Molecular and Physiological Logics of the Pyruvate-Induced Response of a Novel Transporter in *Bacillus subtilis*. *mBio* **2017**, *8*, e00976-17. [CrossRef]
36. Ahn, S.J.; Deep, K.; Turner, M.E.; Ishkov, I.; Waters, A.; Hagen, S.J.; Rice, K.C. Characterization of LrgAB as a stationary phase-specific pyruvate uptake system in *Streptococcus mutans*. *BMC Microbiol.* **2019**, *19*, 223. [CrossRef]
37. Popa, G.L.; Papa, M.I. *Salmonella* spp. Infection—A continuous threat worldwide. *Germs* **2021**, *11*, 88–96. [CrossRef] [PubMed]

38. Christopherson, M.R.; Schmitz, G.E.; Downs, D.M. YjgF is required for isoleucine biosynthesis when *Salmonella enterica* is grown on pyruvate medium. *J. Bacteriol.* **2008**, *190*, 3057–3062. [CrossRef]
39. Garai, P.; Lahiri, A.; Ghosh, D.; Chatterjee, J.; Chakravortty, D. Peptide utilizing carbon starvation gene *yjiY* is required for flagella mediated infection caused by *Salmonella*. *Microbiology* **2016**, *162*, 100–116. [CrossRef] [PubMed]
40. Tenor, J.L.; McCormick, B.A.; Ausubel, F.M.; Aballay, A. *Caenorhabditis elegans*-based screen identifies *Salmonella* virulence factors required for conserved host-pathogen interactions. *Curr. Biol.* **2004**, *14*, 1018–1024. [CrossRef]
41. Wong, V.K.; Pickard, D.J.; Barquist, L.; Sivaraman, K.; Page, A.J.; Hart, P.J.; Arends, M.J.; Holt, K.E.; Kane, L.; Mottram, L.F.; et al. Characterization of the *yehUT* two-component regulatory system of *Salmonella enterica* Serovar Typhi and Typhimurium. *PLoS ONE* **2013**, *8*, e84567. [CrossRef]
42. Holt, K.E.; Parkhill, J.; Mazzoni, C.J.; Roumagnac, P.; Weill, F.X.; Goodhead, I.; Rance, R.; Baker, S.; Maskell, D.J.; Wain, J.; et al. High-throughput sequencing provides insights into genome variation and evolution in *Salmonella* Typhi. *Nat. Genet.* **2008**, *40*, 987–993. [CrossRef] [PubMed]
43. Sambrook, J.; Fritsch, E.; Maniatis, T. *Molecular Cloning: A Laboratory Manual*, 2nd ed.; Cold Spring Harbor Laboratory Press: Cold Spring Harbor, NY, USA, 1989.
44. Karlinsey, J.E. lambda-Red genetic engineering in *Salmonella enterica* serovar Typhimurium. *Methods Enzymol.* **2007**, *421*, 199–209. [CrossRef] [PubMed]
45. Datsenko, K.A.; Wanner, B.L. One-step inactivation of chromosomal genes in *Escherichia coli* K-12 using PCR products. *Proc. Natl. Acad. Sci. USA* **2000**, *97*, 6640–6645. [CrossRef] [PubMed]
46. Brameyer, S.; Hoyer, E.; Bibinger, S.; Burdack, K.; Lassak, J.; Jung, K. Molecular design of a signaling system influences noise in protein abundance under acid stress in different γ-Proteobacteria. *J. Bacteriol.* **2020**, *202*, e00121-20. [CrossRef]
47. Lassak, J.; Henche, A.L.; Binnenkade, L.; Thormann, K.M. ArcS, the cognate sensor kinase in an atypical Arc system of *Shewanella oneidensis* MR-1. *Appl. Environ. Microbiol.* **2010**, *76*, 3263–3274. [CrossRef]
48. Hoiseth, S.K.; Stocker, B.A. Aromatic-dependent *Salmonella* typhimurium are non-virulent and effective as live vaccines. *Nature* **1981**, *291*, 238–239. [CrossRef]
49. Maier, L.; Vyas, R.; Cordova, C.D.; Lindsay, H.; Schmidt, T.S.; Brugiroux, S.; Periaswamy, B.; Bauer, R.; Sturm, A.; Schreiber, F.; et al. Microbiota-derived hydrogen fuels *Salmonella* typhimurium invasion of the gut ecosystem. *Cell Host Microbe* **2013**, *14*, 641–651. [CrossRef]
50. Inoue, H.; Nojima, H.; Okayama, H. High efficiency transformation of *Escherichia coli* with plasmids. *Gene* **1990**, *96*, 23–28. [CrossRef]
51. Gödeke, J.; Heun, M.; Bubendorfer, S.; Paul, K.; Thormann, K.M. Roles of two *Shewanella oneidensis* MR-1 extracellular endonucleases. *Appl. Environ. Microbiol.* **2011**, *77*, 5342–5351. [CrossRef]
52. Guzman, L.M.; Belin, D.; Carson, M.J.; Beckwith, J. Tight regulation, modulation, and high-level expression by vectors containing the arabinose PBAD promoter. *J. Bacteriol.* **1995**, *177*, 4121–4130. [CrossRef] [PubMed]
53. Harwood, C.R.; Cutting, S.M. *Molecular Biological Methods for Bacillus*; Harwood, C.R.C., Simon, M., Eds.; Wiley: Chichester, UK, 1990.
54. Schneider, C.A.; Rasband, W.S.; Eliceiri, K.W. NIH Image to ImageJ: 25 years of image analysis. *Nat. Methods* **2012**, *9*, 671–675. [CrossRef] [PubMed]
55. Darias, J.A.; García-Fontana, C.; Lugo, A.C.; Rico-Jiménez, M.; Krell, T. Qualitative and quantitative assays for flagellum-mediated chemotaxis. *Methods Mol. Biol.* **2014**, *1149*, 87–97. [CrossRef] [PubMed]
56. Sievers, F.; Wilm, A.; Dineen, D.; Gibson, T.J.; Karplus, K.; Li, W.; Lopez, R.; McWilliam, H.; Remmert, M.; Söding, J.; et al. Fast, scalable generation of high-quality protein multiple sequence alignments using Clustal Omega. *Mol. Syst. Biol.* **2011**, *7*, 539. [CrossRef] [PubMed]
57. Saier, M.H.; Reddy, V.S.; Moreno-Hagelsieb, G.; Hendargo, K.J.; Zhang, Y.; Iddamsetty, V.; Lam, K.J.K.; Tian, N.; Russum, S.; Wang, J.; et al. The Transporter Classification Database (TCDB): 2021 update. *Nucleic Acids Res.* **2021**, *49*, D461–D467. [CrossRef]
58. UniProt, C. UniProt: The universal protein knowledgebase in 2021. *Nucleic Acids Res.* **2021**, *49*, D480–D489. [CrossRef]
59. Kraxenberger, T.; Fried, L.; Behr, S.; Jung, K. First insights into the unexplored two-component system YehU/YehT in *Escherichia coli*. *J. Bacteriol.* **2012**, *194*, 4272–4284. [CrossRef] [PubMed]
60. Neumann, S.; Grosse, K.; Sourjik, V. Chemotactic signaling via carbohydrate phosphotransferase systems in *Escherichia coli*. *Proc. Natl. Acad. Sci. USA* **2012**, *109*, 12159–12164. [CrossRef] [PubMed]
61. Somavanshi, R.; Ghosh, B.; Sourjik, V. Sugar influx sensing by the phosphotransferase system of *Escherichia coli*. *PLoS Biol.* **2016**, *14*, e2000074. [CrossRef]
62. Richardson, A.R.; Payne, E.C.; Younger, N.; Karlinsey, J.E.; Thomas, V.C.; Becker, L.A.; Navarre, W.W.; Castor, M.E.; Libby, S.J.; Fang, F.C. Multiple targets of nitric oxide in the tricarboxylic acid cycle of *Salmonella enterica* serovar typhimurium. *Cell Host Microbe* **2011**, *10*, 33–43. [CrossRef]
63. Kröger, C.; Colgan, A.; Srikumar, S.; Händler, K.; Sivasankaran, S.K.; Hammarlöf, D.L.; Canals, R.; Grissom, J.E.; Conway, T.; Hokamp, K.; et al. An Infection-Relevant Transcriptomic Compendium for *Salmonella enterica* Serovar Typhimurium. *Cell Host Microbe* **2013**, *14*, 683–695. [CrossRef]
64. Balaban, N.Q.; Merrin, J.; Chait, R.; Kowalik, L.; Leibler, S. Bacterial persistence as a phenotypic switch. *Science* **2004**, *305*, 1622–1625. [CrossRef]

65. Lewis, K. Persister cells. *Annu. Rev. Microbiol.* **2010**, *64*, 357–372. [CrossRef]
66. Vilhena, C.; Kaganovitch, E.; Shin, J.Y.; Grünberger, A.; Behr, S.; Kristoficova, I.; Brameyer, S.; Kohlheyer, D.; Jung, K. A single-cell view of the BtsSR/YpdAB pyruvate sensing network in *Escherichia coli* and its biological relevance. *J. Bacteriol.* **2018**, *200*, e00536-00517. [CrossRef]
67. Helaine, S.; Cheverton, A.M.; Watson, K.G.; Faure, L.M.; Matthews, S.A.; Holden, D.W. Internalization of *Salmonella* by macrophages induces formation of nonreplicating persisters. *Science* **2014**, *343*, 204–208. [CrossRef] [PubMed]
68. Stapels, D.A.C.; Hill, P.W.S.; Westermann, A.J.; Fisher, R.A.; Thurston, T.L.; Saliba, A.E.; Blommestein, I.; Vogel, J.; Helaine, S. *Salmonella* persisters undermine host immune defenses during antibiotic treatment. *Science* **2018**, *362*, 1156–1160. [CrossRef]
69. Löber, S.; Jäckel, D.; Kaiser, N.; Hensel, M. Regulation of *Salmonella* pathogenicity island 2 genes by independent environmental signals. *Int. J. Med. Microbiol.* **2006**, *296*, 435–447. [CrossRef]
70. Brugiroux, S.; Beutler, M.; Pfann, C.; Garzetti, D.; Ruscheweyh, H.J.; Ring, D.; Diehl, M.; Herp, S.; Lötscher, Y.; Hussain, S.; et al. Genome-guided design of a defined mouse microbiota that confers colonization resistance against *Salmonella enterica* serovar Typhimurium. *Nat. Microbiol.* **2016**, *2*, 16215. [CrossRef]
71. Eberl, C.; Weiss, A.S.; Jochum, L.M.; Durai Raj, A.C.; Ring, D.; Hussain, S.; Herp, S.; Meng, C.; Kleigrewe, K.; Gigl, M.; et al. *E. coli* enhance colonization resistance against *Salmonella* Typhimurium by competing for galactitol, a context-dependent limiting carbon source. *Cell Host Microbe* **2021**, *29*, 1680–1692.e1687. [CrossRef] [PubMed]
72. Gilbert, J.A.; Blaser, M.J.; Caporaso, J.G.; Jansson, J.K.; Lynch, S.V.; Knight, R. Current understanding of the human microbiome. *Nat. Med.* **2018**, *24*, 392–400. [CrossRef]
73. Clavel, T.; Lagkouvardos, I.; Blaut, M.; Stecher, B. The mouse gut microbiome revisited: From complex diversity to model ecosystems. *Int. J. Med. Microbiol.* **2016**, *306*, 316–327. [CrossRef]
74. Weiss, A.S.; Burrichter, A.G.; Durai Raj, A.C.; von Strempel, A.; Meng, C.; Kleigrewe, K.; Münch, P.C.; Rössler, L.; Huber, C.; Eisenreich, W.; et al. In vitro interaction network of a synthetic gut bacterial community. *ISME J.* **2021**, *16*, 1095–1109. [CrossRef] [PubMed]
75. Pontrelli, S.; Szabo, R.; Pollak, S.; Schwartzman, J.; Ledezma-Tejeida, D.; Cordero, O.X.; Sauer, U. Metabolic cross-feeding structures the assembly of polysaccharide degrading communities. *Sci. Adv.* **2022**, *8*, eabk3076. [CrossRef] [PubMed]
76. Girinathan, B.P.; DiBenedetto, N.; Worley, J.N.; Peltier, J.; Arrieta-Ortiz, M.L.; Immanuel, S.R.C.; Lavin, R.; Delaney, M.L.; Cummins, C.K.; Hoffman, M.; et al. *In vivo* commensal control of *Clostridioides difficile* virulence. *Cell Host Microbe* **2021**, *29*, 1693–1708 e1697. [CrossRef]
77. Ducret, A.; Quardokus, E.M.; Brun, Y.V. MicrobeJ, a tool for high throughput bacterial cell detection and quantitative analysis. *Nat Microbiol* **2016**, *1*, 16077. [CrossRef] [PubMed]

5 Establishing large- and small-scale methods to identify and analyze pyruvate export in *Escherichia coli*

Manuscript

Paulini S, Jung K. 2022.

ABSTRACT

Proteobacteria excrete pyruvate when growing in rich medium and take it up again to balance intracellular pyruvate levels. Whereas the uptake of pyruvate has been investigated well during the recent years, nothing is known yet about pyruvate excretion. This study aimed to identify a pyruvate exporter protein in *Escherichia coli*. We established large-scale screening methods based on a reporter system which is activated by excreted pyruvate in combination with knockout libraries. Promising mutants were tested further for pyruvate excretion during growth in rich medium. We found one deletion mutant candidate (*sdaC*) with abolished pyruvate excretion. However, we monitored a clear excretion of pyruvate for both the *sdaC* deletion mutant and the complemented mutant using right-side-out membrane vesicles, independent of a potential substrate outside of the vesicles. This indicated that the serine transporter SdaC is not the unknown pyruvate exporter nor a serine-pyruvate-antiporter, but the uptake of serine by SdaC is crucial for the excretion of pyruvate by the living cells in rich medium. The established large-scale screenings need to be continued and a number of promising candidates needs to be investigated further. This study lays the methodological foundation to identify and analyze the pyruvate exporter(s) in *E. coli*.

INTRODUCTION

Proteobacteria were shown to excrete pyruvate when growing fast in a rich medium due to a so-called overflow metabolism under conditions of high pyruvate production [1-4]. By this means, the cells regulate intracellular pyruvate levels to remain constant. The excreted pyruvate is reclaimed from the medium in a later growth phase. For the uptake of pyruvate, *E. coli* possesses three (putative) pyruvate transporters: BtsT and CstA were proven to transport pyruvate into the cell [5, 6], but only a mutant lacking *btsT*, *cstA* and *yhjX* is unable to grow on pyruvate, indicating that YhjX might be a third pyruvate transporter. Whereas *cstA* is activated by nutrient limitation in the stationary growth phase, the other two (putative) pyruvate transporters are only produced when extracellular pyruvate is present: Expression of *btsT* is activated by the two-component system BtsS/BtsR on sensing of pyruvate with a low threshold concentration of 50 µM [7], and expression of *yhjX* is activated by the two-component system PyrS/PyrR on sensing pyruvate with a higher threshold concentration of 600 µM [8].

In contrast to what is known about pyruvate uptake, the mechanism of pyruvate excretion is still unknown. We assume that the excretion of pyruvate does not happen passively, as intracellular pyruvate levels must be tightly controlled and some species excrete very large

amounts of pyruvate [1, 9, 10]. Thus, the cells need to use a transporter protein to bring pyruvate outside trough the cell membrane, just as the transporters BtsT and CstA carry it inside the cells. The aim of this project was to identify the responsible pyruvate exporter protein(s) in *E. coli*. Pyruvate is not only a valuable compound for the cells to use it as a metabolite, but it also serves as a scavenger for reactive oxygen species [11-13]. Thus, pyruvate excretion can be seen as an oxidative defense mechanism [14]. To find the responsible exporter protein in *E. coli* and subsequently to identify homologs in other species could reveal important insights into pyruvate excretion. By using deletion mutants it could be observed what happens if pyruvate excretion is abolished, for instance in pathogens or specific members of the intestinal microbiota.

RESULTS AND DISCUSSION

For the search of a pyruvate exporter in *E. coli*, we used a reporter strategy based on the fact that the expression of *btsT* is activated only in the presence of extracellular pyruvate by the pyruvate sensing system BtsS/BtsR. It was shown previously that pyruvate activates *btsT* expression [7]. Moreover, *btsT* expression is directly dependent on the concentration of pyruvate outside of the cells: In diluted LB medium, beginning with a threshold concentration of 10 µM, the expression of *btsT* increases according to an increasing pyruvate concentration in the medium, until reaching saturation at 1 mM pyruvate [7]. Thus, *btsT* expression can be taken as a quantitative tool to indirectly measure external pyruvate concentrations. A strain lacking the gene(s) coding for the pyruvate exporter(s) is expected to show no *btsT* expression when grown in LB medium. To this end, we used different reporter assays for *btsT* expression in deletion mutant libraries to find a strain with strongly reduced *btsT* expression, which is an indicator that no external pyruvate is present and thus that the deleted gene is involved in pyruvate excretion, putatively coding for a pyruvate exporter protein. The mechanism how pyruvate excretion is linked to *btsT* expression is illustrated in Figure 1.

Untargeted large-scale transformation of Keio deletion mutants with a luciferase-based reporter plasmid for *btsT* expression reveals YrbG as a first candidate

As a first screening, we used a plasmid-based reporter system for *btsT* expression with luciferase expression as a readout. It was successfully used before to show *btsT* expression and even pyruvate concentration dependency by Behr *et al*. [7], but they used a mutant strain lacking *yhjX* and diluted LB to which pyruvate was added.

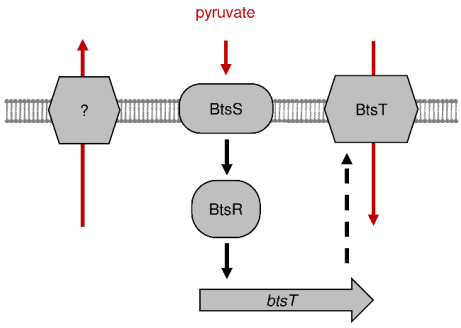

Figure 1. Activation of *btsT* by excreted pyruvate. Schematic illustration of pyruvate excretion via an unknown exporter protein (marked with ?), activation of the two-component system BtsS/BtsR upon sensing the external pyruvate, which leads to expression of *btsT* coding for the protein BtsT transporting the excreted pyruvate back into the cell.

To test if this system is applicable to monitor the excretion of pyruvate in LB medium and even to point out differences in pyruvate concentration, we transformed *E. coli* MG1655 wild-type cells with the respective pBBR-P_{btsT}-*lux* reporter plasmid [15] and measured both the external pyruvate concentration and the luminescence signal over growth to determine *btsT* expression (relative light units [RLU] per OD_{600}). We could clearly see the peak of external pyruvate at the beginning of exponential growth phase and the equivalent peak of *btsT* expression directly afterwards in mid-exponential phase (Figure 2). We conclude that this reporter system can be used to indirectly detect pyruvate excretion.

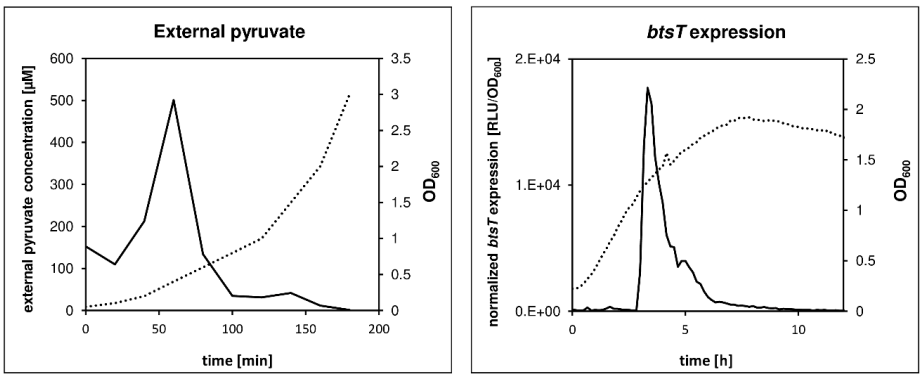

Figure 2. Pyruvate excretion activates *btsT* expression in LB medium. A) External pyruvate: *E. coli* MG1655 wild-type cells were grown in flasks in LB medium at 37 °C, growth was monitored (dotted lines) and samples were taken every 20 min to determine external pyruvate concentrations (solid line) via an enzymatic assay. **B) *btsT* expression:** *E. coli* MG1655 wild-type cells harboring a reporter plasmid for *btsT* expression (pBBR1-MCS5-P_{btsT}-*lux*) were grown in LB medium in a plate reader at 37 °C. Growth (dotted line) and *btsT* expression (RLU/OD_{600}, solid line) were monitored over time.

We used this plasmid-based luciferase reporter system in combination with the Keio collection of single knockout strains [16] and aimed to find a strain with very low *btsT* expression. The Keio collection comprises in total 3985 knockout mutants, which is a high number to be transformed and tested. For the simultaneous transformation of several Keio knockout mutants in the 96-well format, we established a large-scale conjugation. To this end we used the diaminopimelic acid auxotroph *E. coli* strain WM3064 harboring the pBBR-P_{btsT}-*lux* reporter plasmid as the donor, plated it as a lawn and dropped the recipients of the Keio collection on top for mating, as described in detail in the material and methods section. The transformed mutants were then selected by re-streaking on the appropriate antibiotics. After testing several other protocols, this technique allowed the most rapid and efficient transformation of whole 96-well plates. In total, 30 plates of the Keio collection were transformed with the pBBR-P_{btsT}-*lux* reporter plasmid, which means a sum of approximately 2880 mutants or 72 % of the whole collection. Some few strains did not regrow before or after transformation, but for those with knockouts of putatively relevant transporter genes, the procedure was repeated and transformation was successful in the second trial. An overview of all transformed Keio plates can be found in table S1.

The transformed knockout mutants were then used for *btsT* expression measurements. Growth and luciferase expression in LB medium were monitored over time in a plate reader and the maximal *btsT* expression of each single mutant was determined. To each plate, the wild-type harboring the reporter plasmid was added in one well (replacing an "irrelevant" mutant with a deleted gene not coding for a membrane protein) as a control for normal *btsT* expression. By this means, a fold change in relation to the wild-type expression value could be calculated for each strain, which allowed a rough comparison of different tested plates among each other. In table S1, *btsT* expression values as well as calculated fold changes for all tested Keio strains are listed.

19 mutants, which showed very low *btsT* expression, were collected and tested again in one plate, together with the wild-type. All values of *btsT* expression and the fold change in relation to the wild-type of these 19 mutants, as well as the products of the deleted genes are listed in table 1. The 12 strains with the lowest *btsT* expression (Figure 3) and which have a deletion of a gene coding for a putative transporter protein were selected for further testing.

These 12 most promising mutant candidates were tested directly for pyruvate excretion during growth in LB medium. To allow the simultaneous testing of this number of strains, only three samples were taken in the beginning of the exponential growth phase (OD_{600} = 0.2 - 0.6), the

time point at which the peak of external pyruvate is supposed to occur. Pyruvate concentrations were determined using an enzymatic assay. The basal pyruvate concentration in the LB medium (100-200 µM, measured for every experiment) was subtracted to see the amount of excreted pyruvate for each strain. In table 1, the maximal external pyruvate concentration for each of the tested candidates is listed. The maximal external pyruvate concentration for the wild type was 501 µM and almost all 12 mutants had similar values (Figure 3). Only one candidate (*yrbG*) had a very low maximum of external pyruvate (71 µM) and was thus investigated further.

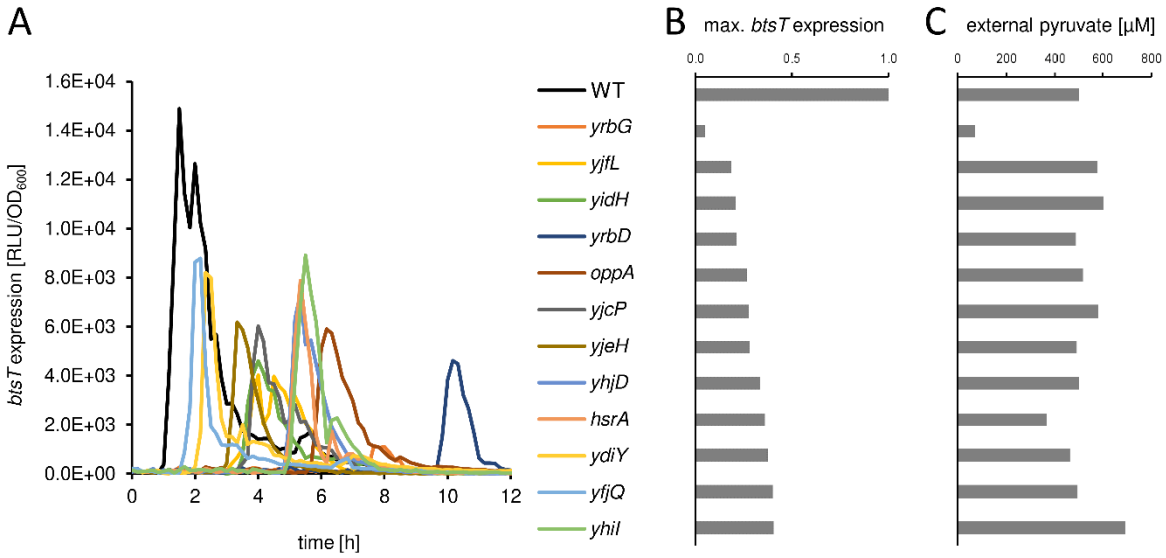

Figure 3. *btsT* expression and external pyruvate of 12 selected Keio deletion mutants as most promising candidates after untargeted screening of 30 Keio collection plates. The indicated Keio mutants and the wild-type harboring the pBBR1-MCS5-P_{btsT}-*lux* reporter plasmid were grown in LB medium at 37 °C. Luminescence (RLU) and growth (OD_{600}) were monitored over time in a plate reader and *btsT* expression was calculated as RLU/OD_{600}. For external pyruvate measurements, samples were taken at the exponential growth phase to determine pyruvate concentrations with an enzymatic assay. **A)** *btsT* expression over time. **B)** Maximal *btsT* expression. **C)** External pyruvate concentration.

YrbG is an uncharacterized membrane protein with 10 predicted transmembrane domains and belongs to the Ca^{2+}:cation antiporter family [17]. First, the correct knockout of the *yrbG* gene was confirmed by PCR. Then, we aimed to complement the deletion mutant by expression of *yrbG* from a plasmid (pBAD24-*yrbG*), but the low *btsT* expression was not complemented (Figure S1). However, a clear effect of the added arabinose concentration on growth was observed for the mutant harboring the pBAD24-*yrbG* expression plasmid (Figure S1), indicating that the expression of the transporter protein worked and might be harmful for the cells when expressed in a high number. As a consequence, we assumed that the reduced

pyruvate excretion and thus decreased *btsT* expression we observed for the *yrbG* deletion mutant did not result from the deletion of *yrbG*, but rather from any other mutation in the genome. A second measurement of external pyruvate provided a maximal external pyruvate concentration of 294 µM. This time, samples were taken over the whole growth period, which could explain the low value of the first measurement with having missed the correct time point of the excretion peak. Thus, we did not follow up on this candidate.

Besides the untargeted transformation and testing of 96-well plates of the Keio collection as a whole, also a targeted transformation of several potential candidates with the pBBR-P_{btsT}-*lux* reporter plasmid was performed, which was based on three different targeted strategies:

Targeted strategy A: Transformation of selected Keio deletion mutants with a luciferase-based reporter plasmid for *btsT* based on increased protein synthesis rates in the presence of amino acids reveals SdaC as a putative serine-pyruvate-antiporter

As a first targeted strategy, we analyzed the ribosome profiling data from Li *et al*. [18], who investigated protein synthesis of *E. coli* MG1655 in different media. As pyruvate excretion occurs under conditions of overflow metabolism in an amino-acid rich medium, we assumed for our sought-after pyruvate exporter to find a strongly increased protein synthesis rate in minimal medium supplemented with amino acids in comparison to minimal medium without supplement. We sorted the data according to this ratio of synthesis rate in medium with amino acids to the synthesis rate in minimal medium without amino acids, and filtered the remaining list of proteins for putative transporters. After excluding all protein candidates for which the corresponding Keio deletion mutants had been already transformed and tested before and showed normal *btsT* expression, a list of 25 candidates remained. The corresponding deletion mutants were selected from the Keio collection, transformed with the pBBR-P_{btsT}-*lux* reporter plasmid and *btsT* expression was measured.

Out of these 25 candidates, five had a fold change lower than 0.7 for *btsT* expression in comparison to the wild-type (Figure 4) and were selected for further measurements of external pyruvate. The *btsT* expression and fold change values of all 25 candidates are listed in table 1, as well as the products of their deleted genes. The five potential mutant candidates were tested for external pyruvate in comparison to the wild type (Figure 4). Samples were taken every 15 minutes during growth in LB medium and pyruvate concentrations were measured with an enzymatic assay.

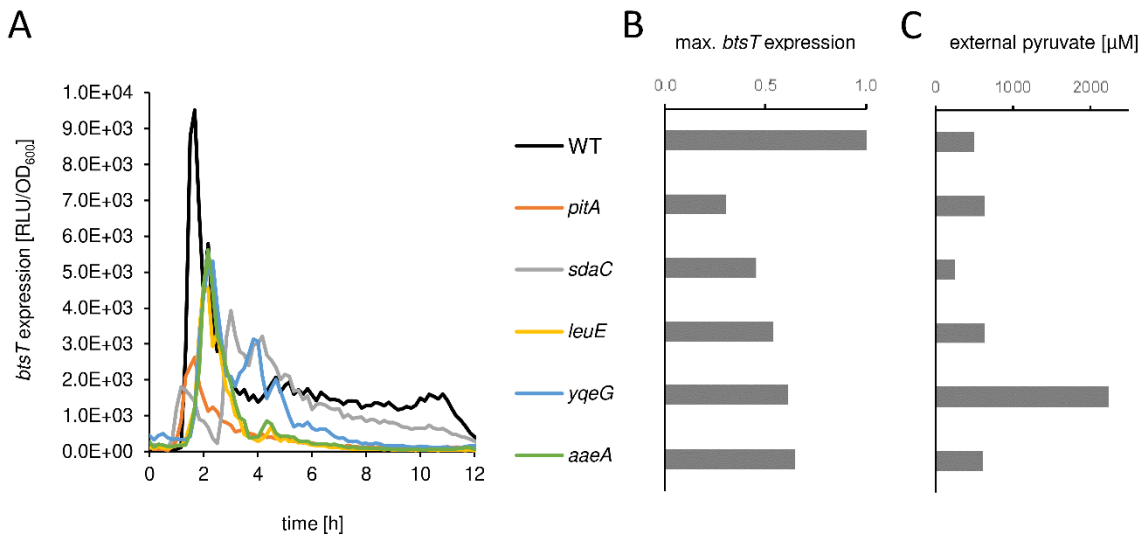

Figure 4. *btsT* expression and external pyruvate of selected Keio deletion mutants based on targeted strategy A. The indicated Keio mutants and the wild-type harboring the pBBR1-MCS5-P_{btsT}-*lux* reporter plasmid were grown in LB medium at 37 °C. Luminescence (RLU) and growth (OD_{600}) were monitored over time in a plate reader and *btsT* expression was calculated as RLU/OD_{600}. For external pyruvate measurements, samples were taken every 15 minutes to determine pyruvate concentrations with an enzymatic assay. **A)** *btsT* expression over time. **B)** Maximal *btsT* expression. **C)** External pyruvate concentration.

One candidate excreted a very high amount of pyruvate, three strains were comparable with the wild type showing a peak of external pyruvate in early exponential growth phase, but for one mutant (*sdaC*) the concentration of external pyruvate remained almost constant over time and only a small peak could be observed, with a maximal pyruvate concentration of 247 µM (Figure 5). The measurement was repeated and the pyruvate concentration again did not change much over time, with a maximum of 188 µM. After confirming the correct knockout of the *sdaC* gene via PCR, we constructed an expression plasmid for *sdaC* to complement the deletion mutant (pBAD24-*sdaC*). Inducing the plasmid with 0.02 % arabinose, we observed complementation of both *btsT* expression and pyruvate excretion in the Keio *sdaC* deletion mutant back to at least wild-type level (Figure 5). Thus, this gene was a very promising candidate to code for a potential pyruvate exporter. Further experiments to check if SdaC can indeed export pyruvate were performed by creating right-side-out membrane vesicles.

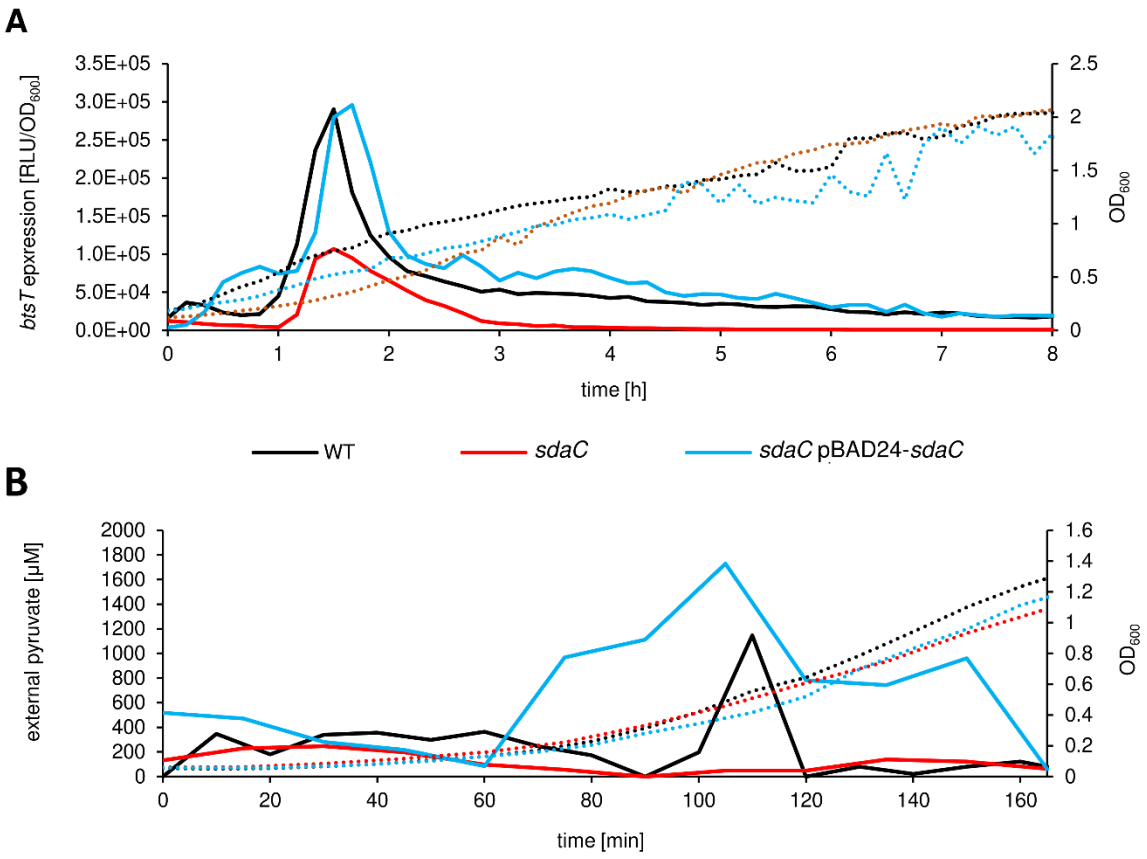

Figure 5. *btsT* expression and pyruvate excretion of Keio *sdaC* deletion mutant in comparison to the wild type and the complemented mutant. A) Time course of *btsT* expression: The indicated cells harbored the pBBR1-MCS5-P_{btsT}-*lux* reporter plasmid and were grown in LB medium at 37 °C. Luminescence (RLU) and growth (OD_{600}, dotted lines) were monitored over time in a plate reader and *btsT* expression was calculated (RLU/OD_{600}, solid lines). **B) External pyruvate during growth:** The indicated cells were grown in LB medium at 37 °C. Growth was monitored (dotted lines) and samples were taken every 15 minutes to determine pyruvate concentrations in the medium (solid lines).

Direct monitoring of pyruvate excretion with right-side-out membrane vesicles shows that SdaC is no pyruvate exporter

SdaC is characterized as a highly specific L-serine transporter of the hydroxy/aromatic amino acid permease (HAAAP) family, which is energized by a proton cotransport [19-21]. It was also shown that SdaC plays a role in maintaining amino acid homeostasis during shifts in nutrient availability [22], that it might be involved in ampicillin sensitivity and phage infection [23] and might work as an inner membrane receptor of colicin V [24].

To show pyruvate export by SdaC directly, we generated right-side-out membrane vesicles of the Keio *sdaC* deletion mutant, either with the pBAD24-*sdaC* expression plasmid for

complementation or with the empty vector pBAD24. Cells were grown in LB medium and the expression plasmid was induced with 0.2 % arabinose. Following the protocol of Kaback (1971), as described in the material and methods section and illustrated in Figure 6, we first monitored the formation of spheroplasts under the microscope. Before the right-side-out membrane vesicles were formed, we added 10 mM pyruvate to the buffer to pre-load the vesicles. Then we added 10 mM of different compounds (either sucrose, serine, succinate or threonine) to the final buffer to balance the molarity and to offer a substrate for a putative symport. After confirming the correct formation of ride-side-out membrane vesicles under the microscope (Figure 6), we conducted export experiments with them.

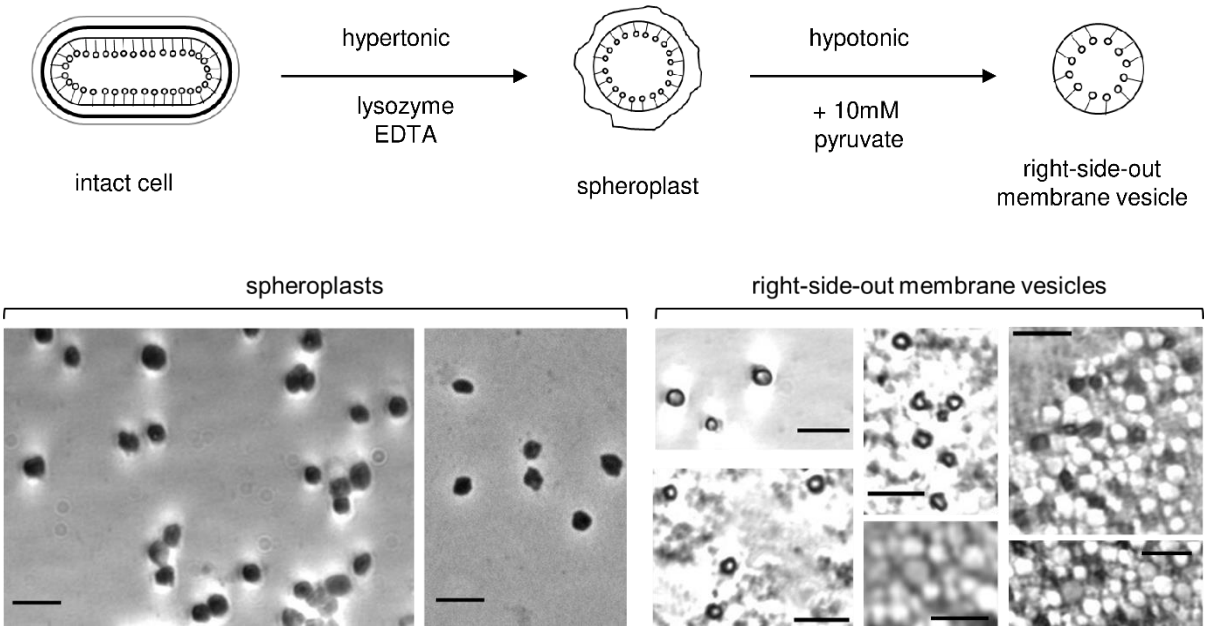

Figure 6. Formation of spheroplasts and right-side-out membrane vesicles. *E. coli sdaC* Keio deletion mutant cells formed spheroplasts when resuspended in a hypertonic solution with lysozyme and EDTA, visible as dark round spheres. After fast dilution into a hypotonic solution, ride-side-out membrane vesicles were formed, visible as light, almost transparent spheres. In this step, the vesicles were pre-loaded with 10 mM pyruvate for subsequent export experiments. Scale bar 5 µm.

After addition of PMS and ascorbate, we took samples at different time points and immediately centrifuged the vesicles at 4 °C to then measure the pyruvate concentration in the supernatant with an enzymatic assay. We could show fast pyruvate export by the right-side-out membrane vesicles for both the Keio *sdaC* deletion mutant with the empty vector and with the pBAD24-*sdaC* expression plasmid (Figure 7). This export was independent of the compound provided in the buffer (same export with serine, threonine, succinate or sucrose outside), indicating that

pyruvate export is not based on an antiport or symport. Without addition of PMS and ascorbate, we did not see any transport anymore (Figure 7), indicating that the export of pyruvate is depending on an electric potential and/or a proton gradient. These new precious facts about a potential pyruvate exporter were applied in further screenings.

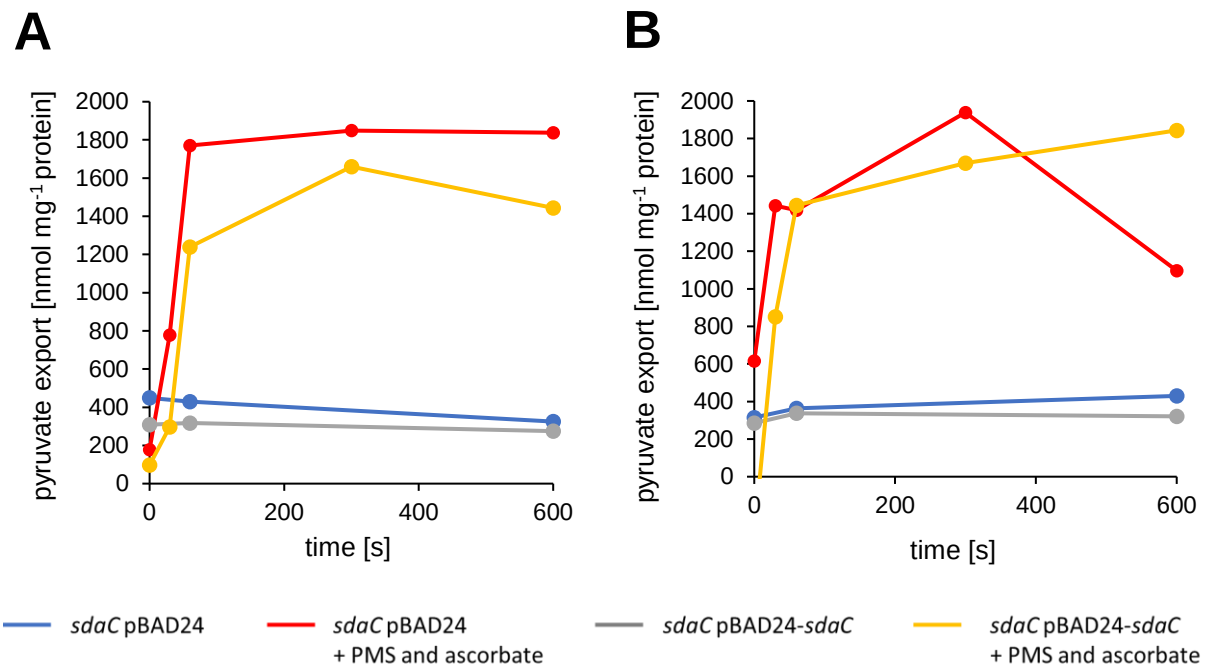

Figure 7. Pyruvate export with right-side-out membrane vesicles. *E. coli sdaC* Keio deletion mutant cells harboring either the empty vector pBAD24 or pBAD24-*sdaC* for complementation were converted to right-side-out membrane vesicles and preloaded with 10 mM pyruvate. Export experiments were performed at RT in 100 mM Tris-Mes buffer, pH 7.0, containing either **A)** 10 mM threonine or **B)** 10 mM serine. PMS (100 µM) and ascorbate (20 µM) were added to the samples where indicated. Pyruvate concentration in the buffer after different time periods was determined with an enzymatic assay.

This leads to the conclusion that SdaC is not the pyruvate exporter we were looking for. The abolished pyruvate excretion in the *sdaC* deletion mutant must be explained with physiological reasons due to a reduced serine uptake without SdaC. Serine is the first amino acid to be consumed and half of it is converted to pyruvate [26, 27]. It was shown that uptake of serine from the medium leads to pyruvate excretion [7]. Interestingly, we found that the deletion of two other serine transporter genes, *sstT* and *tdcC*, did not have any influence on *btsT* expression (Figure S2). Only if *sdaC* was deleted, alone or in addition to *sstT* and *tdcC*, expression of *btsT* was reduced. This indicates that a specific property of SdaC must be crucial for pyruvate excretion, which does not have to be necessarily serine uptake. It has been shown that SdaC

plays a role in maintaining amino acid homeostasis during shifts in nutrient availability with an unknown mechanism [22]. As pyruvate excretion normally happens during early exponential phase, this unexplored role of SdaC could also apply here. Further research is necessary to elucidate the interplay of serine uptake and pyruvate excretion in *E. coli*.

Targeted strategy B: Transformation of selected Keio deletion mutants with a luciferase-based reporter plasmid for *btsT* based on logical narrowing down of a transporter list reveals 5 candidates for further investigation

As a second targeted strategy, we analyzed the *E. coli* transporter database list from Elbourne *et al*. [28] and created a selection of candidates according to all the facts about the sought-for pyruvate exporter which we could conclude after the first experiments: We were looking for a transport which is depending on an electric potential and/or a proton gradient, and no antiport or symport. It has to be mentioned that the online transporter list might be incomplete, as BtsT for instance is not listed. Thus, there is the possibility that the pyruvate exporter might not be included there neither and our candidate selection must be handled with care.

For 62 putative candidates, the corresponding deletion mutants were selected from the Keio collection, transformed with the pBBR-P_{btsT}-*lux* reporter plasmid and *btsT* expression was measured. In Table 1, all *btsT* expression and fold change values for these 62 candidates are listed and which transporter their deleted genes code for. The ten mutants with the lowest expression values (fold change lower than 0.3, Table 1, Figure 8) were selected for further measurements of external pyruvate.

Samples for external pyruvate were taken every 15 minutes during growth in LB medium and pyruvate concentrations were measured with an enzymatic assay. From the ten tested mutants, five showed a maximal external pyruvate concentration similar to that of the wild type, whereas five mutants had a lower pyruvate excretion (228 – 341 µM, Table1, Figure 8). The other five strains were tested again and also this time, their pyruvate excretion was lower than that of the wild type. These results were unexpected, as we hypothesized to find rather only one deletion mutant of a putative pyruvate exporter gene with strongly reduced pyruvate excretion.

We barely assume that all these five genes are coding for pyruvate exporter proteins. As they all code for transporters, a gene deletion could have an impact on the physiological state of the cells, impairing the high production of pyruvate and thus an overflow metabolism which normally leads to pyruvate excretion in full medium. This needs to be investigated further. In a

first step, complementation of these candidates needs to be shown to ensure that the deleted genes are the reason for the decreased pyruvate excretion.

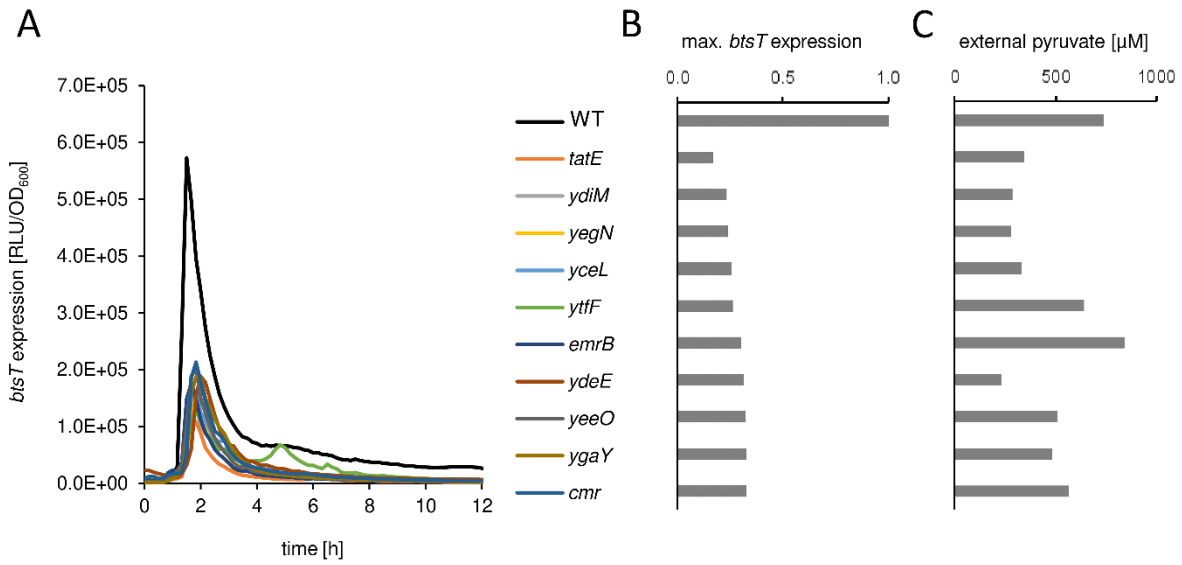

Figure 8. *btsT* expression and external pyruvate of 10 selected Keio deletion mutants based on targeted strategy B. The indicated Keio mutants and the wild-type harboring the pBBR1-MCS5-P_{btsT}-*lux* reporter plasmid were grown in LB medium at 37 °C. Luminescence (RLU) and growth (OD_{600}) were monitored over time in a plate reader and *btsT* expression was calculated (RLU/OD_{600}). For external pyruvate measurements, samples were taken every 15 minutes. **A)** *btsT* expression over time. **B)** Maximal *btsT* expression. **C)** External pyruvate concentration.

Targeted strategy C: Transformation of selected Keio deletion mutants with a luciferase-based reporter plasmid for *btsT* based on an expression peak in exponential growth phase reveals 12 candidates for further investigation

As a third targeted strategy, we analyzed gene expression data from Smith *et al*. [29] at different time points over growth in full medium. As pyruvate is excreted very fast in the beginning of exponential growth phase, we hypothesized an expression peak of the gene coding for a pyruvate exporter at this time. To this end, we sorted the expression data table by Smith *et al*. [29] for genes with the highest upregulation after 1 or 2 hours and filtered this list for genes coding for putative transporter proteins. After excluding all candidates that were not found in the Keio collection, and those that had been already transformed and tested before and showed normal *btsT* expression, a list of 12 gene candidates remained. The corresponding deletion mutants were selected from the Keio collection, transformed with the pBBR-P_{btsT}-*lux* reporter plasmid and *btsT* expression was measured.

Interestingly, all 12 candidates showed a much lower *btsT* expression than the wild-type (Figure 9, Table 1). As we cannot expect that all these genes are involved in pyruvate excretion, we assume that the gene deletions might affect physiological features of the cells in exponential growth phase leading for instance to an abolished overproduction of pyruvate which as a consequence is not excreted. However, these measurements should first be repeated carefully to confirm that these 12 mutants have a reduced *btsT* expression, before measuring external pyruvate for all of them. It also needs to be taken into consideration that the wild-type expression values in these experiment were very high, mostly higher than all expression values of the tested mutants. Further research is necessary for these candidates.

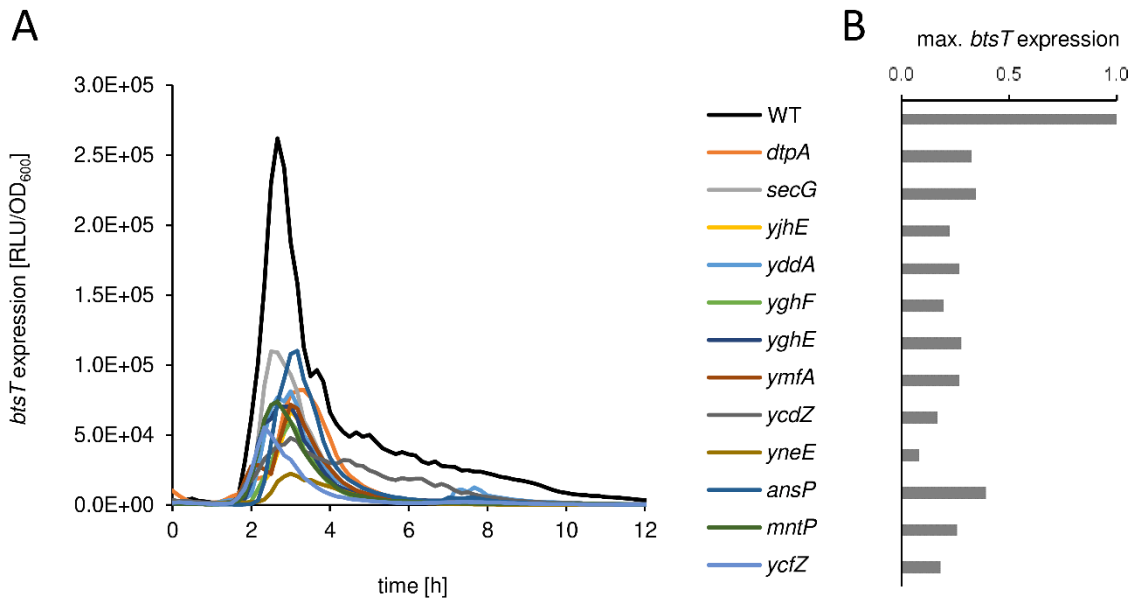

Figure 9. Time course of *btsT* expression of 12 selected Keio deletion mutants based on targeted strategy C. The indicated Keio mutants harboring the pBBR1-MCS5-P_{btsT}-*lux* reporter plasmid were grown in LB medium at 37 °C. Luminescence (RLU) and growth (OD_{600}) were monitored over time in a plate reader and *btsT* expression was calculated (RLU/OD_{600}).

Creation of a transposon library for blue-white screening based on *btsT* expression as an alternative strategy to find a pyruvate exporter

Besides using the luciferase-based reporter system to find a deletion mutant with reduced *btsT* expression, we also established another screening strategy. For this end we used a *lacZ*-based reporter system for *btsT*, which would allow blue-white screening to monitor *btsT* expression rapidly and directly for many cells on plate. In combination with a knockout library, we

expected to be able to select white clones on agar with X-gal for very low *btsT* expression to find by this means a mutant with a deletion of the pyruvate exporter.

In a first step, we tested if the desired reporter system is applicable for blue-white screening by transforming two different *E. coli* strain with the pBBR1-MCS5-P_{btsT}-*lacZ* reporter plasmid: One strain (with deletions of *btsT cstA* and *yhjX* [6]) excretes pyruvate, but is unable to take it up again leading to accumulating pyruvate in the medium, whereas the other strain (*sdaC*, see previous section) does not excrete pyruvate. We mixed them in a 1:10 ratio for *sdaC* : *btsT cstA yhjX* and plated them on LB agar plates containing X-gal. Indeed, we saw roughly 10 percent white colonies in between very blue colonies (Figure 10), indicating that this screening shows *btsT* expression in the form of the blue color – and even when neighboring *btsT cstA yhjX* colonies excreted pyruvate, *sdaC* colonies stayed white due to their own impaired pyruvate excretion. We concluded that this reporter system could be used as a tool in combination with a knockout library to find white clones with abolished pyruvate excretion.

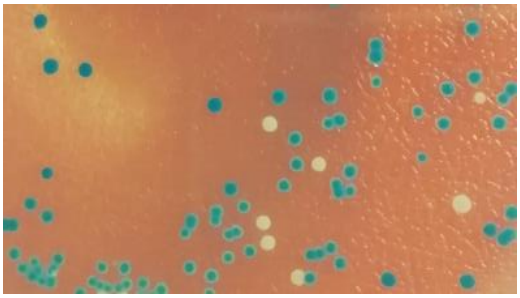

Figure 10. Test for blue-white screening according to *btsT* expression as a result of pyruvate excretion. *E. coli* mutants *sdaC* and *btsT cstA yhjX* harboring the pBBR1-MCS5-P_{btsT}-*lacZ* reporter plasmid were mixed 1:10 and plated on LB agar with X-gal. Plates were incubated overnight at 37 °C.

To this end, we created a mini-Tn*10* transposon library of *E. coli* MG1655 with the plasmid pNK2859 according to the protocol of Freed [30] as described in the material and methods section. A mixture of smaller and larger colonies on the kanamycin plates confirmed that the gene disruption by transposon integration was working. The final library comprised approximately 160 000 single colonies, indicating that a transposon was integrated on average every 30 bp. This library was then pooled and stored in aliquots. One aliquot was transformed with the pBBR1-MCS5-P_{btsT}-*lacZ* reporter plasmid and plated in an appropriate dilution on LB agar plates containing kanamycin, gentamycin and X-gal for blue-white screening. Out of approximately 20 000 single colonies, roughly 120 completely white ones (Figure 11) were selected and re-streaked on fresh plates.

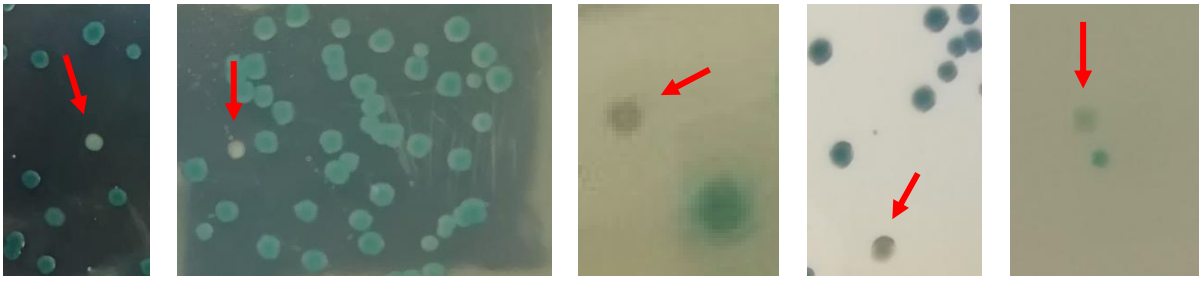

Figure 11. Example pictures of blue-white screening for *btsT* expression. A mini-Tn*10* transposon library of *E. coli* MG1655 harboring the pBBR1-MCS5-P_{btsT}-*lacZ* reporter plasmid was plated on LB agar containing kanamycin, gentamycin and X-gal. After incubation at 37 °C overnight, single white colonies (see red arrows), indicating low *btsT* expression, were collected.

However, most of the streaks turned blue in parts on the fresh plates, indicating that further streaking to clean the white clones would be necessary. After this cleaning, all white clones could be collected to have a pool of candidates with low *btsT* expression for further testing. The next step of this strategy would be to extract the genomic DNA of this "low *btsT* expression library selection", digest it and ligate the DNA fragments into an appropriate vector. *E. coli* cells could then be transformed with this vector-based DNA library and plated on kanamycin to select for clones harboring vectors with a transposon. Sequencing of these vectors could identify all genes in which the transposon was integrated in the white clones. This could lead to a list of genes involved in pyruvate excretion and thus in a final step to candidates for a putative pyruvate exporter.

Further strategies

The strategies presented above were all based on *btsT* expression as a reporter readout for excreted pyruvate. Although this reporter system is well approved and the screenings led to some promising candidates which should definitely be followed up and investigated further, it might be useful to broaden the search also integrating other ways and strategies for screening. Investigating several putative candidates is very time consuming, whereas techniques that narrow down more intensively to a very few strains to test might be faster and lead to more promising results.

Thus, a smart option for future research would be to create a reporter system which leads to lower survival of the cells according to higher *btsT* expression. This could be for instance work via cloning the promoter region of *btsT* upstream of a gene coding for a transcriptional regulator which in turn blocks the expression of an antibiotic resistance cassette. Only in case of low or no *btsT* promoter activity, survival in the presence of the corresponding antibiotic would be

possible. To combine such a system with a knockout library could rapidly reduce the number of potential candidates to test.

Another idea would be to grow a knockout library in very low concentrations of 3-fluoropyruvate, a toxic analog of pyruvate. Mutants without a pyruvate exporter to transport the toxic compound out of the cells would be killed in a higher rate and thus show a reduced growth rate. This method would obviously only work if the pyruvate exporter also transports bromo-pyruvate and if a concentration could be found that is not toxic to all cells, but only to those not able to export the compound again. A combination of this strategy with transcriptomic data of cells grown in the presence of this compound in comparison to cells growing without it could also reveal a detectable upregulation of the sought-after pyruvate exporter gene, as the cells would presumably upregulate this gene to step up their efforts to export the toxin.

CONCLUSION

This study aimed to identify the responsible protein(s) for pyruvate export in *E. coli*. With several different screening methods, one very promising deletion mutant (*sdaC*) was found which indeed did not excrete pyruvate *in vivo*. However, pyruvate excretion could still be shown using right-side-out membrane vesicles. We conclude that the abolished pyruvate excretion of this strain *in vivo* was due to physiology of the cells and a specific property of SdaC is necessary for the excretion of pyruvate.

So far, no pyruvate exporter was identified. Nevertheless, the large- and small-scale methods for screening and analysis were well established and are very promising. Precious information about the pyruvate exporter could be derived from the export experiments. With further investigation of more promising candidates resulting from the different screenings, the chances to narrow down the list and identify the responsible gene(s) for pyruvate export are high. The established methods and strategies lay the foundation to enable further research and screening to finally identify the correct exporter candidate. It would be very interesting and important for different kinds of research areas to investigate the function and relevance of pyruvate excretion by *E. coli* and also by other bacteria – a topic which is fully unexplored yet.

MATERIAL AND METHODS

Strains and plasmids. The following *E. coli* strains were used in this study: *E. coli* MG1655 was used as wild type in relation to all mutants. *E. coli* DH5*α λpir* [31] was used for cloning. *E. coli* WM3064 (W. Metcalf, University of Illinois) was used as a donor for conjugation. The

E. coli Keio collection [16] of single deletion mutants (one gene replaced by a kanamycin resistance cassette) was used for the large-scale conjugation and screening with the luciferase-based reporter assay. The following plasmids were used in this study: To monitor expression of *btsT* with a luciferase-based reporter assay, the pBBR1-MCS5-P_{btsT}-*lux* reporter plasmid [15] was used. For a blue-white-screening based on *btsT* expression, the pBBR1-MCS5-P_{btsT}-*lacZ* plasmid (Jin Qiu, unpublished) was generated by amplifying the promoter region of *btsT* (400 bp upstream of the start codon) by PCR and cloning it into the vector using BamHI and SmaI restriction enzymes. For gene expression to complement deletion mutants, the pBAD24 plasmid [32] was used as backbone. The desired gene was amplified by PCR from genomic DNA and cloned into the vector using EcoRI and XbaI restriction enzymes. Correct cloning of plasmids was confirmed by sequencing.

Growth conditions. Cells were grown aerobically at 37 °C in LB medium (10 g/l tryptone, 5 g/l yeast extract, 10 g/l NaCl) with 20 µg/ml gentamicin, 100 µg/ml ampicillin and/or 50 µg/ml kanamycin if necessary. LB agar plates were made by adding 15 g/l agar to the medium. Growth was monitored by measuring the optical density at 600 nm (OD_{600}) over time.

Molecular biological methods. Molecular methods followed standard protocols [33] or were implemented according to manufacturer's instructions. Kits for the isolation of chromosomal DNA or plasmids and purification of PCR products were purchased from Südlabor. Enzymes were purchased from New England Biolabs. Chemicals were sourced from Roth or Merck.

Large-scale conjugation. To efficiently transform several strains of the Keio collection at the same time with the luciferase-based reporter plasmid, a large-scale conjugation was established for the 96-well format. The donor strain WM3064 harboring the pBBR1-MCS5-P_{btsT}-*lux* reporter plasmid was grown overnight in 20 ml LB medium supplemented with 300 µM diaminopimelic acid due to the strain's auxotrophy and gentamicin to keep the plasmid. The recipients of the Keio collection were grown overnight in a 96-well plate in 200 µl LB medium per well with kanamycin due to their resistance. Both donor and recipients were washed twice with LB medium. The donor was then resuspended in 2 ml LB medium, plated as a lawn on a square LB agar plate containing 300 µM diaminopimelic acid and dried at 37 °C for 30 minutes. The recipients were each resuspended in 10 µl LB medium and small drops of 2 µl were placed with a multichannel pipette on the square agar plate on the donor lawn, keeping the format of the 96-well plate. After all drops were dried, this mating plate was incubated for 4 hours at 37 °C to allow conjugation. Then, the cells were streaked with a multichannel pipette in the 96-

well format on a square LB agar plate containing kanamycin and gentamycin to select for Keio mutants harboring the plasmid and to get rid of the donor.

Luciferase-based expression analysis. The Keio deletion mutants harboring the pBBR1-MCS5-P_{btsT}-*lux* reporter plasmid were grown under agitation in a 96-well plate in 200 µl LB medium with kanamycin and gentamycin in a ClarioStar plate reader at 37 °C. The wild type MG1655 harboring the pBBR1-MCS5-P_{btsT}-*lux* reporter plasmid was added to the 96-well plate (in LB medium with gentamycin) for comparison. Growth and luminescence were measured over time and *btsT* expression was calculated as relative light units (RLU) per OD_{600}. The maximal expression value for each strain was compared with the mean maximal expression value of the wild type, expressed as a fold change.

External pyruvate measurement. Levels of excreted pyruvate were measured using a procedure adapted from O'Donnell-Tormey *et al*. [14]. *E. coli* cells were grown under agitation at 37 °C in LB medium and growth was monitored. At selected time points, 1-ml samples of supernatant were harvested by centrifugation at 4 °C (10 min, 14 000 × g). Proteins were precipitated by the addition of 250 ml of ice-cold 2 M perchloric acid. After a 5-minute incubation on ice, the samples were neutralized with 250 ml of 2.5 M potassium bicarbonate, and precipitates were removed by centrifugation (4 °C, 10 min, 14 000 × g). Pyruvate concentrations of the clear supernatants, diluted 1:5 in 100 mM PIPES buffer (pH 7.5), were determined by using an enzymatic assay based on the conversion of pyruvate and NADH + H^+ to lactate by lactate dehydrogenase. The assay was performed as described before [6]. To determine the basal pyruvate concentration in the medium, clean LB samples were also taken and measured in the same way.

Complementation of deletion mutants. For complementation of deletion mutants, the respective strain from the Keio collection was transformed with the pBAD24 expression vector harboring the gene which was deleted in the mutant. To ensure that the gene was expressed, the promoter was induced with 0.02 % arabinose.

Formation of right-side-out membrane vesicles. The formation of right-side-out membrane vesicles was performed according to Kaback [25]. Shortly, *E. coli* cells were grown in LB medium at 37 °C and harvested by centrifugation (5000 × g, 20 min, 4 °C). The cell pellet was weighed and kept at 4 °C overnight. Then, the cells were resuspended in 80 ml/g wet weight of 30 mM Tris-HCl, pH 8.0, containing 30 % sucrose (w/v) until homogenous. Under slow agitation, lysozyme was added to a final concentration of 50 µg/ml and K_2EDTA (pH 7.0) was added to a final concentration of 10 mM. The cell suspension was stirred at RT for

approximately 45 minutes and the formation of spheroplasts was monitored under the microscope. After centrifugation (16 900 × g, 20 min, RT), the pellet was resuspended with a loosely fitting homogenizer in the smallest possible volume (5-10 ml) of 100 mM Tris-Mes buffer, pH 7.0, containing 20 mM $MgSO_4$, 30 % sucrose, DNaseI and RNaseA (each to a final concentration of 1 mg/ml). Then, the spheroplasts were fastly diluted 1:100 in prewarmed (30 °C) 100 mM Tris-Mes buffer, pH 7.0, containing 100 µM $MgSO_4$, and incubated for 15 minutes at RT. For determination of pyruvate export, 10 mM pyruvate was added to this buffer to preload the right-side-out membrane vesicles, which are formed in this step. K_2EDTA (pH 7.0) was added to a final concentration of 10 mM and $MgSO_4$ was added to a final concentration of 15 mM, followed by 30 minutes incubation at RT. The formation of right-side-out membrane vesicles was monitored under the microscope. After centrifugation (16 000 × g, 60 min, 4 °C), the pellet was resuspended in 100 ml cold 100 mM Tris-Mes buffer, pH 7.0, containing 10 mM K_2EDTA. To test putative antiport, 10 mM serine or sucrose (as a control) were added to this buffer. After the next centrifugation (800 × g, 30 min, 4 °C), the pellet was discarded and the supernatant containing the right-side-out membrane vesicles was centrifuged again (20 800 × g, 30 min, 4 °C). The remaining pellet was resuspended in 10 ml 100 mM Tris-Mes buffer, pH 7.0, containing 10 mM serine, threonine, succinate or sucrose.

Pyruvate export measurements with right-side-out membrane vesicles. Right-side-out membrane vesicles were preloaded with 10 mM pyruvate and suspended in 100 mM Tris-Mes buffer, pH 7.0, containing either 10 mM serine, threonine, succinate or sucrose to test putative antiport. To 1 ml right-side-out membrane vesicles, 100 µM PMS and 20 µM ascorbate were either added or not, and the aliquot was incubated at RT. At different time points, 150 µl were taken out and immediately centrifuged (16000 × g, 1 min, 4 °C). 120 µl clear supernatant were kept on ice. To determine the pyruvate concentration in this 120 µl sample, the same assay as for the external pyruvate measurement was applied (protein precipitation followed by the enzymatic reaction by lactate dehydrogenase) with the samples diluted 1:5 in 100 mM PIPES buffer, pH 7.8. Total protein concentration of the right-side-out membrane vesicles was determined according to Bradford [34] after sonification.

Creation of a mini-Tn*10* transposon library. The mini-Tn*10* transposon library was created according to the protocol of Freed [30] with the plasmid pNK2859 [35] in *E. coli* MG1655. This plasmid carries a P_{tac} promoter which is inducible by IPTG, and the *ats1 ats2* transposase gene that permits relaxed insertion specificity (altered target specificity, ATS) and thus the transposon will use a much higher number of insertion sites. The 1.8 kb mini-Tn*10* transposon

contains a kanamycin resistance marker originating from Tn*903*. The 6.5-kb plasmid is based on pBR322 and contains an ampicillin resistance cassette. First, the donor strain WM3065 was transformed with the pNK2958 plasmid and grown overnight in LB medium supplemented with 300 µM diaminopimelic acid due to the strain's auxotrophy and ampicillin to keep the plasmid. The recipient MG1655 was grown overnight in LB medium. Both strains (1 ml each) were washed twice with LB medium, resuspended and combined in 200 µl LB medium. This volume was carefully dropped on an LB agar plate containing 300 µM diaminopimelic acid, dried and incubated for 4 hours at 37 °C to allow conjugation. The cells were washed off with 2 ml LB containing 1 mM IPTG to induce expression of the transposase on the plasmid and plated in dilutions on LB agar containing kanamycin to select for clones with an inserted transposon. After a test conjugation, the appropriate dilution for plating was determined and the procedure was repeated in larger scale to obtain the desired number of single clones for the library. These clones were washed off from the plates using a sterile scraper and 1 ml PBS per plate. They were pooled in a falkon tube, vortexed and glycerol was added to a final concentration of 15 %. The library was frozen in aliquots of 1 ml cryo-vials.

Blue-white-screening for *btsT* expression. For a blue-white-screening based on *btsT* expression, the transposon library was transformed with the pBBR1-MCS5-P_{btsT}-*lacZ* plasmid. To this end, the donor strain WM3065 was transformed with the plasmid and grown overnight in LB medium supplemented with 300 µM diaminopimelic acid due to the strain's auxotrophy and ampicillin to keep the plasmid. A volume of the donor corresponding to an OD_{600} of 8 was washed twice with LB medium. 200 µl of the frozen transposon library was also washed twice with LB medium. Both pellets were resuspended and combined in 200 µl LB medium. This volume was carefully dropped on an LB agar plate containing 300 µM diaminopimelic acid, dried and incubated for 4 hours at 37 °C to allow conjugation. The cells were washed off with 2 ml LB and plated in dilutions on LB agar containing kanamycin to select for the transposon mutants, gentamicin to keep the reporter plasmid and X-gal to a final concentration of 200 µg/ml. After a test conjugation, the appropriate dilution for plating was determined and the procedure was repeated in larger scale to obtain the desired number of single clones for a sufficient blue-white screening. White clones were re-streaked to fresh plates.

ACKNOWLEDGEMENTS

The authors thank Jin Qiu for her contribution in plasmid construction. This research was funded by the Deutsche Forschungsgemeinschaft (project number 395357507-SFB1371 to K.J.).

TABLES

Table 1. *btsT* expression and external pyruvate of the most promising Keio deletion mutants after untargeted large-scale screening and targeted screening strategies A, B and C. Cells were grown in LB medium at 37 °C. For *btsT* expression, all cells harbored the pBBR1-MCS5-P_{btsT}-*lux* reporter plasmid and fold change values are depicted in relation to the respective wild-type expression value. For external pyruvate measurements, samples were taken at the exponential growth phase (untargeted screening) or every 15 minutes during growth (all other screening strategies).

	Keio strain	Product of the deleted gene	*btsT* expression (RLU/OD_{600})	*btsT* expression fold change in comparison to the wild-type	External pyruvate (µM)
Most promising candidates based on untargeted screening of 30 Keio collection plates	*yrbG*	inner membrane protein, calcium transporter, calcium-cation-antiporter family	1154	0.052	71; 394
	yjfL	inner membrane protein, 4 TMs	4021	0.183	576
	yidH	inner membrane protein, response to oxidative stress, 3 TMs	4606	0.209	601
	yrbD	Intermembrane phospholipid transport system binding protein MlaD, Part of the ABC transporter complex MlaFEDB	4620	0.210	486
	oppA	Periplasmic oligopeptide-binding protein, component of the oligopeptide permease, ATP binding	5900	0.268	516
	yjcP	Multidrug resistance outer membrane protein, transmembrane transport	6018	0.274	581
	yjeH	L-methionine/branched-chain amino acid exporter, catalyzes efflux of L-methionine. Can also export L-leucine, L-isoleucine and L-valine. Activity dependent on electrochemical potential. 11 TMs	6188	0.281	491
	yhjD	inner membrane protein, lipopolysaccharide transmembrane transporter activity, 6 TMs	7358	0.335	501
	hsrA	Probable transport protein, major facilitator superfamily, EmrB family, High-copy suppressor of rspA, 14 TMs	7888	0.359	366
	ydiY	uncharacterized protein, duf481 putative beta barrel porin (duf481) family	8207	0.373	461
	yfjQ	UPF0380 protein, in *Bacillus*: putative ion transporter	8787	0.400	496
	yhiI	uncharacterized protein, ABC superfamily, in *Salmonella*: HlyD family efflux transporter periplasmic adaptor subunit	8918	0.406	691
	cusB	Cation efflux system protein, mediates resistance to copper and silver	9156	0.416	
	yjcD	Guanine/hypoxanthine permease GhxP, 12 TMs	10706	0.487	
	yhgE	uncharacterized protein, putative transporter, 11 TMs	11043	0.502	
	yedR	Inner membrane protein, 2 TMs, in *Shigella*: permease	11181	0.508	
	ydeU	uncharacterized protein, outer membrane, autotransporter domain	11245	0.511	
	yifK	Probable amino-acid or metabolite transport protein, 12 TMs	14187	0.645	

	yebZ	inner membrane protein, copper ion transport, 8 TMs	21155	0.962	
	Wild type	-	21992	1	501
Most promising candidates based on targeted strategy A	Keio strain	Product of the deleted gene	*btsT* expression (RLU/OD_{600})	*btsT* expression fold change in comparison to the wild-type	External pyruvate (µM)
	pitA	Low-affinity inorganic phosphate transporter 1, can also transport arsenate	2630	0.304	630
	sdaC	Serine transporter, import of serine into the cell	3932	0.455	247; 188
	leuE	Exporter of leucine. Can also transport its natural analog L-alpha-amino-n-butyric acid and some other structurally unrelated amino acids, *yeaS*	4668	0.540	630
	yqeG	Inner membrane transport protein, amino acid transport, hydroxy/aromatic amino acid permease (haaap) family, SdaC/TdcC subfamily	5312	0.615	2238
	aaeA	p-hydroxybenzoic acid efflux pump subunit, Forms an efflux pump with AaeB, membrane fusion protein (mfp) family, carboxylic acid transport	5618	0.650	605
	ydiY	Uncharacterized protein YdiY, duf481 putative beta barrel porin (duf481) family	6946	0.804	
	ychE	UPF0056 membrane protein, neutral amino acid transporter (NAAT) family	6978	0.808	
	dtpA	Putative lipoprotein AcfD homolog, type II secretion	7238	0.838	
	panF	Sodium/pantothenate symporter, catalyzes the sodium-dependent uptake of extracellular pantothenate	7327	0.848	
	ydgI	Putative arginine/ornithine antiporter	7826	0.906	
	yeeF	Low-affinity putrescine importer PlaP, required for induction of type 1 pili-driven surface motility	8118	0.939	
	proY	Proline-specific permease ProY, amino acid-polyamine-organocation (APC) family	8360	0.968	
	ansP	L-asparagine permease, amino acid transport, amino acid-polyamine-organocation (APC) family	8579	0.993	
	yicG	UPF0126 inner membrane protein, uncharacterized	8631	0.999	
	yjeM	Inner membrane transporter YjeM, amino acid transport (amino acid-polyamine-organocation (APC) superfamily)	9336	1.080	
	gltP	Proton/glutamate-aspartate symporter, dicarboxylic acid transport, dicarboxylate/amino acid:cation (Na^+ or H^+) symporter (daacs) family	9381	1.086	
	gntP	High-affinity gluconate transporter, fairly broad specificity, gluconate:H^+ symporter (gntp) family	9505	1.100	
	oppC	Oligopeptide transport system permease protein OppC, atp-binding cassette (ABC) superfamily, OppBC subfamily	9639	1.115	
	yaaH	Succinate-acetate/proton symporter SatP, uptake of acetate and succinate	10461	1.211	

	yhjV	Inner membrane transport protein, amino acid transport, response to radiation, hydroxy/aromatic amino acid permease (haaap) family, amino acid/polyamine transporter 2 family, SdaC/TdcC subfamily	10599	1.227	
	yigM	Biotin transporter	12202	1.412	
	ychM	C4-dicarboxylic acid transporter DauA, aerobic transport of succinate from the periplasm to the cytoplasm at acidic pH. Can transport other C4-dicarboxylic acids such as aspartate and fumarate	13990	1.619	
	dinF	Multidrug resistance protein, also able to export peptides	14485	1.676	
	brnQ	Branched-chain amino acid transport system 2 carrier protein, Component of the LIV-II transport system	15015	1.738	
	ydhC	Inner membrane transport protein, major facilitator superfamily (MFS), drug transport, xenobiotic detoxification by export	15935	1.844	
	wild type	-	8641	1	501
Most promising candidates based on targeted strategy B	Keio strain	Product of the deleted gene	*btsT* expression (RLU/OD_{600})	*btsT* expression fold change in comparison to the wild-type	External pyruvate (µM)
	tatE	Sec-independent protein translocase protein TatE	109620	0.149	341; 380
	ydiM	Inner membrane transport protein YdiM, 11 TMs	153779	0.249	288; 163
	yegN	Multidrug resistance protein MdtB, 11 TMs	154938	0.253	281; 355
	yceL	Multidrug resistance protein MdtH, 10 TMs	170594	0.262	333; 297
	ytfF	Inner membrane protein YtfF, 10 TMs	173580	0.262	641
	emrB	Multidrug export protein EmrB, 14 TMs	197756	0.288	843
	ydeE	Uncharacterized MFS-type transporter YdeE, peptide export	204347	0.295	228; 247
	yeeO	Probable FMN/FAD exporter YeeO, 11 TMs	212570	0.295	506
	ygaY	Putative uncharacterized transporter YgaY, 11 TMs	214225	0.298	483
	cmr	Multidrug transporter MdfA, efflux pump driven by the proton motive force	215162	0.300	566
	emrE	Multidrug efflux protein, coupled to an influx of protons	219102	0.318	
	yhfC	Transporter protein TsgA	221186	0.326	
	setB	Sugar efflux transporter B, 12 TMs	222533	0.329	
	ybgH	Dipeptide permease D, 14 TMs	230775	0.332	
	ycaD	Uncharacterized MFS-type transporter YcaD, 12 TMs	232524	0.334	
	tatC	Sec-independent protein translocase protein TatC, part of the TatABC complex	234398	0.348	
	yijE	Probable cystine transporter YijE	234689	0.350	
	yajR	Inner membrane transport protein YajR, 10 TMs	235333	0.352	
	yhjV	Inner membrane transport protein YhjV, 11 TMs	238638	0.352	
	ydgR	Dipeptide and tripeptide permease A, proton dependent	246244	0.353	
	ycaM	Inner membrane transporter YcaM, 12 TMs	253956	0.354	

	yjdL	Dipeptide and tripeptide permease C, proton dependent	264219	0.359	
	rarD	Transport protein, 10 TMs	265335	0.361	
	yegO	Multidrug resistance protein MdtC, 10 TMs	268186	0.362	
	eamA	Probable amino-acid metabolite efflux pump, 10 TMs	268189	0.369	
	yqeG	Inner membrane transport protein YqeG, 10 TMs	268509	0.370	
	ygjI	Inner membrane transporter YgjI, 13 TMs	272730	0.373	
	ynfM	Inner membrane transport protein YnfM, 11 TMs	278542	0.374	
	acrD	Probable aminoglycoside efflux pump, 12 TMs	279428	0.391	
	ybdA	Enterobactin exporter EntS, 12 TMs	281436	0.395	
	yicL	Uncharacterized inner membrane transporter YicL	284838	0.406	
	yjiO	Multidrug resistance protein MdtM	287100	0.406	
	yfbJ	Probable 4-amino-4-deoxy-L-arabinose-phosphoundecaprenol flippase subunit ArnF	288117	0.407	
	yedA	Uncharacterized inner membrane transporter YedA	293754	0.418	
	tatA	Sec-independent protein translocase protein TatA	295219	0.422	
	setA	Sugar efflux transporter A	303275	0.423	
	emrD	Multidrug resistance protein D	304332	0.423	
	dinF	DNA damage-inducible protein F	307103	0.442	
	yhiP	Dipeptide and tripeptide permease B, proton dependent	309182	0.444	
	acrF	Multidrug export protein AcrF, efflux of indole	313680	0.476	
	yfcJ	Uncharacterized MFS-type transporter YfcJ	314926	0.480	
	yjbB	Uncharacterized protein YjbB	320544	0.484	
	bcr	Bicyclomycin resistance protein, peptide export	326772	0.484	
	yhiV	Multidrug resistance protein MdtF	327169	0.495	
	sugE	Guanidinium exporter	328931	0.512	
	ybaT	Inner membrane transport protein YbaT, probable amino-aicd or metabolite transporter	331796	0.521	
	yceE	Multidrug resistance protein MdtG	337192	0.533	
	yigM	Biotin transporter, facilitated by diffusion	341811	0.551	
	yebQ	Uncharacterized transporter YebQ	345103	0.562	
	emrY	Probable multidrug resistance protein EmrY	346389	0.568	
	ydfJ	Putative transporter YdfJ	357541	0.589	
	araJ	Putative transporter AraJ	360745	0.596	
	ydiN	Inner membrane transport protein YdiN	363185	0.600	
	yhhS	Uncharacterized MFS-type transporter YhhS	363486	0.618	
	yhjX	Uncharacterized MFS-type transporter YhjX	381922	0.621	
	yjeM	Inner membrane transporter YjeM	384756	0.622	
	yhaO	Probable serine transporter	419455	0.625	
	yaaJ	Uncharacterized transporter YaaJ	447618	0.651	
	acrB	Multidrug efflux pump subunit AcrB	457235	0.656	
	ydhC	Inner membrane transport protein YdhC	485788	0.664	

	tatB	Sec-independent protein translocase protein TatB	498143	0.704	
	yegB	Putative multidrug resistance protein MdtD	546475	0.717	
	wild type	-	655851	1	738
Most promising candidates based on targeted strategy C	Keio strain	Product of the deleted gene	*btsT* expression (RLU/OD_{600})	*btsT* expression fold change in comparison to the wild-type	External pyruvate (µM)
	yneE	UPF0187 protein YneE, chloride channel	26581	0.082	
	ycdZ	Inner membrane protein	54589	0.169	
	ycfZ	Inner membrane protein	58220	0.180	
	yghF	Putative type II secretion system C-type protein	64644	0.200	
	yjhE	Putative uncharacterized protein	72649	0.225	
	mntP	Probable manganese efflux pump	83857	0.260	
	yddA	Inner membrane ABC transporter ATP-binding protein	87886	0.272	
	ymfA	Inner membrane protein	87996	0.272	
	yghE	Putative type II secretion system L-type protein	89762	0.278	
	dtpA	Proton-dependent permease that transports di- and tripeptides	105822	0.328	
	secG	Protein-export membrane protein	111789	0.346	
	ansP	L-asparagine permease, APC family (*yncF*)	126433	0.391	
	wild type	-	322973	1	

REFERENCES

1. Behr S, Brameyer S, Witting M, Schmitt-Kopplin P, Jung K. 2017. Comparative analysis of LytS/LytTR-type histidine kinase/response regulator systems in γ-proteobacteria. PLoS One 12:e0182993. doi:10.1371/journal.pone.0182993
2. Chubukov V, Gerosa L, Kochanowski K, Sauer U. 2014. Coordination of microbial metabolism. Nat Rev Microbiol 12:327-340. doi:10.1038/nrmicro3238
3. Paczia N, Nilgen A, Lehmann T, Gätgens J, Wiechert W, Noack S. 2012. Extensive exometabolome analysis reveals extended overflow metabolism in various microorganisms. Microb Cell Factories 11:122. doi:10.1186/1475-2859-11-122
4. Yasid NA, Rolfe MD, Green J, Williamson MP. 2016. Homeostasis of metabolites in *Escherichia coli* on transition from anaerobic to aerobic conditions and the transient secretion of pyruvate. R Soc Open Sci 3:160187. doi:10.1098/rsos.160187
5. Kristoficova I, Vilhena C, Behr S, Jung K. 2018. BtsT, a novel and specific pyruvate/H^+ symporter in *Escherichia coli*. J Bacteriol 200:e00599-17. doi:10.1128/jb.00599-17
6. Gasperotti A, Göing S, Fajardo-Ruiz E, Forné I, Jung K. 2020. Function and regulation of the pyruvate transporter CstA in *Escherichia coli*. Int J Mol Sci 21:9068. doi:10.3390/ijms21239068
7. Behr S, Kristoficova I, Witting M, Breland EJ, Eberly AR, Sachs C, Schmitt-Kopplin P, Hadjifrangiskou M, Jung K. 2017. Identification of a high-affinity pyruvate receptor in *Escherichia coli*. Sci Rep 7:1388. doi:10.1038/s41598-017-01410-2
8. Fried L, Behr S, Jung K. 2013. Identification of a target gene and activating stimulus for the YpdA/YpdB histidine kinase/response regulator system in *Escherichia coli*. J Bacteriol 195:807-15. doi:10.1128/jb.02051-12
9. Ruby EG, Nealson KH. 1977. Pyruvate production and excretion by the luminous marine bacteria. Appl Environ Microbiol 34:164-9. doi:10.1128/aem.34.2.164-169.1977
10. Göing S, Gasperotti AF, Yang Q, Defoirdt T, Jung K. 2021. Insights into a Pyruvate Sensing and Uptake System in *Vibrio campbellii* and Its Importance for Virulence. J Bacteriol 203:e0029621. doi:10.1128/jb.00296-21
11. Constantopoulos G, Barranger JA. 1984. Nonenzymatic decarboxylation of pyruvate. Anal Biochem 139:353-358. doi:10.1016/0003-2697(84)90016-2
12. Kładna A, Marchlewicz M, Piechowska T, Kruk I, Aboul-Enein HY. 2015. Reactivity of pyruvic acid and its derivatives towards reactive oxygen species. Luminescence 30:1153-8. doi:10.1002/bio.2879
13. Varma SD, Hegde K, Henein M. 2003. Oxidative damage to mouse lens in culture. Protective effect of pyruvate. Biochim Biophys Acta 1621:246-52. doi:10.1016/s0304-4165(03)00075-8
14. O'Donnell-Tormey J, Nathan CF, Lanks K, DeBoer CJ, de la Harpe J. 1987. Secretion of pyruvate. An antioxidant defense of mammalian cells. J Exp Med 165:500-14. doi:10.1084/jem.165.2.500
15. Kraxenberger T, Fried L, Behr S, Jung K. 2012. First insights into the unexplored two-component system YehU/YehT in *Escherichia coli*. J Bacteriol 194:4272-84. doi:10.1128/jb.00409-12
16. Baba T, Ara T, Hasegawa M, Takai Y, Okumura Y, Baba M, Datsenko KA, Tomita M, Wanner BL, Mori H. 2006. Construction of *Escherichia coli* K-12 in-frame, single-gene knockout mutants: the Keio collection. Mol Syst Biol 2:2006 0008. doi:10.1038/msb4100050
17. UniProt C. 2021. UniProt: the universal protein knowledgebase in 2021. Nucleic Acids Res 49:D480-D489. doi:10.1093/nar/gkaa1100
18. Li GW, Burkhardt D, Gross C, Weissman JS. 2014. Quantifying absolute protein synthesis rates reveals principles underlying allocation of cellular resources. Cell 157:624-35. doi:10.1016/j.cell.2014.02.033
19. Shao Z, Lin RT, Newman EB. 1994. Sequencing and characterization of the sdaC gene and identification of the sdaCB operon in *Escherichia coli* K12. Eur J Biochem 222:901-7. doi:10.1111/j.1432-1033.1994.tb18938.x
20. Ogawa W, Kayahara T, Tsuda M, Mizushima T, Tsuchiya T. 1997. Isolation and characterization of an *Escherichia coli* mutant lacking the major serine transporter, and cloning

of a serine transporter gene. J Biochem 122:1241-5. doi:10.1093/oxfordjournals.jbchem.a021887
21. Hama H, Shimamoto T, Tsuda M, Tsuchiya T. 1988. Characterization of a novel L-serine transport system in *Escherichia coli*. J Bacteriol 170:2236-9. doi:10.1128/jb.170.5.2236-2239.1988
22. Kriner MA, Subramaniam AR. 2020. The serine transporter SdaC prevents cell lysis upon glucose depletion in *Escherichia coli*. Microbiologyopen 9:e960. doi:10.1002/mbo3.960
23. Likhacheva NA, Samsonov VV, Samsonov VV, Sineoky SP. 1996. Genetic control of the resistance to phage C1 of *Escherichia coli* K-12. J Bacteriol 178:5309-15. doi:10.1128/jb.178.17.5309-5315.1996
24. Gerard F, Pradel N, Wu LF. 2005. Bactericidal activity of colicin V is mediated by an inner membrane protein, SdaC, of *Escherichia coli*. J Bacteriol 187:1945-50. doi:10.1128/JB.187.6.1945-1950.2005
25. Kaback H. 1971. Bacterial Membranes, p 99-120, Methods Enzymol, vol 22. Elsevier.
26. Pruss BM, Nelms JM, Park C, Wolfe AJ. 1994. Mutations in NADH:ubiquinone oxidoreductase of *Escherichia coli* affect growth on mixed amino acids. J Bacteriol 176:2143-50. doi:10.1128/jb.176.8.2143-2150.1994
27. Selvarasu S, Ow DS, Lee SY, Lee MM, Oh SK, Karimi IA, Lee DY. 2009. Characterizing *Escherichia coli* DH5alpha growth and metabolism in a complex medium using genome-scale flux analysis. Biotechnol Bioeng 102:923-34. doi:10.1002/bit.22119
28. Elbourne LD, Tetu SG, Hassan KA, Paulsen IT. 2017. TransportDB 2.0: a database for exploring membrane transporters in sequenced genomes from all domains of life. Nucleic Acids Res 45:D320-D324. doi:10.1093/nar/gkw1068
29. Smith A, Kaczmar A, Bamford RA, Smith C, Frustaci S, Kovacs-Simon A, O'Neill P, Moore K, Paszkiewicz K, Titball RW, Pagliara S. 2018. The Culture Environment Influences Both Gene Regulation and Phenotypic Heterogeneity in *Escherichia coli*. Front Microbiol 9:1739. doi:10.3389/fmicb.2018.01739
30. Freed NE. 2017. Creation of a Dense Transposon Insertion Library Using Bacterial Conjugation in Enterobacterial Strains Such As *Escherichia Coli* or *Shigella flexneri*. J Vis Exp. doi:10.3791/56216
31. Inoue H, Nojima H, Okayama H. 1990. High efficiency transformation of *Escherichia coli* with plasmids. Gene 96:23-8. doi:10.1016/0378-1119(90)90336-p
32. Guzman LM, Belin D, Carson MJ, Beckwith J. 1995. Tight regulation, modulation, and high-level expression by vectors containing the arabinose PBAD promoter. J Bacteriol 177:4121-30. doi:10.1128/jb.177.14.4121-4130.1995
33. Sambrook J, Fritsch E, Maniatis T. 1989. Molecular Cloning: A Laboratory Manual, 2nd ed. Cold Spring Harbor Laboratory Press, Cold Spring Harbor, NY.
34. Bradford MM. 1976. A rapid and sensitive method for the quantitation of microgram quantities of protein utilizing the principle of protein-dye binding. Anal Biochem 72:248-54. doi:10.1006/abio.1976.9999
35. Kleckner N, Bender J, Gottesman S. 1991. Uses of transposons with emphasis on Tn10. Methods Enzymol 204:139-80. doi:10.1016/0076-6879(91)04009-d

SUPPLEMENTAL FIGURES

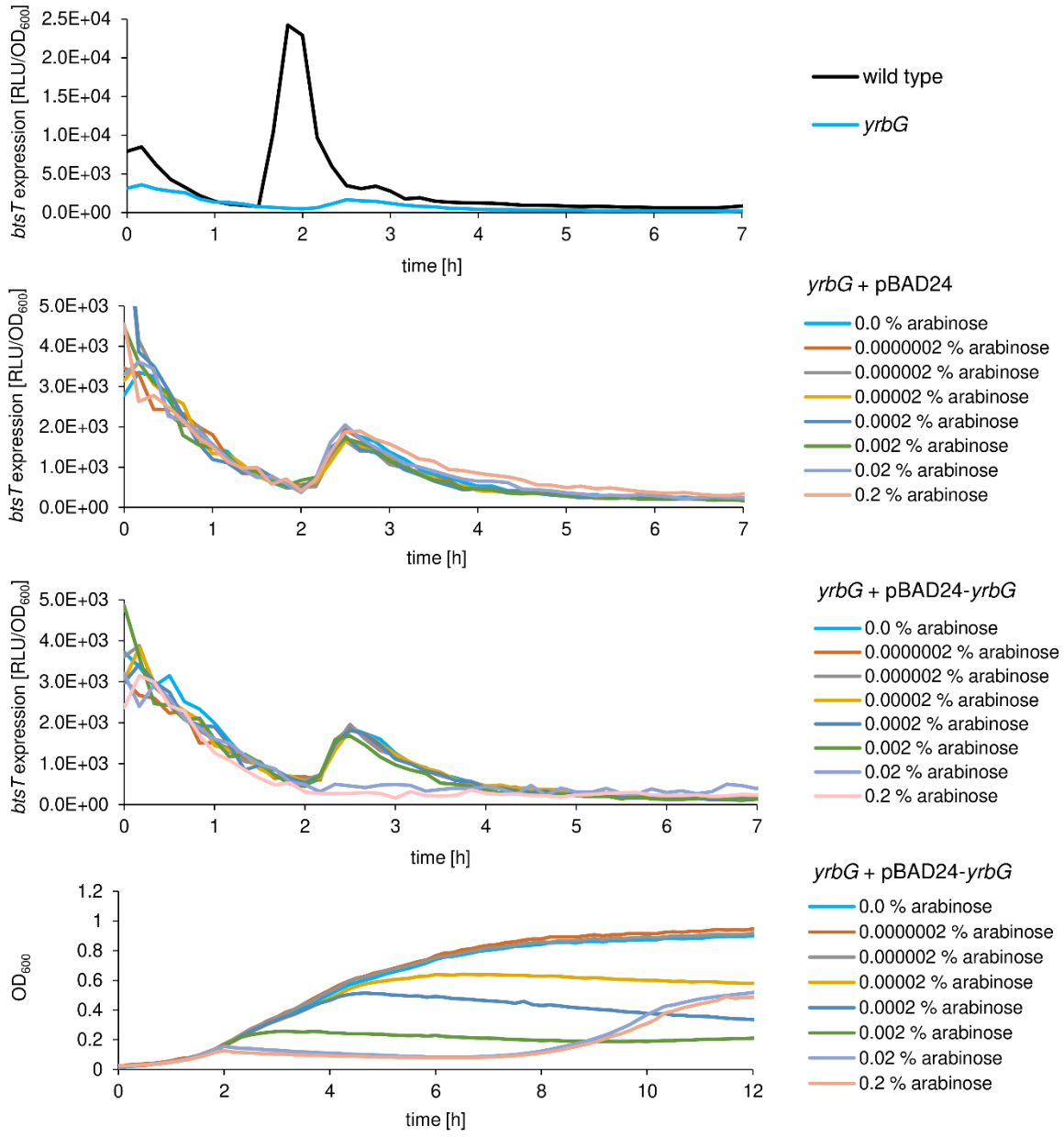

Figure S1. *btsT* expression in *E. coli* Keio deletion mutant *yrbG* with pBAD24 (empty vector as control) or pBAD24-*yrbG* in comparison to the wild type. All cells also harbor the pBBR1-MCS5-P_{btsT}-*lux* reporter plasmid. All strains were grown in LB medium at 37 °C with addition of the indicated arabinose concentrations. Growth (OD_{600}) and luminescence (RLU) were measured in a plate reader and *btsT* expression was calculated (RLU/OD_{600}).

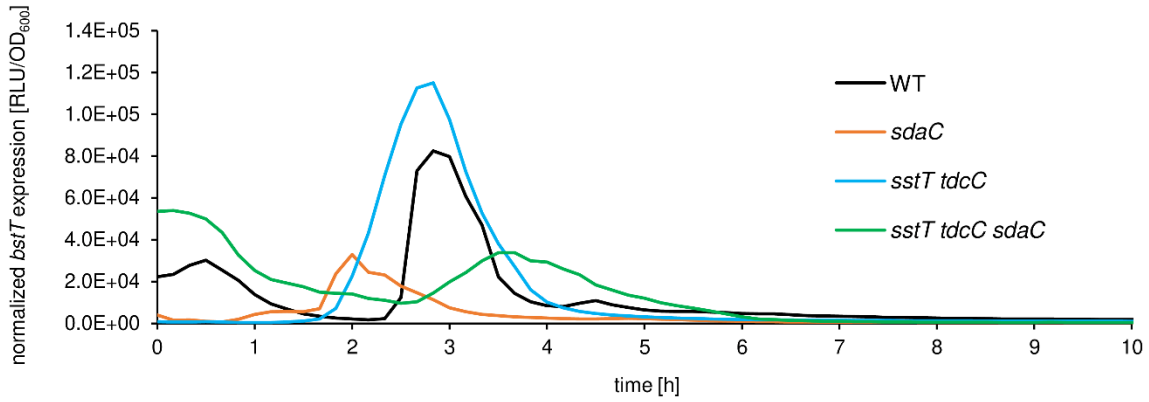

Figure S2. *btsT* expression in *E. coli* Keio deletion mutants *sdaC* (orange), *sstT tdcC* (light blue) and *sstT tdcC sdaC* (green) in comparison to the wild type (black). All cells harbor the pBBR1-MCS5-P_{btsT}-*lux* reporter plasmid. All strains were grown in LB medium at 37 °C. Growth (OD_{600}) and luminescence (RLU) were measured in a plate reader and *btsT* expression was calculated (RLU/OD_{600}).

SUPPLEMENTAL TABLES

Table S1. Overview of all Keio collection plates transformed with the pBBR1-MCS5-P_{btsT}-*lux* reporter plasmid and analyzed for *btsT* expression. All strains were grown in LB medium at 37 °C. Growth (OD_{600}) and luminescence (RLU) were measured in a plate reader and *btsT* expression was calculated (RLU/OD_{600}). Fold change values were calculated based on the mean of the wild-type expression values. This calculation was done in two groups due to different plate readers: Plates 3, 5, 7, 9, 11, 13, 35 and 37 were calculated in one group (wild-type mean for these plates: 18188 RLU/OD_{600}), all other plates were calculated in another group (wild-type mean for these plates: 240470 RLU/OD_{600}).

Plate 3		
	expression	fold change
A02	22009	1.210
A04	23055	1.268
A05	28074	1.544
A06	26049	1.432
A07	22612	1.243
A08	24686	1.357
A09	28537	1.569
A10	33241	1.828
A11	10766	0.592
A12	18650	1.025
B02	13709	0.754
B03	13693	0.753
B04	17059	0.938
B05	20309	1.117
B06	25289	1.390
B07	11566	0.636
B08	22942	1.261
B09	10454	0.575
B10	11719	0.644
B11	14910	0.820
B12	14489	0.797
C01	10954	0.602
C02	19142	1.052
C04	15030	0.826
C05	19137	1.052
C06	18146	0.998
C07	11660	0.641
C08	7168	0.394
C09	5879	0.323
C10	29057	1.598
C11	18160	0.998
C12	9120	0.501
D04	2134	0.117
D05	14483	0.796
D07	12252	0.674
D08	12086	0.665
D09	10699	0.588
D10	18335	1.008
D11	10204	0.561
D12	17489	0.962
E01	12244	0.673
E02	5719	0.314
E03	4012	0.221
E04	15728	0.865
E05	7645	0.420
E06	9398	0.517
E07	5560	0.306
E08	7201	0.396
E09	4958	0.273
E10	17324	0.952
E11	11928	0.656
E12	5422	0.298
F01	6130	0.337
F02	10131	0.557
F03	6767	0.372
F04	16951	0.932
F05	5160	0.284
F06	14461	0.795
F07	17169	0.944
F08	7411	0.407
F09	16896	0.929
F10	14256	0.784
F11	7243	0.398
F12	11436	0.629
G01	4689	0.258
G02	11705	0.644
G03	8270	0.455
G04	8498	0.467
G05	6517	0.358
G06	17613	0.968
G07	15124	0.832
G08	6752	0.371
G09	18730	1.030
G10	11630	0.639
G11	10733	0.590
G12	14886	0.818
H01	9134	0.502
H02	6451	0.355
H03	11991	0.659
H04	7849	0.432
H05	10191	0.560
H06	7422	0.408
H07	10214	0.562
H08	6942	0.382
H09	16117	0.886
H10	23082	1.269
H11	8595	0.473
H12	8311	0.457
WT	17891	0.984

Plate 5		
	expression	fold change
A01	17516	0.963
A02	19186	1.055
A03	17416	0.958
A04	18026	0.991
A05	16170	0.889
A06	21246	1.168
A07	7345	0.404
A08	21901	1.204
A09	28245	1.553
A10	6812	0.375
A11	23764	1.307
A12	19089	1.050
B01	10220	0.562
B02	15855	0.872
B03	14213	0.781
B04	28945	1.591
B05	20027	1.101
B06	15160	0.834
B07	26221	1.442
B08	28363	1.559
B09	18926	1.041
B10	10768	0.592
B11	19892	1.094
B12	11127	0.612
C01	27233	1.497
C02	6632	0.365
C03	10113	0.556
C04	19057	1.048
C05	26749	1.471
C06	16709	0.919
C07	20972	1.153
C08	4545	0.250
C09	17810	0.979
C10	14800	0.814
C11	25878	1.423
C12	22492	1.237
D01	3482	0.191
D02	1987	0.109
D03	10031	0.552
D04	6804	0.374
D05	15547	0.855
D06	16908	0.930
D07	13653	0.751
D08	20612	1.133
D09	12062	0.663
D10	6182	0.340
D11	26116	1.436
D12	100000	5.498
E01	2655	0.146
E02	37917	2.085
E03	8824	0.485
E04	10840	0.596
E05	15757	0.866
E06	20688	1.137
E07	20488	1.126
E08	17470	0.961
E09	11729	0.645
E10	7241	0.398
E11	29780	1.637
E12	80000	4.399
F01	14315	0.787
F02	9940	0.547
F03	5847	0.321
F04	19013	1.045
F05	12121	0.666
F06	10737	0.590
F07	22548	1.240
F08	13882	0.763
F10	18048	0.992
F11	7689	0.423
F12	21300	1.171
G01	13547	0.745
G02	9482	0.521
G03	27054	1.487
G04	33165	1.823
G05	34422	1.893
G06	15880	0.873
G07	11338	0.623
G09	16500	0.907
G10	21092	1.160
G11	10997	0.605
G12	89344	4.912
H01	20017	1.101
H02	11110	0.611
H03	16584	0.912
H04	11120	0.611
H06	11712	0.644
H07	7802	0.429
H08	5676	0.312
H09	37487	2.061
H10	14114	0.776
H11	7959	0.438
WT	6754	0.371

Plate 7		
	expression	fold change
A01	13765	0.757
A02	16893	0.929
A03	21052	1.157
A04	10530	0.579
A05	21297	1.171
A06	9879	0.543
A07	10527	0.579
A08	12138	0.667
A09	20294	1.116
A10	12410	0.682
A11	24293	1.336
A12	6837	0.376
B01	10538	0.579
B02	15817	0.870
B03	20208	1.111
B04	15141	0.832
B05	14626	0.804
B06	15206	0.836
B07	8584	0.472
B08	17461	0.960
B09	14834	0.816
B10	19122	1.051
B11	21130	1.162
B12	8870	0.488
C02	24296	1.336
C03	18052	0.993
C04	20744	1.141
C05	14129	0.777
C06	8701	0.478
C07	3185	0.175
C08	20807	1.144
C09	19837	1.091
C10	9605	0.528
C11	20996	1.154
C12	31490	1.731
D02	34444	1.894
D03	34175	1.879
D04	9863	0.542
D05	26526	1.458
D06	27622	1.519
D07	14257	0.784
D08	18600	1.023
D09	14348	0.789
D10	12891	0.709
D11	27296	1.501
E01	22787	1.253
E02	27440	1.509
E03	32295	1.776
E04	11425	0.628
E05	21862	1.202
E06	11218	0.617
E07	8984	0.494
E08	12064	0.663
E09	15675	0.862
E10	9743	0.536
E11	20304	1.116
F01	4597	0.253
F02	22230	1.222
F03	24474	1.346
F04	9299	0.511
F05	14366	0.790
F06	3188	0.175
F07	12270	0.675
F08	14359	0.789
F09	13314	0.732
F10	6826	0.375
F11	11313	0.622
F12	34715	1.909
G01	17356	0.954
G02	16433	0.904
G03	10800	0.594
G04	19702	1.083
G05	8455	0.465
G06	20444	1.124
G07	21257	1.169
G08	11156	0.613
G09	19000	1.045
G10	18240	1.003
G11	10168	0.559
G12	9773	0.537
H01	3874	0.213
H02	13500	0.742
H03	14446	0.794
H04	18225	1.002
H05	19515	1.073
H06	14939	0.821
H07	11011	0.605
H08	10066	0.553
H09	11949	0.657
H10	11816	0.650
H11	18578	1.021
H12	17012	0.935

plate 9		
	expression	fold change
A05	12349	0.679
A06	13912	0.765
A07	16486	0.906
A08	14276	0.785
A09	20145	1.108
A10	25850	1.421
A11	26822	1.475
A12	21900	1.204
B01	16922	0.930
B02	24047	1.322
B03	10732	0.590
B04	12710	0.699
B05	11185	0.615
B06	20760	1.141
B07	13308	0.732
B08	11085	0.609
B09	24332	1.338
B10	14174	0.779
B11	15051	0.828
B12	21955	1.207
C01	21400	1.177
C02	30668	1.686
C03	13569	0.746
C04	12629	0.694
C05	11813	0.649
C06	11014	0.606
C07	12034	0.662
C08	14901	0.819
C09	15427	0.848
C10	9757	0.536
C11	16671	0.917
C12	14897	0.819
D01	7928	0.436
D02	11495	0.632
D03	16771	0.922
D04	19917	1.095
D05	12759	0.702
D06	8209	0.451
D07	12871	0.708
D08	14753	0.811
D09	14133	0.777
D10	14491	0.797
D11	17556	0.965
D12	16635	0.915
E01	11712	0.644
E02	11380	0.626
E03	16411	0.902
E04	8962	0.493
E05	9769	0.537
E06	6431	0.354
E07	11449	0.629
E08	12209	0.671
E09	14952	0.822
E10	20380	1.121
E11	9066	0.498
E12	9862	0.542
F01	9717	0.534
F02	7353	0.404
F03	11442	0.629
F04	13145	0.723
F05	9167	0.504
F06	6084	0.335
F07	6227	0.342
F08	9422	0.518
F09	16419	0.903
F10	7740	0.426
F11	12538	0.689
F12	13652	0.751
G01	6923	0.381
G02	14573	0.801
G03	5109	0.281
G04	8212	0.451
G05	6519	0.358
G06	6012	0.331
G07	7693	0.423
G08	6226	0.342
G09	9324	0.513
G10	9945	0.547
G11	4258	0.234
G12	4449	0.245
H01	8738	0.480
H02	7802	0.429
H03	5377	0.296
H04	5530	0.304
H05	4006	0.220
H06	1960	0.108
H07	5430	0.299
H08	8893	0.489
H09	4876	0.268
H10	6598	0.363
H11	7107	0.391
H12	5540	0.305
WT	17709	0.974

plate 11		
	expression	fold change
A02	17132	0.942
A03	10756	0.591
A04	17231	0.947
A05	13935	0.766
A06	12912	0.710
A07	10853	0.597
A08	16857	0.927
A09	11787	0.648
A10	14934	0.821
A11	13797	0.759
A12	7565	0.416
B01	17146	0.943
B02	15168	0.834
B03	24500	1.347
B04	20673	1.137
B05	16948	0.932
B06	18984	1.044
B07	23878	1.313
B08	16107	0.886
B09	12253	0.674
B10	11575	0.636
B11	10445	0.574
B12	15627	0.859
C01	19421	1.068
C02	9716	0.534
C03	19275	1.060
C04	20020	1.101
C05	13463	0.740
C06	17761	0.977
C07	15664	0.861
C08	15490	0.852
C09	10820	0.595
C10	16819	0.925
C11	11883	0.653
C12	10971	0.603
D01	17605	0.968
D02	15295	0.841
D03	6062	0.333
D04	13375	0.735
D05	5480	0.301
D06	14756	0.811
D07	19682	1.082
D08	6752	0.371
D09	20310	1.117
D10	16270	0.895
D11	163	0.009
D12	9846	0.541
E01	9839	0.541
E02	5352	0.294
E03	13928	0.766
E04	20237	1.113
E05	14816	0.815
E06	22068	1.213
E07	17872	0.983
E08	6173	0.339
E09	15969	0.878
E10	13275	0.730
E11	14509	0.798
E12	9674	0.532
F01	14620	0.804
F02	6992	0.384
F03	5075	0.279
F04	8421	0.463
F05	10030	0.551
F06	12560	0.691
F07	14079	0.774
F08	7548	0.415
F09	6793	0.374
F10	17958	0.987
F11	17457	0.960
F12	4841	0.266
G01	14307	0.787
G02	5964	0.328
G03	10323	0.568
G04	11285	0.620
G05	10104	0.556
G06	6540	0.360
G07	9960	0.548
G08	7119	0.391
G09	7784	0.428
G10	6789	0.373
G11	8827	0.485
G12	9235	0.508
H01	36565	2.010
H02	11651	0.641
H03	8905	0.490
H04	5639	0.310
H05	3375	0.186
H06	11381	0.626
H07	5269	0.290
H08	1122	0.062
H09	7053	0.388
H10	7515	0.413
H11	9369	0.515
H12	7381	0.406
WT	15055	0.828

plate 13		
	expression	fold change
A01	9338	0.513
A02	7930	0.436
A03	4686	0.258
A04	11482	0.631
A05	12303	0.676
A06	18707	1.029
A07	7045	0.387
A08	13622	0.749
A09	12739	0.700
A10	15674	0.862
A11	13696	0.753
A12	26169	1.439
B02	15496	0.852
B03	11548	0.635
B04	12484	0.686
B05	11747	0.646
B06	40877	2.248
B07	22136	1.217
B08	21390	1.176
B09	52223	2.871
B10	16380	0.901
B12	16085	0.884
C01	11788	0.648
C02	6040	0.332
C03	24286	1.335
C04	11490	0.632
C05	25043	1.377
C06	25459	1.400
C07	34300	1.886
C08	26722	1.469
C09	31744	1.745
C10	14482	0.796
C11	2956	0.163
C12	8627	0.474
D01	7197	0.396
D02	18164	0.999
D03	24879	1.368
D04	33042	1.817
D05	37413	2.057
D06	15990	0.879
D07	32768	1.802
D08	17239	0.948
D09	30435	1.673
D10	24968	1.373
D11	29476	1.621
D12	13793	0.758
E01	5139	0.283
E02	11144	0.613
E03	4319	0.237
E04	32966	1.813
E05	19050	1.047
E06	13045	0.717
E08	28107	1.545
E09	29650	1.630
E10	12864	0.707
E11	26320	1.447
E12	18344	1.009
F01	8884	0.488
F02	3965	0.218
F03	6075	0.334
F04	23961	1.317
F05	40614	2.233
F06	12497	0.687
F07	6065	0.333
F08	19875	1.093
F09	20868	1.147
F10	7185	0.395
F11	9679	0.532
F12	11934	0.656
G01	6534	0.359
G02	9316	0.512
G03	12865	0.707
G04	17877	0.983
G05	20392	1.121
G06	6700	0.368
G07	4452	0.245
G08	6609	0.363
G09	4006	0.220
G10	9710	0.534
G11	22554	1.240
G12	6335	0.348
H02	11547	0.635
H03	5789	0.318
H04	7553	0.415
H05	9152	0.503
H06	3936	0.216
H07	3330	0.183
H08	10804	0.594
H09	4859	0.267
H10	5233	0.288
H11	12280	0.675
H12	27044	1.487
WT	10718	0.589

plate 15		
	expression	fold change
A01	77918	0.324
A02	76332	0.317
A03	108166	0.450
A04	26669	0.111
A05	56057	0.233
A06	59071	0.246
A07	35909	0.149
A08	106071	0.441
A09	97141	0.404
A10	94042	0.391
A11	112789	0.469
B01	95473	0.397
B02	99506	0.414
B03	73269	0.305
B04	73250	0.305
B05	27329	0.114
B06	88104	0.366
B07	140756	0.585
B08	53933	0.224
B09	52268	0.217
B10	91592	0.381
B11	120980	0.503
B12	98508	0.410
C01	131102	0.545
C02	52389	0.218
C03	66191	0.275
C04	36328	0.151
C05	82988	0.345
C06	75818	0.315
C07	88728	0.369
C08	24222	0.101
C09	85958	0.357
C10	148724	0.618
C11	55941	0.233
C12	92660	0.385
D01	79754	0.332
D02	36527	0.152
D03	79214	0.329
D04	74871	0.311
D05	64166	0.267
D06	30977	0.129
D07	122519	0.509
D08	69340	0.288
D09	91257	0.379
D10	110806	0.461
D11	102880	0.428
D12	99006	0.412
E01	112837	0.469
E02	79232	0.329
E03	78055	0.325
E04	50027	0.208
E05	58730	0.244
E06	92770	0.386
E07	115889	0.482
E08	80220	0.334
E09	111787	0.465
E10	55588	0.231
E11	53451	0.222
E12	63141	0.263
F01	58654	0.244
F02	113630	0.473
F03	63382	0.264
F04	50186	0.209
F05	58826	0.245
F06	101592	0.422
F07	45843	0.191
F08	75876	0.316
F09	99164	0.412
F10	248938	1.035
F11	101050	0.420
F12	72162	0.300
G01	117716	0.490
G02	100355	0.417
G03	76932	0.320
G04	61817	0.257
G05	100727	0.419
G06	108597	0.452
G07	66998	0.279
G08	135747	0.565
G09	94827	0.394
G10	71123	0.296
G11	32753	0.136
G12	85151	0.354
H01	66294	0.276
H02	78325	0.326
H03	68749	0.286
H04	83165	0.346
H05	81244	0.338
H06	30684	0.128
H07	80063	0.333
H08	77190	0.321
H09	104093	0.433
H10	71845	0.299
H11	25463	0.106
H12	96852	0.403
WT	214083	0.890

plate 17		
	expression	fold change
A01	170874	0.711
A02	92693	0.385
A03	132214	0.550
A04	164204	0.683
A05	63000	0.262
A06	89364	0.372
A07	124771	0.519
A08	86870	0.361
A09	87288	0.363
A10	253980	1.056
A11	82090	0.341
A12	120995	0.503
B01	101721	0.423
B02	111736	0.465
B03	92653	0.385
B04	100215	0.417
B05	74114	0.308
B06	148623	0.618
B07	205933	0.856
B08	122615	0.510
B09	94125	0.391
B10	165477	0.688
B11	86552	0.360
B12	181934	0.757
C01	76513	0.318
C02	168851	0.702
C03	162693	0.677
C04	94085	0.391
C05	57882	0.241
C06	142640	0.593
C07	192328	0.800
C08	103247	0.429
C09	76536	0.318
C10	140329	0.584
C11	132923	0.553
C12	75923	0.316
D01	124302	0.517
D02	114182	0.475
D03	71416	0.297
D04	96348	0.401
D05	89271	0.371
D06	121802	0.507
D07	78159	0.325
D08	87609	0.364
D09	71075	0.296
D10	88788	0.369
D11	152979	0.636
D12	189532	0.788
E01	123052	0.512
E02	33512	0.139
E03	173791	0.723
E04	97854	0.407
E05	101489	0.422
E06	76592	0.319
E07	81834	0.340
E08	82267	0.342
E09	195900	0.815
E10	51224	0.213
E11	99884	0.415
E12	158075	0.657
F01	43591	0.181
F02	131030	0.545
F03	128124	0.533
F04	90111	0.375
F05	63784	0.265
F06	67402	0.280
F07	188693	0.785
F08	74440	0.310
F09	166166	0.691
F10	100000	0.416
F11	78085	0.325
F12	160513	0.667
G01	147211	0.612
G02	177312	0.737
G03	112571	0.468
G04	167000	0.694
G05	76773	0.319
G06	68958	0.287
G07	79824	0.332
G08	61843	0.257
G09	135489	0.563
G11	77502	0.322
G12	136909	0.569
H01	87939	0.366
H02	148637	0.618
H03	72590	0.302
H04	86542	0.360
H05	98107	0.408
H06	120705	0.502
H07	146497	0.609
H08	104137	0.433
H09	193774	0.806
H10	157829	0.656
H11	110916	0.461
H12	168557	0.701
WT	176953	0.736

plate 19		
	expression	fold change
A01	98348	0.409
A02	98510	0.410
A03	163690	0.681
A04	82434	0.343
A05	131855	0.548
A07	96032	0.399
A08	89696	0.373
A09	176311	0.733
A10	208155	0.866
A11	97969	0.407
A12	195005	0.811
B01	142643	0.593
B02	149868	0.623
B03	87225	0.363
B04	123356	0.513
B05	100457	0.418
B06	131124	0.545
B07	185387	0.771
B08	202625	0.843
B09	176671	0.735
B10	118859	0.494
B11	130667	0.543
B12	83585	0.348
C01	85085	0.354
C02	100664	0.419
C03	84526	0.352
C04	187583	0.780
C05	82853	0.345
C06	70490	0.293
C07	123822	0.515
C08	73333	0.305
C09	179634	0.747
C10	136195	0.566
C11	233466	0.971
C12	115573	0.481
D01	190905	0.794
D02	90433	0.376
D03	82330	0.342
D04	157854	0.656
D05	152895	0.636
D06	154231	0.641
D07	96980	0.403
D08	122299	0.509
D09	135431	0.563
D10	80138	0.333
D11	83545	0.347
D12	123477	0.513
E01	88820	0.369
E02	91070	0.379
E03	107822	0.448
E04	83606	0.348
E05	106664	0.444
E06	95182	0.396
E07	100707	0.419
E08	186800	0.777
E09	99977	0.416
E10	95609	0.398
E11	52992	0.220
E12	87038	0.362
F01	179163	0.745
F02	88905	0.370
F03	128855	0.536
F04	149787	0.623
F05	52731	0.219
F06	129450	0.538
F07	108400	0.451
F08	177146	0.737
F09	101856	0.424
F10	78348	0.326
F11	38881	0.162
F12	102112	0.425
G01	134194	0.558
G02	100716	0.419
G03	144060	0.599
G04	51934	0.216
G05	201449	0.838
G06	44791	0.186
G07	151868	0.632
G08	61931	0.258
G09	69173	0.288
G10	109283	0.454
G11	100397	0.418
G12	97208	0.404
H01	164115	0.682
H02	96482	0.401
H03	57021	0.237
H04	89194	0.371
H05	108451	0.451
H06	93385	0.388
H07	100655	0.419
H08	119327	0.496
H09	179798	0.748
H10	114667	0.477
H11	116276	0.484
H12	195691	0.814
WT	115475	0.480

plate 21		
	expression	fold change
A01	204943	0.852
A02	140519	0.584
A03	102165	0.425
A04	99034	0.412
A05	207082	0.861
A06	156413	0.650
A07	268854	1.118
A09	205213	0.853
A10	284004	1.181
A11	270896	1.127
A12	219773	0.914
B01	184700	0.768
B02	89374	0.372
B03	125856	0.523
B04	125395	0.521
B05	109811	0.457
B06	106355	0.442
B08	97291	0.405
B09	223911	0.931
B10	159863	0.665
B11	260851	1.085
B12	173786	0.723
C01	242006	1.006
C02	108110	0.450
C03	173775	0.723
C04	226408	0.942
C05	117026	0.487
C06	130420	0.542
C09	179950	0.748
C10	140433	0.584
C11	229280	0.953
C12	81065	0.337
D02	164821	0.685
D03	154871	0.644
D04	69615	0.289
D05	128127	0.533
D06	172144	0.716
D07	51221	0.213
D08	185238	0.770
D09	117836	0.490
D10	139664	0.581
D11	117690	0.489
D12	270169	1.124
E01	115182	0.479
E02	181342	0.754
E03	240554	1.000
E04	135787	0.565
E05	125690	0.523
E06	146326	0.608
E07	178265	0.741
E08	129116	0.537
E09	228082	0.948
E10	209002	0.869
E11	153536	0.638
E12	192687	0.801
F01	122207	0.508
F03	148631	0.618
F04	134475	0.559
F05	137811	0.573
F06	32548	0.135
F07	237414	0.987
F08	246915	1.027
F09	124253	0.517
F10	168916	0.702
F11	273243	1.136
F12	205527	0.855
G01	134413	0.559
G02	236392	0.983
G03	256753	1.068
G04	85478	0.355
G05	128974	0.536
G06	156398	0.650
G07	117781	0.490
G08	198446	0.825
G09	246166	1.024
G10	221767	0.922
G11	215948	0.898
G12	98248	0.409
H01	107644	0.448
H02	95694	0.398
H03	104528	0.435
H04	135839	0.565
H05	116085	0.483
H06	122762	0.511
H08	120841	0.503
H09	109355	0.455
H10	218527	0.909
H11	270057	1.123
H12	187739	0.781
WT	146380	0.609

plate 23		
	expression	fold change
A01	97068	0.404
A04	184647	0.768
A05	290441	1.208
A06	46363	0.193
A07	130258	0.542
A08	79060	0.329
A09	124525	0.518
A10	141333	0.588
A11	131826	0.548
A12	92363	0.384
B01	86774	0.361
B02	108513	0.451
B03	118676	0.494
B05	64308	0.267
B06	143353	0.596
B07	104845	0.436
B08	66052	0.275
B09	205521	0.855
B10	159145	0.662
B11	239788	0.997
B12	108358	0.451
C01	147144	0.612
C02	158809	0.660
C03	121791	0.506
C04	55191	0.230
C05	139747	0.581
C06	138951	0.578
C07	72836	0.303
C08	155890	0.648
C09	74962	0.312
C10	132716	0.552
C11	169294	0.704
C12	177647	0.739
D01	96078	0.400
D02	109926	0.457
D04	58391	0.243
D06	119931	0.499
D07	79271	0.330
D08	171405	0.713
D09	202749	0.843
D10	150690	0.627
D11	178390	0.742
D12	131270	0.546
E01	169223	0.704
E02	104576	0.435
E03	69940	0.291
E04	112773	0.469
E06	159430	0.663
E07	94546	0.393
E08	106978	0.445
E09	77796	0.324
E10	202607	0.843
E11	234967	0.977
E12	172294	0.716
F01	61657	0.256
F02	103137	0.429
F03	124068	0.516
F08	130572	0.543
F09	123013	0.512
F10	131449	0.547
F11	217301	0.904
F12	167282	0.696
G01	161736	0.673
G02	98811	0.411
G03	84666	0.352
G04	140693	0.585
G05	24436	0.102
G07	134338	0.559
G08	127063	0.528
G09	103225	0.429
G10	209812	0.873
G11	99529	0.414
G12	79961	0.333
H01	178602	0.743
H02	180464	0.750
H03	141513	0.588
H04	94361	0.392
H05	90850	0.378
H06	62886	0.262
H07	125449	0.522
H08	92372	0.384
H09	104591	0.435
H10	123168	0.512
H11	69417	0.289
H12	202516	0.842
WT	130981	0.545

plate 25		
	expression	fold change
A01	332265	1.382
A02	111989	0.466
A03	209154	0.870
A04	146957	0.611
A05	296980	1.235
A06	243366	1.012
A08	297699	1.238
A09	330282	1.373
A10	279642	1.163
A11	75872	0.316
A12	313301	1.303
B01	182861	0.760
B02	179389	0.746
B03	285581	1.188
B04	132349	0.550
B05	92817	0.386
B06	224826	0.935
B07	324902	1.351
B08	248787	1.035
B09	197271	0.820
B10	104000	0.432
B12	90005	0.374
C01	229500	0.954
C02	332192	1.381
C03	202801	0.843
C04	197322	0.821
C05	276182	1.149
C06	149853	0.623
C07	184953	0.769
C08	161603	0.672
C09	303824	1.263
C10	180316	0.750
C11	147623	0.614
C12	145606	0.606
D01	123653	0.514
D02	208403	0.867
D03	298411	1.241
D04	178300	0.741
D05	150760	0.627
D06	241069	1.002
D07	254418	1.058
D08	199190	0.828
D09	49583	0.206
D10	82779	0.344
D11	109290	0.454
D12	69098	0.287
E01	349868	1.455
E03	286027	1.189
E04	196984	0.819
E05	331439	1.378
E07	189497	0.788
E08	138932	0.578
E09	313071	1.302
E10	142923	0.594
E11	111891	0.465
E12	113938	0.474
F01	111716	0.465
F02	178923	0.744
F03	96753	0.402
F04	112591	0.468
F05	128881	0.536
F06	137149	0.570
F07	233172	0.970
F08	200417	0.833
F09	217674	0.905
F10	213232	0.887
F11	170732	0.710
F12	183795	0.764
G01	193149	0.803
G02	316166	1.315
G03	204110	0.849
G05	203049	0.844
G06	63114	0.262
G07	230726	0.959
G08	275113	1.144
G09	268543	1.117
G10	306529	1.275
G11	165922	0.690
G12	147583	0.614
H01	151450	0.630
H02	313061	1.302
H03	203683	0.847
H04	152064	0.632
H05	213154	0.886
H06	167096	0.695
H07	138581	0.576
H09	264605	1.100
H10	53577	0.223
H11	115870	0.482
H12	253226	1.053
WT	175271	0.729

plate 27		
	expression	fold change
A01	332265	1.382
A02	111989	0.466
A03	209154	0.870
A04	146957	0.611
A05	296980	1.235
A06	243366	1.012
A08	297699	1.238
A09	330282	1.373
A10	279642	1.163
A11	75872	0.316
A12	313301	1.303
B01	182861	0.760
B02	179389	0.746
B03	285581	1.188
B04	132349	0.550
B05	92817	0.386
B06	224826	0.935
B07	324902	1.351
B08	248787	1.035
B09	197271	0.820
B10	104000	0.432
B12	90005	0.374
C01	229500	0.954
C02	332192	1.381
C03	202801	0.843
C04	197322	0.821
C05	276182	1.149
C06	149853	0.623
C07	184953	0.769
C08	161603	0.672
C09	303824	1.263
C10	180316	0.750
C11	147623	0.614
C12	145606	0.606
D01	123653	0.514
D02	208403	0.867
D03	298411	1.241
D04	178300	0.741
D05	150760	0.627
D06	241069	1.002
D07	254418	1.058
D08	199190	0.828
D09	49583	0.206
D10	82779	0.344
D11	109290	0.454
D12	69098	0.287
E01	349868	1.455
E02	175271	0.729
E03	286027	1.189
E04	196984	0.819
E05	331439	1.378
E07	189497	0.788
E08	138932	0.578
E09	313071	1.302
E10	142923	0.594
E11	111891	0.465
E12	113938	0.474
F01	111716	0.465
F02	178923	0.744
F03	96753	0.402
F04	112591	0.468
F05	128881	0.536
F06	137149	0.570
F07	233172	0.970
F08	200417	0.833
F09	217674	0.905
F10	213232	0.887
F11	170732	0.710
F12	183795	0.764
G01	193149	0.803
G02	316166	1.315
G03	204110	0.849
G05	203049	0.844
G06	63114	0.262
G07	230726	0.959
G08	275113	1.144
G09	268543	1.117
G10	306529	1.275
G11	165922	0.690
G12	147583	0.614
H02	313061	1.302
H03	203683	0.847
H04	152064	0.632
H05	213154	0.886
H06	167096	0.695
H07	138581	0.576
H09	264605	1.100
H10	53577	0.223
H11	115870	0.482
H12	253226	1.053
WT	151450	0.630

plate 29		
	expression	fold change
A01	237649	0.988
A02	168590	0.701
A03	53580	0.223
A04	274511	1.142
A05	229077	0.953
A06	194193	0.808
A07	129583	0.539
A08	142653	0.593
A09	187266	0.779
A10	41469	0.172
A11	164104	0.682
A12	182417	0.759
B01	126375	0.526
B02	117371	0.488
B03	188827	0.785
B04	107587	0.447
B05	162788	0.677
B06	179248	0.745
B07	156258	0.650
B08	141060	0.587
B09	164883	0.686
B10	199005	0.828
B11	146728	0.610
B12	52266	0.217
C01	102646	0.427
C02	130466	0.543
C03	112372	0.467
C04	137267	0.571
C05	170638	0.710
C06	233303	0.970
C07	205669	0.855
C08	151320	0.629
C09	131818	0.548
C10	229972	0.956
C11	133682	0.556
C12	199261	0.829
D01	215558	0.896
D02	104619	0.435
D03	100619	0.418
D04	134946	0.561
D05	177784	0.739
D06	112835	0.469
D07	255647	1.063
D08	149640	0.622
D09	97860	0.407
D10	155370	0.646
D11	220654	0.918
E01	131995	0.549
E02	160373	0.667
E03	232299	0.966
E04	144463	0.601
E05	173124	0.720
E06	191717	0.797
E07	167173	0.695
E08	170514	0.709
E09	98254	0.409
E10	150843	0.627
E11	127205	0.529
E12	101938	0.424
F01	139908	0.582
F02	63274	0.263
F03	142342	0.592
F04	173687	0.722
F05	191983	0.798
F07	207404	0.862
F08	125343	0.521
F09	138741	0.577
F10	165753	0.689
F11	308922	1.285
F12	210698	0.876
G01	227026	0.944
G02	132124	0.549
G03	128238	0.533
G04	125124	0.520
G05	182141	0.757
G06	154126	0.641
G07	146387	0.609
G08	194147	0.807
G09	75147	0.313
G10	76413	0.318
G11	172848	0.719
G12	222019	0.923
H01	180760	0.752
H02	139979	0.582
H03	199282	0.829
H04	108498	0.451
H05	111556	0.464
H06	166628	0.693
H07	128288	0.533
H08	172299	0.717
H09	190233	0.791
H10	163015	0.678
H11	178962	0.744
WT	145296	0.604

plate 31		
	expression	fold change
A01	270287	1.124
A02	138474	0.576
A03	213330	0.887
A04	201535	0.838
A05	82618	0.344
A06	154668	0.643
A07	72673	0.302
A08	142567	0.593
A09	16802	0.070
A10	179378	0.746
A11	417325	1.735
A12	112956	0.470
B01	192218	0.799
B03	229659	0.955
B04	112964	0.470
B05	156251	0.650
B06	181144	0.753
B07	253272	1.053
B08	135522	0.564
B09	290659	1.209
B10	109120	0.454
B11	115021	0.478
B12	270985	1.127
C01	154483	0.642
C02	336553	1.400
C03	292645	1.217
C04	123883	0.515
C05	167155	0.695
C06	198906	0.827
C07	249008	1.036
C08	129173	0.537
C09	140061	0.582
C10	162154	0.674
C11	191844	0.798
C12	213788	0.889
D01	182650	0.760
D02	179012	0.744
D03	161226	0.670
D04	173729	0.722
D05	90828	0.378
D06	198210	0.824
D07	393638	1.637
D08	157258	0.654
D09	215184	0.895
D10	385663	1.604
D11	232981	0.969
D12	204622	0.851
E01	164757	0.685
E02	138147	0.574
E03	199546	0.830
E04	102407	0.426
E05	167063	0.695
E06	224501	0.934
E07	111796	0.465
E08	217971	0.906
E09	262136	1.090
E10	328404	1.366
E11	83873	0.349
E12	107380	0.447
F01	175678	0.731
F02	202073	0.840
F03	147844	0.615
F04	158673	0.660
F05	251925	1.048
F06	182936	0.761
F07	182437	0.759
F08	158569	0.659
F09	167473	0.696
F10	25922	0.108
F11	99291	0.413
F12	237852	0.989
G01	71260	0.296
G02	132495	0.551
G03	254738	1.059
G04	187530	0.780
G05	224515	0.934
G06	157998	0.657
G07	207843	0.864
G08	199951	0.832
G09	245317	1.020
G10	141878	0.590
G11	228272	0.949
G12	233046	0.969
H01	185476	0.771
H02	131915	0.549
H03	243391	1.012
H04	165022	0.686
H05	112805	0.469
H06	174304	0.725
H07	27514	0.114
H08	219883	0.914
H09	160083	0.666
H10	161025	0.670
H11	164305	0.683
WT	239905	0.998

plate 33		
	expression	fold change
A01	160121	0.666
A02	170171	0.708
A03	105686	0.439
A04	196995	0.819
A05	96913	0.403
A06	132703	0.552
A07	103990	0.432
A08	150511	0.626
A09	131868	0.548
A10	107797	0.448
A11	229418	0.954
A12	197947	0.823
B01	116796	0.486
B02	103190	0.429
B03	127596	0.531
B04	148709	0.618
B05	140407	0.584
B06	183844	0.765
B07	118435	0.493
B08	74207	0.309
B09	139755	0.581
B10	83952	0.349
B11	183794	0.764
B12	72754	0.303
C01	146537	0.609
C02	137685	0.573
C03	111260	0.463
C04	96858	0.403
C05	147918	0.615
C06	156135	0.649
C07	89987	0.374
C08	135725	0.564
C09	138567	0.576
C10	172823	0.719
C11	127131	0.529
C12	78023	0.324
D01	304406	1.266
D02	214354	0.891
D03	165036	0.686
D04	179990	0.748
D05	194703	0.810
D06	150094	0.624
D07	200573	0.834
D08	106655	0.444
D09	130046	0.541
D10	96661	0.402
D11	225863	0.939
D12	102861	0.428
E01	136060	0.566
E02	209767	0.872
E03	333597	1.387
E04	177097	0.736
E05	84868	0.353
E06	140021	0.582
E07	63410	0.264
E08	132624	0.552
E09	174489	0.726
E10	89408	0.372
E11	112817	0.469
E12	110414	0.459
F02	80127	0.333
F03	104238	0.433
F04	130255	0.542
F05	118395	0.492
F06	144709	0.602
F07	138851	0.577
F08	109309	0.455
F09	141341	0.588
F10	133856	0.557
F11	75072	0.312
F12	60535	0.252
G01	139299	0.579
G02	172281	0.716
G03	132239	0.550
G04	151409	0.630
G05	82478	0.343
G06	138023	0.574
G07	114599	0.477
G08	138509	0.576
G09	114472	0.476
G10	142674	0.593
G11	118154	0.491
G12	96726	0.402
H03	111275	0.463
H04	103540	0.431
H05	95425	0.397
H06	59555	0.248
H07	190036	0.790
H08	108073	0.449
H09	172467	0.717
H10	136865	0.569
H11	83659	0.348
H12	81000	0.337
WT	252799	1.051

plate 35		
	expression	fold change
A01	10245	0.563
A02	26952	1.482
A03	773	0.042
A05	7612	0.419
A06	16632	0.914
A07	18623	1.024
A08	13442	0.739
A09	14481	0.796
A10	20626	1.134
A11	5168	0.284
A12	9608	0.528
B01	14683	0.807
B02	24180	1.329
B03	11638	0.640
B04	18371	1.010
B05	18360	1.009
B06	19319	1.062
B07	20323	1.117
B08	16823	0.925
B09	18841	1.036
B10	17414	0.957
B11	5898	0.324
B12	17141	0.942
C01	13727	0.755
C02	10813	0.595
C03	24887	1.368
C04	21603	1.188
C05	12700	0.698
C06	26257	1.444
C07	13263	0.729
C08	7872	0.433
C09	10252	0.564
C10	18873	1.038
C11	5248	0.289
C12	10458	0.575
D01	3763	0.207
D02	17916	0.985
D04	12419	0.683
D05	14324	0.788
D06	28296	1.556
D07	21924	1.205
D08	13472	0.741
D09	3822	0.210
D10	16541	0.909
D11	16152	0.888
D12	18213	1.001
E01	13101	0.720
E02	24014	1.320
E03	20854	1.147
E04	1159	0.064
E05	10710	0.589
E07	1702	0.094
E09	12030	0.661
E11	16711	0.919
E12	7332	0.403
F01	723	0.040
F02	6443	0.354
F03	6351	0.349
F04	1625	0.089
F05	10964	0.603
F06	9296	0.511
F10	28911	1.590
F11	13958	0.767
F12	5378	0.296
G01	8241	0.453
G02	20529	1.129
G03	4237	0.233
G04	790	0.043
G05	10408	0.572
G06	7925	0.436
G07	13162	0.724
G08	8484	0.466
G09	2934	0.161
G10	10854	0.597
G11	16227	0.892
H01	5993	0.330
H02	6068	0.334
H03	6747	0.371
H04	10193	0.560
H05	10707	0.589
H06	7128	0.392
H07	8329	0.458
H09	7791	0.428
H10	11172	0.614
H11	30769	1.692
H12	12497	0.687

plate 37		
	expression	fold change
A01	17505	0.962
A02	4230	0.233
A03	5357	0.295
WT	23334	1.283
A05	13025	0.716
A06	7026	0.386
A07	3719	0.205
A08	15973	0.878
A09	7052	0.388
A10	12019	0.661
A11	2336	0.128
A12	4615	0.254
B01	5729	0.315
B02	22812	1.254
B03	15302	0.841
B04	2977	0.164
B05	7005	0.385
B06	10686	0.588
B07	9155	0.503
B08	11261	0.619
B09	19382	1.066
B10	11987	0.659
B11	13707	0.754
B12	3271	0.180
C01	6455	0.355
C02	11387	0.626
C03	11292	0.621
C04	8674	0.477
C07	16435	0.904
C08	16736	0.920
C09	10149	0.558
C10	14225	0.782
C11	26909	1.480
C12	5772	0.317
D01	7103	0.391
D02	12413	0.683
D03	18783	1.033
D04	27552	1.515
D05	8965	0.493
D06	20248	1.113
D07	11848	0.651
D08	12284	0.675
D09	14013	0.770
D10	25134	1.382
D11	29913	1.645
D12	4128	0.227
E01	8392	0.461
E02	13645	0.750
E03	7261	0.399
E04	13548	0.745
E05	13151	0.723
E06	13376	0.735
E07	11956	0.657
E08	9365	0.515
E09	15517	0.853
E10	5446	0.299
E11	13980	0.769
E12	10082	0.554
F01	13667	0.751
F02	14909	0.820
F03	9419	0.518
F04	21834	1.200
F05	11510	0.633
F07	9527	0.524
F08	8649	0.476
F09	28103	1.545
F10	13201	0.726
F11	14313	0.787
F12	4095	0.225
G01	8525	0.469
G02	10138	0.557
G03	1816	0.100
G04	12220	0.672
G05	10089	0.555
G06	8124	0.447
G07	5764	0.317
G08	8678	0.477
G09	3367	0.185
G10	7151	0.393
G11	8188	0.450
G12	13515	0.743
H01	5767	0.317
H02	2782	0.153
H03	11358	0.624
H04	7244	0.398
H05	6977	0.384
H06	4963	0.273
H07	11178	0.615
H08	7753	0.426
H09	3394	0.187
H10	9481	0.521
H11	15004	0.825
H12	3483	0.192

plate 39		
	expression	fold change
A01	170634	0.710
A02	81954	0.341
A03	137237	0.571
A04	51849	0.216
A05	87243	0.363
A06	150489	0.626
A07	179206	0.745
A08	112741	0.469
A09	150213	0.625
A10	122551	0.510
A11	154893	0.644
A12	77728	0.323
B01	173622	0.722
B02	127419	0.530
B03	153990	0.640
B05	144269	0.600
B06	143278	0.596
B07	125842	0.523
B08	185400	0.771
B10	110473	0.459
B11	224175	0.932
B12	65619	0.273
C01	131060	0.545
C02	81546	0.339
C03	116635	0.485
C05	60114	0.250
C06	271867	1.131
C07	215004	0.894
C08	53860	0.224
C09	199701	0.830
C10	162460	0.676
C11	204914	0.852
C12	99693	0.415
D01	88228	0.367
D02	101816	0.423
D03	90627	0.377
D05	66146	0.275
D06	126048	0.524
D07	219691	0.914
D08	222350	0.925
D09	143579	0.597
D10	211774	0.881
D11	173997	0.724
D12	224804	0.935
E01	206127	0.857
E02	167410	0.696
E03	66277	0.276
E04	194575	0.809
E05	106296	0.442
E06	149568	0.622
E07	125071	0.520
E08	27252	0.113
E09	105067	0.437
E10	92736	0.386
E11	121424	0.505
E12	199344	0.829
F01	225487	0.938
F02	88649	0.369
F03	111364	0.463
F05	123998	0.516
F06	97750	0.406
F07	375630	1.562
F08	127224	0.529
F09	296089	1.231
F10	114111	0.475
F11	172507	0.717
F12	123374	0.513
G01	293955	1.222
G02	88158	0.367
G03	143367	0.596
G05	113215	0.471
G06	132197	0.550
G07	40121	0.167
G08	206187	0.857
G09	56798	0.236
G10	93634	0.389
G11	121625	0.506
G12	94764	0.394
H01	125777	0.523
H02	183140	0.762
H03	90202	0.375
H05	120550	0.501
H06	133591	0.556
H07	140430	0.584
H08	35370	0.147
H09	99393	0.413
H10	115297	0.479
H11	96726	0.402
H12	134549	0.560
WT	200264	0.833

plate 41		
	expression	fold change
A01	45591	0.190
A02	80940	0.337
A03	68370	0.284
A04	78946	0.328
A05	55085	0.229
A06	80224	0.334
A07	80232	0.334
A08	96264	0.400
A09	58408	0.243
A10	95914	0.399
A11	74182	0.308
A12	63393	0.264
B01	48395	0.201
B02	41869	0.174
B03	68472	0.285
B04	92066	0.383
B05	77785	0.323
B06	157753	0.656
B07	126597	0.526
B08	79017	0.329
B09	98952	0.411
B10	110947	0.461
B11	139653	0.581
B12	94873	0.395
C01	96962	0.403
C02	105651	0.439
C03	127930	0.532
C04	122473	0.509
C05	124984	0.520
C06	103624	0.431
C07	192710	0.801
C08	108438	0.451
C09	116493	0.484
C10	84482	0.351
C11	88021	0.366
C12	105259	0.438
D01	102252	0.425
D02	98224	0.408
D03	107500	0.447
D04	78396	0.326
D05	181630	0.755
D06	181490	0.755
D07	124686	0.519
D08	102970	0.428
D09	93605	0.389
D10	140377	0.584
D11	120473	0.501
D12	131628	0.547
E01	150361	0.625
E02	205963	0.857
E03	139862	0.582
E04	112859	0.469
E05	159639	0.664
E06	102171	0.425
E07	101180	0.421
E08	117150	0.487
E09	101422	0.422
E10	149965	0.624
E11	129433	0.538
E12	145991	0.607
F01	179380	0.746
F02	201111	0.836
F03	133847	0.557
F04	117851	0.490
F05	87793	0.365
F06	106051	0.441
F07	78055	0.325
F08	98429	0.409
F09	89879	0.374
F10	115064	0.478
F11	100922	0.420
F12	135848	0.565
G01	93109	0.387
G02	122526	0.510
G03	217425	0.904
G04	107131	0.446
G05	73914	0.307
G06	106156	0.441
G07	184854	0.769
G08	72520	0.302
G09	106220	0.442
G10	145874	0.607
G11	103316	0.430
G12	110805	0.461
H01	126361	0.525
H02	55283	0.230
H03	110914	0.461
H05	92043	0.383
H06	95943	0.399
H07	70494	0.293
H08	65120	0.271
H09	74219	0.309
H10	53765	0.224
H11	65111	0.271
H12	78073	0.325
WT	139880	0.582

plate 43		
	expression	fold change
A01	104625	0.435
A02	96933	0.403
A03	42448	0.177
A04	152862	0.636
A05	88813	0.369
A06	135922	0.565
A07	126341	0.525
A08	10088	0.042
A09	124846	0.519
A10	205338	0.854
A11	87533	0.364
A12	188594	0.784
B01	78739	0.327
B02	53224	0.221
B03	134002	0.557
B04	180998	0.753
B05	155594	0.647
B06	143288	0.596
B07	159258	0.662
B08	117050	0.487
B09	133068	0.553
B10	219906	0.914
B11	137861	0.573
B12	132492	0.551
C01	94558	0.393
C02	89029	0.370
C03	201356	0.837
C04	101202	0.421
C05	139315	0.579
C06	83058	0.345
C07	244007	1.015
C08	162844	0.677
C09	141837	0.590
C10	190726	0.793
C11	196980	0.819
C12	210552	0.876
D01	72039	0.300
D02	197681	0.822
D03	160092	0.666
D04	127666	0.531
D05	149765	0.623
D06	146866	0.611
D07	121308	0.504
D08	153342	0.638
D09	177534	0.738
D10	103750	0.431
D11	222092	0.924
D12	208091	0.865
E01	138346	0.575
E02	143533	0.597
E03	119112	0.495
E04	128421	0.534
E05	169070	0.703
E06	157668	0.656
E07	160468	0.667
E08	193366	0.804
E09	155615	0.647
E10	290343	1.207
E11	203527	0.846
E12	67886	0.282
F01	145037	0.603
F03	379513	1.578
F04	165785	0.689
F05	151418	0.630
F06	149067	0.620
F07	158938	0.661
F08	255354	1.062
F09	175921	0.732
F10	213311	0.887
F11	205419	0.854
F12	284564	1.183
G01	96658	0.402
G02	267991	1.114
G03	177979	0.740
G04	199376	0.829
G05	186558	0.776
G06	200482	0.834
G07	202428	0.842
G08	149763	0.623
G09	125108	0.520
G10	200032	0.832
G11	230491	0.959
G12	122037	0.507
H01	101662	0.423
H02	111694	0.464
H03	222057	0.923
H04	149296	0.621
H05	142617	0.593
H06	48071	0.200
H07	180991	0.753
H08	75694	0.315
H09	108566	0.451
H10	137080	0.570
H11	209376	0.871
H12	109937	0.457
WT	257546	1.071

plate 45		
	expression	fold change
A01	123933	0.515
A02	146559	0.609
A03	114715	0.477
A04	60548	0.252
A05	95657	0.398
A06	99396	0.413
A07	66735	0.278
A08	103632	0.431
A09	141388	0.588
A10	237799	0.989
A11	85815	0.357
A12	150067	0.624
B01	142599	0.593
B02	140786	0.585
B03	20819	0.087
B04	160303	0.667
B05	99961	0.416
B06	172730	0.718
B07	165096	0.687
B08	95978	0.399
B09	53560	0.223
B10	127065	0.528
B11	116246	0.483
B12	120920	0.503
C01	159643	0.664
C02	148829	0.619
C03	92237	0.384
C04	89031	0.370
C05	149325	0.621
C06	220831	0.918
C07	67152	0.279
C08	135328	0.563
C09	46175	0.192
C10	132496	0.551
C11	86842	0.361
C12	86446	0.359
D01	89848	0.374
D02	88090	0.366
D03	107525	0.447
D04	28645	0.119
D05	173223	0.720
D06	91670	0.381
D07	98786	0.411
D08	101089	0.420
D09	106357	0.442
D10	133150	0.554
D11	99298	0.413
D12	61900	0.257
E02	110051	0.458
E04	126416	0.526
E05	115863	0.482
E06	143661	0.597
E07	85885	0.357
E08	321468	1.337
E09	73212	0.304
E10	112362	0.467
E11	100188	0.417
E12	186770	0.777
F01	90979	0.378
F02	138273	0.575
F03	73830	0.307
F04	168136	0.699
F05	88027	0.366
F06	77025	0.320
F07	127727	0.531
F08	54155	0.225
F09	68131	0.283
F10	157061	0.653
F11	67973	0.283
F12	54992	0.229
G01	184950	0.769
G02	97626	0.406
G03	155914	0.648
G04	181874	0.756
G05	95752	0.398
G06	40508	0.168
G07	154848	0.644
G08	100779	0.419
G09	177107	0.737
G10	160133	0.666
G11	113049	0.470
G12	69495	0.289
H01	162851	0.677
H02	161561	0.672
H03	81924	0.341
H04	123288	0.513
H05	114273	0.475
H06	160526	0.668
H07	93521	0.389
H08	59005	0.245
H09	136698	0.568
H10	98389	0.409
H12	57032	0.237
WT	124750	0.519

plate 47		
	expression	fold change
A01	97607	0.406
A02	80280	0.334
A03	124242	0.517
A04	163180	0.679
A05	43092	0.179
A06	29917	0.124
A07	168411	0.700
A08	167882	0.698
A09	116162	0.483
A10	112926	0.470
A11	59144	0.246
A12	67516	0.281
B01	129462	0.538
B02	79323	0.330
B03	132641	0.552
B04	114051	0.474
B05	110643	0.460
B06	58262	0.242
B07	104590	0.435
B08	99828	0.415
B09	136909	0.569
B10	44382	0.185
B11	63249	0.263
B12	149427	0.621
C01	119701	0.498
C02	85665	0.356
C03	129283	0.538
C04	69583	0.289
C05	76483	0.318
C06	69583	0.289
C07	84199	0.350
C08	104209	0.433
C09	92662	0.385
C10	83485	0.347
C11	58651	0.244
C12	67372	0.280
D01	90095	0.375
D02	101023	0.420
D03	144609	0.601
D04	106959	0.445
D05	100386	0.417
D06	119277	0.496
D07	212457	0.884
D08	97020	0.403
D09	71705	0.298
D10	64734	0.269
D11	74914	0.312
D12	92491	0.385
E01	192397	0.800
E02	78130	0.325
E03	74841	0.311
E04	188888	0.785
E05	196799	0.818
E06	191332	0.796
E07	137313	0.571
E08	81335	0.338
E09	137978	0.574
E10	82650	0.344
E11	63750	0.265
E12	188225	0.783
F01	142136	0.591
F02	82040	0.341
F03	131558	0.547
F04	59775	0.249
F05	134933	0.561
F06	178477	0.742
F07	148899	0.619
F08	95195	0.396
F09	2524	0.010
F10	117082	0.487
F11	97488	0.405
F12	57120	0.238
G01	102663	0.427
G02	138776	0.577
G03	187607	0.780
G04	175929	0.732
G05	174595	0.726
G06	271317	1.128
G07	141020	0.586
G08	127643	0.531
G09	113123	0.470
G10	140290	0.583
G11	97166	0.404
G12	110152	0.458
H02	103095	0.429
H03	137657	0.572
H04	152839	0.636
H05	129438	0.538
H06	178580	0.743
H07	132155	0.550
H08	99643	0.414
H09	66208	0.275
H10	93074	0.387
H11	118763	0.494
H12	105227	0.438
WT	166293	0.692

plate 49		
	expression	fold change
A01	459343	1.910
A02	241945	1.006
A03	274179	1.140
A04	555114	2.308
A05	389233	1.619
A06	206907	0.860
A07	281651	1.171
A08	175674	0.731
A09	185493	0.771
A10	194874	0.810
A11	91433	0.380
A12	273861	1.139
B01	202156	0.841
B02	84831	0.353
B03	614846	2.557
B04	145211	0.604
B05	272513	1.133
B06	128832	0.536
B07	520926	2.166
B08	68500	0.285
B09	50561	0.210
B10	286682	1.192
B11	89783	0.373
B12	244813	1.018
C01	407779	1.696
C02	65011	0.270
C03	102297	0.425
C04	188460	0.784
C06	366942	1.526
C07	229507	0.954
C08	89966	0.374
C09	145451	0.605
C10	138984	0.578
C11	76100	0.316
C12	2132553	8.868
D01	149875	0.623
D02	168295	0.700
D03	275647	1.146
D04	129741	0.540
D05	640676	2.664
D06	570422	2.372
D07	95851	0.399
D08	241532	1.004
D09	88234	0.367
D10	145275	0.604
D11	206141	0.857
D12	309112	1.285
E01	186476	0.775
E02	53768	0.224
E03	71462	0.297
E04	94488	0.393
E05	93128	0.387
E06	267926	1.114
E07	104171	0.433
E08	390053	1.622
E09	109770	0.456
E10	207780	0.864
E11	272541	1.133
E12	577857	2.403
F01	188243	0.783
F02	97322	0.405
F03	580217	2.413
F04	196438	0.817
F05	165129	0.687
F06	436495	1.815
F07	600319	2.496
F08	405031	1.684
F09	124679	0.518
F10	378613	1.574
F11	115647	0.481
F12	314324	1.307
G01	329244	1.369
G02	77497	0.322
G03	66826	0.278
G04	112418	0.467
G05	132649	0.552
G06	383920	1.597
G07	543159	2.259
G08	405050	1.684
G09	164940	0.686
G10	183834	0.764
G11	359623	1.495
G12	256057	1.065
H01	252189	1.049
H02	293571	1.221
H03	124988	0.520
H04	1448448	6.023
H05	226901	0.944
H06	543803	2.261
H08	319840	1.330
H09	69916	0.291
H10	179088	0.745
H11	390934	1.626
H12	254768	1.059
WT	443576	1.845

plate 51		
	expression	fold change
A01	401632	1.670
A02	563998	2.345
A03	379288	1.577
A04	395380	1.644
A05	310146	1.290
A06	251686	1.047
A07	271972	1.131
A08	261532	1.088
A09	655936	2.728
A10	268975	1.119
A11	292867	1.218
A12	335863	1.397
B01	399660	1.662
B02	406879	1.692
B03	296729	1.234
B04	417826	1.738
B05	211906	0.881
B06	271000	1.127
B07	216430	0.900
B08	206671	0.859
B09	414694	1.725
B11	208855	0.869
B12	385314	1.602
C01	314668	1.309
C02	550359	2.289
C03	337008	1.401
C04	285306	1.186
C05	148153	0.616
C06	293294	1.220
C07	145131	0.604
C08	337506	1.404
C09	388000	1.614
C10	486531	2.023
C11	419181	1.743
C12	249359	1.037
D01	251785	1.047
D02	499795	2.078
D03	228196	0.949
D04	160042	0.666
D05	217069	0.903
D06	494905	2.058
D07	292682	1.217
D08	377859	1.571
D09	156577	0.651
D10	375656	1.562
D11	159797	0.665
D12	167481	0.696
E01	277122	1.152
E02	358341	1.490
E03	264630	1.100
E04	457971	1.904
E05	198775	0.827
E06	268229	1.115
E07	452371	1.881
E08	328809	1.367
E09	251996	1.048
E10	348755	1.450
E11	244387	1.016
E12	286248	1.190
F02	126912	0.528
F03	146349	0.609
F04	138671	0.577
F05	147902	0.615
F06	323005	1.343
F07	287085	1.194
F08	693662	2.885
F09	444728	1.849
F10	306838	1.276
F11	280575	1.167
F12	160869	0.669
G02	49977	0.208
G03	616148	2.562
G04	155549	0.647
G05	300030	1.248
G06	468229	1.947
G07	269951	1.123
G08	447869	1.862
G09	211828	0.881
G10	414113	1.722
G11	204926	0.852
G12	172322	0.717
H02	249165	1.036
H03	170213	0.708
H04	456634	1.899
H05	407428	1.694
H06	488735	2.032
H07	208414	0.867
H08	343250	1.427
H09	387342	1.611
H10	198348	0.825
H11	165405	0.688
H12	152430	0.634
WT	285103	1.186

plate 53		
	expression	fold change
A01	659234	2.741
A02	133700	0.556
A03	226304	0.941
A04	303026	1.260
A05	246821	1.026
A06	307510	1.279
A07	574906	2.391
A08	312189	1.298
A09	448686	1.866
A10	155800	0.648
A11	439631	1.828
A12	258675	1.076
B01	401364	1.669
B02	180523	0.751
B03	444058	1.847
B04	240391	1.000
B06	529964	2.204
B07	87776	0.365
B08	204111	0.849
B09	289456	1.204
B10	175651	0.730
B11	322709	1.342
B12	228286	0.949
C01	207899	0.865
C02	831551	3.458
C03	141731	0.589
C04	133110	0.554
C05	239449	0.996
C06	423825	1.762
C07	522946	2.175
C08	400683	1.666
C09	590917	2.457
C10	44112	0.183
C11	813764	3.384
C12	322077	1.339
D01	344357	1.432
D02	239876	0.998
D03	423043	1.759
D04	101069	0.420
D05	298863	1.243
D06	144796	0.602
D07	397245	1.652
D08	254684	1.059
D09	273901	1.139
D10	209636	0.872
D11	592523	2.464
D12	201973	0.840
E01	735935	3.060
E02	837475	3.483
E03	355386	1.478
E04	304343	1.266
E06	218709	0.910
E07	551458	2.293
E08	513182	2.134
E09	117011	0.487
E10	215768	0.897
E12	337405	1.403
F01	266011	1.106
F02	464381	1.931
F03	249602	1.038
F04	553289	2.301
F05	311707	1.296
F06	303988	1.264
F07	125514	0.522
F08	245483	1.021
F09	198408	0.825
F10	252377	1.050
G01	375725	1.562
G02	521137	2.167
G03	202639	0.843
G04	110181	0.458
G05	238159	0.990
G06	425703	1.770
G07	151237	0.629
G08	365459	1.520
G09	246312	1.024
G10	114874	0.478
H01	657906	2.736
H02	671369	2.792
H03	268637	1.117
H04	417657	1.737
H05	461571	1.919
H06	130921	0.544
H07	340751	1.417
H08	527261	2.193
H10	345839	1.438
H11	174506	0.726
H12	184544	0.767
WT	307017	1.277

plate 55		
	expression	fold change
A01	12046	0.050
A02	243902	1.014
A03	12000	0.050
A04	11325	0.047
A05	841313	3.499
A06	225351	0.937
A07	293125	1.219
A08	354814	1.476
A09	460249	1.914
A10	426878	1.775
A11	6870	0.029
A12	4389	0.018
B01	322785	1.342
B02	18593	0.077
B03	163681	0.681
B04	19415	0.081
B05	563248	2.342
B06	582374	2.422
B07	363866	1.513
B08	406250	1.689
B09	279898	1.164
B10	208686	0.868
B11	321739	1.338
B12	350731	1.459
C01	114596	0.477
C02	214756	0.893
C03	276419	1.149
C04	508930	2.116
C05	20447	0.085
C06	213237	0.887
C07	409367	1.702
C08	330865	1.376
C09	17146	0.071
C10	8828	0.037
C11	325933	1.355
C12	227658	0.947
D01	435243	1.810
D02	340002	1.414
D03	172126	0.716
D04	569294	2.367
D05	15968	0.066
D06	345692	1.438
D07	449475	1.869
D08	379276	1.577
D09	329315	1.369
D10	13798	0.057
D11	175163	0.728
D12	424183	1.764
E01	491724	2.045
E02	399554	1.662
E03	473222	1.968
E04	250832	1.043
E05	240421	1.000
E06	348498	1.449
E07	711560	2.959
E08	566970	2.358
E09	416576	1.732
E10	270799	1.126
E11	304259	1.265
E12	474773	1.974
F01	298678	1.242
F02	311008	1.293
F03	105814	0.440
F04	11354	0.047
F05	18062	0.075
F06	272616	1.134
F07	508333	2.114
F08	372193	1.548
F09	364718	1.517
F10	383159	1.593
F11	281576	1.171
F12	831273	3.457
G01	18638	0.078
G02	222204	0.924
G03	241059	1.002
G04	12916	0.054
G05	434943	1.809
G06	330889	1.376
G07	104759	0.436
G08	365771	1.521
G09	19905	0.083
G10	475150	1.976
G11	189248	0.787
G12	447842	1.862
H01	661166	2.749
H03	393907	1.638
H04	370183	1.539
H05	169708	0.706
H06	430648	1.791
H07	91039	0.379
H08	245291	1.020
H09	216474	0.900
H10	355089	1.477
H11	179840	0.748
H12	491059	2.042
WT	446205	1.856

plate 57		
	expression	fold change
A01	204051	0.849
A02	278800	1.159
A03	86994	0.362
A04	140569	0.585
A05	406546	1.691
A06	361373	1.503
A07	238207	0.991
A08	376090	1.564
A09	307844	1.280
A10	517143	2.151
A11	73583	0.306
A12	253264	1.053
B01	306688	1.275
B02	227068	0.944
B03	110767	0.461
B04	80971	0.337
B05	864417	3.595
B06	333000	1.385
B07	516667	2.149
B08	257646	1.071
B09	132211	0.550
B10	418969	1.742
B11	244394	1.016
B12	337229	1.402
C01	161537	0.672
C02	621702	2.585
C03	260641	1.084
C04	309660	1.288
C05	572431	2.380
C06	326623	1.358
C07	335346	1.395
C08	695353	2.892
C09	141771	0.590
C10	354661	1.475
C11	300983	1.252
C12	266676	1.109
D01	92671	0.385
D02	291302	1.211
D03	274804	1.143
D04	320252	1.332
D05	260392	1.083
D06	616090	2.562
D07	404105	1.680
D08	570956	2.374
D09	434407	1.806
D10	129506	0.539
D11	658066	2.737
D12	323900	1.347
E01	239815	0.997
E02	513758	2.136
E03	234291	0.974
E04	131000	0.545
E05	381534	1.587
E06	374554	1.558
E07	571368	2.376
E08	517566	2.152
E09	445951	1.854
E10	255193	1.061
E11	330687	1.375
E12	265271	1.103
F01	105882	0.440
F02	314912	1.310
F03	149171	0.620
F04	200775	0.835
F05	765357	3.183
F06	408117	1.697
F07	218283	0.908
F08	714689	2.972
F09	270330	1.124
F10	458438	1.906
F11	740339	3.079
F12	63741	0.265
G01	484808	2.016
G02	165208	0.687
G03	192490	0.800
G04	668822	2.781
G05	296199	1.232
G06	746895	3.106
G07	483602	2.011
G08	529425	2.202
G09	310365	1.291
G10	438493	1.823
G11	119627	0.497
G12	80417	0.334
H02	121297	0.504
H03	208322	0.866
H04	425333	1.769
H05	315802	1.313
H06	417051	1.734
H07	439534	1.828
H09	148862	0.619
H10	80678	0.335
H11	319822	1.330
H12	425721	1.770
WT	431394	1.794

plate 59		
	expression	fold change
A01	299034	1.244
A02	968408	4.027
A03	550901	2.291
A04	556997	2.316
A05	211735	0.881
A06	381565	1.587
A07	172149	0.716
A08	272040	1.131
A09	221952	0.923
A10	252222	1.049
A11	379378	1.578
A12	381099	1.585
B01	314154	1.306
B02	256759	1.068
B03	290332	1.207
B04	315538	1.312
B05	125670	0.523
B06	143267	0.596
B07	522302	2.172
B08	347379	1.445
B09	144900	0.603
B10	103554	0.431
B11	241997	1.006
B12	427291	1.777
C01	337363	1.403
C02	240259	0.999
C03	384511	1.599
C04	251343	1.045
C05	616343	2.563
C06	136105	0.566
C07	292170	1.215
C08	319205	1.327
C09	496455	2.065
C10	135036	0.562
C11	277272	1.153
C12	284900	1.185
D02	183522	0.763
D03	446786	1.858
D04	110312	0.459
D05	176644	0.735
D06	716485	2.980
D07	373627	1.554
D08	89010	0.370
D09	225073	0.936
D10	92757	0.386
D11	108025	0.449
D12	435643	1.812
E01	763151	3.174
E02	223796	0.931
E03	113495	0.472
E04	320142	1.331
E05	114681	0.477
E06	158394	0.659
E07	177614	0.739
E08	58216	0.242
E09	443241	1.843
E10	288035	1.198
E11	346369	1.440
E12	494638	2.057
F01	378756	1.575
F02	188864	0.785
F03	128980	0.536
F04	485014	2.017
F05	442850	1.842
F06	395075	1.643
F07	584366	2.430
F08	290008	1.206
F09	113685	0.473
F10	271604	1.129
F11	323584	1.346
F12	285443	1.187
G01	502304	2.089
G02	80385	0.334
G03	179282	0.746
G04	534317	2.222
G05	275466	1.146
G06	184992	0.769
G07	136711	0.569
G08	429733	1.787
G09	157412	0.655
G10	194771	0.810
G11	494985	2.058
G12	399087	1.660
H01	410662	1.708
H02	150438	0.626
H03	268050	1.115
H04	111027	0.462
H05	234099	0.974
H06	466037	1.938
H07	253238	1.053
H09	207670	0.864
H10	230857	0.960
H11	456942	1.900
H12	450823	1.875
WT	285537	1.187

plate 61		
	expression	fold change
A01	227995	0.948
A02	356942	1.484
A03	155301	0.646
A04	300389	1.249
A05	290275	1.207
A06	386398	1.607
A07	121678	0.506
A08	325989	1.356
A09	174961	0.728
A10	512919	2.133
A11	390767	1.625
A12	394258	1.640
B01	329827	1.372
B02	345656	1.437
B03	161258	0.671
B04	406491	1.690
B05	311441	1.295
B06	49606	0.206
B07	136346	0.567
B08	189988	0.790
B09	257565	1.071
B10	284887	1.185
B11	230090	0.957
B12	271525	1.129
C01	234414	0.975
C02	251943	1.048
C03	359514	1.495
C04	429160	1.785
C05	362636	1.508
C06	435949	1.813
C07	190614	0.793
C08	166962	0.694
C09	113539	0.472
C10	226327	0.941
C11	154876	0.644
C12	482829	2.008
D01	311977	1.297
D02	291260	1.211
D04	326165	1.356
D05	135974	0.565
D06	451292	1.877
D07	226900	0.944
D08	201233	0.837
D09	350336	1.457
D10	218903	0.910
D11	225745	0.939
D12	320508	1.333
E01	201308	0.837
E03	202750	0.843
E04	297765	1.238
E05	594099	2.471
E06	347358	1.444
E07	374985	1.559
E08	359198	1.494
E09	320517	1.333
E10	203716	0.847
E11	300459	1.249
E12	358427	1.491
F01	78810	0.328
F02	314214	1.307
F03	242293	1.008
F04	316763	1.317
F05	401086	1.668
F06	230393	0.958
F07	348360	1.449
F08	474465	1.973
F09	365227	1.519
F10	243207	1.011
F11	131206	0.546
F12	209017	0.869
G01	335482	1.395
G03	526812	2.191
G04	297850	1.239
G05	438667	1.824
G06	278512	1.158
G07	178092	0.741
G08	272966	1.135
G10	280409	1.166
G11	123497	0.514
G12	323047	1.343
H01	372733	1.550
H03	183353	0.762
H04	423861	1.763
H05	168354	0.700
H06	198446	0.825
H07	123715	0.514
H08	366816	1.525
H09	297316	1.236
H10	196493	0.817
H11	193214	0.803
H12	185673	0.772
WT	459388	1.910

plate 63		
	expression	fold change
A01	191255	0.795
A02	776202	3.228
A03	225277	0.937
A04	103837	0.432
A05	199402	0.829
A06	203905	0.848
A07	301899	1.255
A08	602916	2.507
A09	459497	1.911
A10	375488	1.561
A11	463193	1.926
A12	363492	1.512
B01	349050	1.452
B02	314605	1.308
B03	248926	1.035
B04	286869	1.193
B05	112186	0.467
B06	416765	1.733
B07	514644	2.140
B08	328321	1.365
B09	349079	1.452
B10	163666	0.681
B11	442579	1.840
B12	351540	1.462
C01	146917	0.611
C02	630900	2.624
C03	238277	0.991
C04	326557	1.358
C05	307514	1.279
C06	226712	0.943
C07	341500	1.420
C08	346286	1.440
C09	321222	1.336
C10	448967	1.867
C11	285347	1.187
C12	289286	1.203
D01	226681	0.943
D02	334688	1.392
D03	321906	1.339
D04	326942	1.360
D05	569018	2.366
D06	249597	1.038
D07	346807	1.442
D08	496524	2.065
D09	224108	0.932
D10	498259	2.072
D11	192351	0.800
D12	429256	1.785
E01	319275	1.328
E02	294833	1.226
E03	429569	1.786
E04	332170	1.381
E05	286467	1.191
E06	248856	1.035
E07	194868	0.810
E08	283309	1.178
E09	290917	1.210
E10	425386	1.769
E11	587658	2.444
E12	359901	1.497
F01	273714	1.138
F02	232822	0.968
F03	417058	1.734
F04	433105	1.801
F05	278788	1.159
F06	394301	1.640
F07	230665	0.959
F08	407683	1.695
F09	294207	1.223
F10	293441	1.220
F11	584292	2.430
F12	450517	1.873
G01	219904	0.914
G02	231150	0.961
G03	410387	1.707
G04	300507	1.250
G05	401244	1.669
G06	357422	1.486
G07	466405	1.940
G08	218777	0.910
G09	362963	1.509
G10	48629	0.202
G11	434489	1.807
G12	386636	1.608
H01	212806	0.885
H02	442061	1.838
H03	107424	0.447
H04	260777	1.084
H05	405178	1.685
H06	316654	1.317
H07	311993	1.297
H08	283475	1.179
H09	379910	1.580
H10	317962	1.322
H11	290083	1.206
WT	235267	0.978

7 Concluding discussion

This thesis describes sensing, uptake and excretion of pyruvate in gamma-proteobacteria, focusing on the three model gamma-proteobacteria *E. coli* (chapter 2 and 5), *V. campbellii* (chapter 3) and *S.* Typhimurium (chapter 4). The research presented here is mainly based on experiments with deletion mutants, reporter strains and infection models.

7.1 Comparison of pyruvate sensing and uptake systems in three model bacteria

It has been assumed and partly demonstrated previously that proteobacteria are able to sense and take up pyruvate, but knowledge about the responsible proteins, mechanisms and impacts has been scarce, especially regarding a comparison between different species and a focus on pathogenic bacteria. Here, it is shown that *E. coli*, *S.* Typhimurium and *V. campbellii* possess different numbers and kinds of molecular systems to perceive pyruvate in their environment and to transport it into their cells, as illustrated in figure 5.

For *E. coli*, it was shown previously that the bacterium possesses two different two-component systems for pyruvate sensing, the high-affinity system BtsS/BtsR and the low-affinity system PyrS/PyrR [59, 61, 63, 64], which both activate expression of a gene coding for a transporter protein, *btsT* and *yhjX*, respectively, but so far only BtsT has been characterized as a pyruvate/H^+ symporter [62]. It was suggested that in addition a constitutive pyruvate uptake system exists [81, 82]. In this thesis, CstA is identified as a second specific pyruvate transporter (see chapter 2). The two transporters BtsT and CstA both have 18 suggested transmembrane domains, belong to the "Putative Peptide Transporter Carbon Starvation (CstA)" family and share a high degree of similarity, but in contrast to the high-affinity transporter BtsT, CstA has a moderate substrate affinity (K_m: 242 µM). Like for BtsT, pyruvate uptake by CstA is specific and driven by a protonmotive force. The expression of *cstA* is also regulated by the cyclic AMP receptor protein (CRP) and post-transcriptionally by the carbon storage regulator A (CsrA) [83, 99]. However, *cstA* shows a different activating stimulus and expression pattern during growth than *bstT*: Induction of *cstA* does not follow sensing the presence of external pyruvate in the medium and activation by a two-component system, but it is downregulated by the transcriptional regulator protein Fis during exponential growth. Fis is suggested to block the binding site for CRP until stationary phase, so that *cstA* is finally expressed then. The result of this regulation is a growth-stage dependent activation of *cstA* for pyruvate uptake in contrast to the expression of *bstT* and *yhjX* as soon as pyruvate is accessible.

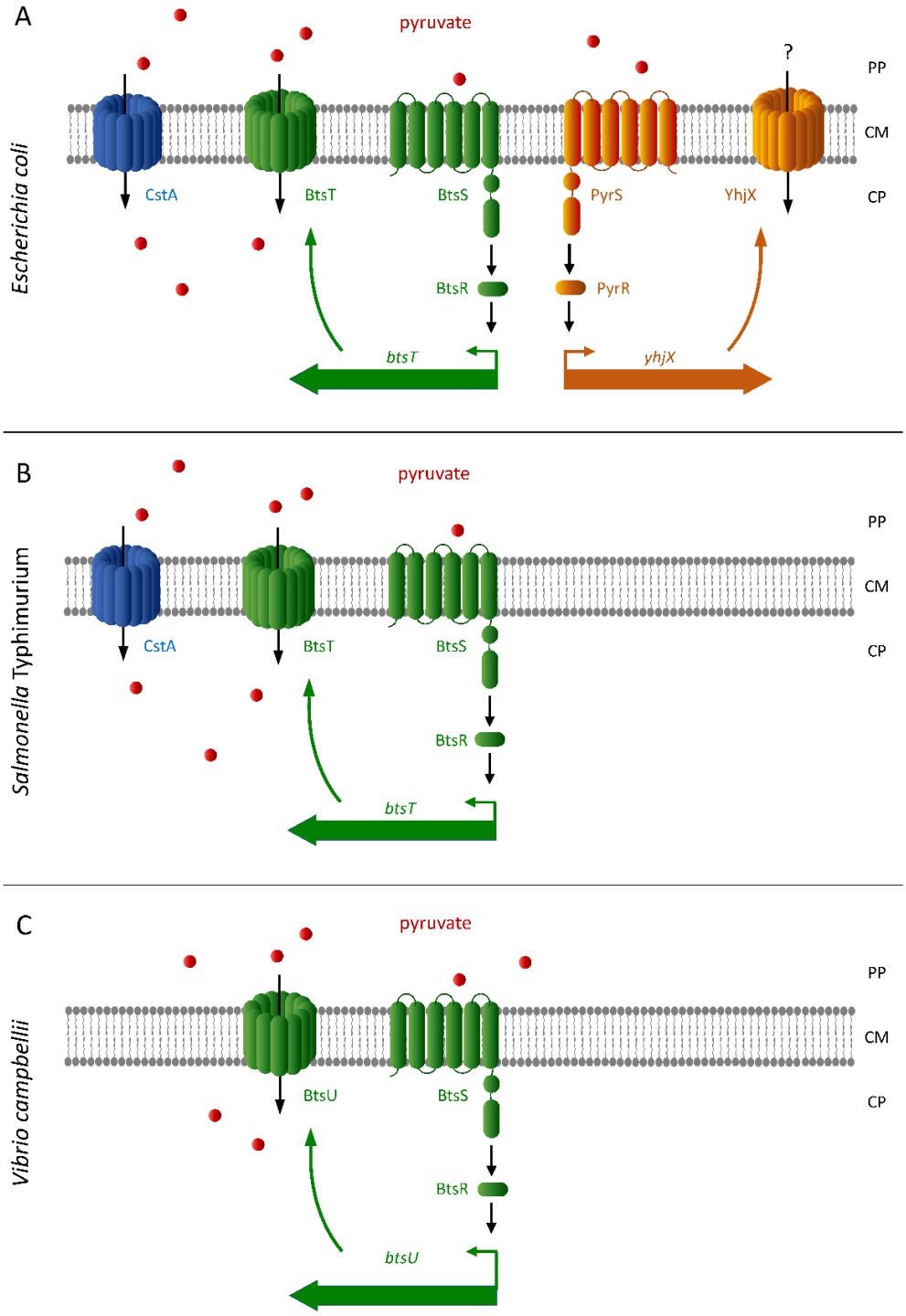

Figure 5. Schematic and simplified illustration of pyruvate uptake and sensing systems in the three model bacteria *E. coli, S.* Typhimurium and *V. campbellii*. A) In *E. coli*: The pyruvate transporter CstA (blue), the pyruvate transporter BtsT (green) with the two- component system BtsS/BtsR (green), consisting of the histidine kinase BtsS sensing pyruvate and the response regulator BtsR activating expression of *btsT* upon signal transduction, and the putative pyruvate transporter YhjX (orange) with the two-component system PyrS/PyrR (orange), consisting of the histidine kinase PyrS sensing pyruvate and the response regulator PyrR activating expression of *yhjX* upon signal transduction. **B) In *S.* Typhimurium:** The pyruvate transporter CstA (blue), and the pyruvate transporter BtsT (green) with the two- component system BtsS/BtsR (green), consisting of the histidine kinase BtsS sensing pyruvate

and the response regulator BtsR activating expression of *btsT* upon signal transduction. **C) In *V. campbellii*:** The pyruvate transporter BtsU (green) with the two- component system BtsS/BtsR (green), consisting of the histidine kinase BtsS sensing pyruvate and the response regulator BtsR activating expression of *btsU* upon signal transduction. PP, periplasm; CM, cytoplasmic membrane; CP, cytoplasm.

It is shown here, that an *E. coli* mutant lacking the three genes *btsT*, *yhjX* and *cstA* is unable to grow on pyruvate. The deletion of only one or two of these genes is not sufficient to achieve this phenotype. This is a strong indicator that YhjX might also transport pyruvate and that no further system for the uptake of pyruvate exists in *E. coli* besides BtsT, CstA and YhjX. Comparing the expression of all three transporter genes, it becomes obvious that at each time during exponential growth at least one transporter is expressed and thus pyruvate can be taken up. Having two different systems for pyruvate sensing and three different systems for pyruvate uptake allows the cells of an *E. coli* population a very effective usage of the valuable compound in every growth phase and specialized for every external pyruvate concentration, without wasting energy or membrane space with all transporters being produced throughout. This shows a high degree of adaptation for *E. coli*, which has to apply strategies to survive in the competitive environment of the human intestinal tract.

A comparative analysis previously revealed that in contrast to *E. coli*, most gamma-proteobacteria possess only one of the two LytS/LytTR-type two-component systems, the BtsS/BtsR-type system [72]. This applies also for the two other gamma-proteobacteria this thesis focuses on, *V. campbellii* and *S.* Typhimurium. Until now, nothing has been known about pyruvate sensing and uptake in these two species – or about the role that this metabolite plays for them.

Here, it is demonstrated that *V. campbellii* senses extracellular pyruvate also with the two-component system BtsS/BtsR, which then activates the expression of a target gene homologous to *E. coli*'s *btsT* coding for a pyruvate transporter protein (see chapter 3 and figure 5). Strikingly, this transporter, which was named BtsU, shares only 19 percent protein sequence identity with *E. coli*'s BtsT and has 12 predicted transmembrane domains instead of 18. Evidence is shown here that BtsU is the only pyruvate transporter in *V. campbellii*. Without *btsU*, the marine pathogen is no longer able to take up pyruvate, since there is no spare transporter to substitute the function of pyruvate uptake. Furthermore, it is confirmed here that *V. campbellii* excretes extraordinarily large amounts of pyruvate during exponential growth in rich medium and reclaims it fast and completely in stationary phase. Transport of pyruvate by BtsU was

monitored directly using radioactively labeled pyruvate and is found to be depending on the proton motive force. This indicates that the mechanism of pyruvate uptake by BtsT in *E. coli* and BtsU in *V. campbellii* is similar.

For the human pathogen *S.* Typhimurium, the two-component system BtsS/BtsR has been investigated in one study before, which could not identify a stimulus or function of the system, but found it to regulate the homologous gene of E. coli's *btsT* [73]. Interestingly, several non-synonymous mutations have accumulated in this operon, potentially due to host adaptation, indicating a specific importance of the system for the pathogen [74]. Here, it is shown that in *S.* Typhimurium, BtsS/BtsR is activated by external pyruvate, which leads to the expression of *btsT* coding for a pyruvate transporter (see chapter 4 and figure 5). In contrast to *V. campbellii*, this pyruvate transporter protein in *S.* Typhimurium is very similar to BtsT of *E. coli* (97 percent protein sequence identity and at least 16 predicted transmembrane domains). In addition to *btsS/btsR/btsT*, *S.* Typhimurium also harbors homologs of *E. coli*'s *cstA* gene. Here, it is shown that CstA is a second pyruvate transporter that *S.* Typhimurium possesses. Without *btsT* and *cstA*, *S.* Typhimurium is no longer able to take up pyruvate, indicating that no further pyruvate transporter exists in this species. Direct transport measurements with *btsT* and *cstA* deletion mutants show that BtsT seems to be able to substitute the transport function of CstA, whereas a deletion of *btsT* results in reduced pyruvate uptake. This leads to the conclusion that BtsT might be a more important pyruvate transporter in *S.* Typhimurium than CstA.

Quite similar expression can be monitored for the respective transporters in all three species during growth in LB medium: There is always one expression peak for *btsT*/*btsU* in the exponential growth phase, depending on sensing the excreted pyruvate with BtsS/BtsR. This indicates that the expression of this transporter is induced by external pyruvate, which is excreted in this growth phase. The same applies for *yhjX*, which is only present in *E. coli*, presumably as a backup system activated by higher pyruvate concentrations. For *cstA*, the expression reaches a peak in the stationary phase both in *E. coli* and *S.* Typhimurium, indicating an induction by nutrient limitation. For all three species, a strong increase in *btsT*/*btsU* expression is seen in mutants lacking *btsT*/*btsU*, which has been shown before also for the pyruvate transporter gene *pftAB* in *B. subtilis* [70] and has been suggested to rely on a feedback inhibition of the produced transporter protein or the elevated intracellular pyruvate level [65]. Interestingly, only in *V. campbellii*, all three genes of the *btsS/btsR/btsT/U* system are located adjacent to each other on the chromosome, whereas both in *E. coli* and in *S.* Typhimurium, *btsT* is positioned many kb away from the *btsS/btsR* operon.

In rough comparison, *E. coli* excretes twice as much pyruvate as *S.* Typhimurium during exponential growth, but *V. campbellii* excretes even three times more pyruvate than *E. coli* – and is able to take it up again very fast and completely with its one pyruvate transporter. This emphasizes the important role that BtsU plays in *V. campbellii* and raises the question why this species in particular possesses no back-up system to reclaim these amounts of a valuable compound, whereas *S.* Typhimurium needs two pyruvate transporters, but excretes least pyruvate than *E. coli* with its three transporters. An explanation might be found when considering the different habitat the three species live in and the role they have to fulfil to thrive: *V. campbellii* lives in the sea and infects animals like fish or shrimps – a quite specialized habitat and challenge. It did not evolve mechanisms to fight against many competing pathogens. It may be sufficient to have only one system for sensing and uptake of pyruvate. The enormous pyruvate excretion on the other hand could depict a specific advantage for *V. campbellii* during infection.

S. Typhimurium has to hold its ground in a very challenging situation: It not only has to find a way to survive in the competitive environment of the human intestine – which is the same for *E. coli* that is best equipped with three pyruvate transporters in a fine-tuned regulatory network – but it has to overcome the colonization resistance of the host against pathogens provided by the commensal microbiota. Moreover, as a facultative intracellular pathogen, *S.* Typhimurium can enter and survive in macrophages to reach distant organs. This requires a specific adaptation and could make a second system to take up pyruvate very useful. Nevertheless, in comparison to *E. coli*, *S.* Typhimurium succeeds in a more specific niche inside of macrophages, which could explain the existence of one pyruvate transporter less.

E. coli in the end needs to be best equipped out of the three model species, living in a habitat full of challenges and competitions – where it is very successful: It was shown that over 90 percent of human adults carry *E. coli* in their intestinal microbiota and it is one of the first bacteria colonizing the gut of new-born babies [100, 101]. Since it can be a live-long resident, it must have the best molecular equipment. A high redundancy serves as a backup-adaptation for all challenges this metabolic generalist might have to face, with only 10 percent of its metabolic network being essential [102]. Pathogens such as *S.* Typhimurium or *V. campbellii* in contrast have a broader redundancy and thus flexibility regarding their pathogenicity and infection properties, allowing them to thrive in a more specific habitat. This could be a hint to understand the numeric hierarchy regarding the different numbers of molecular systems for the sensing and uptake of pyruvate.

In summary, the tree model organisms investigated in this theses have different numbers and kinds of pyruvate sensing and uptake systems. Expression and regulation of the homologous pyruvate transporter genes seems to be similar, whereas the excretion of pyruvate in rich medium differs regarding the amount.

7.2 The biological relevance of pyruvate for three model bacteria

It was shown previously that pyruvate is not only very important as a metabolite, but has also several functions that go beyond. It acts as a scavenger of ROS and promotes the resuscitation of VBNC cells. Furthermore, its importance for virulence and inflammation has been demonstrated in several studies (see chapter 1.5). In this thesis, it was investigated which role pyruvate plays for the three model bacteria *E. coli*, *V. campbellii* and *S.* Typhimurium. Using deletion mutants unable to take up pyruvate, several phenotypes are described in the three species which reveal differences in comparison to the wild type. An overview of the role of pyruvate for the three model species is illustrated in Figure 6.

For all three species, it is found that without pyruvate uptake, the ability of the cells to react chemotactically to pyruvate, is abolished, meaning the cells fail to move along a gradient towards the attractant (see chapters 2, 3 and 4). This leads to the conclusion that the chemotaxis system must be activated intracellularly by the increasing pyruvate concentration. In *E. coli*, it was shown that the cytoplasmic phosphotransferase system (PTS) monitors not only the influx of PTS sugars but also nutrients like pyruvate – probably via the pyruvate to phosphoenolpyruvate (PEP) ratio – and then transfers this signal linearly to the chemotaxis system [103, 104]. Thus, the disruption of pyruvate uptake could lead to a decrease in the intracellular pyruvate/PEP ratio which then prevents an activation of the chemotaxis network. The results presented here suggest that this might also apply for *V. campbellii* and *S.* Typhimurium. However, the molecular mechanisms are not solved yet and the possibility cannot be excluded that the abolished chemotactic reaction to pyruvate might be due to another molecular reason. Generally, being able to move towards pyruvate as soon as it is close by could depict an important advantage for the species, especially in competitive environments when the cells need the compound either as a metabolite or due to its other valuable properties. It can be concluded that pyruvate uptake is crucial for all three model bacteria to perform chemotaxis towards pyruvate.

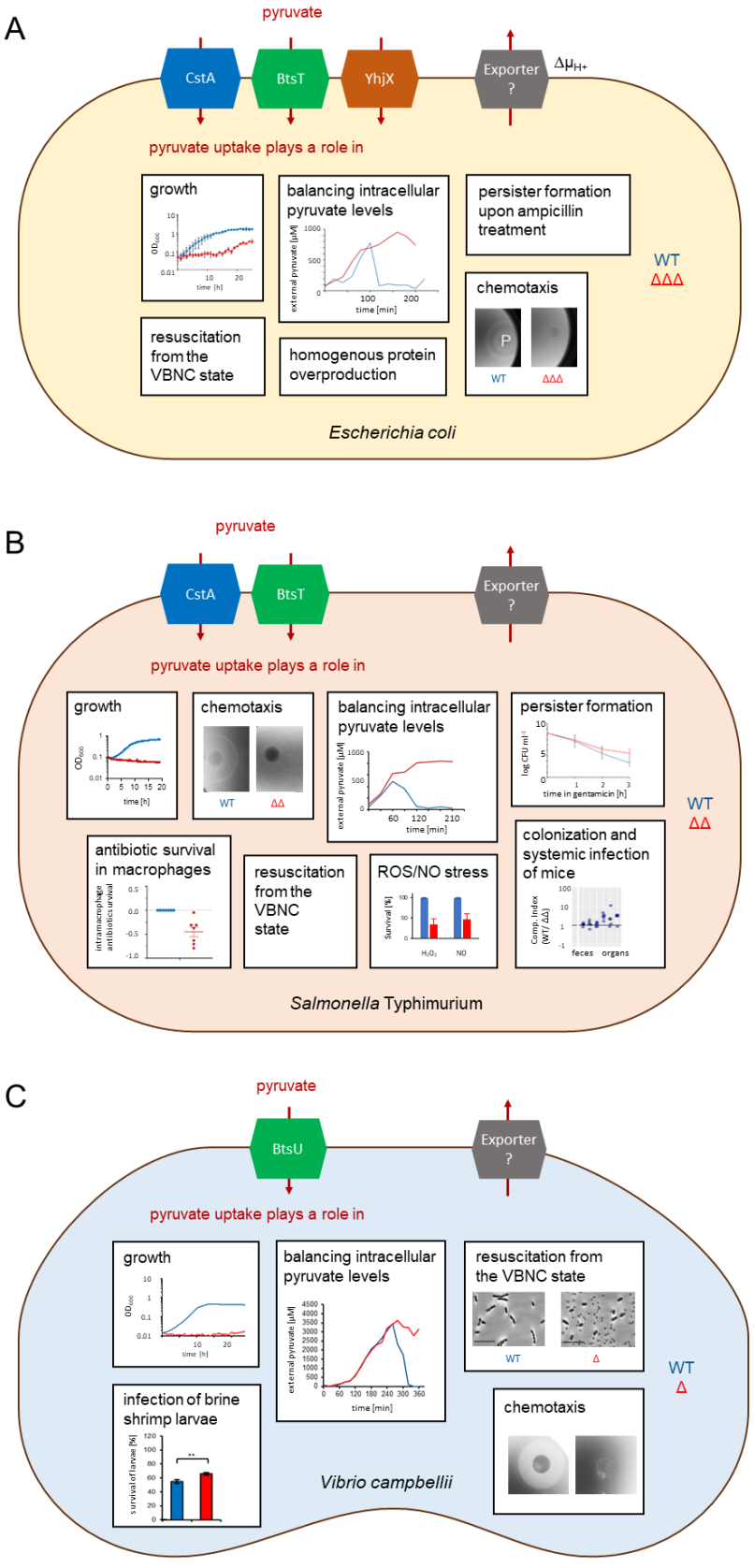

Figure 6. The biological relevance of pyruvate for the three model bacteria *E. coli, S.* Typhimurium and *V. campbellii*. Schematic illustration of the three bacterial cells with their (putative) pyruvate transporter proteins and the summarized role of pyruvate for each species. **A)** The role of

pyruvate for *E. coli*, based on results presented in this thesis and from Vilhena *et al*. [46, 66]; WT: wild type; ΔΔΔ: Δ*btsT* Δ*cstA* Δ*yhjX* deletion mutant; **B)** The role of pyruvate for *S*. Typhimurium, based on results presented in this thesis and from Liao *et al*. [45]; WT: wild type; ΔΔ: Δ*btsT* Δ*cstA* deletion mutant; **C)** The role of pyruvate for *V. campbellii*, based on results presented in this thesis; WT: wild type; Δ: Δ*btsU* deletion mutant. Implemented and partly modified miniature figures are all based on results presented in this thesis. Results from manuscripts which are not included in this thesis are implemented as text.

In *E. coli*, it has been shown previously that pyruvate fulfils several important functions beside metabolic ones: For deletion mutants lacking both pyruvate sensing systems, a part of the population has significant problems to overproduce a protein, indicating that pyruvate sensing and thus pyruvate uptake by BtsT and YhjX is important for the population to homogeneously fulfil this challenging task [66]. Moreover, without pyruvate sensing systems, a larger fraction of *E. coli* cells forms persister cells upon antibiotic treatment [66]. It was also shown that pyruvate is important for VBNC *E. coli* cells to return from this dormant state back to culturability by taking up the compound with BtsT [46]. It is not surprising that *btsT* is upregulated in VBNC *E. coli* cells [46]. These results show that when *E. coli* cells are impaired to use pyruvate, they tend to enter and/or stay in a persisting state. For *S*. Typhimurium, it has been found before as well that pyruvate can effectively restore culturability of VBNC cells [45]. Here, it is shown that also the marine pathogen *V. campbellii* can be resuscitated with pyruvate from the VBNC state (see chapter 3). Mutants lacking pyruvate sensing and/or uptake systems lose culturability after the same time period in long-term storage at low temperature under nutrient starvation as wild-type cells. However, the mutants cannot be resuscitated with pyruvate, which is the most effective means to "wake up" the cells. This can be explained with the fact that pyruvate is not only a nutrient which can be metabolized very easily without prior phosphorylation, but it also scavenges ROS – an important property for cells in long-term storage. Bacteria enter the VBNC state upon environmental stress and can thereby even withstand refrigeration, antibiotic treatment or detection [41]. Without being able to return to culturability, they are trapped in dormancy. Taken together, for all three species, pyruvate is a crucial factor for the resuscitation from the VBNC state.

Furthermore, it is shown here that also in *S*. Typhimurium, just as in *E. coli*, the inability of pyruvate uptake leads to an increasing proportion of persister cells upon antibiotic treatment (see chapter 4). This phenotype occurs in *E. coli* upon treatment with ampicillin, a beta-lactam antibiotic inhibiting the transpeptidase, but in *S*. Typhimurium upon treatment with gentamicin, a aminoglycoside antibiotic interacting with the 30S ribosomal subunit. No phenotype was

found for *S.* Typhimurium mutants upon ampicillin treatment. This indicates that pyruvate uptake seems to play a different role for the two species regarding the effect of and the reaction to antibiotics. However, it must be taken into consideration that for *E. coli*, the mutants used for this experiment are still able to take up pyruvate with their third pyruvate transporter CstA, whereas for *S.* Typhimurium mutants, all systems for pyruvate uptake are deleted. Interestingly, *yhjX* in *E. coli* was found to be upregulated in the presence of gentamicin in a previous study [105]. *S.* Typhimurium does not possess a homolog of *yhjX*, but in the *E. coli* mutants used here, *yhjX* expression was impaired by the deletion of *ypdA*/*ypdB*. Performing the same experiment with *E. coli* triple pyruvate transporter mutants, as well as with gentamicin instead of ampicillin would be very interesting. So far, it can be concluded that in *E. coli*, a reduced pyruvate uptake causes more cells to form persisters when the cell wall synthesis gets inhibited. In comparison, the complete abolishment of pyruvate uptake in *S.* Typhimurium leads to an increase in persister formation when the ribosomal function is affected. In both cases, pyruvate seems to be important for the cells to prevent them entering a persisting state and slowing down their metabolism and active functions.

For *S.* Typhimurium, a further phenotype is demonstrated here for mutants with deleted pyruvate transporter genes. When pyruvate uptake is abolished, less cells survive oxidative stress by H_2O_2, as well as nitrosative stress by nitric oxide (NO). Thus, pyruvate uptake is important for the pathogen to stand up against these aggressive compounds. This is not surprising, since pyruvate serves as a scavenger of ROS and it was shown previously that *btsT* and *cstA* are slightly upregulated under oxidative stress [106]. In the host, which produces ROS and NO as an antimicrobial defense [107], this scavenging capability could be very useful and help the pathogen to survive and successfully infect the body. Certainly, this phenotype found here in the *in vitro* setting does not necessarily have to lead to the assumption that pyruvate uptake by BtsT and CstA really plays a role for *S.* Typhimurium *in vivo* in the host. It is a further indicator that pyruvate might be useful for the cells under stress conditions.

In this theses, also the results of *in vivo* infection experiments with the two pathogens *V. campbellii* and *S.* Typhimurium are shown. Using appropriate animal models, wild-type cells and mutants lacking all pyruvate uptake systems were compared regarding the ability to infect their host. For *S.* Typhimurium, first experiments with macrophages were performed, which the pathogen can infect and use as means of transportation trough the body to cause systemic infection. It is shown here, that mutants lacking pyruvate transporters have a slightly decreased survival of cefotaxime treatment in macrophages, assuming that this is due to aggravated

recovery and regrowth after persisting inside the macrophages, since pyruvate has been shown before to be important for bacteria to leave a persisting state. Furthermore, competition experiments were performed, in which wild-type and mutant bacteria were brought together into the host, in this case mice with a defined minimal microbiota, and numbers of wild-type and mutant bacteria were compared afterwards in different organs. It is demonstrated here, that mutants unable to take up pyruvate have a small disadvantage regarding systemic infection of the host. This experiment was also performed with a non-virulent *S.* Typhimurium strain leading to a non-inflamed environment in the gut, as well as in mice with a less diverse microbiota leading to a higher nutrient availability in the gut and an abolished colonization resistance against the pathogen. In the non-inflamed gut, pyruvate uptake provides a small advantage for gut colonization. The microbiota and thus the nutrient availability however make no difference. Systemic infection, i.e. bacteria invading lymph nodes, liver or spleen, cannot be addressed with the avirulent strain due to its inability to infect. It can be concluded that for *S.* Typhimurium, pyruvate uptake definitely plays a role in host infection, even if only a small one. It was expected to see a more pronounced effect – especially since pyruvate concentrations have been found to be significantly higher in mice infected with *S.* Typhimurium than in uninfected mice, indicating that the ability to take this pyruvate up might provide an advantage [53]. Nevertheless, regarding the fact that many different factors come into play during colonization and infection *in vivo*, also a small effect is not to be neglected. The clear phenotypes seen *in vitro* might be mitigated *in vivo* and other properties presumably fall more into weight.

The most striking phenotype shown in this thesis is the role of pyruvate regarding host infection for *V. campbellii* – of all things the species which possesses only one pyruvate sensing system and one pyruvate transporter. Mutants lacking pyruvate sensing or uptake systems, have a significantly reduced ability to infect and kill gnotobiotic brine shrimp larvae. This leads to the conclusion that pyruvate must be important for the virulence of the marine pathogen. Since bacterial infections represent a severe burden for the increasing aquaculture production, these results are crucial to better understand one of the responsible pathogens and offer different ways to fight them, especially regarding antibiotic resistances.

It can be concluded that pyruvate is very important for all three model bacteria. When pyruvate sensing and/or uptake are/is abolished, we see phenotypic effects in all three species which lead to clear disadvantages. Interestingly, the effects go far beyond the role of pyruvate as a metabolite and are not the same in the three species.

7.3 Achievements on the way to identify a pyruvate exporter in *Escherichia coli*

It has been shown previously that cells excrete pyruvate under specific conditions. Pyruvate excretion is even used as a defense or profitable advantage (see chapter 1.5). Since pyruvate is an interesting product for biotechnology, metabolic engineering of bacteria for enhanced pyruvate excretion gained growing interest in the recent years [96, 108-111]. Nevertheless, in contrast to pyruvate sensing and uptake, almost nothing is known yet about the mechanism and involved molecular systems of pyruvate excretion. It is shown here that for the three investigated species, deletion of the characterized pyruvate transporters does not affect pyruvate excretion (see chapters 2, 3 and 4), indicating that these transporters just perform pyruvate uptake and are not involved in pyruvate export. Thus another system must exist to fulfil this task. To this end, this thesis aimed to identify one (or more) pyruvate exporter protein(s) in the model bacterium *E. coli* to investigate the function and impact of pyruvate excretion.

As shown here, assays were established to screen for genes which are crucial for the excretion of pyruvate. A plasmid-based reporter system was used, which is activated by external pyruvate and deletion mutants were transformed with this plasmid via large-scale transformations. It is demonstrated that this luciferase-based reporter system is functional to monitor the amount of excreted pyruvate in rich medium. This enabled screening of in total almost 3000 mutants regarding their pyruvate excretion, with a targeted focus on particularly promising transporter genes. By this means one mutant was identified which does not excrete pyruvate during growth in rich medium, a strain with a deletion of the gene *sdaC* coding for a serine transporter.

Moreover, the excretion of pyruvate could be monitored directly using right-side-out membrane vesicles from *E. coli* cells with a different genetic background. However, based on this technique, it is shown that the promising mutant strain lacking *sdaC* is still able to excrete pyruvate. It can be assumed that in rich medium the uptake of serine by SdaC is required for the overflow metabolism leading to the excretion of pyruvate. The results of the export experiments provide valuable information on the function and properties of the unknown pyruvate exporter in *E. coli*, which relies on an electric potential and/or a proton gradient, but not on an antiport of a specific substrate.

As an alternative strategy it is demonstrated here that a blue-white screening with a plasmid-based reporter system is likewise functional to monitor excreted pyruvate in *E. coli*. Furthermore, this screening can be used in combination with a self-created transposon library

to identify genes that impact the excretion of pyruvate. Several other approaches are also presented which could be applied to find a pyruvate exporter protein.

So far, the search did not lead to the identification of a pyruvate exporter in *E. coli*. The project of establishing the necessary methods and plans was successful, but further investigation is necessary. Moreover, it has to be taken into consideration that the excretion of pyruvate relies on several cellular functions, as well as on specific growth conditions. This leads to aggravated prerequisites regarding a screen based on pyruvate excretion of living cells. The mutant lacking *sdaC* is the best example of a strain which indeed does not excrete pyruvate any more, whereby the cause is however not due to the fact that the pyruvate exporter is missing, but the uptake of serine seems to impact the excretion of pyruvate under conditions which usually lead to this cellular reaction. This could be the case for several transporter genes that are crucial to induce an overflow metabolism. Furthermore, the reporter system is based on the expression of *btsT* via the two-component system BtsS/BtsR upon sensing external pyruvate. Not all details about the activation and downregulation of *btsT* in different metabolic contexts of living *E. coli* cells are known yet. A deletion of *btsT* itself leads to an even stronger activation of its promoter by BtsS/BtsR, suggesting some kind of feedback inhibition. Thus, a reduced expression of *btsT* in the screening approach does not necessarily need to be due to low external pyruvate concentrations – and vice versa.

Nevertheless, especially the measurements of pyruvate export using right-side-out membrane vesicles described here are a precious tool for the fast test and characterization of potential exporter candidates. For the functional analysis of the L-lysine exporter MglE, *Xenopus laevis* oocytes expressing *mglE* were used in combination with radioactively labeled L-lysine, representing a much more complex assay to test and measure the export of a compound [112], whereas our experimental system is direct, fast, easy and adaptable for different genetic backgrounds in the original organism.

7.4 Conclusion and outlook

Primary metabolites play a very important role for bacteria. In microbial communities, their presence or absence contributes to form networks, niches, to bring benefits for specific species and disadvantages for others. In this thesis, a part of the puzzle was revealed, how one important primary metabolite – pyruvate – is sensed, taken up and excreted.

In three different model gamma-proteobacteria pyruvate sensing and uptake systems and their biological relevance were characterized, thereby observing that even though these three species have different numbers and kinds of pyruvate sensing and uptake systems, pyruvate is important for all of them, with different biological impacts – which go wide beyond metabolism. This shows the differences between the three model bacteria, as well as the complexity of molecular systems and their functions.

However, there are still several open questions for future research: Even though strong evidence is provided here that YhjX in *E. coli* is a third pyruvate transporter, its function remains elusive. To confirm the transport of pyruvate by YhjX would complete the picture of pyruvate sensing and uptake in *E. coli*. Recently, expression of *yhjX* has been shown to be activated by low intracellular pH [113], indicating that pyruvate transport measurements might require cytoplasmic acidification to lead to measurable results.

Moreover, in contrast to the pathogens *V. campbellii* and *S.* Typhimurium, the role of pyruvate for the virulence of pathogenic *E. coli* strains was not directly investigated, although it was suggested that pyruvate sensing and uptake systems play a role in uropathogenic *E. coli* [65]. Therefore, it would be very interesting to perform infection experiments with pyruvate transporter deletion mutants of pathogenic *E. coli* strains. *YhjX* has been identified as a potential pathotype marker gene of mammary pathogenic *E. coli* [114], making infection experiments with deletion mutants of this strain even more interesting. Regarding the significance of pyruvate for virulence, it is worth mentioning that for the here described infection experiments with *V. campbellii*, germ-free brine shrimp larvae were used and for *S.* Typhimurium, we worked with mice carrying a minimal microbiota. This raises the question what effect would be seen for both pathogens in a more competitive environment. Would the sensing and uptake of pyruvate play a smaller or a larger role? Would the disadvantage for *V. campbellii* mutants in comparison to the wild type still be stronger than for *S.* Typhimurium mutants? A native microbiota could provide colonization resistance and prevent infection. On the other hand, within a complex microbiota, when not all nutrients are available, the ability to take up pyruvate might fall more into weight. The uptake of nutrients which are easily to metabolize, like pyruvate, could provide advantages in competitive environments like the gut [67]. For *S.* Typhimurium, one study reported that *btsT* is crucial for the colonization of the mouse gut [75]. Albeit the authors did not show any complementation to confirm *btsT* as cause of this phenotype, they found a significant disadvantage for mutants lacking *btsT*. Since mice with a complex microbiota were used in that study, the question arises if the microbiota might be

responsible for the stronger effects in contrast to the findings presented here. Experiments with animals carrying a native microbiota are necessary to provide answers to these questions.

Further insights are also required regarding the molecular connection between pyruvate uptake, the PTS and the chemotaxis network. How does the PTS sense intracellular pyruvate? Does this happen via the pyruvate/PEP ratio? Is this reaction linear?

Persister formation upon treatment with different antibiotics is another topic which needs to be investigated more closely. Conclusions can only be drawn and impacts of molecular systems on persister formation can only be compared between species after the experiments have been performed with the respective other bacterium and antibiotic, as well as using the appropriate comparable mutants.

Moreover, after the findings about CstA in *E. coli*, it was recently also shown that CstA in *Clostridioides difficile* imports pyruvate – and that the pathogen requires pyruvate for biofilm formation [115]. A previous study found *E. coli*'s *btsT* to be slightly upregulated in a biofilm in the presence of diarrheagenic enteroaggregative *E. coli* bacteria [116], and BtsSR has been shown before to regulate also the gene *csgD*, coding for a master regulator of biofilm production, as well as the *csg* operon coding for curli fimbriae [67]. Based on these results, it would be very interesting to investigate also the importance of pyruvate uptake for biofilm production in *E. coli*, *V. campbellii* and *S.* Typhimurium.

It remains unclear, how the export of pyruvate is performed and which protein(s) is/are responsible. Functioning screening systems and monitoring methods for the pyruvate exporter search and analysis have been established in *E. coli* and some promising candidates still need to be pursued, which could bring answers to this question in the near future. Jones *et al*. present an overview of exporter proteins in bacteria, thus comparing how they have been identified could be helpful to find appropriate strategies [117]. Applying exactly the same technique described here (using deletions of the Keio collection of single deletion mutants and screening potential candidates for the desired phenotype of low external concentrations of the compound of interest), other exporter protein could already be identified – even though several exporters existed which fulfilled the same task [118]. This indicates that the strategy pursued here could indeed be successful in the near future. In addition to continue testing the remaining promising candidates, functional metagenomic approaches for the discovery of exporter proteins might be worth testing, like the one presented by Malla *et al*. [112], who combined an expression library with selective concentrations of the respective compound. The general concept to apply a screen

based on hypersensitivity has already led to the identification of many exporter proteins [119, 120]. Furthermore, transcriptomic profile comparisons between conditions leading to an excretion of the respective compound and conditions of no excretion would be of interest and could advance the exporter search [121]. To this end, it is necessary to examine more closely under which conditions *E. coli* excretes pyruvate the most and the least.

The role of serine uptake by SdaC for the excretion of pyruvate *in vivo* is another question to be addressed. Recently it has been shown in uropathogenic *E. coli* that the deamination of serine to pyruvate is an important tool for the pathogen to resist acid stress – and it was suggested that YhjX might function as a pyruvate exporter [122]. The data presented here clearly demonstrate that mutants lacking *yhjX* still excrete pyruvate. However, since it has been shown before that function and regulation of pyruvate sensing and uptake systems might work differently in pathogenic *E. coli* strains, in which for instance BtsS interacts with the non-cognate response regulator YpdB to activate *yhjX* [65], only further research can solve these inconsistencies. The larger aim of the project presented here is to investigate the role of pyruvate excretion for proteobacteria in general. After the identification of the correct pyruvate exporter protein, an interesting starting point would be to work with the corresponding deletion mutants of uropathogenic *E. coli* to investigate the significance of pyruvate excretion for this pathogen in its acidic habitat. Then, using pyruvate exporter deletion mutants of different gastro-intestinal species could show how abolished pyruvate excretion changes the composition of the intestinal microbiota and the colonization resistance against pathogens, as well as an impact of excreted pyruvate on infection and inflammation.

The comparative analysis presented in this dissertation shows the varying impact that primary metabolites can have – and raises even more need for further research about pyruvate in different species and in the human host. Intestinal pyruvate concentration data from patients and healthy individuals would be important, as well as more knowledge about the molecular pyruvate uptake and sensing system also in other bacteria. The fact that pyruvate is not only a precious metabolite, but also fulfils other valuable functions for bacteria to varying extents, emphasizes how exciting further research on this primary metabolite would be.

References for chapters 1 and 7

1. Boor KJ. 2006. Bacterial stress responses: what doesn't kill them can make then stronger. PLoS Biol 4:e23. doi:10.1371/journal.pbio.0040023
2. Ulrich LE, Koonin EV, Zhulin IB. 2005. One-component systems dominate signal transduction in prokaryotes. Trends Microbiol 13:52-6. doi:10.1016/j.tim.2004.12.006
3. Staron A, Sofia HJ, Dietrich S, Ulrich LE, Liesegang H, Mascher T. 2009. The third pillar of bacterial signal transduction: classification of the extracytoplasmic function (ECF) sigma factor protein family. Mol Microbiol 74:557-81. doi:10.1111/j.1365-2958.2009.06870.x
4. Wuichet K, Cantwell BJ, Zhulin IB. 2010. Evolution and phyletic distribution of two-component signal transduction systems. Curr Opin Microbiol 13:219-25. doi:10.1016/j.mib.2009.12.011
5. Zschiedrich CP, Keidel V, Szurmant H. 2016. Molecular Mechanisms of Two-Component Signal Transduction. J Mol Biol 428:3752-75. doi:10.1016/j.jmb.2016.08.003
6. Stock AM, Robinson VL, Goudreau PN. 2000. Two-component signal transduction. Annu Rev Biochem 69:183-215. doi:10.1146/annurev.biochem.69.1.183
7. Beier D, Gross R. 2006. Regulation of bacterial virulence by two-component systems. Curr Opin Microbiol 9:143-52. doi:10.1016/j.mib.2006.01.005
8. Alm E, Huang K, Arkin A. 2006. The evolution of two-component systems in bacteria reveals different strategies for niche adaptation. PLoS Comput Biol 2:e143. doi:10.1371/journal.pcbi.0020143
9. Heermann R, Jung K. 2009. Stimulus Perception and Signaling in Histidine Kinases, p 135-161. *In* Krämer R, Jung K (ed), Bacterial Signaling. Wiley-VCH Verlag GmbH & Co. KGaA.
10. Shi X, Wegener-Feldbrugge S, Huntley S, Hamann N, Hedderich R, Sogaard-Andersen L. 2008. Bioinformatics and experimental analysis of proteins of two-component systems in *Myxococcus xanthus*. J Bacteriol 190:613-24. doi:10.1128/JB.01502-07
11. Schramke H, Wang Y, Heermann R, Jung K. 2016. Stimulus Perception by Histidine Kinases, p 282-300. *In* de Bruijn FJ (ed), Stress and Environmental Regulation of Gene Expression and Adaptation in Bacteria. Wiley-Blackwell.
12. Hancock L, Perego M. 2002. Two-component signal transduction in *Enterococcus faecalis*. J Bacteriol 184:5819-25. doi:10.1128/JB.184.21.5819-5825.2002
13. Mascher T, Helmann JD, Unden G. 2006. Stimulus perception in bacterial signal-transducing histidine kinases. Microbiol Mol Biol Rev 70:910-38. doi:10.1128/MMBR.00020-06
14. Gao R, Stock AM. 2009. Biological insights from structures of two-component proteins. Annu Rev Microbiol 63:133-54. doi:10.1146/annurev.micro.091208.073214
15. Rajeev L, Garber ME, Mukhopadhyay A. 2020. Tools to map target genes of bacterial two-component system response regulators. Environ Microbiol Rep 12:267-276. doi:10.1111/1758-2229.12838
16. Wadhams GH, Armitage JP. 2004. Making sense of it all: bacterial chemotaxis. Nat Rev Mol Cell Biol 5:1024-37. doi:10.1038/nrm1524
17. Jung K, Fried L, Behr S, Heermann R. 2012. Histidine kinases and response regulators in networks. Curr Opin Microbiol 15:118-24. doi:10.1016/j.mib.2011.11.009
18. Vilhena CSJ. 2018. Phenotypic heterogeneity and the biological significance of a pyruvate sensing network in *Escherichia coli*. Ludwig-Maximilians-Universität München, Munich.
19. Nikaido H, Saier MH, Jr. 1992. Transport proteins in bacteria: common themes in their design. Science 258:936-42. doi:10.1126/science.1279804

20. Tetsch L, Jung K. 2009. The regulatory interplay between membrane-integrated sensors and transport proteins in bacteria. Mol Microbiol 73:982-91. doi:10.1111/j.1365-2958.2009.06847.x
21. Heermann R, Jung K. 2010. The complexity of the 'simple' two-component system KdpD/KdpE in *Escherichia coli*. FEMS Microbiol Lett 304:97-106. doi:10.1111/j.1574-6968.2010.01906.x
22. Davies SJ, Golby P, Omrani D, Broad SA, Harrington VL, Guest JR, Kelly DJ, Andrews SC. 1999. Inactivation and regulation of the aerobic C(4)-dicarboxylate transport (*dctA*) gene of *Escherichia coli*. J Bacteriol 181:5624-35. doi:10.1128/JB.181.18.5624-5635.1999
23. Scheu PD, Witan J, Rauschmeier M, Graf S, Liao YF, Ebert-Jung A, Basche T, Erker W, Unden G. 2012. CitA/CitB two-component system regulating citrate fermentation in *Escherichia coli* and its relation to the DcuS/DcuR system in vivo. J Bacteriol 194:636-45. doi:10.1128/JB.06345-11
24. Kato A, Tanabe H, Utsumi R. 1999. Molecular characterization of the PhoP-PhoQ two-component system in *Escherichia coli* K-12: identification of extracellular $Mg2^{+}$-responsive promoters. J Bacteriol 181:5516-20. doi:10.1128/JB.181.17.5516-5520.1999
25. Wright JS, Olekhnovich IN, Touchie G, Kadner RJ. 2000. The histidine kinase domain of UhpB inhibits UhpA action at the *Escherichia coli uhpT* promoter. J Bacteriol 182:6279-86. doi:10.1128/JB.182.22.6279-6286.2000
26. Gilbert JA, Blaser MJ, Caporaso JG, Jansson JK, Lynch SV, Knight R. 2018. Current understanding of the human microbiome. Nat Med 24:392-400. doi:10.1038/nm.4517
27. Medlock GL, Carey MA, McDuffie DG, Mundy MB, Giallourou N, Swann JR, Kolling GL, Papin JA. 2018. Inferring Metabolic Mechanisms of Interaction within a Defined Gut Microbiota. Cell Syst 7:245-257 e7. doi:10.1016/j.cels.2018.08.003
28. Faith JJ, Guruge JL, Charbonneau M, Subramanian S, Seedorf H, Goodman AL, Clemente JC, Knight R, Heath AC, Leibel RL, Rosenbaum M, Gordon JI. 2013. The long-term stability of the human gut microbiota. Science 341:1237439. doi:10.1126/science.1237439
29. Sung J, Kim S, Cabatbat JJT, Jang S, Jin YS, Jung GY, Chia N, Kim PJ. 2017. Global metabolic interaction network of the human gut microbiota for context-specific community-scale analysis. Nat Commun 8:15393. doi:10.1038/ncomms15393
30. Gralka M, Szabo R, Stocker R, Cordero OX. 2020. Trophic Interactions and the Drivers of Microbial Community Assembly. Curr Biol 30:R1176-R1188. doi:10.1016/j.cub.2020.08.007
31. Ratzke C, Barrere J, Gore J. 2020. Strength of species interactions determines biodiversity and stability in microbial communities. Nat Ecol Evol 4:376-383. doi:10.1038/s41559-020-1099-4
32. Brugiroux S, Beutler M, Pfann C, Garzetti D, Ruscheweyh HJ, Ring D, Diehl M, Herp S, Lötscher Y, Hussain S, Bunk B, Pukall R, Huson DH, Münch PC, McHardy AC, McCoy KD, Macpherson AJ, Loy A, Clavel T, Berry D, Stecher B. 2016. Genome-guided design of a defined mouse microbiota that confers colonization resistance against *Salmonella enterica* serovar Typhimurium. Nat Microbiol 2:16215. doi:10.1038/nmicrobiol.2016.215
33. Troxell B, Zhang JJ, Bourret TJ, Zeng MY, Blum J, Gherardini F, Hassan HM, Yang XF. 2014. Pyruvate protects pathogenic spirochetes from H_2O_2 killing. PLoS One 9:e84625. doi:10.1371/journal.pone.0084625
34. O'Donnell-Tormey J, Nathan CF, Lanks K, DeBoer CJ, de la Harpe J. 1987. Secretion of pyruvate. An antioxidant defense of mammalian cells. J Exp Med 165:500-14. doi:10.1084/jem.165.2.500
35. Desagher S, Glowinski J, Premont J. 1997. Pyruvate protects neurons against hydrogen peroxide-induced toxicity. J Neurosci 17:9060-7.

36. Woo YJ, Taylor MD, Cohen JE, Jayasankar V, Bish LT, Burdick J, Pirolli TJ, Berry MF, Hsu V, Grand T. 2004. Ethyl pyruvate preserves cardiac function and attenuates oxidative injury after prolonged myocardial ischemia. J Thorac Cardiovasc Surg 127:1262-9. doi:10.1016/j.jtcvs.2003.11.032
37. Constantopoulos G, Barranger JA. 1984. Nonenzymatic decarboxylation of pyruvate. Anal Biochem 139:353-358. doi:10.1016/0003-2697(84)90016-2
38. Varma SD, Hegde K, Henein M. 2003. Oxidative damage to mouse lens in culture. Protective effect of pyruvate. Biochim Biophys Acta 1621:246-52. doi:10.1016/s0304-4165(03)00075-8
39. Redanz S, Treerat P, Mu R, Redanz U, Zou Z, Koley D, Merritt J, Kreth J. 2020. Pyruvate secretion by oral streptococci modulates hydrogen peroxide dependent antagonism. ISME J 14:1074-1088. doi:10.1038/s41396-020-0592-8
40. Oliver JD. 2005. The viable but nonculturable state in bacteria. J Microbiol 43 Spec No:93-100.
41. Dong K, Pan H, Yang D, Rao L, Zhao L, Wang Y, Liao X. 2020. Induction, detection, formation, and resuscitation of viable but non-culturable state microorganisms. Compr Rev Food Sci 19:149-183. doi:10.1111/1541-4337.12513
42. Li L, Mendis N, Trigui H, Oliver JD, Faucher SP. 2014. The importance of the viable but non-culturable state in human bacterial pathogens. Front Microbiol 5:258. doi:10.3389/fmicb.2014.00258
43. Mizunoe Y, Wai SN, Takade A, Yoshida S. 1999. Restoration of culturability of starvation-stressed and low-temperature-stressed *Escherichia coli* O157 cells by using H_2O_2-degrading compounds. Arch Microbiol 172:63-7. doi:10.1007/s002030050741
44. Morishige Y, Fujimori K, Amano F. 2013. Differential resuscitative effect of pyruvate and its analogues on VBNC (viable but non-culturable) *Salmonella*. Microbes Environ 28:180-6. doi:10.1264/jsme2.me12174
45. Liao H, Jiang L, Zhang R. 2018. Induction of a viable but non-culturable state in *Salmonella* Typhimurium by thermosonication and factors affecting resuscitation. FEMS Microbiol Lett 365:fnx249. doi:10.1093/femsle/fnx249
46. Vilhena C, Kaganovitch E, Grünberger A, Motz M, Forné I, Kohlheyer D, Jung K. 2019. Importance of pyruvate sensing and transport for the resuscitation of viable but nonculturable *Escherichia coli* K-12. J Bacteriol 201:e00610-18. doi:10.1128/jb.00610-18
47. Basta DW, Bergkessel M, Newman DK. 2017. Identification of Fitness Determinants during Energy-Limited Growth Arrest in *Pseudomonas aeruginosa*. mBio 8. doi:10.1128/mBio.01170-17
48. Bücker R, Heroven AK, Becker J, Dersch P, Wittmann C. 2014. The pyruvate-tricarboxylic acid cycle node: a focal point of virulence control in the enteric pathogen *Yersinia pseudotuberculosis*. J Biol Chem 289:30114-30132. doi:10.1074/jbc.M114.581348
49. Schär J, Stoll R, Schauer K, Loeffler DI, Eylert E, Joseph B, Eisenreich W, Fuchs TM, Goebel W. 2010. Pyruvate carboxylase plays a crucial role in carbon metabolism of extra- and intracellularly replicating *Listeria monocytogenes*. J Bacteriol 192:1774-84. doi:10.1128/jb.01132-09
50. Petrova OE, Schurr JR, Schurr MJ, Sauer K. 2012. Microcolony formation by the opportunistic pathogen *Pseudomonas aeruginosa* requires pyruvate and pyruvate fermentation. Mol Microbiol 86:819-35. doi:10.1111/mmi.12018
51. Goodwine J, Gil J, Doiron A, Valdes J, Solis M, Higa A, Davis S, Sauer K. 2019. Pyruvate-depleting conditions induce biofilm dispersion and enhance the efficacy of antibiotics in killing biofilms *in vitro* and *in vivo*. Sci Rep 9:3763. doi:10.1038/s41598-019-40378-z

52. Abernathy J, Corkill C, Hinojosa C, Li X, Zhou H. 2013. Deletions in the pyruvate pathway of *Salmonella* Typhimurium alter SPI1-mediated gene expression and infectivity. J Anim Sci Biotechnol 4:5. doi:10.1186/2049-1891-4-5
53. Anderson CJ, Medina CB, Barron BJ, Karvelyte L, Aaes TL, Lambertz I, Perry JSA, Mehrotra P, Gonçalves A, Lemeire K, Blancke G, Andries V, Ghazavi F, Martens A, van Loo G, Vereecke L, Vandenabeele P, Ravichandran KS. 2021. Microbes exploit death-induced nutrient release by gut epithelial cells. Nature 596:262-267. doi:10.1038/s41586-021-03785-9
54. Harper L, Balasubramanian D, Ohneck EA, Sause WE, Chapman J, Mejia-Sosa B, Lhakhang T, Heguy A, Tsirigos A, Ueberheide B, Boyd JM, Lun DS, Torres VJ. 2018. *Staphylococcus aureus* responds to the central metabolite pyruvate to regulate virulence. mBio 9:e02272-17. doi:10.1128/mBio.02272-17
55. Dubois T, Dancer-Thibonnier M, Monot M, Hamiot A, Bouillaut L, Soutourina O, Martin-Verstraete I, Dupuy B. 2016. Control of *Clostridium difficile* Physiopathology in Response to Cysteine Availability. Infect Immun 84:2389-405. doi:10.1128/IAI.00121-16
56. Xie T, Pang R, Wu Q, Zhang J, Lei T, Li Y, Wang J, Ding Y, Chen M, Bai J. 2019. Cold tolerance regulated by the pyruvate metabolism in *Vibrio parahaemolyticus*. Front Microbiol 10:178. doi:10.3389/fmicb.2019.00178
57. Warburg O, Wind F, Negelein E. 1927. The metabolism of tumors in the body. J Gen Physiol 8:519-30. doi:10.1085/jgp.8.6.519
58. Galperin MY. 2008. Telling bacteria: do not LytTR. Structure 16:657-9. doi:10.1016/j.str.2008.04.003
59. Behr S, Kristoficova I, Witting M, Breland EJ, Eberly AR, Sachs C, Schmitt-Kopplin P, Hadjifrangiskou M, Jung K. 2017. Identification of a high-affinity pyruvate receptor in *Escherichia coli*. Sci Rep 7:1388. doi:10.1038/s41598-017-01410-2
60. Miyake Y, Inaba T, Watanabe H, Teramoto J, Yamamoto K, Ishihama A. 2019. Regulatory roles of pyruvate-sensing two-component system PyrSR (YpdAB) in *Escherichia coli* K-12. FEMS Microbiol Lett 366. doi:10.1093/femsle/fnz009
61. Kraxenberger T, Fried L, Behr S, Jung K. 2012. First insights into the unexplored two-component system YehU/YehT in *Escherichia coli*. J Bacteriol 194:4272-84. doi:10.1128/jb.00409-12
62. Kristoficova I, Vilhena C, Behr S, Jung K. 2018. BtsT, a novel and specific pyruvate/H^+ symporter in *Escherichia coli*. J Bacteriol 200:e00599-17. doi:10.1128/jb.00599-17
63. Fried L, Behr S, Jung K. 2013. Identification of a target gene and activating stimulus for the YpdA/YpdB histidine kinase/response regulator system in *Escherichia coli*. J Bacteriol 195:807-15. doi:10.1128/jb.02051-12
64. Behr S, Fried L, Jung K. 2014. Identification of a novel nutrient-sensing histidine kinase/response regulator network in *Escherichia coli*. J Bacteriol 196:2023-2029. doi:10.1128/jb.01554-14
65. Steiner BD, Eberly AR, Hurst MN, Zhang EW, Green HD, Behr S, Jung K, Hadjifrangiskou M. 2018. Evidence of cross-regulation in two closely related pyruvate-sensing systems in uropathogenic *Escherichia coli*. J Membr Biol 251:65-74. doi:10.1007/s00232-018-0014-2
66. Vilhena C, Kaganovitch E, Shin JY, Grünberger A, Behr S, Kristoficova I, Brameyer S, Kohlheyer D, Jung K. 2018. A single-cell view of the BtsSR/YpdAB pyruvate sensing network in *Escherichia coli* and its biological relevance. J Bacteriol 200:e00536-17. doi:10.1128/jb.00536-17

67. Ogasawara H, Ishizuka T, Yamaji K, Kato Y, Shimada T, Ishihama A. 2019. Regulatory role of pyruvate-sensing BtsSR in biofilm formation by *Escherichia coli* K-12. FEMS Microbiol Lett 366:fnz251. doi:10.1093/femsle/fnz251
68. Conover MS, Hadjifrangiskou M, Palermo JJ, Hibbing ME, Dodson KW, Hultgren SJ. 2016. Metabolic Requirements of *Escherichia coli* in Intracellular Bacterial Communities during Urinary Tract Infection Pathogenesis. mBio 7:e00104-16. doi:10.1128/mBio.00104-16
69. Zhu T, Lou Q, Wu Y, Hu J, Yu F, Qu D. 2010. Impact of the *Staphylococcus epidermidis* LytSR two-component regulatory system on murein hydrolase activity, pyruvate utilization and global transcriptional profile. BMC Microbiol 10:287. doi:10.1186/1471-2180-10-287
70. Charbonnier T, Le Coq D, McGovern S, Calabre M, Delumeau O, Aymerich S, Jules M. 2017. Molecular and Physiological Logics of the Pyruvate-Induced Response of a Novel Transporter in *Bacillus subtilis*. mBio 8:e00976-17. doi:10.1128/mBio.00976-17
71. Ramos AL, Aquino M, Garcia G, Gaspar M, de la Cruz C, Saavedra-Flores A, Brom S, Cervantes-Rivera R, Galindo-Sanchez CE, Hernandez R, Puhar A, Lupas AN, Sepulveda E. 2022. RpuS/R Is a Novel Two-Component Signal Transduction System That Regulates the Expression of the Pyruvate Symporter MctP in *Sinorhizobium fredii* NGR234. Front Microbiol 13:871077. doi:10.3389/fmicb.2022.871077
72. Behr S, Brameyer S, Witting M, Schmitt-Kopplin P, Jung K. 2017. Comparative analysis of LytS/LytTR-type histidine kinase/response regulator systems in γ-proteobacteria. PLoS One 12:e0182993. doi:10.1371/journal.pone.0182993
73. Wong VK, Pickard DJ, Barquist L, Sivaraman K, Page AJ, Hart PJ, Arends MJ, Holt KE, Kane L, Mottram LF, Ellison L, Bautista R, McGee CJ, Kay SJ, Wileman TM, Kenney LJ, MacLennan CA, Kingsley RA, Dougan G. 2013. Characterization of the *yehUT* two-component regulatory system of *Salmonella enterica* Serovar Typhi and Typhimurium. PLoS One 8:e84567. doi:10.1371/journal.pone.0084567
74. Holt KE, Parkhill J, Mazzoni CJ, Roumagnac P, Weill FX, Goodhead I, Rance R, Baker S, Maskell DJ, Wain J, Dolecek C, Achtman M, Dougan G. 2008. High-throughput sequencing provides insights into genome variation and evolution in *Salmonella* Typhi. Nat Genet 40:987-93. doi:10.1038/ng.195
75. Garai P, Lahiri A, Ghosh D, Chatterjee J, Chakravortty D. 2016. Peptide utilizing carbon starvation gene *yjiY* is required for flagella mediated infection caused by *Salmonella*. Microbiology (Reading) 162:100-116. doi:10.1099/mic.0.000204
76. Hosie AH, Allaway D, Poole PS. 2002. A monocarboxylate permease of *Rhizobium leguminosarum* is the first member of a new subfamily of transporters. J Bacteriol 184:5436-48. doi:10.1128/jb.184.19.5436-5448.2002
77. Jolkver E, Emer D, Ballan S, Krämer R, Eikmanns BJ, Marin K. 2009. Identification and characterization of a bacterial transport system for the uptake of pyruvate, propionate, and acetate in *Corynebacterium glutamicum*. J Bacteriol 191:940-8. doi:10.1128/jb.01155-08
78. Ahn SJ, Deep K, Turner ME, Ishkov I, Waters A, Hagen SJ, Rice KC. 2019. Characterization of LrgAB as a stationary phase-specific pyruvate uptake system in *Streptococcus mutans*. BMC Microbiol 19:223. doi:10.1186/s12866-019-1600-x
79. Kornberg HL, Smith J. 1967. Genetic control of the uptake of pyruvate by *Escherichia coli*. Biochim Biophys Acta 148:591-2. doi:10.1016/0304-4165(67)90167-5
80. Lang VJ, Leystra-Lantz C, Cook RA. 1987. Characterization of the specific pyruvate transport system in *Escherichia coli* K-12. J Bacteriol 169:380-5. doi:10.1128/jb.169.1.380-385.1987
81. Kreth J, Lengeler JW, Jahreis K. 2013. Characterization of pyruvate uptake in *Escherichia coli* K-12. PLoS One 8:e67125. doi:10.1371/journal.pone.0067125

82. Hwang S, Choe D, Yoo M, Cho S, Kim SC, Cho S, Cho BK. 2018. Peptide transporter CstA imports pyruvate in *Escherichia coli* K-12. J Bacteriol 200:e00771-17. doi:10.1128/jb.00771-17
83. Schultz JE, Matin A. 1991. Molecular and functional characterization of a carbon starvation gene of *Escherichia coli*. J Mol Biol 218:129-40. doi:10.1016/0022-2836(91)90879-b
84. Bricker DK, Taylor EB, Schell JC, Orsak T, Boutron A, Chen YC, Cox JE, Cardon CM, Van Vranken JG, Dephoure N, Redin C, Boudina S, Gygi SP, Brivet M, Thummel CS, Rutter J. 2012. A mitochondrial pyruvate carrier required for pyruvate uptake in yeast, *Drosophila*, and humans. Science 337:96-100. doi:10.1126/science.1218099
85. Wenes M, Jaccard A, Wyss T, Maldonado-Perez N, Teoh ST, Lepez A, Renaud F, Franco F, Waridel P, Yacoub Maroun C, Tschumi B, Dumauthioz N, Zhang L, Donda A, Martin F, Migliorini D, Lunt SY, Ho PC, Romero P. 2022. The mitochondrial pyruvate carrier regulates memory T cell differentiation and antitumor function. Cell Metab 34:731-746 e9. doi:10.1016/j.cmet.2022.03.013
86. Bensard CL, Wisidagama DR, Olson KA, Berg JA, Krah NM, Schell JC, Nowinski SM, Fogarty S, Bott AJ, Wei P, Dove KK, Tanner JM, Panic V, Cluntun A, Lettlova S, Earl CS, Namnath DF, Vazquez-Arreguin K, Villanueva CJ, Tantin D, Murtaugh LC, Evason KJ, Ducker GS, Thummel CS, Rutter J. 2020. Regulation of Tumor Initiation by the Mitochondrial Pyruvate Carrier. Cell Metab 31:284-300 e7. doi:10.1016/j.cmet.2019.11.002
87. Guimaraes NC, Alves DS, Vilela WR, de-Souza-Ferreira E, Gomes BRB, Ott D, Murgott J, P ENdS, de Sousa MV, Galina A, Roth J, Fabro de Bem A, Veiga-Souza FH. 2021. Mitochondrial pyruvate carrier as a key regulator of fever and neuroinflammation. Brain Behav Immun 92:90-101. doi:10.1016/j.bbi.2020.11.031
88. Zangari J, Petrelli F, Maillot B, Martinou JC. 2020. The Multifaceted Pyruvate Metabolism: Role of the Mitochondrial Pyruvate Carrier. Biomolecules 10. doi:10.3390/biom10071068
89. Ruby EG, Nealson KH. 1977. Pyruvate production and excretion by the luminous marine bacteria. Appl Environ Microbiol 34:164-9. doi:10.1128/aem.34.2.164-169.1977
90. Kodaki T, Murakami H, Taguchi M, Izui K, Katsuki H. 1981. Stringent control of intermediary metabolism in *Escherichia coli*: pyruvate excretion by cells grown on succinate. J Biochem 90:1437-44. doi:10.1093/oxfordjournals.jbchem.a133610
91. Chubukov V, Gerosa L, Kochanowski K, Sauer U. 2014. Coordination of microbial metabolism. Nat Rev Microbiol 12:327-340. doi:10.1038/nrmicro3238
92. Paczia N, Nilgen A, Lehmann T, Gätgens J, Wiechert W, Noack S. 2012. Extensive exometabolome analysis reveals extended overflow metabolism in various microorganisms. Microb Cell Factories 11:122. doi:10.1186/1475-2859-11-122
93. Yasid NA, Rolfe MD, Green J, Williamson MP. 2016. Homeostasis of metabolites in *Escherichia coli* on transition from anaerobic to aerobic conditions and the transient secretion of pyruvate. R Soc Open Sci 3:160187. doi:10.1098/rsos.160187
94. Surowitz KG, Pfister RM. 1985. Glucose metabolism and pyruvate excretion by Streptomyces alboniger. Can J Microbiol 31:702-706. doi:10.1139/m85-133
95. Madden T, Ward JM, Ison AP. 1996. Organic acid excretion by *Streptomyces lividans* TK24 during growth on defined carbon and nitrogen sources. Microbiology (Reading) 142:3181-5. doi:10.1099/13500872-142-11-3181
96. Benson PJ, Purcell-Meyerink D, Hocart CH, Truong TT, James GO, Rourke L, Djordjevic MA, Blackburn SI, Price GD. 2016. Factors altering pyruvate excretion in a glycogen storage mutant of the Cyanobacterium, *Synechococcus* PCC7942. Front Microbiol 7:475. doi:10.3389/fmicb.2016.00475

97. Yin C, He D, Chen S, Tan X, Sang N. 2016. Exogenous pyruvate facilitates cancer cell adaptation to hypoxia by serving as an oxygen surrogate. Oncotarget 7:47494-47510. doi:10.18632/oncotarget.10202
98. Morita N, Umemoto E, Fujita S, Hayashi A, Kikuta J, Kimura I, Haneda T, Imai T, Inoue A, Mimuro H, Maeda Y, Kayama H, Okumura R, Aoki J, Okada N, Kida T, Ishii M, Nabeshima R, Takeda K. 2019. GPR31-dependent dendrite protrusion of intestinal CX3CR1^{+} cells by bacterial metabolites. Nature 566:110-114. doi:10.1038/s41586-019-0884-1
99. Dubey AK, Baker CS, Suzuki K, Jones AD, Pandit P, Romeo T, Babitzke P. 2003. CsrA regulates translation of the *Escherichia coli* carbon starvation gene, *cstA*, by blocking ribosome access to the *cstA* transcript. J Bacteriol 185:4450-60. doi:10.1128/JB.185.15.4450-4460.2003
100. Tenaillon O, Skurnik D, Picard B, Denamur E. 2010. The population genetics of commensal *Escherichia coli*. Nat Rev Microbiol 8:207-17. doi:10.1038/nrmicro2298
101. Mueller NT, Bakacs E, Combellick J, Grigoryan Z, Dominguez-Bello MG. 2015. The infant microbiome development: mom matters. Trends Mol Med 21:109-17. doi:10.1016/j.molmed.2014.12.002
102. Mahadevan R, Lovley DR. 2008. The degree of redundancy in metabolic genes is linked to mode of metabolism. Biophys J 94:1216-20. doi:10.1529/biophysj.107.118414
103. Neumann S, Grosse K, Sourjik V. 2012. Chemotactic signaling via carbohydrate phosphotransferase systems in *Escherichia coli*. PNAS 109:12159-64. doi:10.1073/pnas.1205307109
104. Somavanshi R, Ghosh B, Sourjik V. 2016. Sugar influx sensing by the phosphotransferase system of *Escherichia coli*. PLoS Biol 14:e2000074. doi:10.1371/journal.pbio.2000074
105. Zhou S, Zhuang Y, Zhu X, Yao F, Li H, Li H, Zou X, Wu J, Zhou H, Nuer G, Huang Y, Li S, Peng Q. 2019. YhjX Regulates the Growth of *Escherichia coli* in the Presence of a Subinhibitory Concentration of Gentamicin and Mediates the Adaptive Resistance to Gentamicin. Front Microbiol 10:1180. doi:10.3389/fmicb.2019.01180
106. Kröger C, Colgan A, Srikumar S, Händler K, Sivasankaran Sathesh K, Hammarlöf Disa L, Canals R, Grissom Joe E, Conway T, Hokamp K, Hinton Jay CD. 2013. An Infection-Relevant Transcriptomic Compendium for *Salmonella enterica* Serovar Typhimurium. Cell Host Microbe 14:683-695. doi:10.1016/j.chom.2013.11.010
107. Richardson AR, Payne EC, Younger N, Karlinsey JE, Thomas VC, Becker LA, Navarre WW, Castor ME, Libby SJ, Fang FC. 2011. Multiple targets of nitric oxide in the tricarboxylic acid cycle of *Salmonella enterica* serovar typhimurium. Cell Host Microbe 10:33-43. doi:10.1016/j.chom.2011.06.004
108. Causey TB, Shanmugam KT, Yomano LP, Ingram LO. 2004. Engineering *Escherichia coli* for efficient conversion of glucose to pyruvate. Proc Natl Acad Sci U S A 101:2235-40. doi:10.1073/pnas.0308171100
109. Zhu Y, Eiteman MA, Altman R, Altman E. 2008. High glycolytic flux improves pyruvate production by a metabolically engineered *Escherichia coli* strain. Appl Environ Microbiol 74:6649-55. doi:10.1128/AEM.01610-08
110. Wieschalka S, Blombach B, Eikmanns BJ. 2012. Engineering *Corynebacterium glutamicum* for the production of pyruvate. Appl Microbiol Biotechnol 94:449-59. doi:10.1007/s00253-011-3843-9
111. Kawata Y, Nishimura T, Matsushita I, Tsubota J. 2016. Efficient production and secretion of pyruvate from *Halomonas* sp. KM-1 under aerobic conditions. AMB Express 6:22. doi:10.1186/s13568-016-0195-y

112. Malla S, van der Helm E, Darbani B, Wieschalka S, Forster J, Borodina I, Sommer MOA. 2022. A Novel Efficient L-Lysine Exporter Identified by Functional Metagenomics. Front Microbiol 13:855736. doi:10.3389/fmicb.2022.855736
113. Kannan G, Wilks JC, Fitzgerald DM, Jones BD, Bondurant SS, Slonczewski JL. 2008. Rapid acid treatment of *Escherichia coli*: transcriptomic response and recovery. BMC Microbiol 8:37. doi:10.1186/1471-2180-8-37
114. Jung D, Park S, Ruffini J, Dussault F, Dufour S, Ronholm J. 2021. Comparative genomic analysis of *Escherichia coli* isolates from cases of bovine clinical mastitis identifies nine specific pathotype marker genes. Microb Genom 7. doi:10.1099/mgen.0.000597
115. Tremblay YDN, Durand BAR, Hamiot A, Martin-Verstraete I, Oberkampf M, Monot M, Dupuy B. 2021. Metabolic adaption to extracellular pyruvate triggers biofilm formation in *Clostridioides difficile*. ISME J 15:3623-3635. doi:10.1038/s41396-021-01042-5
116. Da Re S, Valle J, Charbonnel N, Beloin C, Latour-Lambert P, Faure P, Turlin E, Le Bouguenec C, Renauld-Mongenie G, Forestier C, Ghigo JM. 2013. Identification of commensal *Escherichia coli* genes involved in biofilm resistance to pathogen colonization. PLoS One 8:e61628. doi:10.1371/journal.pone.0061628
117. Jones CM, Hernandez Lozada NJ, Pfleger BF. 2015. Efflux systems in bacteria and their metabolic engineering applications. Appl Microbiol Biotechnol 99:9381-93. doi:10.1007/s00253-015-6963-9
118. Sugiyama Y, Nakamura A, Matsumoto M, Kanbe A, Sakanaka M, Higashi K, Igarashi K, Katayama T, Suzuki H, Kurihara S. 2016. A Novel Putrescine Exporter SapBCDF of *Escherichia coli*. J Biol Chem 291:26343-26351. doi:10.1074/jbc.M116.762450
119. Yamada S, Awano N, Inubushi K, Maeda E, Nakamori S, Nishino K, Yamaguchi A, Takagi H. 2006. Effect of drug transporter genes on cysteine export and overproduction in *Escherichia coli*. Appl Environ Microbiol 72:4735-42. doi:10.1128/AEM.02507-05
120. Hori H, Yoneyama H, Tobe R, Ando T, Isogai E, Katsumata R. 2011. Inducible L-alanine exporter encoded by the novel gene *ygaW* (*alaE*) in *Escherichia coli*. Appl Environ Microbiol 77:4027-34. doi:10.1128/AEM.00003-11
121. Gunasekera TS, Striebich RC, Mueller SS, Strobel EM, Ruiz ON. 2013. Transcriptional profiling suggests that multiple metabolic adaptations are required for effective proliferation of *Pseudomonas aeruginosa* in jet fuel. Environ Sci Technol 47:13449-58. doi:10.1021/es403163k
122. Wiebe MA, Brannon JR, Steiner BD, Bamidele A, Schrimpe-Rutledge AC, Codreanu SG, Sherrod SD, McLean JA, Hadjifrangiskou M. 2022. Serine Deamination Is a New Acid Tolerance Mechanism Observed in Uropathogenic *Escherichia coli*. mBio:e0296322. doi:10.1128/mbio.02963-22

Supplemental material for chapter 2

Gasperotti AF, Göing S, Ruiz EF, Forne I, Jung K. 2020. Function and regulation of the pyruvate transporter CstA in *Escherichia coli*. Int J Mol Sci 21:E9068. https://doi.org/10.3390/ijms21239068

Supplementary Materials

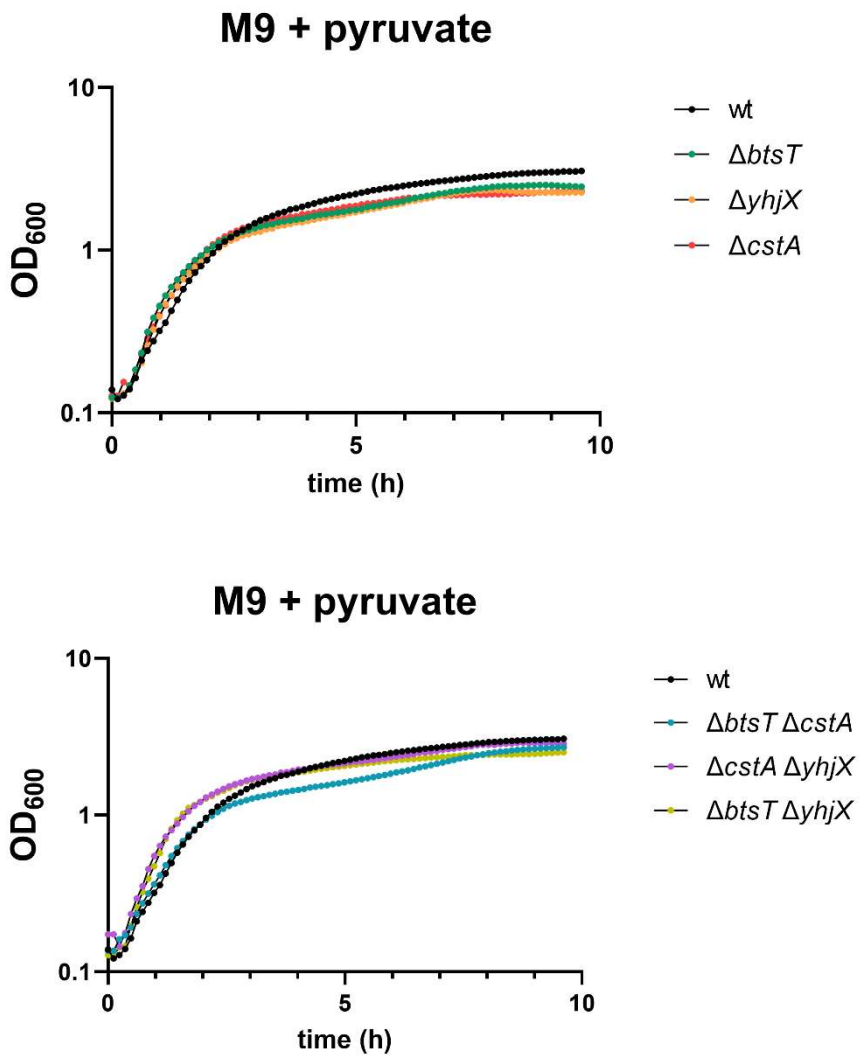

Figure S1. Growth of *E. coli* MG1655 and the different single and double mutants with pyruvate as C-source. Cells of *E. coli* MG1655 and the indicated single (upper panel) or double mutants (lower panel) were grown in M9 minimal medium with 40 mM pyruvate as C-source at 37°C under constant agitation. Samples were taken and OD_{600} was measured at different time points. The graphs show the mean of three independent replicates. The standard deviations from the mean were less than 10%.

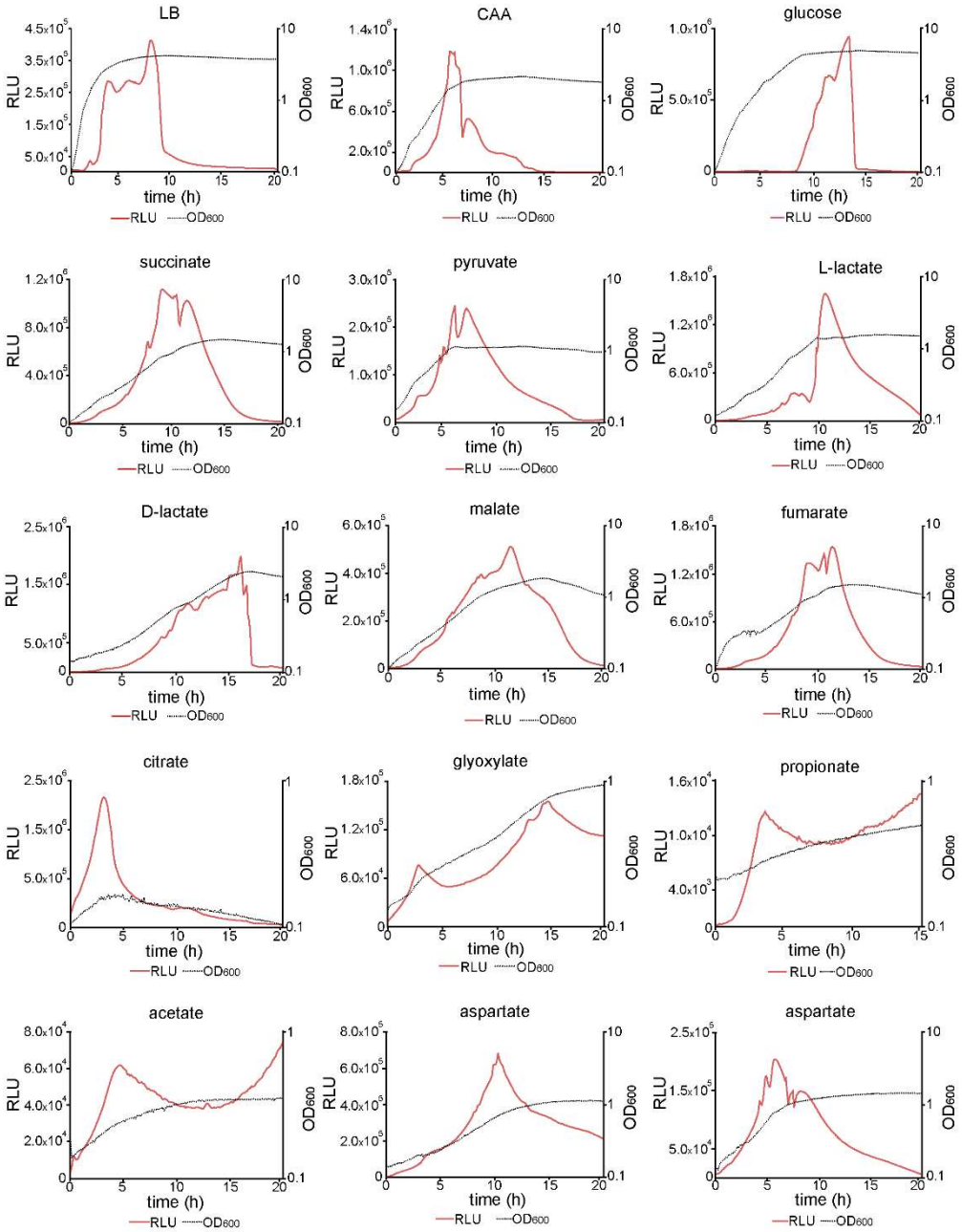

Figure S2. Activation of the *cstA* promoter under various growth conditions. *E. coli* MG1655 cells were transformed with pBBR1-*cstA*prom-lux and grown at 37°C in M9 minimal medium supplemented with 40 mM of the indicated C-source. Luminescence levels and OD_{600} were measured over time. Luminescence normalized to an optical density (OD_{600}) of 1 (RLU) and growth of cells is plotted over time. CAA, casamino acids.

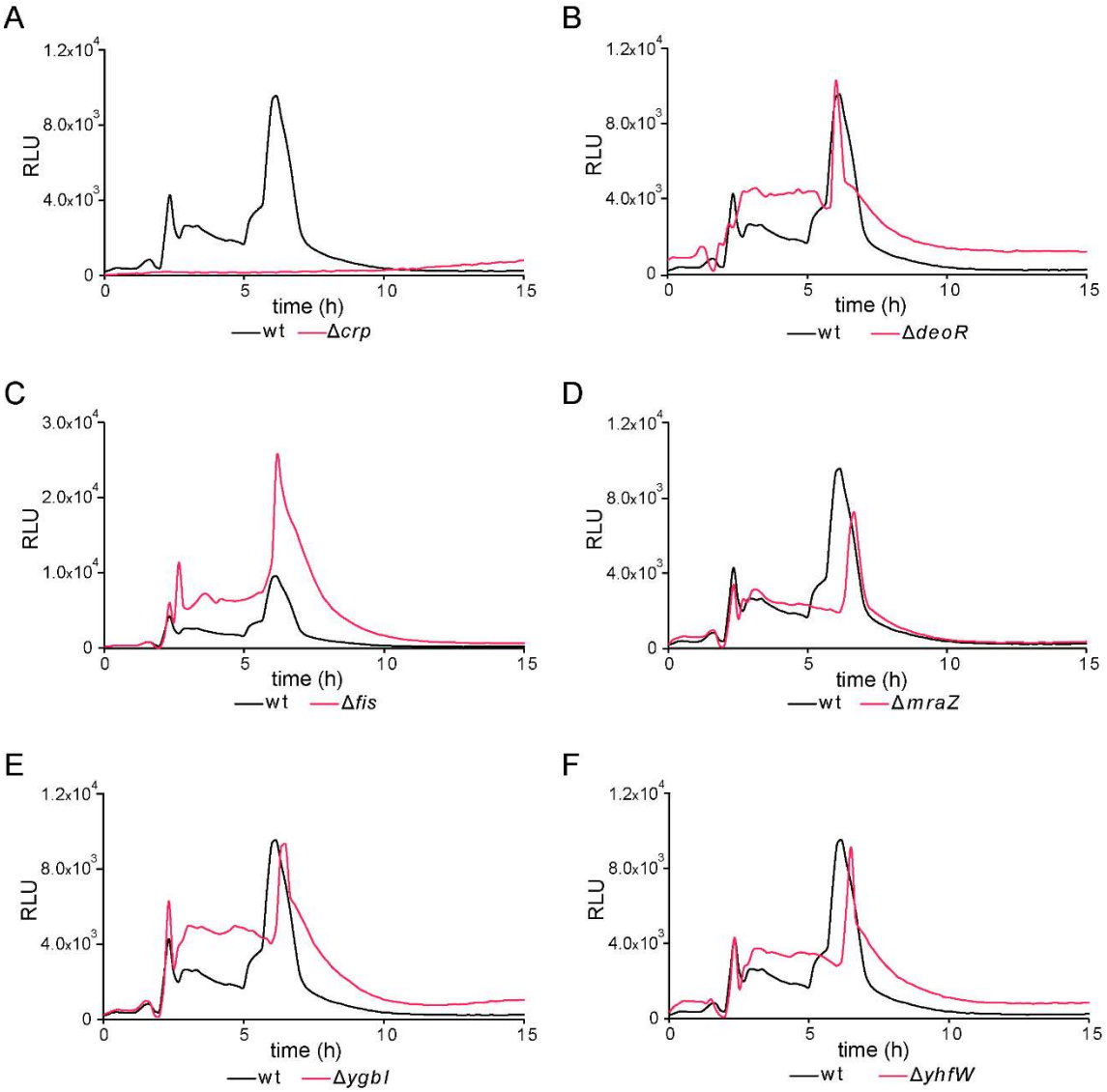

Figure S3. Promoter activity of *cstA* in different *E. coli* mutants. A luciferase-based reporter assay was used to monitor the promoter activity of *cstA* in the indicated *E. coli* BW25113 mutants. All strains were transformed with the plasmid pBBR1-*cstA*prom-lux. Bacteria were cultivated in LB medium under aerobic conditions, and the growth and activity of the reporter were continuously monitored. Luciferase activity normalized to an optical density (OD_{600}) of 1 (RLU) is plotted over time. A) expression in the Δ*crp* mutant compared to the wt strain. B) expression in the Δ*deoR* mutant compared to the wt strain. C) expression in the Δ*fis* mutant compared to the wt strain. D) expression in the Δ*mraZ* mutant compared to the wt strain. E) expression in the Δ*ygbI* mutant compared to the wt strain. F) expression in the Δ*yhfW* mutant compared to the wt strain.

Table S1. List of oligonucleotides used in this work.

Name	Sequence (5′ – 3′)	Description
dYhjX forward	TTTATTACTGCAGGAATACTG CCATGACACCTTCAAATTATC AGCGTACCAATTAACCCTCAC TAAAGGGCG	Upstream primer for in-frame deletion of *yhjX*, using the Quick and Easy *E. coli* gene deletion kit (Gene Bridges)
dYhjX reverse	CAGTAGCTCGCGGCTGAGCAT TAAAGGGAGCCATGCGCCTCA CGCAACATTAATACGACTCAC TATAGGGCTC	downstream primer for in-frame deletion of *yhjX*, using the Quick and Easy *E. coli* gene deletion kit (Gene Bridges)

dbtsT forward	GGCCAACTATTAATCAATACA TGCCAGGTTTTACTATGGATA CTAAAAAGAATTAACCCTCAC TAAAGGGCG	Upstream primer for in-frame deletion of *btsT,* using the Quick and Easy *E. coli* gene deletion kit (Gene Bridges)
dbtsT reverse	AGAACAAAGCCCCGCCGAAG CGGGGCTAAACACGGTTAGTG GTGCGAAGATAATACGACTCA CTATAGGGCTC	downstream primer for in-frame deletion of *btsT,* using the Quick and Easy *E. coli* gene deletion kit (Gene Bridges)
dcstA forward	TAACATCTCTATGGACACGCA CACGGATAACAACTatgAACA AATCAGGGAATTAACCCTCAC TAAAGGGCG	Upstream primer for in-frame deletion of *cstA,* using the Quick and Easy *E. coli* gene deletion kit (Gene Bridges)
dcstA reverse	CCAACATTCGCCAACATCCCC CCCTCACTCTGACTTTAGTGTG CGCCTTTTAATACGACTCACT ATAGGGCTC	downstream primer for in-frame deletion of *cstA,* using the Quick and Easy *E. coli* gene deletion kit (Gene Bridges)
CstA_pBAD_fw	GGAATTCACCATGGTACCCAT GAACAAATCAGGGAAATAC	Gibson assembly fragment 1 forward primer, overlap region of pBAD24 and beginning of *cstA*
CstA_oI_rev	CCAGGTCAACTGCACGCCGGT AAAG	Gibson assembly fragment 1 reverse primer, internal primer on *cstA* coding region.
CstA_oI_fw	CTTTACCGGCGTGCAGTTGAC CTGG	Gibson assembly fragment 2 forward primer, internal primer on *cstA* coding region.
CstA_pBAD_rev	GGTCGACTCTAGAGGATCCCC TTAGTGGTGATGGTGATGATG GTGTGCGCCTTTTGCCTGC	Gibson assembly fragment 2 reverse primer, end sequence of *cstA*, 6 his tag and overlap region of pBAD24
XbaI-CstAprom-Fw	CTATTCTCTAGACGCGGCGTC TGCCAGCCGCTGCATC	300 bp upstream starting codon, for *cstA* promoter cloning in pBBR1-lux using XbaI
XhoI-CstAprom-Rv	CCCCCCCTCGAGAGTTGTTAT CCGTGTGCGTGTCCAT	upstream ATG for *cstA* promoter cloning in pBBR1-lux using XhoI
cstApFw	[Btn]GTCGTTTTCGATGAACAG GGGC	biotinilated forward primer for DNA affinity-capture, *cstA* promoter region. 300 bp upstream of start codon.
cstApRv	CTGTCCAGACGAGGTATTTCC C	reverse primer for DNA affinity purification, *cstA* promoter region upstream ATG
cstAcFw	[Btn]GTGGCCTGCTTTATGATC ATGG	biotinilated forward primer for DNA affinity purification. Control fragment: *cstA* gene inner region
cstAcRv	AGGTCAACTGCACGCCGGTAA A	reverse primer for DNA affinity purification. Control fragment: *cstA* gene inner region

Supplemental material for chapter 3

Göing S, Gasperotti AF, Yang Q, Defoirdt T, Jung K. 2021. Insights into a pyruvate sensing and uptake system in *Vibrio campbellii* and its importance for virulence. J Bacteriol 203:e00296-21. https://doi.org/10.1128/jb.00296-21

SUPPLEMENT

SUPPLEMENTAL METHODS

Bioluminescence measurement. *V. campbellii* wild type, Δ*btsU* and Δ*btsSR* were grown in Autoinducer Bioassay (AB) medium (1) at 30°C in a plate reader (Tecan). Cells of overnight cultures were diluted 1:5,000-fold in fresh AB medium. OD_{600} and bioluminescence were measured over time and relative light units (RLU * OD_{600}^{-1}) were determined.

Swimming motility test. *V. campbellii* wild type, Δ*btsU* and Δ*btsSR* cells were grown in LM medium to mid-exponential phase and adjusted to OD_{600} = 1. Drops of 5 µl were spotted on LM soft agar plates (0.3 % agar, w/v), incubated at 30 °C for 18 hours and diameter sizes of motility halos were determined.

Aggregation assay. *V. campbellii* wild type, Δ*btsU* and Δ*btsSR* were grown in tubes with 5 ml LM medium, inoculated from overnight cultures, grown to an OD_{600} = 1.5 and kept standing at 30°C for 24 h. Every hour, samples were taken from the upper 5 mm of the culture and OD_{600} was determined.

External indole measurement. *V. campbellii* wild type, Δ*btsU* and Δ*btsSR* were grown aerobically in LM medium. Growth was monitored and samples were taken periodically for measurement of indole concentration. According to Mueller *et al.* (2), samples were centrifuged (4°C, 10 min, 10,000 x *g*), 250 µl supernatant were mixed with 250 µl 20 % trichloroacetic acid, incubated on ice for 15 min and centrifuged again to remove precipitates. Supernatants were mixed 1:1 with Kovac's reagent (5 g dimethylaminobenzaldehyde, 75 ml isoamylalcohol, 25 ml concentrated HCl), vortexed and incubated at room temperature for at least 15 min. Absorbance at 571 nm of the upper layer was determined with a plate reader (Tecan). Standards of 0 µM, 200 µM,

400 μM, 600 μM, 800 μM and 1 mM indole were used for a calibration curve to allow quantification.

pH of culture supernatants. *V. campbellii* wild type, Δ*btsU* and Δ*btsSR* were grown in LM medium. Growth was monitored and samples were taken periodically to determine the pH of the medium after centrifugation.

Macrocolony formation. *V. campbellii* wild type, Δ*btsU* and Δ*btsSR* were grown in LM medium, adjusted to OD_{600} =1 and drops of 5 μl were spotted on LM plates (2 % agar, w/v). During incubation at 30°C, pictures of emerging macrocolonies were taken at different time points with a Canon EOS M50 camera and bioluminescence of macrocolonies was visualized with a luminescence imaging chamber (Peqlab).

SUPPLEMENTAL FIGURES

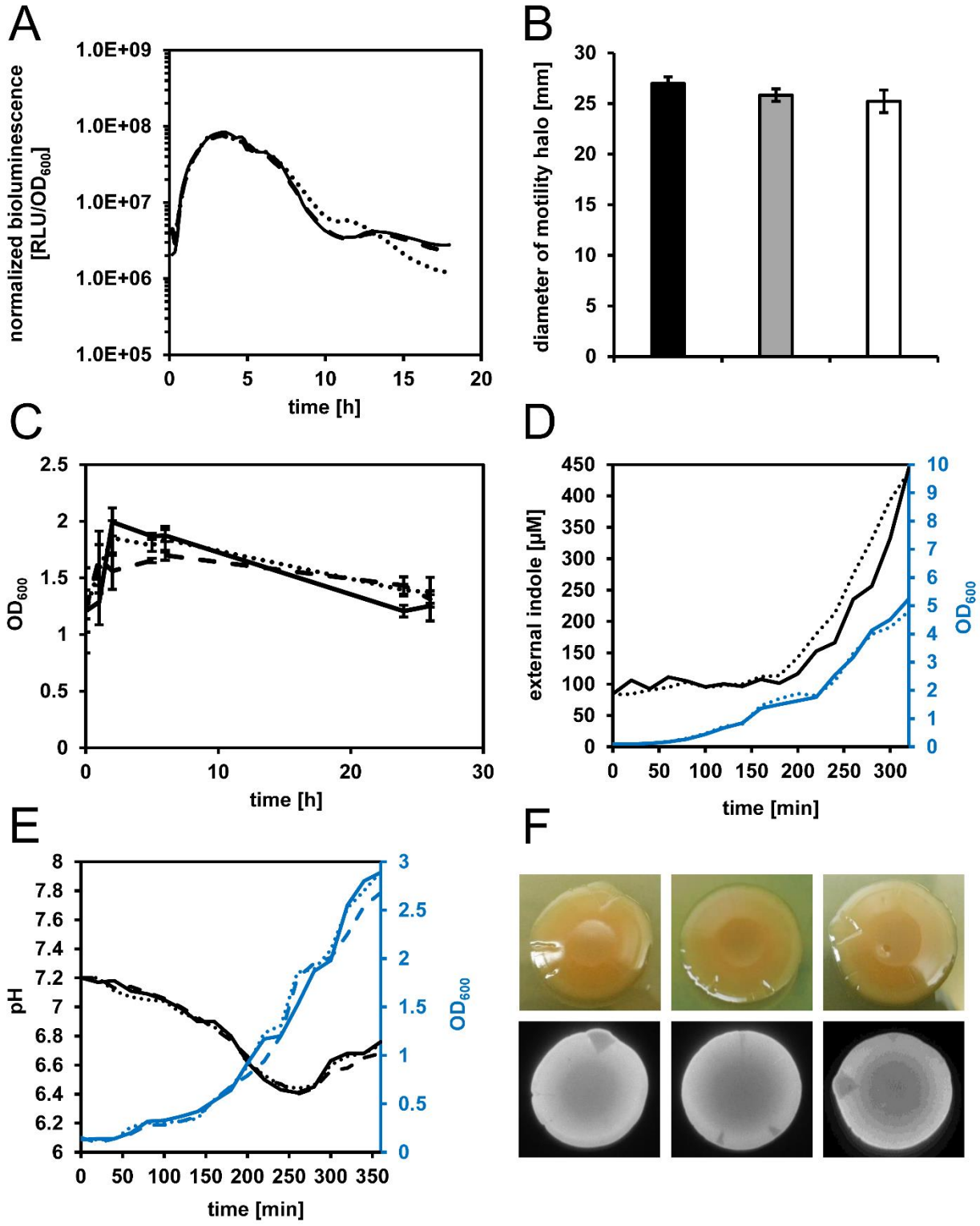

FIG S1. Phenotypes of *V. campbellii* that were not affected by deletions of *btsU* or *btsSR*. **A) Bioluminescence.** *V. campbellii* wild type (solid line), Δ*btsU* (dotted line) and Δ*btsSR* (dashed line) were grown in AB medium at 30°C and bioluminescence was measured over time in a plate reader. **B) Swimming motility.** Droplets with equal numbers of *V. campbellii* wild type (black), Δ*btsU* (grey) and Δ*btsSR* (white) cells were spotted on LM soft agar plates (0.3 % agar, w/v), incubated at 30°C for 18 hours and motility halo diameters were determined. **C) Cell aggregation.** *V. campbellii* wild type (solid line), Δ*btsU* (dotted line) and Δ*btsSR* (dashed line) were grown to OD_{600} = 1.5 and kept standing at 30°C for 24 h. Samples were taken every hour from the upper 5 mm of the culture and OD_{600} was determined. **D) Indole excretion.** *V. campbellii* wild type (solid line) and Δ*btsU* (dotted line) were grown in LM medium at 30°C, samples were taken every 20 min and indole concentration was determined. **E) Extracellular pH.** *V. campbellii* wild type (solid line), Δ*btsU* (dotted line) and Δ*btsSR* (dashed line) were grown in LM medium at 30°C, samples were taken every 20 min and the pH of the medium was determined. **F) Macrocolony formation.** Droplets with equal numbers of *V. campbellii* wild type (left), Δ*btsU* (middle) and Δ*btsSR* (right) cells were spotted on LM agar plates (2 % agar, w/v) and incubated for 8 days at 30°C. Pictures were taken (upper image) and bioluminescence was detected (lower image).

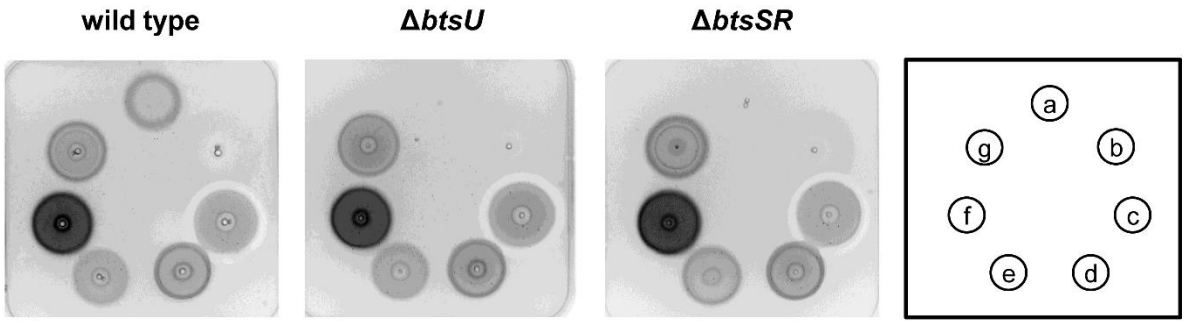

FIG S2. Chemotaxis defect of *V. campbellii* Δ*btsU* and Δ*btsSR* is specific for pyruvate. *V. campbellii* wild type, Δ*btsU* and Δ*btsSR* cells were tested for chemotaxis towards different substances using the plug-in-pond assay (3). The organization of the test plate is schematically illustrated on the right. Cells were mixed with M9 minimal medium soft agar without carbon source (2 % NaCl, 0.3 % agar, w/v) and poured over hard agar plugs (1.5 % agar, w/v) containing (a) pyruvate, (b) H_2O as negative control, (c) alanine, (d) fumarate, (e) acetate, (f) gluconate and (g) glucose (each 20 mM). Plates were incubated for 3 hours at 30°C and accumulation of cells around the plugs was visualized by bioluminescence detection.

SUPPLEMENTAL TABLES

TABLE S1. Oligonucleotides used in this study

	DNA sequence	Description
#1	CGGCTGGCGCCAAGCTTCTC TGCAGGAGCGATCGGCAAT GCTCAATGCGC	Primer 1 for deletion of *V. campbellii btsU* with pNTPS-R6KT, PstI site

#2	GACAATAGCTATGATGTGGT TTCTATCAGAAACCGCATAA TGAATCCCTT	Primer 2 for deletion of *V. campbellii btsU* with pNTPS-R6KT, amplifies 15 last bp, overlap with #3
#3	AAGGGATTCATTATGCGGTT TCTGATAGAAACCACATCAT AGCTATTGTC	Primer 3 for deletion of *V. campbellii btsU* with pNTPS-R6KT, amplifies 15 first bp, overlap with #2
#4	CCGAAGCTAGCGAATTCGTG GATCCAAAAAGATCTTTTTC ATGTTTCTAT	Primer 4 for deletion of *V. campbellii btsU* with pNTPS-R6KT, BamHI site
#5	CGGCTGGCGCCAAGCTTCTC TGCAGTTCATCGGGAATTGC TACATGAGTT	Primer 1 for deletion of *V. campbellii btsS* with pNTPS-R6KT, PstI site
#6	TAGGTTCGCTATGGAACTGG TCATCCCCCACTCGCGATAA GTACAGTGAA	Primer 2 for deletion of *V. campbellii btsS* with pNTPS-R6KT, amplifies 15 last bp, overlap with #7
#7	TTCACTGTACTTATCGCGAG TGGGGGATGACCAGTTCCAT AGCGAACCTA	Primer 3 for deletion of *V. campbellii btsS* with pNTPS-R6KT, amplifies 15 first bp, overlap with #6
#8	CCGAAGCTAGCGAATTCGTG GATCCTCTACGGTGCAATGA TTGGTGAAGG	Primer 4 for deletion of *V. campbellii btsS* with pNTPS-R6KT, BamHI site
#9	CGGCTGGCGCCAAGCTTCTC TGCAGCCGTACGCCAAGAA GCGAAGTCTCG	Primer 1 for deletion of *V. campbellii btsR* with pNTPS-R6KT, PstI site

#10	GTAGTCTTGGATGTTAACCG CACTCGGTATCAGTAGCTAA GCTCAGGCTC	Primer 2 for deletion of *V. campbellii btsR* with pNTPS-R6KT, amplifies 15 last bp, overlap with #11
#11	GAGCCTGAGCTTAGCTACTG ATACCGAGTGCGGTTAACAT CCAAGACTAC	Primer 3 for deletion of *V. campbellii btsR* with pNTPS-R6KT, amplifies 15 first bp, overlap with #12
#12	CCGAAGCTAGCGAATTCGTG GATCCCTGCAAATTGGGATC TGCGTTGATC	Primer 4 for deletion of *V. campbellii btsR* with pNTPS-R6KT, BamHI site
#13	TAGGTTCGCTATGGAACTGG TCATCGGTATCAGTAGCTAA GCTCAGGCTC	Primer 2 for double deletion of *V. campbellii btsR* and *btsS* with pNTPS-R6KT, amplifies 15 last bp of *btsR*, overlap with #14, use together with #8
#14	GAGCCTGAGCTTAGCTACTG ATACCGATGACCAGTTCCAT AGCGAACCTA	Primer 3 for double deletion of *V. campbellii btsR* and *btsS* with pNTPS-R6KT, amplifies 15 first bp of *btsS*, overlap with #13, used together with #12
#15	ATATCTGGATCCTCATGTTT CTATTTCACTTCTGATT	Primer 1 for complementation of *V. campbellii btsU* at the native locus, BamHI site
#16	GCCGAAGCTAGCAAAGGTC GCTGAGTACTTTTCAAAA	Primer 2 for complementation of *V. campbellii btsU* at the native locus, NheI site
#17	ATATCTGGATCCTTATCTGG TGTGCTATTGCTCTGTC	Primer 1 for complementation of *V. campbellii btsSR* at the native locus, BamHI site
#18	GCCGAAGCTAGCATTTAACA GTATTCGATGCAACGTG	Primer 2 for complementation of *V. campbellii btsSR* at the native locus, NheI site

#19	AAAAAACTGCAGGATCGTA GTCACCTTGCTTAGCATT	Primer 1 to amplify the promoter region of *V. campbellii btsU* (500 bp), PstI site
#20	ACCATGCCGCTAGTTGCCAT AGCTATTGTCCTTGGTTTAA	Primer 2 to amplify promoter of *V. campbellii btsU* (500 bp), overlap to *mcherry*
#21	TTAAACCAAGGACAATAGCT ATGGCAACTAGCGGCATGGT	Primer 1 to amplify *mcherry*, overlap to promoter of *V. campbellii btsU*
#22	AAAAAAGGATCCTTATTTGT ATAGTTCATCCATGCCA	Primer 2 to amplify *mcherry*, BamHI site

SUPPLEMENTAL REFERENCES

1. Greenberg E, Hastings JW, Ulitzur S. 1979. Induction of luciferase synthesis in *Beneckea harveyi* by other marine bacteria. Arch Microbiol 120:87-91.
2. Mueller RS, Beyhan S, Saini SG, Yildiz FH, Bartlett DH. 2009. Indole acts as an extracellular cue regulating gene expression in *Vibrio cholerae*. J Bacteriol 191:3504-16.
3. Darias JA, García-Fontana C, Lugo AC, Rico-Jiménez M, Krell T. 2014. Qualitative and quantitative assays for flagellum-mediated chemotaxis. Methods Mol Biol 1149:87-97.

Supplemental material for chapter 4

Paulini S, Fabiani FD, Weiß AS, Moldoveanu AL, Helaine S, Stecher B, Jung K. 2022. The Biological Significance of Pyruvate Sensing and Uptake in *Salmonella enterica* Serovar Typhimurium. Microorganisms 10:1751. https://doi.org/10.3390/microorganisms10091751

Supplementary material

The biological significance of pyruvate sensing and uptake in *Salmonella enterica* serovar Typhimurium

Stephanie Paulini [1], Florian D. Fabiani [1,†], Anna S. Weiss [2], Ana Laura Moldoveanu [3], Sophie Helaine [3,‡], Bärbel Stecher [2,4] and Kirsten Jung [1,*]

[1] Department of Microbiology, Ludwig-Maximilians-University Munich, 82152 Planegg-Martinsried, Germany
[2] Max von Pettenkofer Institute of Hygiene and Medical Microbiology, Faculty of Medicine, Ludwig-Maximilians-University Munich, 80336 Munich, Germany
[3] MRC Centre for Molecular Bacteriology and Infection, Imperial College London, London SW7 2DD, UK
[4] German Center for Infection Research (DZIF), Partner Site LMU Munich, 80337 Munich, Germany
* Correspondence: jung@lmu.de; Tel.: +49-(0)89/2180-74500
† Present affiliation: Bayer AG, 13353 Berlin, Germany.
‡ Present affiliation: Department of Microbiology, Harvard Medical School, Boston, MA 02115, USA.

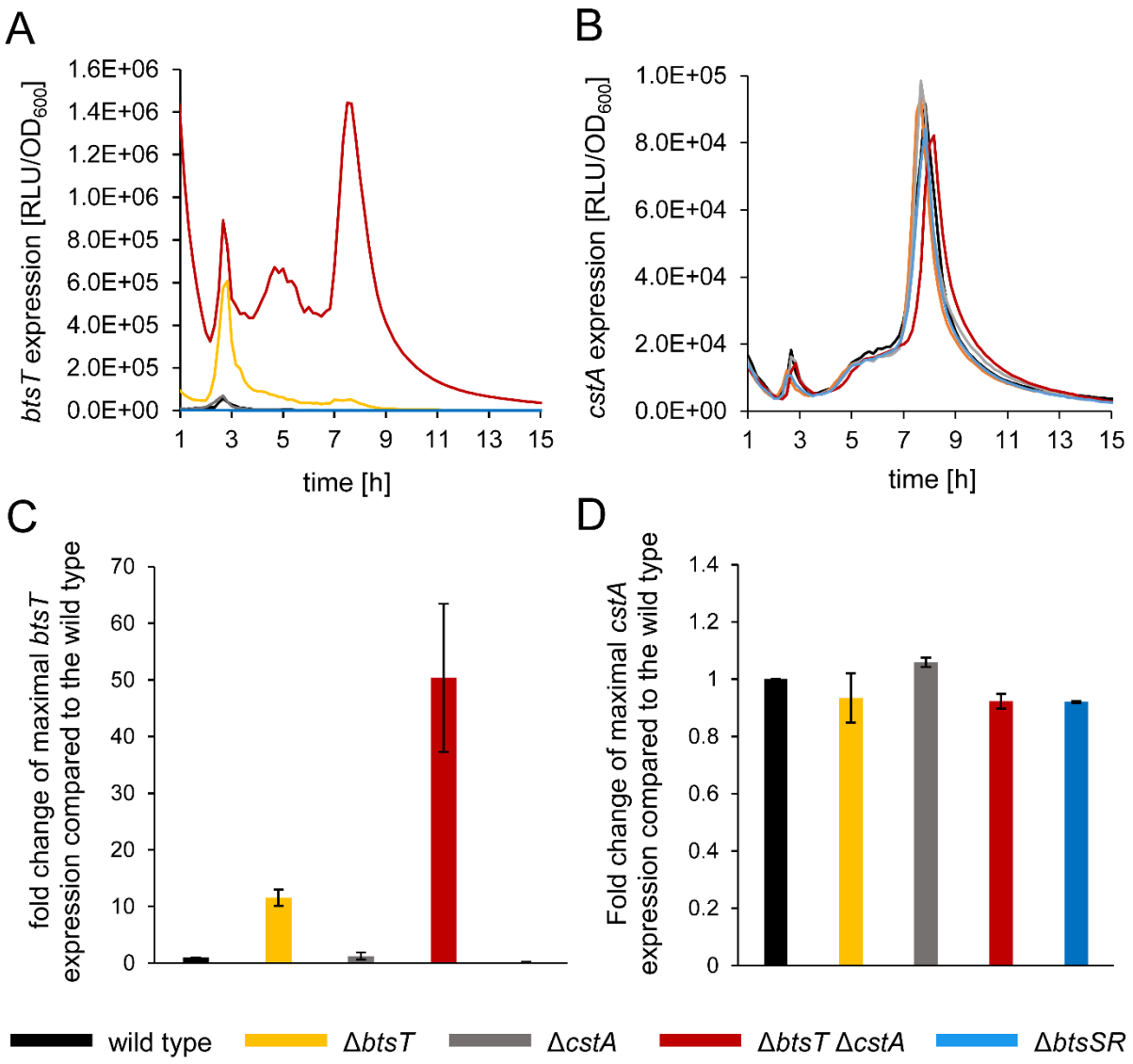

Figure S1. Expression of *btsT* and *cstA* in *S*. Typhimurium mutants. SL1344 wild-type (black), Δ*btsT* (yellow), Δ*cstA* (grey), Δ*btsT*Δ*cstA* (red) and Δ*btsSR* (blue) cells harboring the reporter plasmid for *btsT* (pBBR1-MCS5-*PbtsT-lux*) or for *cstA* (pBBR1-MCS5-*PcstA-lux*) were grown in LB medium in a plate reader at 37 °C. Luminescence values were measured over time and gene expression was determined as RLU per 1 OD_{600}. **A)** Expression of *btsT* during growth. **B)** Expression of *cstA* during growth. **C)** Maximal *btsT* expression depicted as fold change from wild-type value. **D)** Maximal *cstA* expression depicted as fold change from the wild-type value. A, B: graphs represent the mean of three independent replicates. the standard deviations were below 10%. C, D: Error bars represent the standard deviations of the mean of three independent replicates.

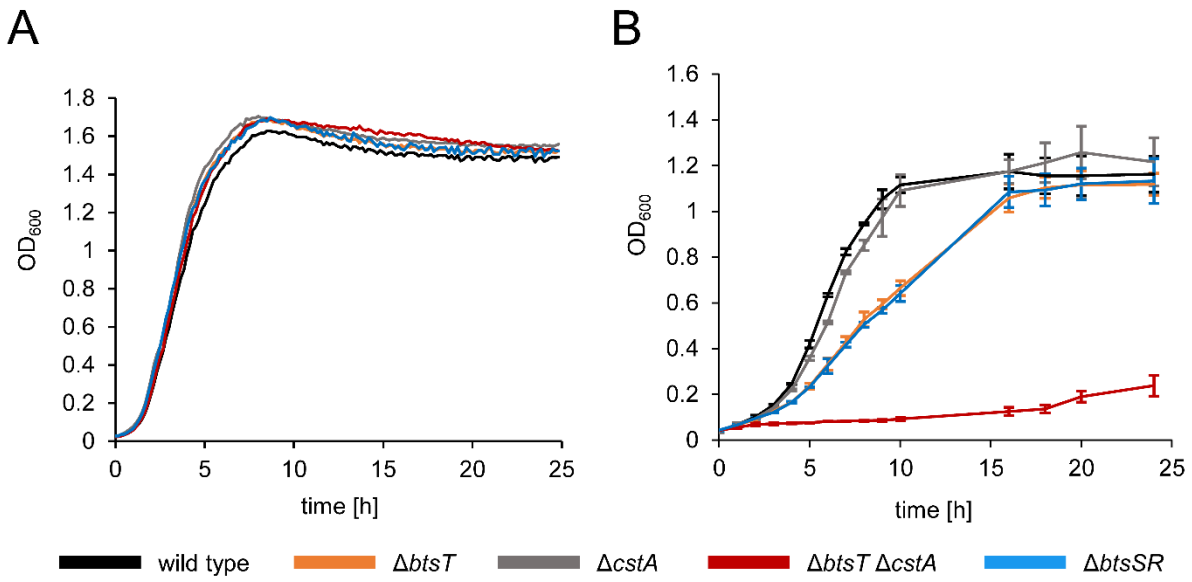

Figure S2. Growth of *S.* Typhimurium mutants. SL1344 wild-type (black), Δ*btsT* (yellow), Δ*cstA* (grey), Δ*btsT*Δ*cstA* (red) and Δ*btsSR* (blue) cells were grown for 24 hours at 37°C in **A)** LB medium or **B)** M9 minimal medium with 60 mM pyruvate.

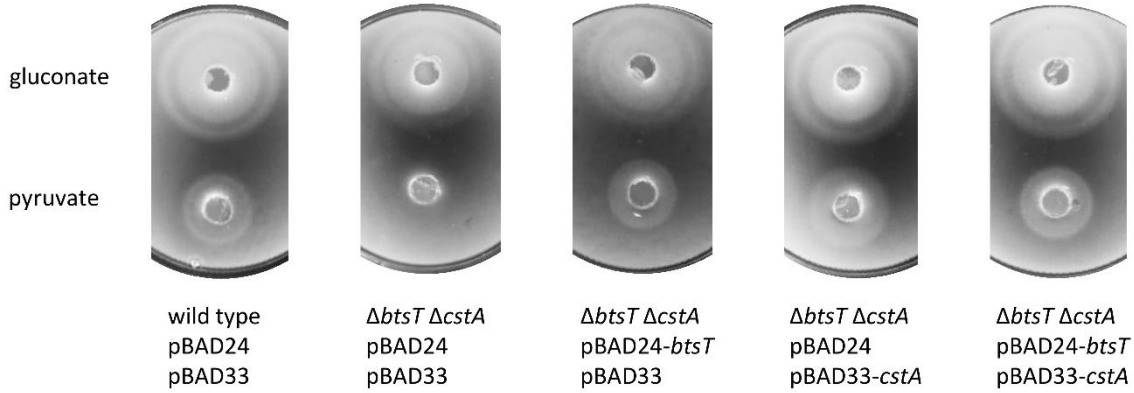

Figure S3. *S*. Typhimurium Δ*btsT*Δ*cstA* mutant lost chemotactic response to pyruvate. Chemotaxis was tested by mixing SL1344 wild-type or Δ*btsT*Δ*cstA* cells harboring the indicated expression plasmids for *btsT* (pBAD24-*btsT*) and/or *cstA* (pBAD33-*cstA*) or the empty vectors with 0.3% (wt/vol) M9 soft agar and pouring them over 1.5% (wt/vol) M9 agar plugs containing either 60 mM gluconate (above) or 60 mM pyruvate (below). Plates were incubated at 37 °C for 4 hours, and the pictures are representative of three independent experiments.

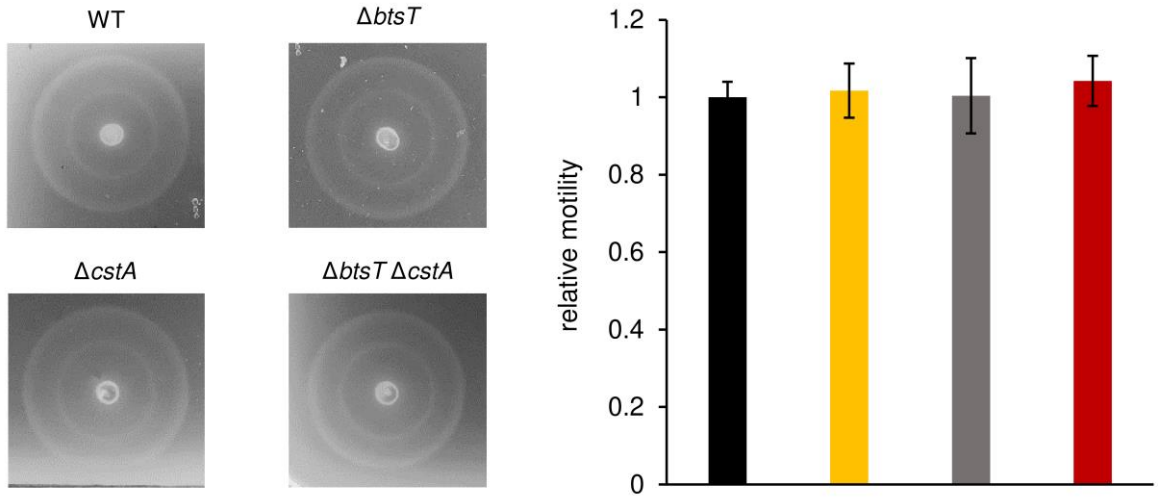

Figure S4. Motility of *S.* Typhimurium is not affected by deletions of *btsT* or *cstA*. Motility of SL1344 wild type (upper left, black), Δ*btsT* (upper right, yellow), Δ*cstA* (lower left, grey) and Δ*btsT*Δ*cstA* (lower right, red) cells was tested by spotting equal numbers of cells on 0.3% LB soft agar, incubating the plates at 37°C for 3 hours and measuring the diameter of the ring with the software ImageJ [54]. Images of rings are representative of four independent experiments and relative motility was determined in relation to the mean diameter of the wild type ring.

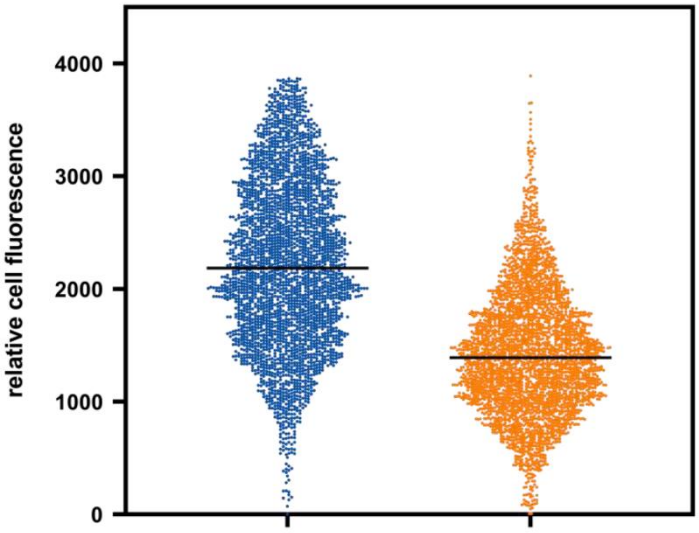

Figure S5. Expression of *btsT* in *S*. Typhimurium under SPI2 inducing conditions. Strain SL1344 *btsT*::*mNeonGreen*, which chromosomally encodes a fusion between *btsT* and *mNeonGreen,* was used to measure expression of *btsT* in single cells. Cells were grown in NonSPI2 (blue) or InSPI2 (orange) medium with 4 μg/ml histidine and 60 mM pyruvate as C-source until mid-exponential phase. Samples were taken for fluorescence microscopy. To quantify relative fluorescence intensities of single cells, phase contrast and fluorescent images were analyzed using the ImageJ [54] plugin MicrobeJ [77]. In total >1000 cells were quantified per condition.

Table S1. Oligonucleotides used in this study.

	DNA sequence	Description
#1	CGCTGTGCGCTACCCGGCATCAGTTTTAGTGGTGTGAAGATTAAGACCCACTTTCACATT	Primer 1 for tetRA-insertion by λ-Red recombination in *btsT*
#2	ATTAAACTTACAACCAGGTTTTACTATGGATACGAAAAAGCTAAGCACTTGTCTCCTG	Primer 2 for tetRA-insertion by λ-Red recombination in *btsT*
#3	ATTAAACTTACAACCAGGTTTTACTATGGATACGAAAAAGTCTTCACACCACTAAAACTG	Primer 1 for clean deletion of btsT
#4	AGTCCGGAATACCAATCAACA	Primer 2 for clean deletion of btsT
#5	ACCGCTTAAACCGCCATACA	Primer 1 for sequencing of Δ*btsT*
#6	ACGTTCGCGGAAGAACTCTT	Primer 2 for sequencing of Δ*btsT*
#7	GGCAAAACGATATTCTAACAGTCTTTTACAGGCCAATCGCTTAAGACCCACTTTCACATT	Primer 1 for tetRA-insertion by λ-Red recombination in *btsSR*
#8	TTTAATTGAAGTGTGGTTTGCGGGTATGTACGAGTTTAATCTAAGCACTTGTCTCCTG	Primer 2 for tetRA-insertion by λ-Red recombination in *btsSR*
#9	TTGTTGATACGACGTTCCGC	Primer 1 for clean deletion of btsSR
#10	TTTAATTGAAGTGTGGTTTGCGGGTATGTACGAGTTTAATGCGATTGGCCTGTAAAAGAC	Primer 2 for clean deletion of btsSR
#11	TGGAACACCCAAACGGACAACAACTATGAATAAATCAGGGTAGGCTGGAGCTGCTTCGAA	Primer 1 to amplify the FRT-kanamycin-FRT cassette from pKD46 for replacement of *cstA*
#12	GGAGAGGGCTATTGATGTAAAAAGATTAGTGCGCGCCTTTTCCTCCTTAGTTCCTATTCC	Primer 2 to amplify the FRT-kanamycin-FRT cassette from pKD46 for replacement of *cstA*
#13	CTCTTTGACGAGCAGGGGAG	Primer 1 for sequencing of Δ*cstA*
#14	CGTCTGATCCGGATGCGTTA	Primer 2 for sequencing of Δ*cstA*
#15	AAAAAATCTAGAGCGATGACGTGCTGGAGGCG	Primer 1 to amplify the promoter of *cstA* to create pBBR1-MCS5-*PcstA-lux*, XbaI site
#16	AAAAAACTCGAGAGTTGTTGTCCGTTTGGGTG	Primer 2 to amplify the promoter of *cstA* to create pBBR1-MCS5-*PcstA-lux*, XhoI site
#17	AAAAAATCTAGAAGTTTGCAATACGGTGAAGT	Primer 1 to amplify the promoter of *btsT* to create pBBR1-MCS5-*PbtsT-lux*, XbaI site
#18	AAAAAACTCGAGAGTAAAACCTGGTTGTAAGT	Primer 2 to amplify the promoter of *btsT* to create pBBR1-MCS5-*PbtsT-lux*, XhoI site
#19	GCGCGCGAATTCACTATGGATACGAAAAAGATATT	Primer 1 to amplify *btsT* to create pBAD24-*btsT*, EcoRI site

#20	GCTAGCAAGCTTTTAGTGATGGTGATGG TGATGGTGGTGTGAAGAGATCTTCA	Primer 2 to amplify *btsT* to create pBAD24-*btsT*, HindIII site
#21	GCGCGCGAATTCACTATGAATAAATCAG GGAAATA	Primer 1 to amplify *cstA* to create pBAD3-*cstA*, EcoRI site
#22	GCTAGCAAGCTTTTAGTGATGGTGATGG TGATGGTGCGCGCCTTTCGCCTGCG	Primer 2 to amplify *cstA* to create pBAD3-*cstA*, HindIII site

Supplementary methods

Strain construction of SL1344 *btsT*::*mNeonGreen*. Chromosomal fusions were created by double homologous recombination using the pNPTS138-R6KT suicide plasmid [47]. SL1344 *btsT* was amplified by PCR from SL1344 genomic DNA with oligonucleotides #38 and #39, without keeping the stop codon. The *mNeonGreen* gene was amplified by PCR from a plasmid (Peter Graumann, Marburg) with oligonucleotides #40 and #41. An 800 bp region directly downstream of *btsT* was amplified by PCR from SL1344 genomic DNA with oligonucleotides #42 and #43. The pNPTS138-R6KT backbone was linearized with oligonucleotides #37 and #44. All fragments were created with overlaps of 20 bp for assembly using the NEBuilder kit (New England Biolabs, Ipswich, MA, USA). The final pNPTS138-R6KT-*btsT*::*mNeonGreen* plasmid was first transformed into *E. coli* DH5α and confirmed by sequencing. Then it was transferred into *E. coli* WM3064 for conjugation with SL1344. Double homologous recombination was induced as described in the main manuscript. Oligonucleotide sequences are listed in table S1.

***In vivo* single cell fluorescence measurements.** SL1344 cells with the chromosomal fusion *btsT*::*mNeonGreen* were grown in InSPI2 and NonSPI2 medium [69] with 4 μg/ml histidine and 60 mM pyruvate as carbon source, inoculated from overnight culture to an initial OD_{600} of 0.05. In exponential growth phase, samples were taken and 2 μl of the culture were spotted on 1% (wt/vol) agarose prepared with PBS on a microscope slide and sealed with a cover slide. Microscopy was performed using a DMI6000 B fluorescence microscope (Leica Microsystems, Wetzlar, Germany), with an excitation wavelength of 485 nm and a 510-nm emission filter. To quantify single cell fluorescence, 1000 cells per condition (InSPI2 or NonSPI2) were analyzed using the plug-in MicrobeJ [77] of the software ImageJ [54], as described before [46]. The background was subtracted for each cell.

Acknowledgements

The last years went by so fast and I somehow feel like moving out from home after all this time in the microbiology department of the LMU. I'm leaving very thankful!

First of all, I want to thank Prof. Kirsten Jung, who gave me the opportunity to stay in this group after my master thesis as a doctoral student, which was the perfect decision for me. You were not only my supervisor, but also such a good motivator! Whenever my experiments were not working as expected or when I was not sure how the big picture of the story should look like, you were always able to re-light my fire and make me excited about my work again. You gave me the trust and freedom to work on my own, and at the same time your door was always open for me. I really enjoyed working in your group and writing our publications together.

I also would like to thank the LMU for being my second home since 2009, the DFG for funding my projects and the CRC1371 for making me being a part of such an excellent group of scientists and for all the nice courses, retreats, events and our graduate school. Moreover, I thank my collaborators for all their work, time, inspiration and all our publications. Special thanks to Prof. Bärbel Stecher and Prof. Silke Robatzek for all your time and help as my TAC members, and also to the other members of my examination board.

I deeply want to thank all members of AG K. Jung, AG H. Jung and AG Lassak for making the last years so wonderful! The pyruvate lab with Ana, Jin, Nathalie, Florian, Elena and all students that passed the way for your friendship, for helping, laughing, chatting and advising in G 01.005. My office mate Urte for being a wonderful friend in our most relaxed office. Alina, Judith and Ralph for your friendship and all our moments of joy. Julia, Franzi, Kilian, Bibakhya, Sophie, Grazyna, Ingrid and numerous students for making each lunch break in the sun my daily highlight. The running group for the best sporty summer experiences. Nicola, Michelle, Sabine, Korinna, Tina, Dimitar, Lingyun, Tatjana, Jürgen, Tania, Prof. Heinrich Jung and of course everybody I might have forgotten for making me feel happy and at home here every single day. You all made this time very special and I will miss you all so much.

Without the support and love of my family I wouldn't be who and where I am today and I can't thank you enough. You are the best. Oskar, you are my sun, my moon, my stars and my whole world and there are no words to thank you enough.

At last, thanks to all my bacteria – you did a great job and I will miss you, my little Stinkies!

“Die Rolle des unendlich Kleinen in der Natur ist unendlich groß.“

Louis Pasteur